

Novel models towards predictive control of advanced building systems and occupant comfort in buildings

THÈSE N° 6440 (2015)

PRÉSENTÉE LE 8 MAI 2015

À LA FACULTÉ DE L'ENVIRONNEMENT NATUREL, ARCHITECTURAL ET CONSTRUIT
LABORATOIRE D'ÉNERGIE SOLAIRE ET PHYSIQUE DU BÂTIMENT
PROGRAMME DOCTORAL EN GÉNIE CIVIL ET ENVIRONNEMENT

ÉCOLE POLYTECHNIQUE FÉDÉRALE DE LAUSANNE

POUR L'OBTENTION DU GRADE DE DOCTEUR ÈS SCIENCES

PAR

Nikolaos ZARKADIS

acceptée sur proposition du jury:

Prof. M. Bierlaire, président du jury
Prof. J.-L. Scartezzini, Dr N. Morel, directeurs de thèse
Prof. J. Hennebert, rapporteur
Prof. C. N. Jones, rapporteur
Dr D. Lindelöf, rapporteur



ÉCOLE POLYTECHNIQUE
FÉDÉRALE DE LAUSANNE

Suisse
2015

To my family & Bénédicte
for all their love and support.

*You might slide, you might tumble and fall by the road side;
don't you ever let nobody drag your spirit down.
Remember you're walkin' up to heaven, don't let nobody turn you round.
Walk with the rich, walk with the poor; learn from everybody that's what life is for;
don't you ever let nobody drag your spirit down.*

(Charlotte Hoglund, Eric Bibb)

ABSTRACT

People in developed countries spend today most of their time inside buildings as part of the modern way of life. As a result, the building sector accounts for almost 40% of the total energy consumption and a big part of the energy bill goes to maintain the visual and thermal comfort of their occupants. At the same time, awareness is being raised during the last decades about the greenhouse gas emissions and the possibly irreversible effects of global warming; both linked to excessive use of non-renewable primary energy sources which still power most of the world, including our buildings. Thus, moderating the energy consumed in them is a top priority. However, this does not imply a horizontal cut in energy consumption that would result in a drop of user comfort.

Instead, we suggest that improving energy efficiency in buildings while maintaining or even improving the user comfort is the optimal solution. It is indeed the core of this thesis that there is a great energy saving potential in refining the control of building systems such as electric lighting, heating, cooling and ventilation, which more than often consume a lot of energy without delivering the analogous amount of visual and thermal comfort.

In this direction, this thesis proposes the development of a novel predictive control algorithm for the control of electrochromic glazing using a low cost sky scanner using a simple web camera. The developed algorithm demonstrated an average prediction accuracy of 92% and integrates and controls the blinds and electric lighting to maximise visual comfort taking into account outdoor and indoor conditions, presence and user actions. Measurements and extensive simulations showed that the elaborated algorithm improves thermal and visual comfort when compared to standard glazing coupled with blinds and exhibits acceptable levels of energy consumption for space heating and electric lighting.

In the same subject of improving building control, a novel approach for controlling building systems by using state-based stochastic data-driven models to identify "season" is defined and developed. We reason that the season variable is unique to every building and it depends on weather conditions, user behaviour and building construction. The developed models identified "season" with an accuracy that ranged from 69 to 91% and it was shown through simulations that a controller based on Hidden Markov Models can reduce energy

demand for heating and improve the thermal comfort of occupants in different building construction types.

Finally, the use of Hidden Markov Models was further explored in this thesis by suggesting a novel model for the estimation of occupants' visual comfort in buildings. The proposed model is based on horizontal workplane illuminance measurements using ceiling-mounted sensors as well on vertical illuminance monitoring at the observer's eyes plane (pupillary illuminance) by means of wearable portable sensors. We argue that the proposed model improves greatly over the various existing discomfort glare indices and metrics and it is also convincingly demonstrated that it can be seamlessly integrated and used in building automation systems based on fuzzy logic.

Keywords: integrated control of building systems, electrochromic windows, predictive control, fuzzy logic, visual and thermal comfort, energy saving, Hidden Markov Models, machine learning, clouds motion prediction, sky prediction, stochastic modelling, user adaptation, season modelling, HVAC systems

RÉSUMÉ

Dans les pays développés, les gens passent aujourd'hui la plupart de leur temps à l'intérieur des bâtiments dans le cadre de la vie moderne. Par conséquent, le secteur du bâtiment est responsable de près de 40% de la consommation totale d'énergie et une grande partie de la facture d'énergie concerne la production du confort visuel et thermique de leurs occupants. Dans le même temps, au cours des dernières décennies, le public est de plus en plus concerné par le sujet des émissions de gaz à effet de serre et des effets peut-être irréversibles du réchauffement climatique; tous deux liés à une utilisation excessive des sources d'énergie primaires non renouvelables qui alimentent l'ensemble de nos activités, y compris l'énergie consommée dans nos bâtiments. Ainsi, modérer la consommation de ces énergies non renouvelables est une priorité absolue. Mais, est-ce que cela signifie une réduction drastique de notre consommation d'énergie et donc une baisse de notre confort et de notre niveau de vie?

Pas du tout, répondons-nous dans cette thèse, où nous suggérons que l'amélioration de l'efficacité énergétique dans les bâtiments tout en maintenant, voire en améliorant le confort de l'utilisateur est le chemin à parcourir. En particulier, la position de cette thèse est qu'il y a un grand potentiel pour des grandes économies d'énergie dans l'affinage du contrôle des systèmes, tels que l'éclairage électrique, le chauffage, la climatisation et la ventilation, qui en plus consomment souvent beaucoup d'énergie sans fournir un réel confort visuel et thermique.

Dans cette direction, la thèse propose le développement d'un nouvel algorithme de contrôle prévisionnel de fenêtres électrochromiques utilisant un « sky-scanner » à faible coût dont le capteur est une simple caméra web. L'algorithme développé démontre une précision de prédiction de 92% en moyenne et il intègre et il contrôle les stores et l'éclairage électrique afin de maximiser le confort visuel en tenant compte des conditions à l'extérieur et à l'intérieur du bâtiment, de la présence et des actions des utilisateurs. Des mesures et des simulations ont montré que l'algorithme développé améliore le confort thermique et visuel des occupants par rapport à un vitrage standard couplé avec des stores et présente des niveaux de consommation d'énergie acceptables pour le chauffage et l'éclairage électrique.

En relation avec le même sujet de l'amélioration du contrôle des systèmes dans les bâtiments, une nouvelle approche pour identifier la « saison » en utilisant des modèles stochastiques tels que les modèles de Markov cachés est définie et développée. Nous considérons que la variable « saison » est unique à chaque bâtiment et qu'elle dépend des conditions météorologiques, du comportement de l'utilisateur et de la construction (typologie) du bâtiment. Les modèles développés identifient la « saison » avec une précision comprise entre 69 et 91%. Ainsi, il a été montré par le biais de simulations qu'un contrôleur basé sur des modèles de Markov cachés peut réduire la demande d'énergie pour le chauffage et améliorer le confort thermique des occupants dans différentes typologies de bâtiments.

Finalement, l'utilisation de modèles de Markov cachés a été approfondie dans cette thèse en proposant un modèle nouveau pour l'estimation de confort visuel des occupants dans les bâtiments. Le modèle proposé est basé sur des mesures d'éclairement dans le plan de travail horizontal utilisant des capteurs montés au plafond, ainsi que sur des mesures de l'éclairement dans le plan vertical des yeux de l'observateur au moyen de nouveaux capteurs portables. Nous soutenons que le modèle présente une amélioration face aux différents indices d'éblouissement existants et montrons de manière convaincante qu'il peut être intégré et utilisé dans le contrôle automatique des installations techniques du bâtiment basé sur la logique floue.

Mots-clés: contrôle intégré des installations techniques du bâtiment, fenêtres électrochromiques, contrôle prévisionnel, logique floue, confort visuel et thermique, économies d'énergie, modèles de Markov cachés, prédiction de mouvement des nuages, modélisation stochastique, adaptation aux préférences des utilisateurs, modélisation de la saison, systèmes CVC

ΠΕΡΙΛΗΨΗ

Οι μοντέρνοι ρυθμοί ζωής στις αναπτυγμένες χώρες θέλουν τους ανθρώπους να περνούν το μεγαλύτερο ποσοστό του χρόνου τους μέσα στα κτίρια. Ως εκ τούτου, ο κτιριακός τομέας ευθύνεται για το 40% της συνολικής τελικής κατανάλωσης ενέργειας, μεγάλο μέρος της οποίας φροντίζει για την θερμική και οπτική άνεση των ενοίκων τους (κλιματισμός και φωτισμός). Ταυτόχρονα, τις τελευταίες δεκαετίες σημαντικό μέρος της κοινής γνώμης έχει ευαισθητοποιηθεί σχετικά με την κλιματική αλλαγή και τις πιθανά μη αναστρέψιμες επιπτώσεις που αυτή έχει στη βιόσφαιρα και κατανοεί πως αυτή οφείλεται κατά κύριο λόγο στην αλόγιστη χρήση μη ανανεώσιμων πηγών ενέργειας. Αυτές οι «μη καθαρές» πηγές ενέργειας τροφοδοτούν κατά κανόνα και τα κτίριά μας, ενώ η ελάττωση της ενέργειας που καταναλώνουμε σε αυτά αποτελεί προτεραιότητα και αναπόσπαστο πλέον κομμάτι πολιτικών σε εθνικό και παγκόσμιο επίπεδο. Η εξοικονόμηση όμως της ενέργειας δεν είναι επιθυμητή όταν γίνεται οριζόντια και με τρόπο βλαπτικό ως προς την ποιότητα ζωής του χρήστη. Αντίθετα, θα πρέπει να επιτυγχάνεται στοχευμένα μέσω της αύξησης της ενεργειακής απόδοσης των κτιρίων και της ταυτόχρονης διατήρησης (ή ακόμα και βελτίωσης) των συνθηκών διαβίωσης σε αυτά.

Αυτή ακριβώς η λογική αποτελεί τον πυρήνα γύρω από τον οποίο αναπτύχθηκε η παρούσα διατριβή, η οποία υποστηρίζει πως η βελτιστοποίηση του ελέγχου των ενεργοβόρων κτιριακών συστημάτων όπως ο φωτισμός και ο κλιματισμός μπορεί να απελευθερώσει μεγάλο δυναμικό εξοικονόμησης ενέργειας και ταυτόχρονα να διασφαλίσει πως αυτά προσφέρουν τις καλύτερες δυνατές συνθήκες στους χρήστες τους.

Σε αυτήν την κατεύθυνση, στα πλαίσια της παρούσας διατριβής αναπτύχθηκε ένας καινοτόμος αλγόριθμος ελέγχου ηλεκτροχρωμικών παραθύρων ο οποίος προβλέπει τοπικά τη νεφοκάλυψη και την ηλιοφάνεια μέσω μιας απλής κάμερας ηλεκτρονικού υπολογιστή. Ο αλγόριθμος επιτυγχάνει πρόγνωση με ακρίβεια 92% και ελέγχει (εκτός των ηλεκτροχρωμικών υαλοπινάκων) και τα συστήματα σκίασης και ηλεκτρικού φωτισμού, λαμβάνοντας υπόψη τις καιρικές συνθήκες, την παρουσία και τις ενέργειες του χρήστη. Επί τόπου μετρήσεις καθώς και εκτενείς προσομοιώσεις έδειξαν πως το προτεινόμενο ολοκληρωμένο σύστημα ελέγχου βελτιώνει τα επίπεδα θερμικής και οπτικής άνεσης, ενώ κρατάει τα επίπεδα κατανάλωσης ενέργειας σε αποδεκτά επίπεδα (συγκρινόμενο με κλασικά συστήματα υαλοπινάκων με εξωτερικά σκιάδια).

Στην ίδια θεματική ενότητα (αυτήν της βελτίωσης της απόδοσης κτιριακών συστημάτων), αναπτύχθηκε μία νέα προσέγγιση ελέγχου συστημάτων κλιματισμού, η οποία βασίζεται σε Κρυφά Μοντέλα Μαρκόφ (Hidden Markov Models) και μηχανική μάθηση και η οποία προτείνει έναν καινοτόμο ορισμό της έννοιας της «εποχής». Συγκεκριμένα, προτείνεται πως η παράμετρος της «εποχής» – σύμφωνα με την οποία αποφασίζεται συνήθως η λειτουργία των συστημάτων θέρμανσης, ψύξης και κλιματισμού – είναι μοναδική για κάθε κτίριο ή ακόμα και τμήμα του κτιρίου και εξαρτάται από τις καιρικές συνθήκες, την κατασκευή του κτιρίου και τους ίδιους τους ενοίκους (συμπεριφορά, χρήση, επιθυμίες). Τα μοντέλα που αναπτύχθηκαν επέτυχαν να αποδώσουν σωστά την «εποχή» με ακρίβεια που κυμαίνεται από 69 έως 91%, ενώ προσομοιώσεις που πραγματοποιήθηκαν σε διαφορετικές τυπολογίες κτιρίων έδειξαν πως η ενσωμάτωση τέτοιων αλγορίθμων σε κτιριακά συστήματα ελέγχου μπορεί να μειώσει την κατανάλωση ενέργειας για θέρμανση και να βελτιώσει τα επίπεδα θερμικής άνεσης των ενοίκων τους.

Τέλος, η χρήση των Κρυφών Μοντέλων Μαρκόφ επεκτάθηκε και στην εκτίμηση της οπτικής άνεσης των ατόμων εντός των κτιρίων γραφείων. Τα προτεινόμενα μοντέλα βασίζονται σε μετρήσεις των επιπέδων του φωτισμού στην (οριζόντια) επιφάνεια εργασίας των χρηστών καθώς και στο επίπεδο των οφθαλμών τους (κάθετα) μέσω των αντίστοιχων κάθε φορά αισθητήρων. Τα μοντέλα που αναπτύχθηκαν στα πλαίσια της παρούσας διατριβής παρουσιάζουν αρκετά πλεονεκτήματα σε σχέση με τα υπάρχοντα μοντέλα και δείκτες (είναι λιγότερο πολύπλοκα, πιο ακριβή, ιδιαίτερα όταν κάνουν χρήση του φωτισμού στο κάθετο επίπεδο, προσαρμόζονται στις προτιμήσεις του κάθε ατόμου κ.α.), ενώ αποδεικνύεται πως δύναται να ενσωματωθούν εύκολα σε αυτόματα συστήματα φωτισμού τα οποία βασίζονται τη λειτουργία τους στην Ασαφή Λογική (fuzzy logic).

Λέξεις-κλειδιά: Ολοκληρωμένος έλεγχος κτιριακών συστημάτων, ηλεκτροχρωμικά παράθυρα, έλεγχος βασισμένος σε μοντέλα πρόγνωσης, ασαφής λογική (fuzzy logic), οπτική και θερμική άνεση, εξοικονόμηση ενέργειας, Κρυφά Μοντέλα Μαρκόφ, μηχανική μάθηση, πρόγνωση κίνησης νεφών και ηλιοφάνειας, στοχαστικές μέθοδοι και μοντέλα, συστήματα ψύξης-θέρμανσης-κλιματισμού

ACKNOWLEDGEMENTS

I am very grateful to my thesis supervisors Jean-Louis Scartezzini and Nicolas Morel for providing me the opportunity to perform doctoral research at the Solar Energy and Building Physics Laboratory (LESO-PB) at EPFL, where they allowed me to work in an autonomous manner while provided their valuable guidance and scientific rigour along the way whenever I needed it.

Further, I would like to express my gratitude to the members of the jury, Michel Bierlaire (Transportation and Mobility Laboratory, EPFL), Colin Jones (Automatic Control Laboratory 3, EPFL), Jean Hennebert (Institute of Complex Systems, HES-SO Fribourg) and David Lindelöf (Neurobat AG) for their participation in the examination, their thorough reading and their constructive remarks that greatly improved this thesis.

My gratitude is also extended to the Swiss Federal Office of Energy as well as to the Hasler Foundation who provided the financial support for the research projects 'Automatic Control of An Electrochromic Window' and 'Green-Mod' respectively, without which this work would not have been possible. Many thanks too to our partners of the 'Green-Mod' project from the University of Applied Sciences at HES-SO Fribourg, Jean Hennebert, G  r  me Bovet and especially Antonio Ridi whose hard work on Hidden Markov Model algorithms was instrumental to this thesis.

I express my gratitude to all the researchers of LESO-PB whose high-calibre work has been both an inspiration and the catalyst of this thesis. In particular I wish to mention the research work of Antoine Guillemin, David Lindel  f, Manuel Bauer, Friedrich Linhart, Fr  d  ric Haldi, David Daum and of course Jean-Louis Scartezzini and Nicolas Morel.

Furthermore, I would like to thank my colleagues in the laboratory Loesch Pierre, Laurent Deschamps and his team (especially Roulin Pascal, Matteo Winter, S  bastien Hausammann, Rapha  l Mas and Paul Becquelin) for the valuable IT and infrastructure-related support they provided throughout the duration of this thesis. Special thanks to Christian Roecker for allowing us to use his office as the test bed for the research regarding the electrochromic windows. Also, I would like to take the opportunity and thank the secretaries of our laboratory Sylvette Renfer, Suzanne l'Eplattenier, Barbara Smith and Marl  ne Muff for their helpfulness, enthusiasm and kindness through all kinds of administrative and other matters.

The warmest of thanks go to Jérôme Kämpf and Silvia Coccolo with whom I had the great pleasure to share my office and many an interesting conversations with (as well as the occasional laugh!) during most of my time in the laboratory.

I would also like to thank all the colleagues I have had the chance to meet in the laboratory between 2010 and 2015 who contributed in making LESO-PB such an amazing environment to work at. In addition to the people already mentioned before, it was a privilege and a sheer joy to work and share time with Diane Perez, Urs Wilke, Jean Ceppi, Philippe Leroux, Darren Robinson, Alessia Giovanardi, Charlotte Marguerite, Apiparn Borisuit, Chantal Basurto, Marja Edelmann, Raquel Peres Gagliano, Maria Papadopoulou, Gianpiero Caruso, Lenka Maierova, Andrea Cifuentes Cuéllar, Thibault Gruaz, Thibaut Vermeulen, Nesrine Gharbi, Mirjam Münch, Maria Cristina Munari, Andreas Schüler, Martin Joly, Antonio Paone, André Kostro, Virginie Le Caër, Luc Burnier, Nicolas Jolissaint, Thomas Gascou, Govinda Upadhyay, Dapeng Li, Olivia Bouvard, Emmanuel Walter, Kilian Megret, Anna Kramer, Sara Vanzo, Florio Pietro, Dan Assouline, Ali Motamed, Gong Jing, Dasun Perera, Yujie Wu, Dasaraden Mauree, Nahid Mohajeri and Vahid Nik. Extra-special thanks go to my dear friend and colleague Stefan Mertin with whom we shared great moments on and off the laboratory during all these years.

My friends have always been a great support for me. I spare a particular though for Spyros Kalogeras, Theofilos Anastasiou, Marianna Kokkota, Vana Karafylli, Danae Theodosopoulou, Giorgos Karouzakis, the Samara family, Massimo Natale, Agnieszka Majszczyk, Iris Mack, Despoina Sareidaki, Daniel Rüffer, Giuseppe Franco, Andrea Koch, Beat Weber and to all the CouchSurfers I met in Switzerland. Also, many thanks to all the dear people I met during my radio years at Studio Fm1 105.4MHz (Heraklion, Greece) and at Fréquence Banane (Lausanne, Switzerland): you guys rock! Further, all my gratitude to the musicians whose music and songs kept me going through the good and the bad times all this time.

I would like to express my deepest thanks to my former professor, colleague, friend and mentor Nikos Sakkas who has been a great source of inspiration and positive influence on me during my early academic and professional years and a major supporter of my work throughout.

Words are not enough to express my gratitude to my parents, Alexandra & Charis, my sister Katerina and my brother in law Dimitris.

And of course, a whole-hearted thanks to Bénédicte whose constant support and patience (especially during all those long evenings she spent alone) were absolutely vital to the successful completion of this work.

CONTENTS

Abstract	v
Résumé.....	vii
Περίληψη.....	ix
Acknowledgements	xi
Contents	xiii
1. Introduction	1
1.1. Context of the thesis	1
1.1.1. Thermal and visual comfort.....	1
1.1.2. Advanced building systems	2
1.1.3. Building control	3
1.2. Constitutive hypothesis.....	3
1.3. Thesis structure	4
2. Experimental setup	7
2.1. The LESO office building.....	7
2.1.1. Geometric and thermal characteristics of a typical office room	7
2.2. Existing infrastructure	8
2.2.1. Sensors and actuators	10
2.2.2. The LESO database	10
2.3. Electrochromic glazings setup	11
2.3.1. Electrochromic glazing and characteristics.....	11
2.3.2. Control and communication protocols	14
2.4. EnOcean gateways and sensors	15
2.4.1. Components installed, network and communication.....	15
2.4.2. Web of Things (WoT)	15

3. Predictive control algorithm for electrochromic windows.....	17
3.1. Introduction	17
3.1.1. Electrochromic & Switchable glazing	17
3.1.2. Key factors and properties of EC glazings	18
3.2. Previous research work	20
3.2.1. On the control of EC windows.....	20
3.2.2. On sky prediction methods	21
3.3. Methodology	22
3.3.1. The principles	22
3.3.2. Sky prediction algorithm.....	23
3.3.3. Performance analysis of the sky prediction algorithm	28
3.4. Building systems integration.....	30
3.4.1. Why combine EC windows control with blinds and electric lights?	30
3.4.2. Implementation of the integration.....	31
3.4.3. Fuzzy Rule Bases	32
3.5. Discussion.....	34
4. Field measurements and evaluation of the sky prediction approach..	37
4.1. Field measurements.....	37
4.1.1. Measurements and characterization of switching time curves of the EC windows.....	37
4.1.2. Daylight Factor (DF) measurements.....	40
4.1.3. User evaluation surveys	41
4.1.4. Algorithm testing (automatic control)	43
4.1.5. Proposed future field work	44
4.2. Simulations methodology	45
4.2.1. Introduction	45
4.2.2. Simulation tool (thermal model).....	45
4.2.3. Simulated scenarios	47
4.2.4. Description and characteristics of the simulated office room	47
4.2.5. Meteorological data.....	48
4.2.6. Heating control system	48
4.2.7. Electrochromic windows and blind control	48
4.2.8. Electric lighting calculation	49
4.2.9. Occupancy schedule	51
4.3. Simulation results and discussion.....	51

4.3.1. Energy consumption.....	51
4.3.2. Thermal comfort	52
4.3.3. Visual comfort.....	64
4.4. Conclusion.....	70
5. Season modelling using state-based stochastic data-driven models .	71
5.1. Introduction.....	71
5.1.1. General definition of the “season” variable.....	72
5.1.2. Factors affecting the “season” in buildings	73
5.2. Current practice and research status	74
5.2.1. Calendar definition of season	74
5.2.2. Average outdoor temperature approach.....	75
5.2.3. Average outdoor temperature and solar radiation approach	76
5.2.4. State of the art	76
5.3. Methodology.....	79
5.3.1. Model framework (Hidden Markov Models) and definitions.....	79
5.3.2. Observations (features) vector and data mining	80
5.3.3. Building’s time constant	81
5.3.4. Data pre-processing	82
5.3.5. Labelling rules of data sets	83
5.3.6. Model training and testing	84
5.3.7. Model simplification: Feature selection.....	88
5.3.8. Simulations	89
5.4. Results	93
5.4.1. Energy consumption.....	93
5.4.2. Thermal comfort	94
5.5. Discussion and outlook.....	102
5.6. Conclusion.....	104
6. Visual comfort modelling based on stochastic data-driven models..	107
6.1. Introduction.....	107
6.1.1. Definition of visual discomfort	107
6.2. Previous research work	108
6.2.1. Visual discomfort indices.....	108
6.2.2. Limitations of visual discomfort indices	110
6.2.3. User-adaptive, data-driven approaches.....	111

6.3. Methodology	112
6.3.1. Initial model definition: A two-variable model	113
6.3.2. Data sources	113
6.3.3. Monitoring procedure	114
6.3.4. Evaluation and usability of the eye-level plane illuminance measurements taken during the monitoring procedure.....	115
6.3.5. New model definition: Observation vector with one variable	118
6.3.6. Labelling the data sets	119
6.3.7. User actions, data processing and verification.....	119
6.4. Results.....	123
6.4.1. Identification accuracy using the structured data sets: Confusion Matrices	123
6.4.2. Visual comfort identification using random illuminance values: The HMM as a classifier	124
6.4.3. Comparison of the HMM with other classifiers: Simple Bayesian and k-Nearest Neighbors	126
6.4.4. State identification certainty of the HMM: Likelihood of selected states.....	129
6.5. Conclusion	132
7. Conclusion and outlook	135
7.1. Main achievements	135
7.2. Future outlook.....	136
Appendix.....	139
A.1. Communication protocol of "EControl-Glas" glazings	139
A.2. Fuzzy logic controller of Electrochromic Windows	144
A.4. Switching time curves of electrochromic windows.....	154
A.5. Short survey questionnaire.....	156
A.6. Useful information concerning the portable illuminance sensor 'EnOcean'.....	160
Nomenclature	161
List of Figures	163
List of Tables.....	169
Bibliography	171
Curriculum Vitae.....	179

1. INTRODUCTION

1.1. Context of the thesis

People in developed countries spend as much as 80 to 90% of their time inside buildings as part of their residence, work, education, leisure and other activities [1; 2]. As a result, the provision of a sound indoor environment quality is absolutely essential. Leaving other factors aside, visual and thermal comfort are crucial elements of shaping a healthy, productive and pleasant indoor environment [3; 4; 5]. To satisfy these needs, a large amount of energy is required: bibliography indicates that electric lighting accounts for 16 up to 60% of buildings' total electricity load [6; 7; 8; 9], while the energy demand for heating, ventilation and air conditioning (HVAC) systems depending on climate, can represent about half of the energy consumed in buildings [8]. Considering that building sector is responsible for almost 40% of the total energy consumption [8; 10] one can realise the magnitude of these figures and the importance of improving the energy efficiency in buildings, while preserving the users comfort. But, how can this be achieved?

1.1.1. Thermal and visual comfort

In the context of buildings, we distinguish between different aspects of occupants' comfort, such as thermal, visual, acoustic, air quality, etc. In the context of this thesis, we focus on the two first.

Thermal comfort

ASHRAE defines thermal comfort as "*that state of mind which expresses satisfaction with the thermal environment*" [11]. Hence, thermal comfort is largely a matter of preference and its estimation is performed subjectively: most researchers and standards use the seven-point thermal sensation scale introduced by Fanger [12] and later adopted by ISO [13] and ASHRAE, where comfort is rated by the users by means of subjective notions, such as feeling cold, cool, slightly cool, neutral, etc. Thermal comfort models do exist and they never fail to point out the subjective nature of the subject. Fanger's model, which is used widely by the scientific community, computes the predicted mean vote (PMV) of a population of occupants according to which, there is at best 5% of dissatisfied people, which expresses the impossibility of creating thermal conditions satisfying all the occupants, but that it is

possible to create an indoor environment where the relative fraction of satisfied is maximal” [14]. Other models, such as the Adaptive comfort models, mention the neutral or comfort temperature, which is the Operative Temperature at which either the average person will be thermally neutral or at which the largest proportion of a group of people will be comfortable [15].

Visual comfort

Although there are several definitions of visual comfort, most studies agree that horizontal illuminances (especially on the workplane) must be sufficiently high (but not too much), the light flux on the workplane has to be properly distributed (appropriate illuminance uniformities) and discomfort glare (e.g. from luminaires or through windows) must be avoided [16].

On par with thermal comfort, visual comfort is perception-based and as such, differences at preferred illuminance levels can be observed between individuals. For instance, Nabil and Mardaljevic [17] noticed that illuminances spanning between 100 and 500 lx were rated as effective, while at higher levels (500-2000 lx) their perception varies from desirable to tolerable. In a study performed in the LESO building, Lindelöf [18] estimated the probability of visual discomfort when desktop illuminance is between 400 and 500 lx as high as 30%, highlighting among others that no predefined visual conditions can satisfy everyone's preferences.

1.1.2. Advanced building systems

As difficult as it may be to provide for occupant's comfort, all building systems have eventually one universal aim: to offer a comfortable environment to the users while they exercise their numerous indoor tasks. In today's buildings, along with the conventional lighting, shading or HVAC systems, advanced technologies and systems are becoming available with the aim of improving the occupant's comfort while preserving energy the energy resources.

Daylighting systems

Harvesting and using a part of the naturally abundant daylight has a significant energy saving potential [9], affects positively the health and wellbeing of building users [16] and was found to be more comfortable than electric lighting [19]. The energy saving potential consists of an integrated approach where daylighting reduces (directly) the need for electric lighting while in parallel takes into account the thermal aspects of the building, reducing the heating and cooling loads of indoor space by means of appropriate technologies and control strategies (indirect/long-term aspects). On-going research regarding daylighting that has been carried out internationally has resulted in innovative and efficient technologies such as Anidolic Daylighting Systems (ADS) [20] or electrochromic glazing.

Electrochromic glazing

Electrochromic (EC) glazing has been commercially available the last few years as an alternative to the combination of standard window glazings with mobile sun shadings (very often discarded by the architects) or to permanently tinted solar protection glazings. EC glazing has the ability of changing dynamically its optical properties and modulating the transmission of visible light and solar gains through the window, while maintaining at all times the view towards outside [21]. EC windows might replace in the future the vast existing stock of permanently tinted solar protection glazings which are often unsuitable to varying weather conditions while at the same time are not effective for protecting against overheatings. The EC glazings commercially available provide a transmission dynamics with a large enough range [22; 23], which provides a good protection against the overheating when properly controlled. Control in combination with other systems such as blinds can be necessary to address possible glare issues [24].

1.1.3. Building control

To succeed at their role of providing a comfortable indoor environment while saving as much energy as possible, available daylight and other building systems have to be controlled optimally. As it became clear before, comfort is subjective by definition, based on the individual's perception of the indoor environmental conditions. As such, building systems should be able to adapt to each user's personal preferences and comfort boundaries. Personalised or room-based control is envisaged but seldom provided by control systems today (especially in office buildings), in spite the fact that it has been found by multiple studies that occupants' satisfaction with their indoor environment improves when they have the ability to control their environment and that users are also more tolerant towards discomforting influences in buildings that provided good opportunities for occupant control [25; 26]. Also, control systems usually are based on average fixed values without taking into consideration fluctuations due to current or future changes in the real use of the building (user presence and activity) or due to varying weather conditions. This kind of predictive control is crucial, for instance, when controlling systems with a long response time, such as EC windows or HVAC. What is more, automatic control often regards building systems as 'isolated islands' which work independently from each other [27]. Last, the building's characteristics that are unique to each construction are often only partly considered, leading to unsatisfactory HVAC control.

1.2. Constitutive hypothesis

In the research context outlined above, we pointed out that the delicate balance between energy savings and the provision of a comfortable indoor environment to building occupants is often undermined by the inadequate control of building systems. Based on this, we formulated the following hypothesis on which this thesis is based on:

Proper visual and thermal comfort are vital for a healthy, productive and pleasant indoor environment. On the other hand, artificial lighting and HVAC systems are responsible for the greatest part of energy demand in buildings. We believe that a sound automatic control which integrates successfully the different subsystems, respects user wishes and adapts to the building's own characteristics as well as to outdoor variations can reduce the energy consumption and provide for a better visual and thermal environment for the users.

Figure 1-1 illustrates the scope of the doctoral thesis, while its structure is outlined next in Section 1.3.

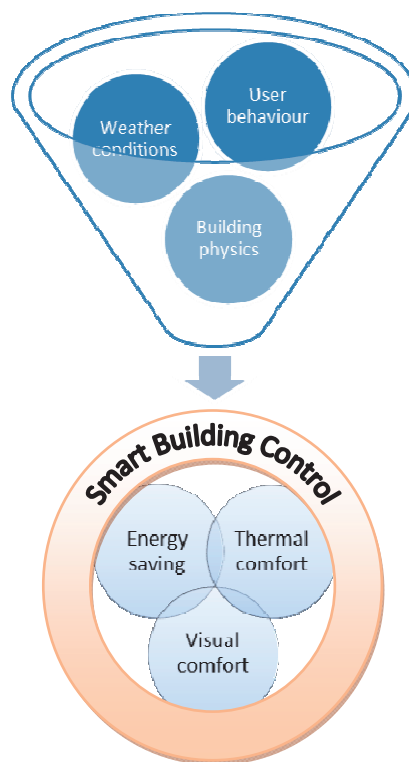


Figure 1-1. General scheme representing the scope of the doctoral thesis.

1.3. Thesis structure

In Chapter 2 we introduce the LESO solar experimental building where data acquisition and the experimental parts of the thesis took place. The existing infrastructure is presented

along new equipment which has been installed specifically in the framework of this work (i.e. the electrochromic windows and the EnOcean sensors network).

Chapter 3 presents the concept, the development and the commissioning of a predictive control algorithm for electrochromic glazing. The algorithm addresses the inherent slow response of electrochromic windows to varying weather conditions by implementing a novel sky-scanner approach which detects the motion of clouds and predicts their probability of obscuring the sun in a time horizon of 3 to 7 minutes. The algorithm also integrates and controls the blinds and electric lighting to maximise visual comfort taking into account outdoor and indoor conditions, presence and user actions.

Chapter 4 presents the evaluation of the control algorithm developed in the previous Chapter, via field measurements (including a short evaluation by actual users) and simulations which focused on the energy demand for heating and electric lighting, as well as on the evaluation of thermal and visual comfort.

In Chapter 5 we define and develop a novel approach for controlling building systems by using state-based stochastic data-driven models for the identification of the “season”. The new model attempts to identify the state of the variable between three possible values: *heating*, *cooling* and *intermediate season*, by taking into account weather conditions, user behaviour and the thermo-physical properties of buildings. The ability of the developed model to reduce energy for heating while preserving thermal comfort has been assessed through simulations.

In Chapter 6 we pursue further the investigation on state-based stochastic data-driven models and suggest a novel model for the estimation of visual comfort which improves greatly over the existing discomfort glare indices.

2. EXPERIMENTAL SETUP

This chapter introduces the LESO solar experimental building where the data acquisition and the experimental parts of the thesis took place. An important part of the infrastructure presented herein had already been in place when the presented work started (i.e. the building itself, the sensors, the EIB/KNX building automation bus, the database), while other components (like the EC glazing and the EnOcean sensors network) have been installed specifically in the framework of the presented thesis. Parts of this section have been published in an article by Zarkadis et al. [28] as well as in a final report for the Swiss Federal Office of Energy by Zarkadis and Morel [29].

2.1. The LESO office building

The LESO solar experimental building is located in EPFL campus near the cities of Ecublens and Lausanne in Switzerland. It is a 3-storey, 20-room building as seen on Figure 2-1. About half of the offices are occupied by a single person while the other half features two to three occupants. Sixteen of all office rooms are south-oriented and equipped on their South facade with both a conventional window on their lower part and an Anidolic Daylighting System (ADS) on the upper one, designed to increase the daylighting illuminance provided at the rear of the room [30; 20] (Figure 2-2). LESO's construction is a heavy one with thick walls and substantial thermal mass. All openings of the southern façade have a wooden frame and are double glazed with IR coating (the IR coating is not present on the ADS). The windows of all south-looking offices are protected by two external textile blinds, one for the normal window (lower) and one for the anidolic one (upper). The building features no active cooling or ventilation system and it is naturally ventilated by a stack effect [28]. More details about LESO in general are provided by Altherr & Gay [31], Morel [32] and in a number of PhD theses, i.e. [33; 18; 16].

2.1.1. Geometric and thermal characteristics of a typical office room

On this thesis, all data as well as all field measurements, experiments or simulations were collected or performed in one or more south-oriented office rooms. Following are the principal characteristics of a typical, south-oriented LESO room [32].

Room size

- Floor area of one room: 15.7 m²

- Room height: 2.8 m

Walls and slabs

All the layers of the construction elements below are given from the inside layer to the outside. Where present, the thermal insulation is mineral wool, glass wool, polystyrene or polyurethane and its conduction coefficient is equal to 0.04 W/m·K.

- Façade wall (South): 5.4 m² light wall (1 cm plaster panel + 12 cm thermal insulation + 1 cm wood) + windows (see below)
- Rear wall (North, gives to internal circulation area): 7.0 m² heavy partition wall (12 cm concrete bricks + 8 cm thermal insulation + 12 cm concrete brick) + 3.0 m² door (2 cm wood)
- Wall to neighbour cell: 13.3 m² heavy partition wall (12 cm concrete bricks + 8 cm thermal insulation + 12 cm concrete bricks)
- Wall to neighbour room of the same thermal cell: 13.3 m² light partition wall (1 cm plaster panel + 4 cm thermal insulation + 1 cm plaster panel)
- Floor: 15.7 m² (1 cm rubber coating + 6 cm screed + 6 cm thermal insulation + 25 cm concrete slab)
- Ceiling (only for the rooms of the 2nd floor immediately under the roof): 15.7 m² (25 cm concrete slab + 16 cm thermal insulation + 10 cm concrete and roof gravel)

Windows

All windows feature double glazing; U-value 1.4 W/m²K; g-value 0.54.

- Normal window: 2.1 m² net glass area with IR coating
- Anidolic window: 1.7 m² net glass area
- Frame area (total for the façade of one room): 0.9 m² wood (U-value 2 W/m²K)

2.2. Existing infrastructure

The LESO building is equipped with an EIB/KNX building management bus provided by Siemens. As detailed below, the heating, the artificial lighting and the blinds systems are all connected and can controlled by the bus or manually via a large number of sensors and actuators installed in the building. All the commands and the signals that travel through the bus are stored in a database.



Figure 2-1. LESO building: (a) ground floor; (b) first floor; (c) second floor; (d) southern façade [28].

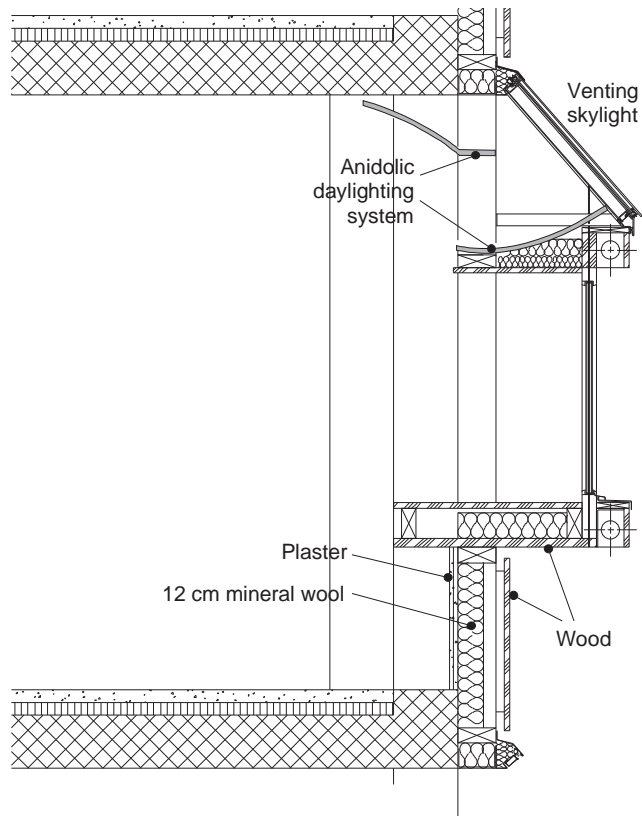


Figure 2-2. Vertical section detail of an office room located in the South façade of LESO building which showcases the conventional window on the lower part and the ADS on the upper one [32].

2.2.1. Sensors and actuators

The EIB/KNX was first installed in 1999; as reported by Lindelöf [18] 240 sensors and actuators were integrated in the system as of August 2004. Today, LESO features 237 sensors and actuators (devices) that generate information on 716 different logic addresses on the EIB/KNX bus. For each room of the building (but also for the common areas where applicable), these inputs control or give information on [28]:

- **Air temperature** (integrated in the control box for the heating and the electric lighting in each room or common area); the sensor measures a weighted average between air temperature and wall temperature (due to the fact that the sensor itself is contained in the box, located on the room wall).
- **Presence** (infra-red sensor mounted on the ceiling).
- **Lighting level** (actually, the sensor is a conventional luminance sensor mounted on the ceiling and looking downwards, measuring the luminance in a given cone; it is used as a illuminance sensor, but this is only valid if the objects in the sensing cone are not too dark or too bright).
- **Window opening** (on/off sensors, one for each openable window).
- **Blinds**: the blinds position is not directly recorded; instead, the basic commands to actuators, i.e. "blind up", "blind down", "stop", are recorded as EIB/KNX telegrams. From these commands and the respective timestamps the actual position is calculated and inserted into the database.
- **Heating**: electric radiators are controlled by an on/off controller, using a pulse width modulation for implementing a proportional controller, with a cycle time of several minutes; like for the blinds, the significant variable, i.e. the average heating power, is not directly available, but only the elementary commands on and off with the respective timestamps, allowing to reconstruct the heating power from the on/off commands.
- **Electric lighting data** (on/off and dimming status).

Additionally, **weather data** (for the whole building) is also recorded by sensors installed on the roof of the building: ambient temperature, solar radiation on a horizontal surface (direct and diffuse components), global horizontal illuminance, wind speed and direction and rain alarm.

2.2.2. The LESO database

Until March 2008, a server was connected to the EIB system via its serial port and run a Java program called *Eibserver*. This server was used as an interface both for data acquisition and for control algorithms implemented on another computer and connected to the EibServer through Java/RMI protocol. Eibserver kept in memory at all times the complete known state of the LESO building; when any variable was modified, that change was committed to memory and logged to disk. The program logged all bus events to disk and a

Perl script that run every day at 5 a.m. read the log files that had been written during the last 24 hours and inserted the corresponding values in a MySQL database. The MySQL database called "leso_eib" includes all the data recorded by Eibserver since it began recording data in 2001 till March 2008 [28; 18]. After May 2010, a different setup has been implemented; however the data used on this thesis was collected when the described setup was in place.

Concerning the origin of the data passed on to the database, it is always possible to distinguish controller commands from user commands. In particular, by looking at the prefix of the device's name recorded in the database ("type" field) one knows whether it was a user-initiated action or a system-originated command sent through Eibserver [28].

2.3. Electrochromic glazings setup

For the development of the proposed predictive control system for EC windows (see Chapter 3), new EC glazings were installed at the LESO building. The chosen room (LE 003) is a typical South-facing office and it can be seen on the pictures and plan drawing of Figure 2-3. This office room it is also the one used in previous research by Page et al. [34] where EC glazings were coupled with an ADS. EC glazings both for the normal windows (lower part) and for the anidolic daylighting system (upper part) were installed.

2.3.1. Electrochromic glazing and characteristics

The newly installed glazings completely replaced the existing ones. Their total area is 5.10 m², their Visible light Transmission (Tv) is in the range of 0.15 - 0.50 while their Solar Heat Gain Coefficient (SHGC) is 0.12 - 0.38. The glazings have been provided by EControl-Glas GmbH and installed by Flachglas AG on February and March 2011. The EC glazings can be seen in the two pictures of Figure 2-4, one taken with the glazing at maximum transmission and the other with the minimum transmission (dark configuration). A dominant blue colour can be seen when the system is in the dark configuration. The principal characteristics of the installed EC glazings are summarized in the Table 2-1 while the images on Figure 2-5 show the schematic representation and a cross section of the glazings. (The information presented was taken from the documentation of EControl-Glas that accompanied the glazings or/and from the website of the company [35]).

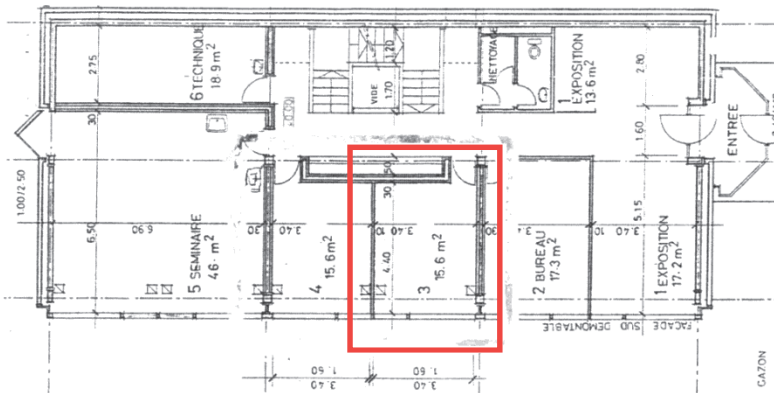


Figure 2-3. Pictures and plan drawing of the LESO solar experimental building and office room LE 003 where the EC glazings have been installed.



EC glazings in the clear configuration ($T_v=50\%$, $SHGC=38\%$).

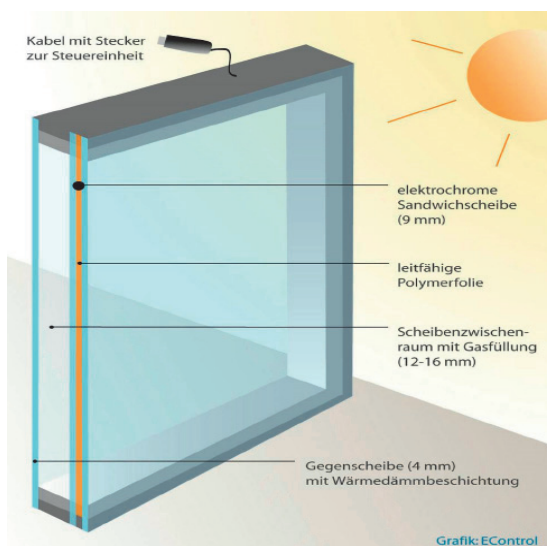


EC glazings in the dark configuration ($T_v=15\%$, $SHGC=12\%$).

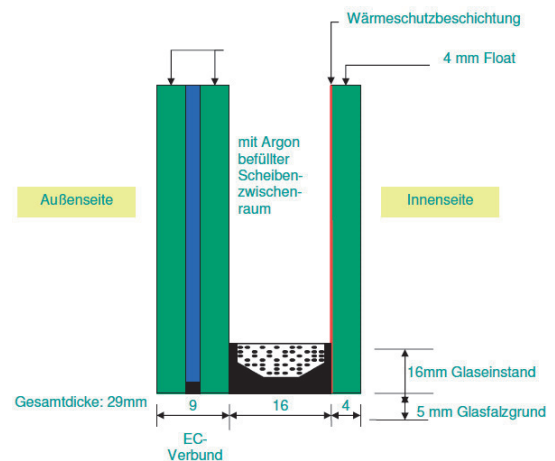
Figure 2-4. EC glazings in the bleached (clear) and fully tinted (dark) states.

Table 2-1: Principal characteristics of the installed EC glazings.

	dark configuration	clear configuration	unit
Light transmission (T_v)	0.15	0.50	-
Energy transmission ($SHGC$)	0.12	0.38	-
U-value	1.1		W/m^2K
type of glazing	double glazing with argon filling and low-e coating		-



Schematic view of the EC glazing



Cross section of the EC glazing

Figure 2-5. Schematic view and cross section of installed EC glazings (images: ©EControl-Glas GmbH).

2.3.2. Control and communication protocols

The EC glazings are connected to their control units through a dedicated cable. Two control units are installed: one for the normal window (3-pane window) and one for the anidolic system (3-pane upper window; see Figure 2-4). Each control unit bears in the front an interface for manual operation featuring 2 pushbuttons which can be pressed sequentially by the user to choose the desired transmission level. Alongside the pushbuttons there are 5 LEDs indicating the 5 transmission regions set either manually or via the control system (Figure 2-6). Moreover, each control unit is connected to a dedicated computer implementing the automatic control algorithm and collecting and storing in a database the EC glazings data (Tv, panes' temperature, status, etc.), through an RS485 serial link interface. At a later stage, it is envisioned to completely integrate the EC glazings with the EIB/KNX building bus.

The “conversation” between the computer and the EC glazings through the control unit is rather complex and had to be implemented from scratch. The industrial partner of the research project and supplier of the EC windows (EControl-Glas GmbH) provided us with the specifications for the communication protocol of the control unit of the glazings (provided in full detail in Appendix A.1). Consequently, the necessary interface modules described in the protocol were built using Matlab software platform [36].

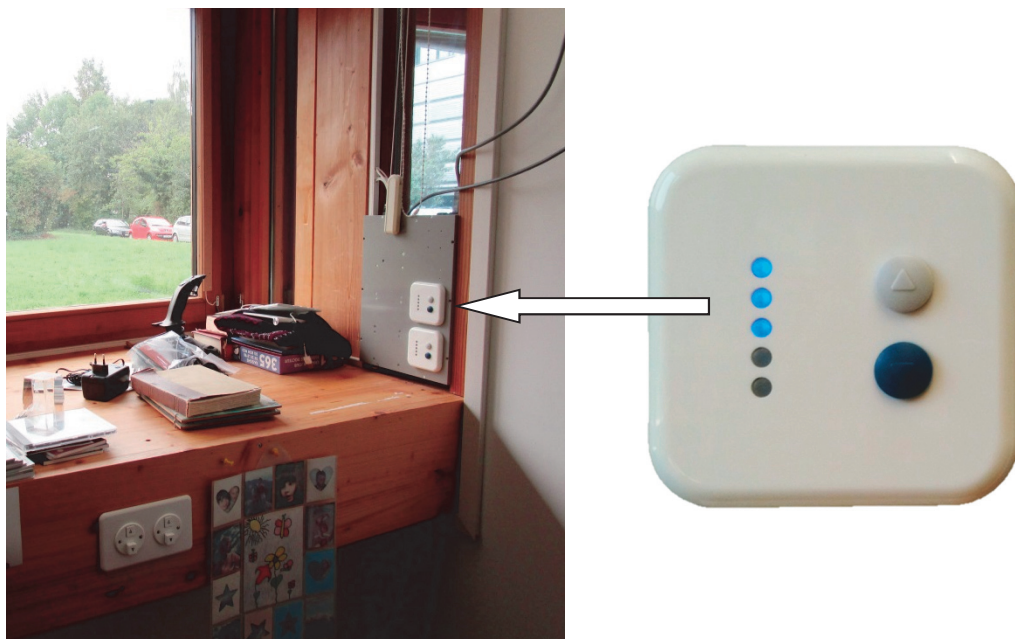


Figure 2-6. One of the two control units of the EC glazings with the manual control panel in the front (right image) and its position inside the office room LE 003.

2.4. EnOcean gateways and sensors

In the framework of the research performed on the visual comfort modelling based on stochastic state-based approaches (Chapter 6), a small network of EnOcean sensors and gateways has been installed in LESO in March 2014. EnOcean is an emerging energy harvesting wireless technology that allows for building automation and sensor data collection while using minimal energy to do so.

2.4.1. *Components installed, network and communication*

In total, 6 illuminance/motion and 4 temperature/CO₂ sensors were installed in 6 single-occupant offices in LESO. The wireless communication between the sensors and the central node takes place through 2 EnOcean gateways. As seen on Figure 2-7, each gateway is implemented using a Raspberry Pi model "B" as base unit, an EnOcean USB 300 dongle and an SD card (which is necessary for the operation of the base unit and carries all the required software). The illuminance and the CO₂ sensors were purchased from Eltako GmbH. In particular, the illuminance sensor is the model FBH63AP Wireless Motion/brightness sensor (Figure 2-7) which measures illuminances in the range of 0 to 2000 lux and transmits a new value to the gateway every 100 seconds, provided that the new value differs more than 10 lux from the old one (not configurable). Power supply can be either provided by 12V DC power supply unit or by AAA batteries or by the built-in solar cell under normal ambient light, in a daily average of at least 200 lux [37]. In our case, the third option has been preferred to keep the sensor portable and without any additional weight.

The telegrams with the new values are transmitted wirelessly from the EnOcean sensors to the gateways and they are stored in a MySQL database residing on the SD card. The gateways are connected via Ethernet (wired connection) to LESO's LAN and they can be accessed (i.e. for data retrieval) through their unique IP addresses. Figure 2-8 provides a schematic with the connection topology for one of the two gateways.

2.4.2. *Web of Things (WoT)*

The implementation of new network and type of sensors in LESO brought forward the issue of the integration of heterogeneous building management systems. In particular, the question that arose was how to integrate the EnOcean infrastructure (or any other installed in the future) with the existing EIB/KNX building management bus. Bovet and Hennebert [38] provided a solution which leverages on the concept of Web-of-Things and uses well implemented standards like the HTTP protocol where the real-time access to the sensors is independent from the underlying infrastructure and takes the simplified form of a logical tree structure (i.e. <http://buildingX.floorY.roomZ.sensorN=status>). A prototype KNX-WoT gateway (based on the Raspberry Pi mini PC) has been installed and tested in LESO in late 2013. Although time constraints did not allow for the use of this technology in the framework

of this thesis, it is believed that it has a lot to offer in the future when a standardised way to interact with devices connected to different networks will be needed.



Figure 2-7. EnOcean gateway connected to Ethernet and to DC power supply (left image) and autonomous EnOcean illuminance/motion sensor with the solar cells around the sensor (image on the right).

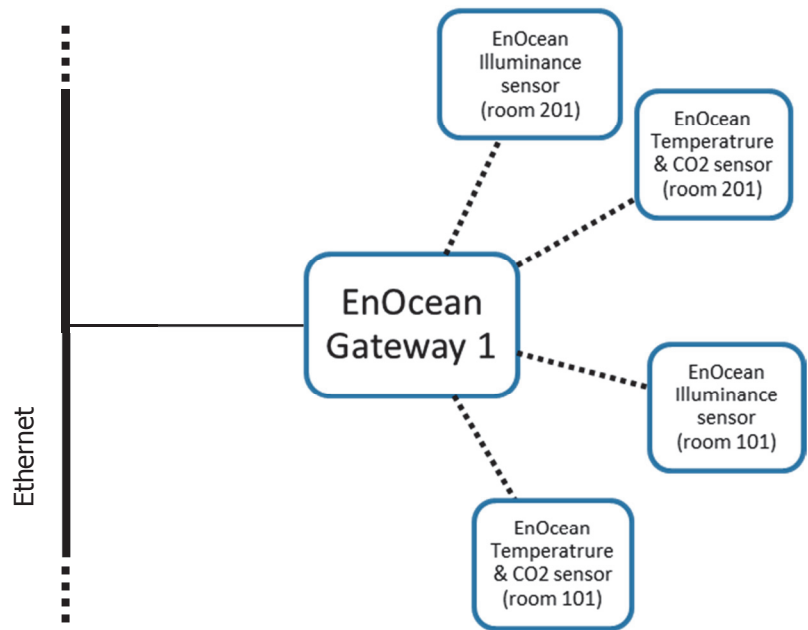


Figure 2-8. Connection topology of EnOcean sensors with the gateway and the local area network (LAN) via Ethernet.

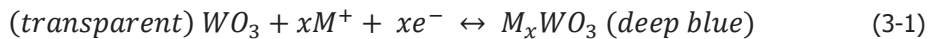
3. PREDICTIVE CONTROL ALGORITHM FOR ELECTROCHROMIC WINDOWS

The development of an advanced control algorithm for an electrochromic (EC) glazing coupled with an anidolic daylighting system (ADS), blinds and dimmable lights taking into account the optimal use of the direct solar gains and the (visual and thermal) comfort of the users is presented in this chapter. To satisfy the visual comfort requirements, the elaborated algorithm integrates a novel sky-scanner approach to predict the probability of clouds obscuring the sun for a time horizon of 3 to 7 minutes which corresponds roughly to the time required by the EC glazings to switch between different transmission states (up to 15 minutes). For the thermal comfort, a wider time horizon is considered, taking into account season, weather, presence, user actions and other data collected from the EIB/KNX bus. Parts of this section have been published by Zarkadis and Morel in an article [39] as well as in a final report for the Swiss Federal Office of Energy [29].

3.1. Introduction

3.1.1. Electrochromic & Switchable glazing

The EC phenomenon of materials was originally discovered in the late 1960s [24] in tungsten oxide (WO_3) thin films which until now remains the material most widely used in applications and research. Electrochromism constitutes a rather complex electrochemical reaction where ion insertion and extraction processes are taking place. Although until today the exact phenomenon cannot be fully described, it can be presented with the following simplified reaction [40]:



where M^+ can be H^+ , Li^+ , Na^+ or K^+ , $0 < x < 1$ and where e^- are denoting electrons. Other EC metal oxides have also been applied in prototype EC windows with nickel oxide, iridium dioxide and niobium pentoxide being the most promising ones [23].

Besides oxide films, organic materials (polymers) have been used in EC devices. Similarly, other types of switchable glazings do exist. *Gasochromic* devices use hydrogen gas (H_2)

instead of voltage to switch between the bleached and coloured states. *Liquid crystal (LC)* devices use as a switching mechanism the change in the orientation of liquid crystal molecules between two conductive electrodes by applying an electric field, resulting in a change of their transmittance. *Electrophoretic or suspended-particle (SP)* glazing is a film-based patented technology similar to that of LC devices [23]. Unless otherwise explicitly noted, any further reference on this thesis to the term “EC” or “switchable” windows will imply tungsten-oxide (WO_3) EC windows.

3.1.2. Key factors and properties of EC glazings

To better understand the need for the development of an advanced control algorithm for EC windows, the issues related with it as well as the user acceptance of such a system (detailed in Chapter 4), the key factors and properties of EC glazing are given next.

Visible transmittance (T_v) and solar heat gain coefficient (SHGC) range

Both values denote the percentage of solar radiation transmitted through the glazing. Baetens et al. reported in 2010 that values of T_v in today's available EC windows are between 0.15 and 0.035 for the dark state and no more than 0.60 for the bleached state, while SHGC values range between 0.09 and 0.48 respectively [23]. However, in 2012 Sbar et al. [41] reported on commercially available EC glazing with less than 2% of T_v in the tinted state. The wider the ranges, the more flexible the EC windows and more capable to respond to different conditions and to a variety of different scenarios, i.e. a T_v lower than 1% maybe necessary for glare protection in the case of direct sunlight [42; 43], while high values of T_v and SHGC are required for maximum daylight harvesting under low-light conditions and when maximum solar gains are needed, respectively.

Colour

As also seen on Figure 2-4, their colour varies from deep blue (when tinted) to fully clear. When the EC window is switching between intermediate states, some non-uniformity may be observed [44].

Switching time

The switching speed of an EC varies with its temperature, size (see below), depth and direction of switching (transition from dark to bleached is generally faster than the opposite [45]). A manufacturer reports that for a pane measuring 100cm x 100cm the transition between the fully bleached ($T_v = 50\%$) to the fully dark setting ($T_v = 15\%$) requires 12 minutes [35]. In measurements carried out by Lee et al. a prototype EC unit of 43cm x 85cm required up to 5 minutes for the switching [45]. Further detailed tests performed by Lee et al. using EC windows of another manufacturer showed that an EC window measuring approximately 46cm x 90cm (35x18-inch) required less than 7 minutes to change completely its state when the surface temperature was greater than 10°C. The same window required

37 minutes to switch from a bleached state to dark (T_v of 0.56 to a T_v of 0.13) with an EC surface temperature between -3°C and -1°C [44].

Detailed measurements of the T_v during the switching were carried out by Fasano et al. [46]. They reported that the switching curve (under a given temperature and pane size) resembles an exponential decay, where:

"[...] the curve steeply decreases during the first minutes, then the curvature changes and the profile is flat until the process finishes."

These reports are confirmed by similar measurements carried out in the framework of this thesis and presented in Section 4.1.1. These observations can help us to describe in a more accurate fashion the terms "switching speed/time" cited in this document and to define switching speed $U(t)$ as follows:

$$U(t) = d \frac{T_v(t)}{dt}, \quad (3-2)$$

where $T_v(t)$ is the visible transmittance curve of the EC glazings as a function of the transition time t .

In general, fast switching speeds are desired for prompt response to variations of external conditions, especially during days with intermediate sky conditions and are reported as being critical for protection against glare and user acceptance [42]. On the other hand, lower switching speeds can be tolerated when controlling the windows with regard only to thermal aspects. Today's commercial products are generally characterized by slow switching speeds and there is a consensus that higher speeds are required [23; 47].

Temperature

The surface temperature of the EC window depends on incident solar radiation levels, wind speed and air temperature and is an important factor affecting switching speed (in general, higher temperature facilitates switching). EC windows have been successfully tested in a temperature range of -10°C to 95°C , but in practice reported temperatures do not exceed 76°C [44].

Surface size

As stated above, the switching speed of an EC window is closely related to its size and larger EC panels tend to have longer switching times. The size of EC glazings has also been reported as being responsible for partial loss of tint uniformity during the switching from one state to another [23; 45]. Also, as technology of EC materials progresses, larger sizes are progressively becoming available. Insulating glass units (IGU) of up to 3m^2 ($125\text{cm} \times 245\text{cm}$) are currently available as commercial products, while sizes of up to $135\text{cm} \times 330\text{cm}$ are expected shortly in the market [35]. On the other hand, professionals claim that a size of 6m^2 ($200\text{cm} \times 300\text{cm}$) is desired for applications [23].

Life expectancy

First-generation commercial EC windows suffered from degradation effects visible to the naked eye^a such as dissolution, corrosion and etching [48]. Although there is still much uncertainty as to the exact causes for the degradation effects, several possible factors have been reported as being responsible: the entry of water vapour into the gap between the panes of an IGU [44], the operation in extreme temperatures, rapid cycling (no relaxation) between the bleached and dark states, UV stress, sudden thermal shocks and delamination of interfaces [48]. Leading manufacturers today serve a 10-year guarantee on their products, but a minimum lifetime of twenty years (and a minimum of 10^5 cycles) is expected [23], which is the standard operating lifetime of a standard IGU [21].

Power consumption

A low DC voltage (usually of 5 Volt) is required by the EC windows for the change of their state. Certain types of EC windows also require a similarly low voltage to maintain their current state. [23; 44]. In particular, the installed glazings in LESO which are used in the presented research require a 24V DC source for the controller, their power consumption during switching is less than 10W (the energy required is 0.5 Wh/m^2 or lower) and they do not require power to maintain their state [35].

3.2. Previous research work

3.2.1. On the control of EC windows

The characteristics of EC windows make them suitable for use in buildings where we can achieve maximum occupant comfort [45]. Nevertheless, the control issue of EC glazings has not been addressed adequately as the vast majority of proposed control schemes failed to address the time the EC glazing requires to switch between the bleached and dark states (~5-15 minutes).

Several research studies have been carried out during the last few years with regard to the use of EC windows in buildings. In some of these, the visual or thermal comfort is evaluated through computer simulations [49; 50; 51; 52; 53; 54] or with the use of small-scale models [55]. This type of research involves an easier setup, is favourable for the study of energy aspects and allows for the execution of different scenarios; nevertheless, it lacks the evaluation by real persons in real-life situations. User acceptance tests were performed in full-scale environments by Scartezzini et al. [43] and by Zinzi et al. [47]. However, both

^a Personal on-site observations of EC windows installed in August 2002 at the LESO solar experimental building, Lausanne.

teams implemented manual control of EC windows, electric lighting and internal blinds. Simple closed-loop schemes have been implemented by laboratories worldwide carried out measurements on EC glazings (see for instance [56] or [57]). In the same vein, Lee et al. [45] developed an automatic closed-loop control strategy, where the transmittance of the EC windows was continuously modulated to maintain the levels of daylight work plane illuminance within a predetermined range. Based on this research, Clear et al. [42] published in 2006 the responses of users of an office room equipped with automatically controllable EC glazings and electric lights, while blinds were available but controlled manually. To the best of the author's knowledge, these two studies were the first (and only) efforts until today to address effectively the slow switching speed issue of EC glazings in a control strategy, albeit on the expense of energy consumption. This was achieved by first changing accordingly the level of dimmable electric lighting (a system with almost immediate response) while waiting for the EC windows to reach the desired transmission state (which can take up to several minutes).

More advanced control systems were also attempted. Fuzzy logic controllers following the principles of the adaptive neuro-fuzzy inference system were developed by Assimakopoulos et al. [54; 50] but they were not tested in a real environment. Fuzzy control was also attempted in LESO by Scartezzini et al. [43] as an attempt to counter-balance the slow switching speed of EC windows; results were reported as "promising".

Regarding the control strategies, whether they are optimized for visual comfort or thermal comfort, bibliography suggests that user presence and user wishes is a key factor to consider when implementing an advanced building control system. Earlier studies carried out in LESO concerning intelligent blind controllers proposed that user presence should determine the adopted control strategy at a given time: When user is present in the room then visual comfort is a priority, while in the absence of users a strategy favouring long term thermal aspects and maximum energy conservation should be implemented [58; 59]. With regard to user wishes, they should be respected at all times (override of the automatic control made possible) while at the same time they should be considered as a valuable source of information allowing for the adaptation of the control system to the user specific needs [33].

3.2.2. On sky prediction methods

As becomes evident from the research performed previously, the characteristic of slow switching speeds of EC windows pose a challenge yet to be met by an advanced control system. On this research, it is proposed to meet this challenge by predicting the sky luminances for a time horizon that equals the time required by the EC windows to switch to the desired transmission status (up to 15 minutes). Towards this short-term prediction, image manipulation of sky images taken by a camera was implemented in a way that blue sky is recognized and separated from clouds and other elements in the image. Other

techniques that do not use a camera do exist, such as the estimation of cloud speed using measurements from multiple irradiance sensors placed in a semi-circular array [60] or stochastic approaches, where the transition probability from one sky type to another sky type is gathered in a transition probability matrix, which can be evaluated by collecting data over a sufficiently long period of time [61]. Nevertheless, these approaches are not further explored here as they fall outside the scope of the proposed work.

Image Correlation and *Image Convolution* techniques are widely used for calculating the changes between two consecutive images [62]. Template matching between the two images is applied within a predefined search area. The motion vector (e.g. of the clouds) can then be determined by the best match position [63]. Zafarifar and With [64] presented a model which is one of the few mentioned in bibliography that explicitly aims at the detection of blue-sky regions. Intended primarily for video enhancement functions in modern TVs, this method performs a classification of sky areas by computing a pixel-accurate sky probability. Lalonde et al. [65] proposed a cloud segmentation algorithm based on the Perez sky model [66] which is expressed as a function of camera parameters. Regularized fitting is applied to the model by the computation of a data-driven prior model of clear skies. More complex than standard image correlation, *Optical flow* method is a collection of techniques used for the estimation of object velocities between two consecutive images or video frames. In particular, the methods of Horn & Schunck [67] and Lucas & Kanade [68] are the most referred ones in bibliography. On a different approach, satellite imagery can be used to detect cloud motion over large areas. *Remote sensing* techniques [63] are largely based on image correlation techniques discussed earlier. However, remote sensing is not directly relevant to the present research as the characteristics of processed images are vastly different (i.e. area covered and resolution, background).

3.3. Methodology

3.3.1. The principles

The proposed algorithm predicts an optimal setting for the EC glazing, the blinds and the electric lighting taking into account all the available data on instantaneous weather condition and building status, including data on room occupancy and user wishes/actions, workplane illuminance, internal air temperature. The algorithm predicts this optimal setting at a time horizon corresponding to the EC glazing latency time (ideally from 5 to 15 minutes; see 4.1.1). Electric lighting is used only complementary when daylight is not sufficient, while blinds are likewise only employed to protect from glare and/or to avoid overheating when protection from EC windows is not sufficient. A longer time horizon is taken into account for the thermal aspects. Moreover, when the room is occupied priority is given to visual comfort, while if the user is absent the algorithm is optimized for thermal comfort [39].

The developed algorithm consists of two parts:

1. A 'child' algorithm that uses a sky scanner approach: the sky is continuously monitored by a simple web camera connected to a computer and the possibility of clouds obscuring the sun is deducted at short time steps (30s to 1 min).
2. A 'mother' algorithm that uses the input of the child algorithm along with all other inputs mentioned above and finally implements the control of EC Windows, electric lights and blinds.

3.3.2. Sky prediction algorithm

To address the problem of the slow switching speed of the EC windows we implemented a predictive algorithm based on the image processing of sky images taken by a standard web camera.

In particular, Matlab computing environment is installed in a LESO PC, to which a standard USB camera has been connected. The camera is placed below the skylight of an office room where it can have an almost unobstructed view of the sky. It faces towards the south at a measured angle ' α ' from the zenith, making sure the sun trajectory is included in the images taken (Figure 3-1). At first, the camera was setup to take automatically images of the sky at fixed-time intervals of 5, 10, 30s and 1, 2 & 5 min. For low to moderate wind speeds the time interval of 1 min is sufficient for the observation of changes in the sky concerning the motion of clouds, similar to other studies [69; 70]. However, it was observed that higher wind speeds require shorter time intervals of 30 or even down to 5s. To cover even the most extreme weather conditions, an interval of 5s is considered. The images taken have a resolution of 640×480 pixels.

First efforts targeted at having the blue parts of the sky recognized and separated from clouds and other elements in the image. Sky detection and cloud separation has been attempted using simple colour thresholding techniques [62; 36] but it became quickly evident that the separation process had still to be optimized. As noted by Lalonde et al. [65], sky images exhibit a varying appearance depending on various parameters such as weather conditions, time in the day and camera parameters. Likewise, colour of the sky can occupy a wide part of the colour space, from saturated blue to gray, and even to orange and red when sun is close to the horizon [64].

Earlier, Perez et al. [66] had pointed out the variability and non-uniformity in the angular distribution of sky luminance. Consequently, "blue" sky exhibits high non-uniformity of colour, hue, brightness and texture across different images or even across areas of the same image, rendering fixed-colour detection (e.g. simple colour thresholding techniques) problematic and rather unsuitable. To solve this problem, Li et al. [71] proposed the Hybrid Thresholding Algorithm (HYTA) that combines fixed-colour and adaptive thresholding methods together with the use of the blue and red channels ratio of the image.

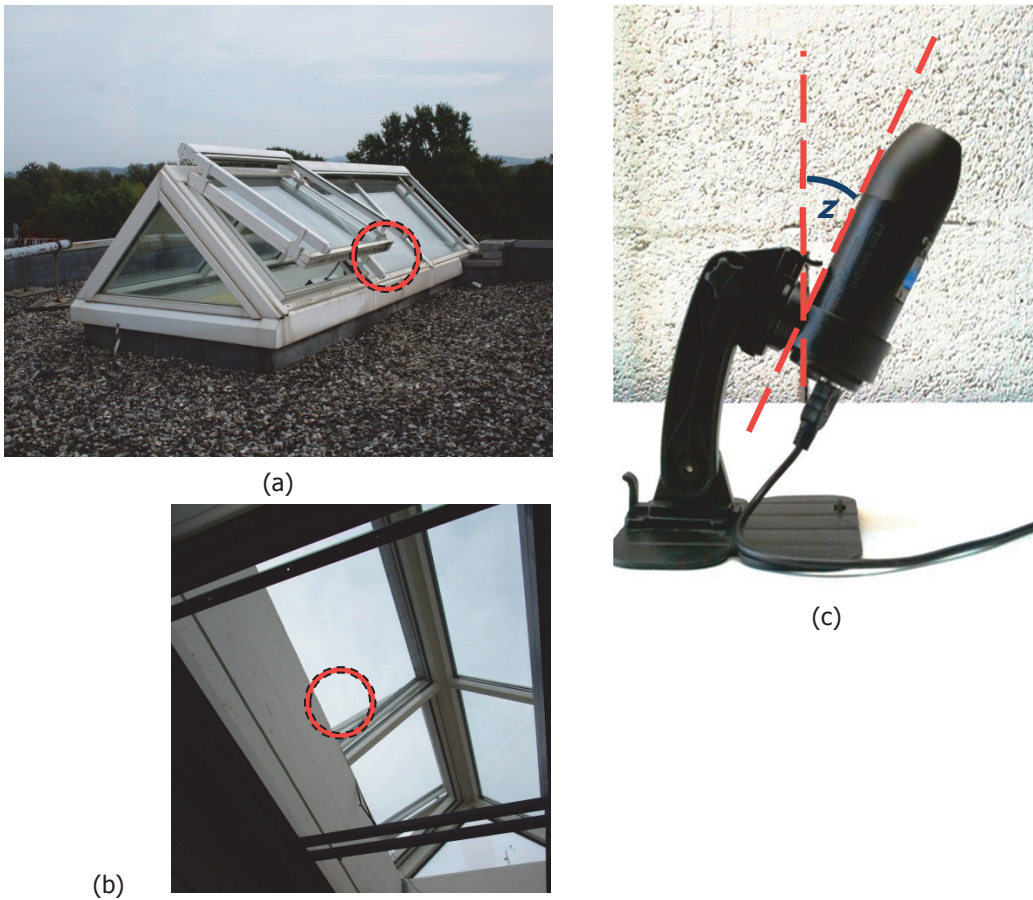


Figure 3-1. (a) Outside and (b) inside view of the skylight in the office room where the camera was placed; the red circles indicate the point where the camera was placed during the measurements; (c) the USB camera “BulletHD PRO 1080p” used for the study, at an angle ‘ z ’ from the zenith. (Image taken while the camera was off-duty, placed on a desk).

An extensive and time-consuming application of Ariadne’s thread problem-solving approach was evolved in a string of trial-and-error, which started formulating the basis of the algorithm. In this course, the sky detection and cloud separation approach was abandoned and replaced by the estimation of cloud motion between two consecutive images.

In specific, *Block Matching* block of Matlab is used and the two images are divided down to blocks of $N_1 \times N_2$ pixels each^b. Each block of pixels from the first image is moved around, compared and eventually matched with a block of pixels in the second one within a predefined search area. For the best match, the Mean Square Error (MSE) is applied to estimate the similarity of the blocks compared; if k is the first image then $k+1$ is the second one and (d_1, d_2) is the displacement pair of values of the centre pixel of the block that minimizes the equation:

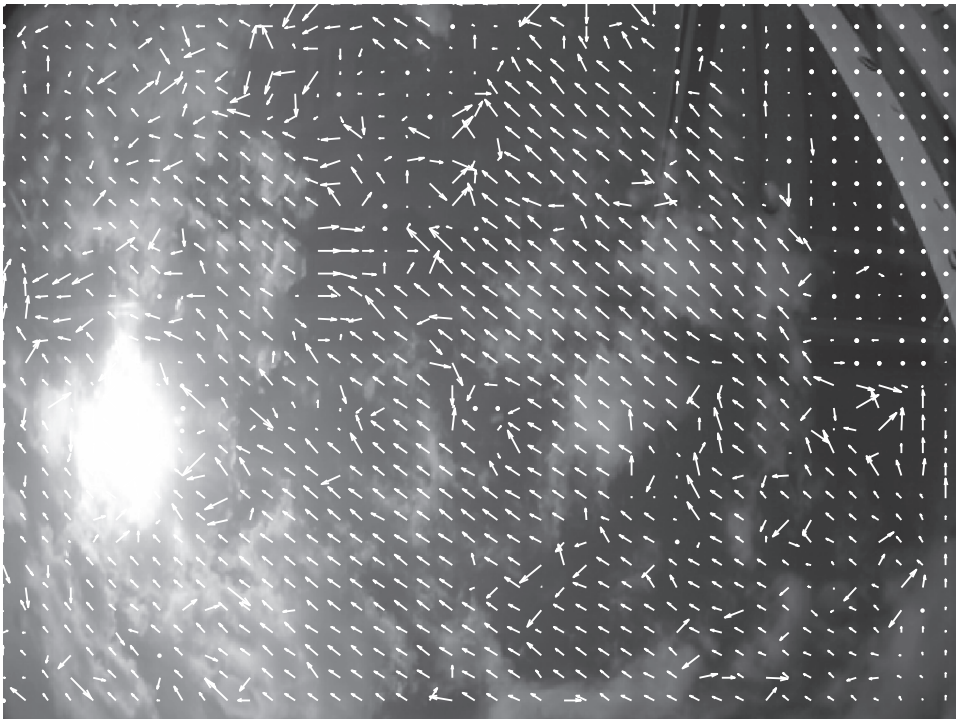
$$MSE(d_1, d_2) = \frac{1}{N_1 \times N_2} \sum_{i=1}^{N_1} \sum_{j=1}^{N_2} [s(i, j, k) - s(i + d_1, j + d_2, k + 1)]^2 \quad (3-3),$$

where $s(i, j, k)$ denotes a pixel's location at coordinates (i, j) of the block in the 1st image [62]. After block matching is performed for all the blocks of the image, the calculated motion vectors (u, v) of all the blocks are inserted in a $\left\lceil \frac{640}{N_1} \right\rceil \times \left\lceil \frac{480}{N_2} \right\rceil$ matrix. On Figure 3-2, the images (a) and (b) are the two original images and on Figure 3-3 the (c) is the combined image (blend) with the calculated motion vectors overlaid on top (1 motion vector per block).

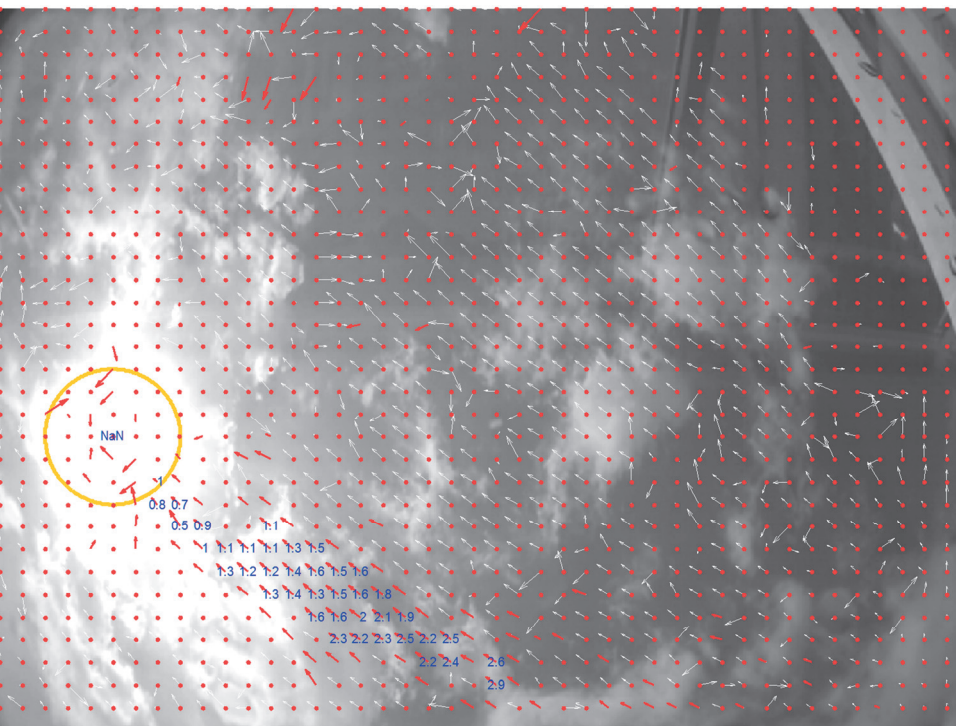


Figure 3-2. Sky prediction image-processing – part I: (a) and (b) show two consecutive original images taken on 2012.06.07 at 10h29m40s and at 10h29m45s (UTC+2), respectively.

^b Both N_1 and N_2 are odd positive integers (≥ 3); this ensures that each block possesses a centre pixel. Furthermore, blocks located at the image borders may overlap with neighbouring blocks to ensure all blocks are of $N_1 \times N_2$ size.



(c)



(d)

Figure 3-3. Sky prediction image-processing – part II: (c) shows the combined image of the two original images with motion vectors grid overlaid; (d) presents the decision image including sun disc position (area inside orange circle), the vectors corresponding to (parts of) clouds heading towards the sun disc (in red) and the part of clouds that can potentially obscure the sun with the time prediction for each of them (blue numbers in min).

A similar technique of “cloud velocity fields” was implemented in posterior research^c by Marquez and Coimbra [70], where the Matlab Particle Image Velocimetry (MPIV) toolbox is used in conjunction with the Minimum Quadratic Difference method [72].

It was observed (and it is partly evident on image (c) of Figure 3-3), that motion vectors in the processed images are rarely uniform in terms of speed and/or direction; clouds in the sky can move towards the prevailing wind direction, others follow a different path (e.g. turbulences) or they can “stay in the same part of the sky” simply changing forms. Thus, only the motion vectors (and hence, the clouds) that are identified consistently in consecutive image correlations and they are heading towards the sun are taken into account. The sun position is known at every time step and is mapped on the image (Figure 3-3d).

Open-source Matlab code^d based on the algorithm of Reda & Andreas [73] is being used to compute the sun position (zenith and azimuth angle at LESO location) as a function of local time and geographic coordinates. Then, the sun position coordinates are transformed from spherical (polar) to rectangular (Cartesian) coordinates. The zenith angle ‘z’ of the camera is taken into consideration to correctly project the computed sun position onto every image. However, the calculated and projected sun position is only a point on the image. To estimate the possibility of clouds passing in front and obscuring the sun we observed that considering only the apparent dimensions of the sun’s disc in the images (about 35 pixels wide) is not enough. After trials, a sun disc with 90 pixels diameter is found to be optimal to identify the cloud vectors pointing towards the sun. On this step, these are represented by the red vectors on Figure 3-3 (d).

The next and final step for the sky prediction algorithm is to keep only those “potential” vectors that consistently appear in consecutive image processing operations. Further, the “density” of these vectors on a given region should also be sufficient to be taken into account: for the given grid (block) size (15×15 pixels) and image frequency (5s) if there are less than 6 “red” vectors around a “red” vector then this is disregarded as having less potential to obscure the sun (most probably corresponding to a part of non-dense or scattered clouds). The remaining vectors are then name-coded “potential” and the time required to obscure the sun is calculated based on their detected (angular) speed and distance from the sun disc (times in blue on Figure 3-3d). The speed is easily calculated since each detected motion vector bears its displacement information dS in the form of (u,v)

^c Marquez and Coimbra published their article in 2013; the work concerning the development of the proposed sky prediction algorithm in this thesis was concluded in the summer of 2012.

^d Code by Vincent Roy; available here: <http://www.mathworks.com/matlabcentral/fileexchange/4605-sun-position-m>

coordinates and the time dt in which this displacement takes place is the time between two consecutive images.

The possibility of the clouds to obscure the sun during the next 5 minutes is estimated and – if necessary – adjusted every 30s (that means after every 6 image processing operations) and subsequently fed into the “mother” algorithm that is responsible for the final control of the EC windows and the other building devices (Section 3.4). The time frame of the prognosis can be higher than 5 minutes if the sky image remains relatively unaltered for longer periods but it can also fall down to only 2 to 3 minutes or less if clouds in the images are moving fast relative to the sun or if the sun is located close to the edge of the images with prevailing wind blowing from that edge.

3.3.3. Performance analysis of the sky prediction algorithm

In a first step, the algorithm’s capacity to estimate accurately the cloud motion vectors and to predict the time needed for the “potential” cloud vectors to obscure the sun was evaluated by multiple visual assessments which demonstrated that the developed algorithm performs quite satisfactorily. To verify objectively its performance, an additional statistical analysis was carried out.

In this analysis, four days with prevailing intermediate sky conditions were chosen from June 2012. The intermediate conditions are the most crucial conditions that a sky prediction algorithm has to work under but they are also the most interesting ones: during days of stable overcast or clear blue skies, the necessity for a sky prediction clearly diminishes.

We tested the capacity of the algorithm to correctly predict whether the sun will be obstructed in a 5-min horizon. As explained in Section 3.3.2, the algorithm gives a prediction every 30s; thus we compared every prediction given by the algorithm between 11:30 and 15:30 (UTC+2) for each of the four days with the actual sky situation. To get the actual sky situation, we went through 1920 images^e and we labelled each one of them accordingly (sun obstructed/sun not obstructed). The specific 4-hour time frame has been chosen because for the given days (of June) and the camera available, the sun stayed well inside the images during this time (solar noon was approximately at 13:30).

Table 3-1 shows the prediction performance of the algorithm for each day and tested hour against the sky conditions which are represented by the average Global Horizontal Irradiance (Ave Igh) and its standard deviation (Stdv Igh). The global accuracy achieved for all the 1920 forecasts analysed was 92%. The prediction is almost perfect (up to 97% accuracy) when the Igh stays stable (Day 1 and partly, Day 3). This is expected since the forecasting

^e $\frac{4h}{day} \times \frac{60min}{h} \times \frac{2images}{min} \times 4days = 1920 images$

task is significantly easier under stable sky conditions. Under heavily changing sky conditions (mostly Days 2 and 4) it still performs very well and the prediction accuracy of the algorithm fluctuates between 86 and 93% for all but one case.

As it shown on Figure 3-4, the prediction accuracy of the algorithm is satisfactorily correlated with the variability of the sky conditions which is represented by the hourly standard deviation of the I_{gh} . However, it should be noted that this correlation is true under the sky conditions tested herein and it may differ for different sky types (e.g. overcast).

Time [h:min]	Ave I_{gh} [W/m²]	Stdv I_{gh} [W/m²]	Prediction Accuracy [%]
<i>Day 1 [June 1, 2012]</i>			
11:30 – 12:29	873	7	96.7
12:30 – 13:29	867	23	96.7
13:30 – 14:29	778	35	95
14:30 – 15:29	639	49	95.8
<i>Day 2 [June 4, 2012]</i>			
11:30 – 12:29	823	276	90.8
12:30 – 13:29	471	216	88.3
13:30 – 14:29	434	221	79.2
14:30 – 15:29	470	232	89.2
<i>Day 3 [June 5, 2012]</i>			
11:30 – 12:29	886	39	96.7
12:30 – 13:29	805	159	93.3
13:30 – 14:29	751	79	95
14:30 – 15:29	651	58	93.3
<i>Day 4 [June 7, 2012]</i>			
11:30 – 12:29	794	201	85.8
12:30 – 13:29	746	130	89.2
13:30 – 14:29	746	83	91.7
14:30 – 15:29	611	158	90

Table 3-1: Accuracy of the sky prediction algorithm to predict sun-obscureness in 5-min forecast horizons for each day and tested hour.

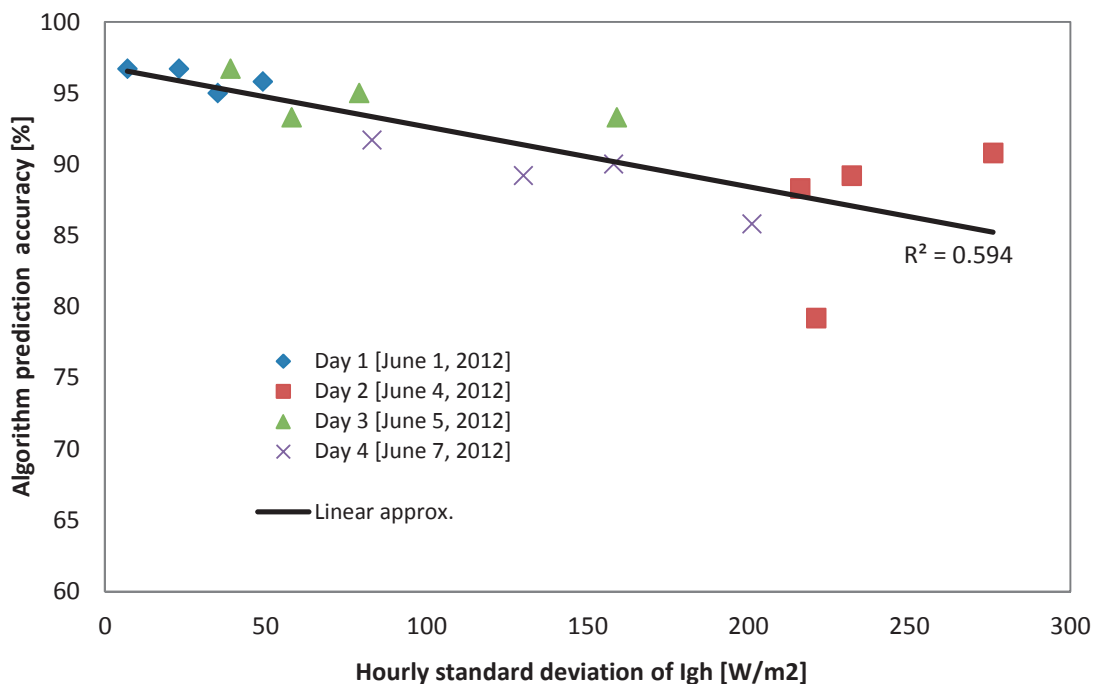


Figure 3-4. Prediction accuracy of the sky scanner algorithm as a function of the variability of the sky conditions (as represented by the hourly standard deviation of the Global Horizontal Irradiance) for the four days analysed.

3.4. Building systems integration

3.4.1. Why combine EC windows control with blinds and electric lights?

One might have expected that a “smart” control algorithm for EC windows (as the sky prediction one presented previously) should only keep to controlling the EC glazings. After all, when EC windows are in place, the use of blinds has proven to be substantially reduced when compared to normal windows [42; 47]. To answer the question above, one should look into certain daylighting issues related with the promising technology of EC Windows. In this regard, when considering the present technology of EC windows and its limitations regarding the minimum T_v value achievable and their slow switching speeds (see 3.1.2), blinds cannot be wiped out from a system wishing to offer an integrated daylighting solution (and visual comfort). As Lee et al. state [24]:

"If the sun (or specular reflections of the sun) is in the field-of-view, the 11%-glazing cannot control its intensity to permit comfortable viewing of the sun or areas of the sky in which the sun is visible. Disability glare will impair the visibility of secondary objects (similar to night roadway visibility with oncoming headlights). The luminance of the sun ranges from several million cd/m^2 when it is near the horizon, to over a

billion cd/m² as it approaches the meridian. Glare calculations suggest that transmittances of less than 0.001 are needed to reduce these luminances to comfortable levels. For these conditions, blocking direct sun with an interior shading device will yield better lighting energy-efficiency. Under partly cloudy conditions and with slow switching speeds, instantly deployed shading devices also have advantages for controlling direct sun."

In addition to the problem of glare, blinds can be also a meaningful means to tackle with the issue of overheating during summer periods, as the minimum value of SHGC is ~10%.

On the other hand, what happens when daylight harvesting is impeded by low intrinsic maximum visible transmittance values? As stated earlier (see 3.1.2), the T_v of today's EC glazings is limited to a maximum of 50%, while T_v values of standard, non-EC IGUs can be significantly higher. This characteristic can potentially render inadequate the luminous flux entering the room under low-light conditions (i.e. overcast skies) and thus makes the use (and hence, the control) of artificial lighting necessary [24]. The same can happen when the EC windows are fully coloured to prevent glare phenomena. A way to increase the efficiency of the system and moderate the increase in energy caused by electric lighting is to couple the EC system with ADS, which can increase the light comfort and reduce the risk for glare [20; 30]. Detailed measurements of daylighting and visual comfort have been previously carried out in a LESO office room equipped with an anidolic system coupled with an EC glazing [34]. The glazing was divided in two independent zones: the lower (larger/main) vertical window was equipped with normal glazing and external tissue blinds; the upper part featured a slanted EC window, the ADS as well as external tissue and internal opaque blinds. The study demonstrated that this is a promising concept but it also concluded that the system's response time (it ranged around 7 minutes) had to be improved. Field research carried out independently [22; 74] as well as parametric studies [75] also favour the implementation of two-zone or multi-zone window panes.

3.4.2. Implementation of the integration

Once we have the output of the 'child' sky prediction algorithm (time in which the sun will likely be obscured by the clouds), we use it as an input to the 'mother' algorithm that is responsible for the integration of all possible controllable building systems. For the implementation of this part we use a rule based fuzzy logic control, building on work previously performed in LESO [33; 58; 59]. In specific, we follow on the work of Daum [76], where a Takagi-Sugeno-Kang (TSK) rule based model is chosen, which requires a relatively small number of rules to describe complex, non-linear models [77; 78]. For example:

IF sun=obscured in 5' AND user=1 AND user action=1 THEN ec, el, bl = C,

mandates that no action (C =constant) is assigned to EC windows (ec), electric lights (el) and blinds (bl) by the mother algorithm when the user is present ($user=1$) and he or she has

performed an override action on one of the building elements (*action=1*), despite the fact that the sun is going to be obscured by the clouds in about 5 minutes (*sun=obscured in 5*).

As seen by this example, one of the important rules of the control algorithm is the prevalence of user actions over any automatic control. Both experience and bibliography suggest that user presence and user wishes is a key factor to consider when implementing an advanced building control system. Earlier studies carried out in LESO concerning intelligent blind controllers proposed that user presence should determine the adopted control strategy at a given time: When user is present in the room then visual comfort is a priority, while in the absence of users a strategy favouring long term thermal aspects and maximum energy conservation should be implemented [58; 59]. As a result, user wishes are respected by the developed algorithm at all times.

Similar to the above example, a rather complex set of rules has been built comprising all available input from the LESO EIB system: instantaneous weather condition (Irradiances and illuminances, external temperature) and building state (room occupancy, user wishes/actions on building systems, workplane illuminance, and internal air temperature). Additional variables including "season" (based on average external temperatures on the last 48 hours) are also incorporated in the rule base. Next, in Section 3.4.3, the framework of the Fuzzy Rule Bases is given. For the complete rule bases including membership functions, see Appendix A.2.

3.4.3. Fuzzy Rule Bases

User Present, "EC Tv" Fuzzy Rule Base

It controls the Tv of the EC windows when the user is present in the room. The visual comfort and the user's wishes are the top priorities followed by thermal comfort and optimal use of thermal gains depending on the season.

Inputs (fuzzy values):

- Sky obscured probability
- Workplane illuminance
- Outdoor average temperature on the last 48 hours
- Room temperature
- User interaction with EC windows

Output (crisp value):

- EC Windows visible light transmission

User Absent, "EC Tv" Fuzzy Rule Base

This scheme controls the EC windows when the user is absent from the room for more than thirty minutes. Priority is given to the optimal use of thermal gains depending on the season.

Whenever allowed by the thermal gains management, the Tv is kept high so the EC windows can provide the maximum possible daylight to the circulation area (corridor) outside the office room (the door is kept open most of the times when the user is absent).

Inputs (fuzzy values):

- Global horizontal solar irradiation
- Outdoor average temperature on the last 48 hours
- Room temperature

Output (crisp value):

- EC Windows visible light transmission

User Present, "Blinds" Fuzzy Rule Base

This controller sets an optimum position for the roller blinds in the room with respect to the user's visual comfort and his/her interaction with the blinds. The blinds are kept completely open and are employed only when the EC windows cannot deal with excessive desktop illuminance.

Inputs (fuzzy and crisp values):

- Workplane illuminance
- EC windows Tv
- User interaction with Blinds

Output (crisp value):

- Blind position

User Absent, "Blinds" Fuzzy Rule Base

This controller is used in parallel with the *User Absent, "EC Tv"* scheme above. It controls the roller blinds in the absence of the user with respect to the optimal use of thermal gains depending on the season. Following the logic explained above, whenever possible it allows for the maximum possible penetration of daylight to the circulation area (corridor).

Inputs (fuzzy and crisp values):

- EC windows Tv
- Global horizontal solar irradiation
- Outdoor average temperature on the last 48 hours
- Room temperature

Output (crisp value):

- Blind position

User Present, "Lights" Fuzzy Rule Base

The controller is activated when the global horizontal illuminance drops below 20 klux^f and it controls the electric dimmable luminaires. Electric lighting is only used when the amount of light on the user's workplane is too low, the blinds are completely rolled up and the Tv of the EC windows is over 41%. Like above, user preferences are always accounted for.

Inputs (fuzzy and crisp values):

- Workplane illuminance
- EC windows Tv
- Blind position
- User interaction with electric lights

Output (crisp value):

- Electric lights power

3.5. Discussion

In this chapter we presented the development of an algorithm that automatically controls the EC windows, the electric lights and the blinds of an office room based on a novel sky-scanner approach. In this approach, images of the sky taken with a camera are logged in a PC and processed in a way that [39]:

1. the relative motion of clouds between two consecutive images is detected;
2. analysis of the cloud motion using a series of images is performed;
3. the possibility of clouds to obscure the sun during the next 5 minutes is deducted and passed on to the main control algorithm so it can issue on time the appropriate commands to the EC windows, blinds and electric lighting.

The development of the sky prediction algorithm was based on a consumer-grade USB camera on purpose, as we wanted to demonstrate that it is feasible to implement a low-cost but rigid solution without the need to invest in dedicated (and costly) traditional sky scanner systems as those referred to in bibliography [70; 69; 79]. In the same vain, no wide angle lens was used in this study. However, a fish-eye lens (or camera) that captures the whole sky dome will allow for a better sky prediction from dusk till dawn and it will also maximize the prediction window. As seen before, the prediction window is currently at about 5 min. As suggested in other studies in which the whole sky is captured in the images, under certain

^f As deduced from the measurements presented in Section 4.1.2, $E_{gh} \approx 20$ klx provides over 400 lx at about 3 m away from the fully bleached EC windows, which is considered sufficient for most occasions.

wind conditions the prognosis window can reach up to 15 to 20 minutes [69], which is needed for controlling EC windows as seen on this chapter.

The inclusion of a fish-eye camera would undoubtedly improve on prediction times, providing a larger time-frame. At the same time, some alterations to the algorithm (like the transformations to rectangular grid implemented by Marquez [70]) would be necessary to correctly compute cloud speeds close to the horizon (at the edges of the image) as every fish-eye lens uses a particular type of projection on the image plane (i.e. hemispherical or angular). On this study, no compensation for the deformation (which is higher on the corners) of the images was applied as the camera possesses a limited field-of-view (FOV) which is $\approx 115^\circ$ on the horizontal and only $\approx 61^\circ$ on the vertical axis^g; values which are far from the 180° of a total sky imager or a fish-eye lens. The only compensation was applied due to the “shrinking” of the image along the horizontal axis due to the 4:3 ratio of the images taken (480x640 pixels)^h.

Also regarding the camera, in other studies the CCD sensor is protected from direct sunlight by means of sun-tracking moving shadow bands in [69; 70]. Such protection appears to be necessary for the longevity of the CCD and its absence from the presented study might be the reason why the camera stopped working a few months after it was first commissioned. Nevertheless, it should be noted that when these protective bands are in place are likely to have an impact on the algorithm’s capacity for short term predictions (in the region of 1 to 3 minutes), especially if wind direction is parallel to them.

Concerning the main control algorithm that implements the final control (fuzzy logic control), although a rather complex set of rules is in place, an elementary fuzzy control is implemented without optimization with artificial neuron networks [59], genetic algorithms [33], or other tuning or adaptive processes [76]. Similarly, the control system does not employ a two-zone window control (i.e. independent control of the normal and ADS EC window) as suggested by relevant research [22; 74; 75].

These limitations of the controller can be explored and eliminated in future research; in the framework of the presented study however the main attention was given in developing a novel image-based prediction algorithm as well as paving the way towards the automatic control of EC windows which until recently remained poorly covered in relevant research.

^g Approximate measurements based on these directions: <http://www.dr-lex.be/info-stuff/viewangle.html>

^h One can notice on the original images (Figure 3-3a/b) the sun’s deformation to an elliptical shape.

4. FIELD MEASUREMENTS AND EVALUATION OF THE SKY PREDICTION APPROACH

This section presents an experimental measurement phase on an office room of the LESO building equipped with EC glazing as well as a parametric study (simulations) comparing the developed algorithm and experimental setup (presented in the previous sections) against other control and setup scenarios. Field measurements, albeit not extensive, were carried out with real persons and aimed principally at the investigation of visual and thermal comfort felt by the user, including the acceptance of a control system incorporating EC glazings by the occupants. Simulations tested different control scenarios of EC windows against a long period of time (one year) and against varying meteorological conditions. The simulations allowed for the comparison of the energy consumption for heating and electric lighting, as well as for the comparison of the estimated thermal comfort and the estimated visual comfort for each of the proposed control setups. Parts of this section have been published by Zarkadis and Morel in an article [39] as well as in a final report for the Swiss Federal Office of Energy [29].

4.1. Field measurements

4.1.1. *Measurements and characterization of switching time curves of the EC windows*

The switching speed of an EC varies with its temperature, size, depth and direction of switching (transition from dark to bleached is generally faster than the opposite [45] but this was not verified in the measurements of the presented study). Following the installation and communication setup between the EC windows and the control computer (see Section 2.3), the switching time curves^a were described through extensive measurements and applied into the newly developed algorithm ('mother' algorithm; Section 3.4.2) as well as into the simulations (Section 4.2.7). Values derived from in-situ measurements of the installed EC

^a The EC transmission values against the time required when switching from one extreme state to the other.

glazings and are specific to them. EC glazings were given numerous times the command to switch between their 2 extreme states (clear and tinted). Their status during transmission change was recorded continuously and logged to a text file. For the switch from clear to dark blue (at about 26°C), the measured visible transmittance (T_v) values were fitted almost perfectly ($R^2=0.9992$) to the equation:

$$y = -0.0049x^3 + 0.3071x^2 - 6.4843x + 65.015, \quad x \in [0.157, 25.77] \quad (4-1)$$

where x denotes time (in min) and y is the T_v . For the reverse change from dark to clear (at about 26°C), the measured T_v values were fitted also perfectly ($R^2=0.9982$) to the equation:

$$y = -0.0012x^4 + 0.0367x^3 - 0.2111x^2 + 1.4903x + 18.037, \quad x \in [0, 17.69] \quad (4-2)$$

Figure 4-1 presents the switching decay curve of the installed EC glazing showing T_v levels (%) vs. switching time (min) during transition from bleached to coloured states for a given temperature (26°C). Figure 4-2 presents the inverse process (transition from coloured to bleached states).

The technical specifications provided by the manufacturer mention the extreme transmission values of the glazings (%): $T_v \text{ EC} = [18, 64]$; $T_v \text{ IGU} = [15, 50]$; $\text{SHGC} = [12, 38]$, where ' $T_v \text{ EC}$ ' is the transmittance of the visible light through the EC element (laminated unit) of the windows, while ' $T_v \text{ IGU}$ ' is the resulting visible light transmittance of the double pane window (Insulated Glass Unit). These extremes were used to extrapolate the values of $T_v \text{ IGU}$ and SHGC (given in the Appendix A.3) from the measured $T_v \text{ EC}$ values. No significant differences were observed between the anidolic (ADS) and the lower (normal) glazing hence there is no necessity for introducing separate fitted curves and matrices.

As it can be observed in Figure 4-1, the switching curve from clear to dark (under the given temperature and glazing dimensions) resembles an exponential decay reproducing with extreme fidelity the outcome of other independent research where "*the curve steeply decreases during the first minutes, then the curvature changes and the profile is flat until the process finishes.*"[46].

These observations can help us to describe in a theoretically accurate fashion the terms "switching speed/time" cited in this thesis and to define switching speed $U(t)$ as follows:

$$U(t) = d \frac{T_v(t)}{dt}, \quad (4-3)$$

where $T_v(t)$ is the visible transmittance curve of the EC glazings as a function of the transition time t (see also Figure 4-1).

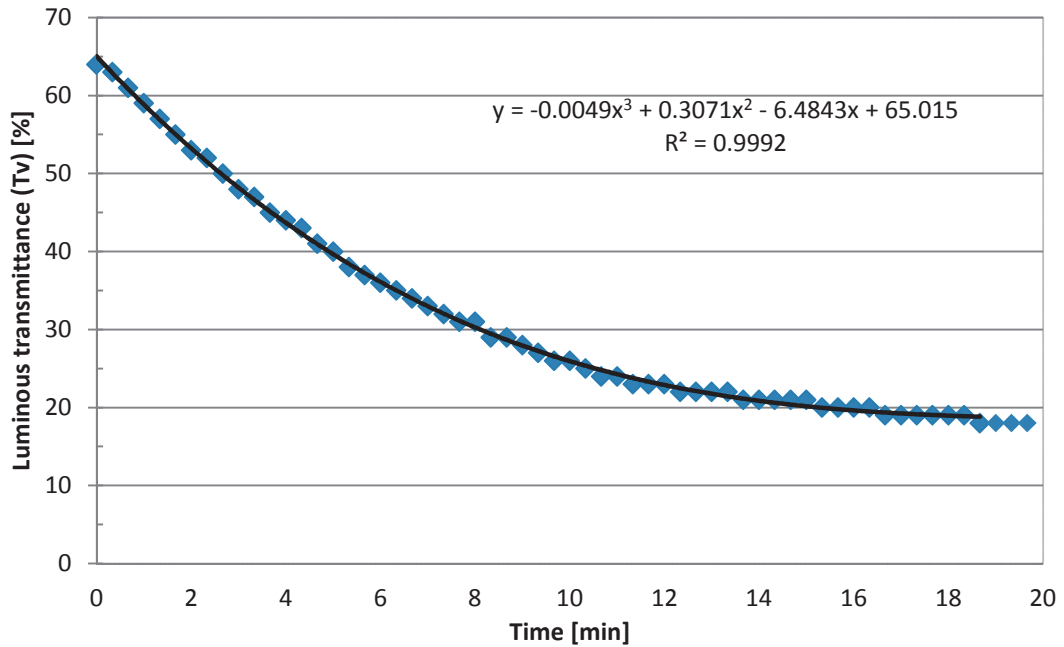


Figure 4-1. Switching decay curve (blue marks) of the EC element (laminated unit) for the installed EC glazing showing Tv levels (%) vs. switching time (min) during transition from bleached to coloured states for a given temperature ($\sim 26^\circ\text{C}$). The black line is the polynomial fit with displayed equation and coefficient of determination.

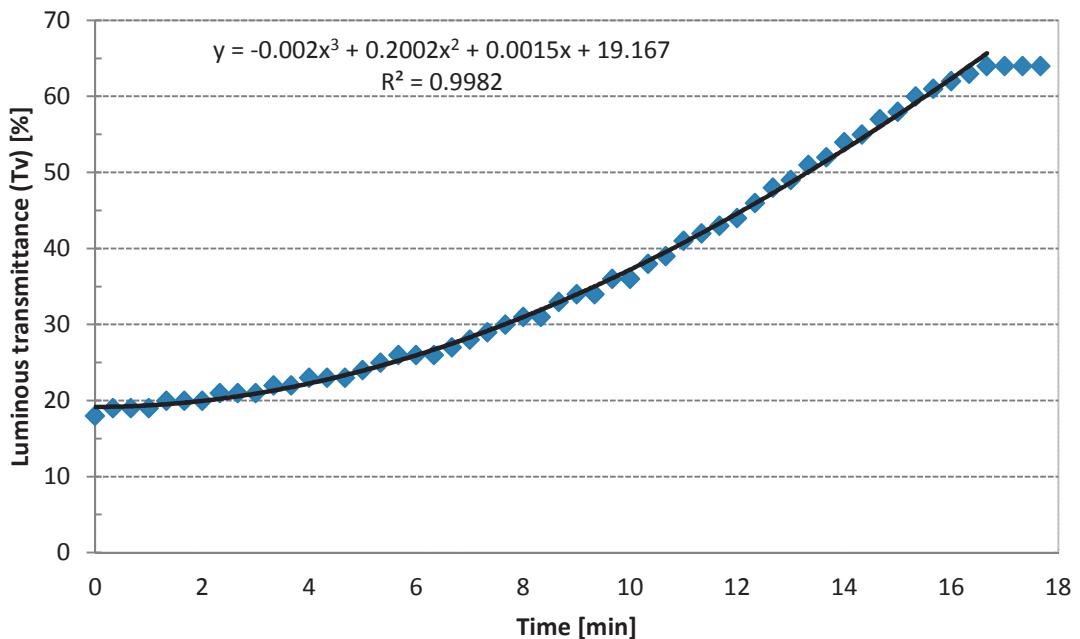


Figure 4-2. Switching decay curve (blue marks) of the EC element (laminated unit) for the installed EC glazing showing Tv levels (%) vs. switching time (min) during transition from coloured to bleached states for a given temperature ($\sim 26^\circ\text{C}$). The black line is the polynomial fit with displayed equation and coefficient of determination.

However, this notion of theoretical approach can have little practical meaning, especially due to the non-linear form of the switching curves. In practice, it is useful to define speed as the time required by the EC glazings to obtain a certain percentage of the total switching depth. For this reason, Table 4-1 provides some meaningful alternative to the theoretically defined EC glazings speed. Transition from the dark to the clear state is remarkably slower than the opposite (e.g. EC glazings perform 50% of the full switch from clear to dark in less than 5 min). On the other hand, a complete change from dark to clear requires 18 min, whereas the opposite direction full transition takes more than 25 min.

Depth of switching [%]	Time required [min]	
	From clear to dark	From dark to clear
30%	2.5	8.5
50%	4.6	11.2
70%	7.4	13.5
80%	9.4	14.7
90%	12.4	16
100%	26	18

Table 4-1: Switching speed of EC Glazings (time required by the EC glazings to execute a certain percentage of the total switching depth).

4.1.2. Daylight Factor (DF) measurements

Illuminance measurements during diffuse light conditions (overcast sky) were carried out to determine the daylight factor (DF), which is used to determine the use of electric lights (Section 4.2.8) and to aid on the estimation of the visual comfort in the simulations presented in Section 4.3.3. The process included multiple measurements of the global horizontal illuminance on the roof (unobstructed 180° view of the sky) and on 5 points on the desktop level of the office room LE 003 where the EC glazings are installed. The 5 points were spread on equal distances (≈ 90 cm) from each other and they were situated on the central axis of the room (vertical to the south façade and parallel to the floor). The first point was chosen at a distance of about 90 cm from the windows plane while the last one was at about 30 cm from the back wall. Measurements were performed with the EC windows fully bleached (DF-15) and fully tinted (DF-50). Values are presented on Table 4-2 and on Figure 4-3 (where the ≈ 90 cm distances are given in meters):

DF for Tv level	Distance from the windows [m]				
	5	4	3	2	1
DF-50	0.68%	0.84%	1.83%	3.08%	4.35%
DF-15	0.38%	0.56%	0.84%	1.43%	1.50%

Table 4-2: Daylight factors for the 2 extreme Tv levels of the EC windows and for each point.

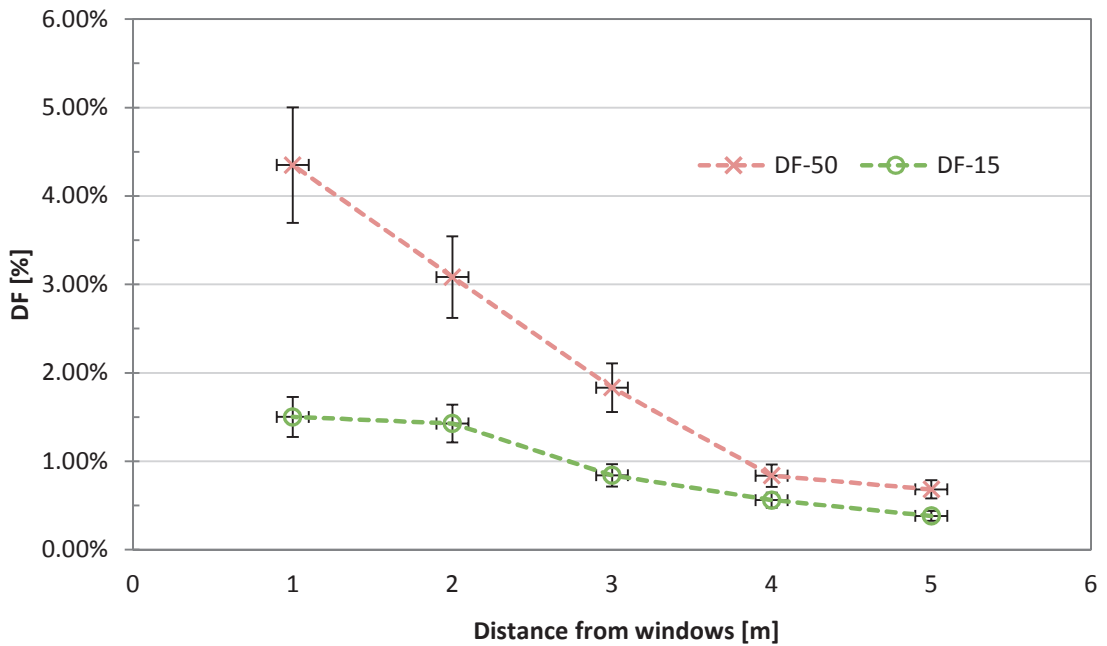


Figure 4-3. Daylight factors for the two extreme T_v levels of the EC windows (50 and 15%) as a function of the distance from the windows (measurement errors: 15% for the DF and ± 0.1 m for the distances). The apparent non-homotheticity of the curves can be attributed to measurement errors and to the presence of the ADS in the upper window.

4.1.3. User evaluation surveys

Short satisfaction surveys were conducted on October 2012 with 9 subjects who volunteered to spend some time inside the office room where the EC glazings are installed. This survey allowed a short-duration assessment of manually controlled EC windows with several persons staying in the room for about two hours each (with similar weather conditions for all the persons). The subjects spanned all age groups, both genders (2 female and 7 male) and spent their time doing ordinary desk work (mainly reading from paper, and computer work) facing all possible directions inside the office room (windows, side and back walls). At the end of the session, they were asked to fill in the short questionnaire which is provided in Appendix A.5 and is partly based on work performed by Clear et al. [42] and Hygge and Løfberg [80]. As the small number of subjects suggests, this survey had a limited scope and was meant as a preliminary user assessment of EC glazings in an office environment. Hence, no thorough statistical analysis (ANOVA, Tukey Test [42] or other [47]) was conducted on the users' answers.

At the time of the survey, all subjects were working at the LESO building and were familiar with the building systems and the controls available to them. Thus, before the beginning of each session they were given only a brief introduction to the technology of EC windows including their principal characteristics and instructions on how to control them. They were

also given the choice between two working places in the room: the first one was at the main desk situated close to the windows (which are on the right of the user who faces the east wall; see Figure 2-4); the second one was a meeting table at the back of the room (about 4m away from the windows) and facing either the windows or the back wall. Subjects were told they could adjust the EC windows, the electric lights, and the blinds available in the office room any time during the session according to their preferences (single-user office room). Then, they were asked to perform their standard working tasks for 2 to 3 hours as they would have done in their usual working place (they were allowed to bring in their personal portable computer, use the desktop terminal already in the room or/and bring any reading or other related material necessary to work with).

Responses showed that most users were not satisfied by the unnatural colour rendering of the room and/or that of the view when looking outside, especially when the windows were fully tinted (Persian blue colour). Glare issues were also mentioned by half of the persons, which eventually motivated them to use the blinds. This was true in cases that direct sunlight hit the desk and/or the computer monitor. Also, some users expressed the wish for a bigger dynamic range of transmissions (on both ends). However, most users are willing to oversee any inconveniences or disadvantages of EC windows and they are generally positive when comparing this daylighting system to a standard one (i.e. blinds) mainly due to the unobstructed view that EC windows offer at all times. Users did not express dissatisfaction regarding the manual control of the EC Windows nor did they seem to consider negatively the slow switching time between different transmission levels.

Interesting additional comments included:

- Since the transition from one state of transmission to another one happens without the user actually noticing the change, there is no way for the user to know if the manual command given to the EC windows is sufficient, underestimated or overestimated (e.g. when blinds are deployed by the user to reduce illuminance or glare, user gets an instant feedback and stops the deployment as soon as they feel satisfied with the resulting visual environment).
- Manual control panels could use a small LCD screen instead of the 5 LED diodes to indicate their transmission level (see also Figure 2-6).
- The colour of the EC windows (also) when windows are fully bleached could be more "clear" and natural. For the tinted state the light Persian blue seems to be cold or dull by many.
- When the person working inside the office leaves the room to visit an adjacent office equipped with normal double glazings, then upon their return time is needed to adjust to the different visual environment and colour rendering.

4.1.4. Algorithm testing (automatic control)

Tests of the algorithm were brief but they allowed for a short check of the elaborated algorithm on the experimental level. Regarding the visual comfort, workplane illuminance was measured by the ceiling-mounted sensor described in Section 2.2.1 while the EC was controlled automatically. A hand held lux meter (BEHA 93408) was used prior to the test to verify that illuminance values reported by the sensor were not affected by the varying reflectance of the desktop surface (i.e. papers or other objects on the desktop can impact the value of the ceiling-mounted sensor).

Measurements took place during a day with intermediate sky conditions (global horizontal irradiance was between 120-320 W/m²) and workplane illuminances were kept inside acceptable visual comfort levels (at around 450-1000 lx) most of the time (Figure 4-4).

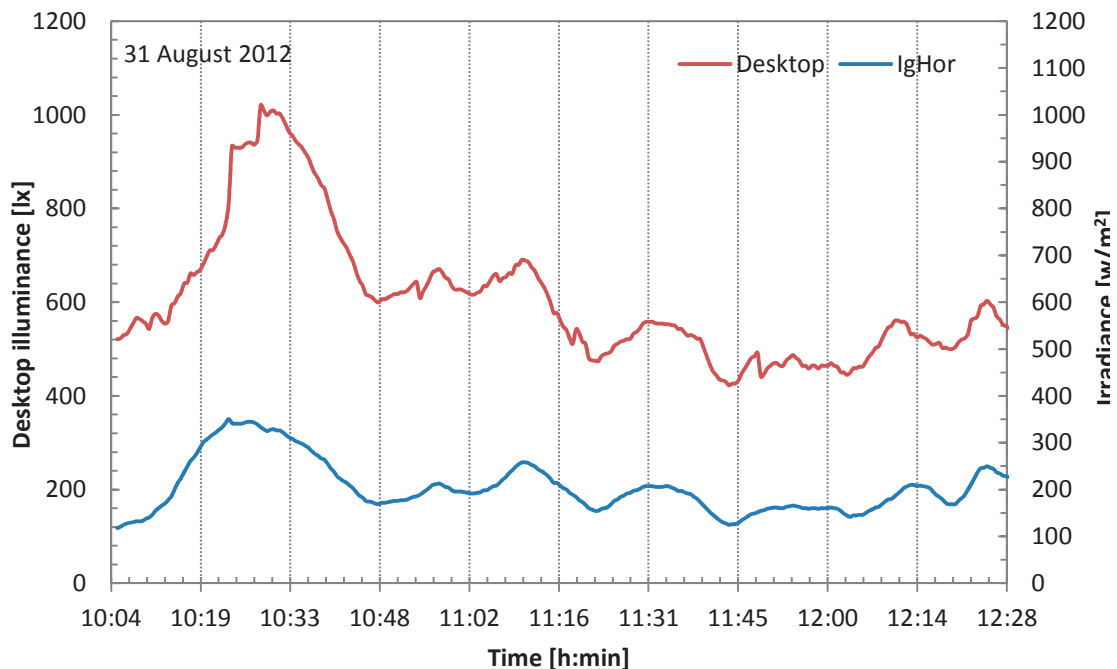


Figure 4-4. Desktop illuminance and Global Horizontal Irradiance (IgHor) measurements before and around noon time on 31 August 2012 (day with intermediate sky conditions).

As it is often the case when a real-life experimental test is being setup, hardware and technical issues plagued the field testing campaign. The computer that communicated with and controlled the EC windows experienced stop errors ('Blue screen') even after the switch to different operating systems and hardware configurations. Most likely this issue originates in the serial port card but no solution has been found during the duration of this study. At the level of the building management bus (EIB/KNX), the meteorological station of LESO and the system that interfaces with the EibServer experienced some serious malfunction and it

was out of operation during most of the testing of the algorithm (the sensors of Global Horizontal Illuminance and Vertical South Illuminance were particularly affected). Last, the waterproof web camera that was purchased for this research not only proved to be a non-wide angle camera, despite the specifications given by the manufacturer^b, but it also ceased to operate about 6 months after its purchase.

Even though a proper user evaluation of the developed control algorithm was not possible due to the aforementioned reasons, short-time checks were promising. The integrated system of EC windows, blinds and electric lighting was controlled in a satisfactory manner and provided good lighting conditions even under changing sky conditions. The sky prediction algorithm seemed to work well, although sometimes the prediction window needs to be bigger.

4.1.5. Proposed future field work

As mentioned previously (Section 4.1.3), only a very limited on-site experimental test of the developed sky prediction algorithm has taken place. Whereas the comprehensive parametric study (presented in Section 4.2) allows for the evaluation of the proposed control system, further field work will allow for the evaluation of the system by real users while at the same time long term measurements will help validate simulation results.

In particular, extensive experimental tests could take place in LE003 office room of the LESO building. They could include long-term data acquisition in the database of the building's central management system of all the relevant parameters from sensors or actuators as instantaneous weather conditions, room conditions as well as user wishes. Simultaneously, EC transmission data will also be logged and user actions could be used as a learning input for the implemented control algorithm. This process could potentially introduce some refinements to the control algorithm. Heating system consumption could be also recorded and then compared with the output of the simulations.

Further, detailed assessment of the user satisfaction (visual and thermal comfort) and acceptance through on-line questionnaires being displayed several times a day on the users' personal computers [14] or smart phones could be performed.

Last, glare risk could be evaluated using novel high dynamic range (HDR) imaging techniques, following recent relevant research by Borisuit and Scartezzini [81; 82] or Inanici [83].

^b Bullet HD Pro 1080; <http://www.bullethd.us/bullethd-best-wearable-sports-waterproof-helmet-camera/bullethd-pro-1080p-helmet-camera/>

4.2. Simulations methodology

In this section, we give a detailed description of the simulation test bed parameters and process.

4.2.1. Introduction

The field measurements realized on LESO building did not allow for a detailed energy comparison, mainly because EC glazings equipment is installed in one office room only. Thus, simulation allowed for the testing of different control scenarios over a long period of time (one year) and against varying meteorological conditions. The simulation presents results for the following parameters:

1. Energy consumption for heating;
2. Energy consumption for electric lighting;
3. Estimated thermal comfort;
4. Estimated visual comfort.

4.2.2. Simulation tool (thermal model)

Simulations were performed using Matlab computing environment [36]. They were based on dynamic thermal simulations code that has been previously developed by the LESO-PB laboratory and used in various research and teaching projects. The choice of Matlab has been made on the grounds of robustness, customization and flexibility^c. The tool had been initially developed for the assessment of heating and cooling needs by comparing different blind control strategies. The calculations are based on a basic dynamic nodal model, taking into account the heat capacity of the construction elements and of the room air. At every time step the heat exchange between all the different nodes is calculated: the room air (first node) exchanges heat with the internal room surfaces (every wall and slab layer is a different node) and external air (last node), while at the same time the energy received and absorbed by the internal surfaces via the windows in the form of solar radiation is also considered. Figure 4-5 presents the distribution of the nodes and the connections via their conductances in a schematic diagram of the model used in the simulations. A detailed general description of a 2-node thermal model including its electric circuit analogy and mathematical description is given by Daum [76 pp. 128-130].

In this study, fourteen (14) nodes were considered during the simulations performed:

- node 1: heated zone air

^c The use of IDA/ICE has been initially considered but quickly aborted because of the difficulty to incorporate a module for EC windows.

- nodes 2, 3: floor screed (surfaces from inside to outside zone)
- nodes 4, 5, 6: ceiling slab (surfaces from inside to outside zone; node 5 is in the middle of the slab)
- nodes 7, 8, 9: internal partition walls (surfaces from inside to outside zone; node 8 is in the middle of the wall)
- nodes 10, 11, 12, 13: facade wall (layers from inside to outside; see 4.2.4)
- node 14: outside air temperature

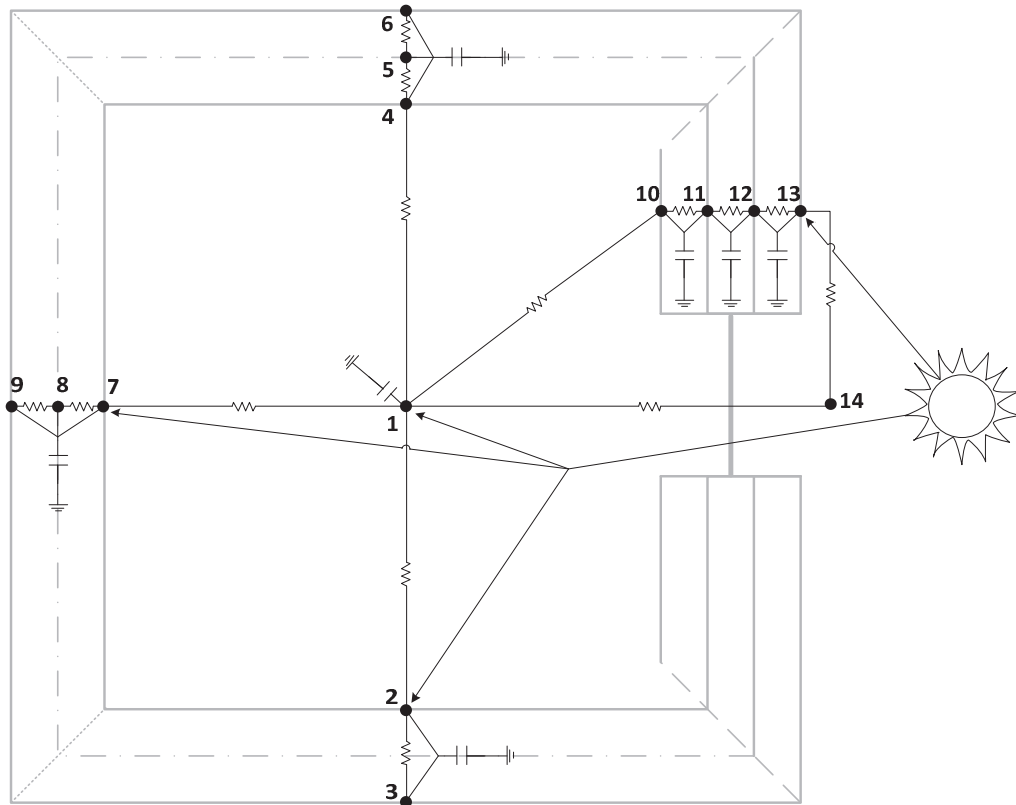


Figure 4-5. A schematic of the thermal model used in the simulations as an equivalent electric circuit.

Also, the Matlab code was modified and expanded accordingly to include:

- An appropriate module to take into account the EC glazing features (switching curves) and control algorithm.
- A module for electrical lighting (illuminance levels on desktop and energy consumption).
- A simple occupancy schedule feature.
- A visual and thermal comfort prediction feature.

- A shorter time step (one minute instead of hourly) to be able to predict illuminances and cater to the visual comfort aspects.

4.2.3. Simulated scenarios

The parametric study compared the following cases of windows for a South-facing office room:

1. Conventional transparent double glazing;
2. Conventional transparent double glazing coupled with blinds;
3. Solar protection glazing with SHGC=0.38 and $T_v=0.50$;
4. Solar protection glazing with SHGC=0.12 and $T_v=0.15$;
5. EC glazing with simple automatic control (See 4.2.7);
6. EC glazing with the proposed sky prediction control algorithm.

4.2.4. Description and characteristics of the simulated office room

The room model used in all simulations is a simplified nodal model of a South-facing office room similar to the LESO building room LE 003 where the EC glazing was installed. North, West and East are partition walls adjacent to other offices and the corridor. Ceiling and roof are also adjacent to other offices. Thus, the room is connected to the outside with only the South wall. The blinds considered are made of textile tissue and they can roll up (completely open) and down (when closed). Window surface was modelled as a single conventional window instead of the coupling of a conventional window with ADS. The room is not occupied; there are no internal gains and only light furniture. The infiltration rate was set to a constant value of $0.3h^{-1}$ in the winter and $0.8h^{-1}$ in the summer and no additional night or day cooling takes place via the windows (they stay closed all the time).

The main characteristics of the room model are as close as possible to the ones of a real LESO office room presented in Section 2.1.1, with only a few differences:

- Floor area of one room: 15.7 m^2
- Room height: 2.8 m
- Facade wall (to South): 5.4 m^2 light wall (2 cm plaster panel + 12 cm thermal insulation [$0.04\text{ W/m}\cdot\text{K}$] + 3 cm wood) + windows (see below)
- Window area including frames: 5.10 m^2 (frames area: 17%)
- Standard glazing: SHGC= 67%; $T_v=78\%$; U-value $1.1\text{ W/m}^2\text{K}$ (U-value the same for all types of glazings including frames)
- Blinds: Textile tissue with 20% solar gains transmission when completely drawn
- Light partition walls with bricks: 10 cm thickness
- Floor screed: 6 cm (concrete)
- Ceiling slab thickness: 25 cm (concrete)

4.2.5. Meteorological data

The meteorological data used for the simulation are synthetic values generated by the Meteonorm software [84]. Data for one year were generated for the city of Ecublens near EPFL and LESO building. Time interval was set at one (1) minute to account for our sky prediction developed algorithm. Simulations used the same time-step (1 minute). The generated data included date, time, external temperature, global horizontal solar radiation, diffuse horizontal solar radiation, global vertical south solar radiation as well as solar height and azimuth angles.

4.2.6. Heating control system

The heating controller is a simple, closed-loop system based on the internal air temperature and the season. The set point for the temperature is 20°C (no night setback schedule is implemented). At every time step the controller checks whether the temperature is below the set point and the season is set to "heating season"; if both conditions are met, then it injects the necessary amount of energy in the room so that the temperature can reach the set point value (no hysteresis is implemented). Heating season is not implemented using a calendar definition. Instead, we consider a given simulation time step as being in "winter" if the average external temperature over the last 7 days is below 10°C.

No (active or passive) cooling system is employed, to reflect the current real situation of LESO building.

4.2.7. Electrochromic windows and blind control

A separate module for the EC windows that gives at any time step the values of the solar heat and visible transmission of EC glazings was implemented and inserted into the simulation code. As explained in the experimental setup chapter (4.1.1), tabular values of switching time curves were produced (see Appendix A.3) and inserted into this simulation module. The time step of the simulation was the same as the time step of the switching curves (1 min).

For the simulation scenario 5 (EC simple automatic control), a simple closed-loop control is used based on the global vertical south solar radiation (I_{gvs})^d and the season^e. In the cooling season the EC windows are kept fully bleached for an I_{gvs} below 100 W/m²; fully tinted if it exceeds 300 W/m² and assigned linearly interpolated *target* values of SHGC

^d The internal air temperature (T_{air}) was initially also considered in the control: In the summer, solar gains were allowed only when $T_{air} < 20^\circ\text{C}$ and during winter were rejected if $T_{air} > 25^\circ\text{C}$. Simulation tests showed no difference so it was excluded from the control scheme.

^e As defined in Section 4.2.6 above.

(between 12 and 38%) and T_v (15-50%) for solar radiation values between 100 and 300 W/m^2 . By “target value” we mean that EC windows at a certain time-step are assigned a desired transmission value. Due to the intrinsically low switching speed of EC glazings (see 3.1.2 and 4.1.1), this value cannot be assigned instantly; instead it will be achieved in the next time steps (next minutes) following the incorporated switching time curves. In the winter, all solar gains are accepted and EC windows act like low solar gains windows with SHGC=38%.

For the simulation scenario 6 (EC with the developed control algorithm), we use the same control variables and limits as above but we consider that a perfect sky prediction allows the EC windows to achieve desired transmittance values at every time step. In this case, the EC windows are always assigned with the right transmission values, as required by the control variables.

Regarding the blinds control in simulation scenario 2 (Conventional glazing coupled with blinds), we follow exactly the same control as above: In the summer, they are fully rolled up if I_{gvs} is lower than 100 W/m^2 ; fully deployed if it exceeds 300 W/m^2 and in an intermediate position linearly interpolated for solar radiation values between 100 and 300 W/m^2 . Likewise, in the winter they are fully open.

Suggested by test simulations, the decision to permit all solar gains during the winter is a conscious compromise between visual comfort (which may be affected negatively due to extreme brightness and/or glare phenomena) and decreasing energy consumption for space heating.

4.2.8. Electric lighting calculation

Electric lighting is commissioned to maintain horizontal illuminance at the user’s workplace on the desktop level at 500 lx when daylight is not sufficient. The dimmable light fixture considered is the one that currently is found inside the office LE 003 of the LESO experimental building and can deliver 250 lx of illuminance on the user’s workplace at a maximum power of 4x36 W. On top of the nominal power of the 4 lamps (144 W), we assume 15% overconsumption due to the fixture ballasts (21.6 W). This power is considered as base power and it is consumed during all work hours when the fixture is not completely switched off. The fixture’s power consumption from 21.6 to 165.6 W is linearly correlated with the required artificial lighting illuminance of 0 to 250 lx.

As it can also be seen in Figure 4-6, electric lights remain switched off when available daylight maintains workplace illuminance above 500 lx. When workplace illuminance due to daylight is between 250 and 500 lx, then electric light is commissioned to contribute the necessary amount of lighting so the resulting desktop illuminance (natural & artificial light) is maintained at 500 lx. When natural daylight yields workplane illuminances equal or lower than 250 lx, then the electric lights are switched on at full power (165.5 W & 250 lx).

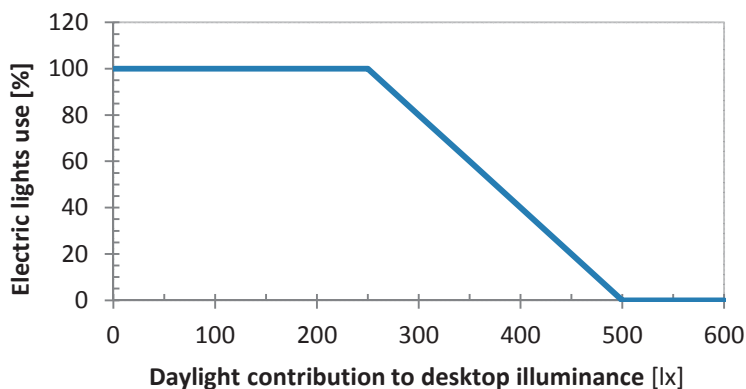


Figure 4-6. Electric lights usage as a function of the natural light-induced desktop illuminance.

To calculate if any additional desktop illuminance is needed, the desktop illuminance due to daylight is first computed. At every time step, it depends on the global horizontal illuminance (E_{gh}), EC windows visual transmission level (T_v) and blinds position. To calculate E_{gh} from global horizontal irradiance (I_{gh}), one normally has to resort to a physically accurate model such as the Perez model [85; 66]. On the practical level, this simulation use an approximation which is only correct for diffuse light conditions according to which the E_{gh} is correlated to I_{gh} : 1 W/m^2 of I_{gh} corresponds to 179 lx of E_{gh} (luminous efficacy of 179 lm/W) [86]. As noted, this approximation is not valid for intermediate or clear sky conditions with a direct illuminance component. We assume that in such cases corresponding illuminance would be higher, resulting in a slight over-estimation of energy used for electric lighting.

Next, we use the measurements of the Daylight Factors (DF) as described previously (Section 4.1.2) for the given user position in the room (at approximately 1.8 m away from the windows) and for the 2 extreme states of the EC windows ($DF_{\text{fully bleached}}=3.13\%$; $DF_{\text{fully tinted}}=1.43\%$). We then interpolate linearly the DF for the actual EC transmission at every time step. Finally, the multiplication of the DF with the estimated E_{gh} , gives us the amount of desktop illuminance due to daylight.

For the simulation scenario where we have standard glazing with the use of blinds (scenario 2), we use results from a study previously performed in LESO by Bauer et al. [58] in an office room identical to the one used here. Following on this research, we estimate for the user position ($\sim 1.8 \text{ m}$ away from the windows) the value of DF for the blinds completely rolled up to be $DF_{\text{no blinds}}=10.4\%$, while for blinds completely rolled down is $DF_{\text{blinds}}= 1.8\%$. For an intermediate blind position the resulting DF is again a linear interpolation between the two values.

4.2.9. Occupancy schedule

For the electric light use, the visual and the thermal comfort we consider the presence of a single occupant only during the working hours with a 9-hour daily schedule of 08.00 to 18.00 with a lunch break (absence) from 12.00 to 13.00, from Monday to Friday.

4.3. Simulation results and discussion

4.3.1. Energy consumption

The results of the simulation study regarding the energy consumption for heating and electric lighting are shown on Figure 4-7 and on Table 4-3. As expected, standard (clear) glazing permits high solar gains during the winter which results in significantly low energy demand for space heating. In these cases, energy required for electric lighting is also reduced when compared to other cases due to the abundant daylight penetrating inside the room. However, both cases of standard glazing offer the worst thermal and visual comfort (overheating and extreme illuminances, respectively) as seen next.

Scenario 4 appears on the other extreme in terms of energy demand. This case features a low solar gain glazing with a very low constant coefficient of solar radiation transmission of 0.12. Solar gains are mostly cut-off and energy demand for heating escalates to over the double in comparison to the other scenarios. Energy demand for electric lighting is also significantly higher (about 40%) when compared to scenarios 3, 5 and 6. This is due to the constant low visible light transmission and the subsequent more frequent use of electric lighting.

The energy demand of the case of low solar gain glazing with a constant coefficient of solar radiation transmission of 0.38 (scenario 3) is comparable to the energy demand by the scenarios 5 and 6 with the EC glazings. It is important to compare these 3 scenarios in respect to the predicted visual and thermal comfort they offer, as it is done next.

Simulation scenario	Heating [kwh/m ²]	Electric lighting [kwh/m ²]	Total [kwh/m ²]
1: Standard glazing	2.7	5.6	8.3
2: Standard glazing+Blinds	4.2	5.6	9.8
3: Low Solar gain glazing (0.38)	13.6	7.9	21.5
4: Low Solar gain glazing (0.12)	36.4	11.1	47.5
5: EC Simple control	14.9	8.0	22.8
6: EC Predictive control	14.9	7.9	22.9

Table 4-3: Annual energy demand for space heating and electric lighting for different simulation scenarios.

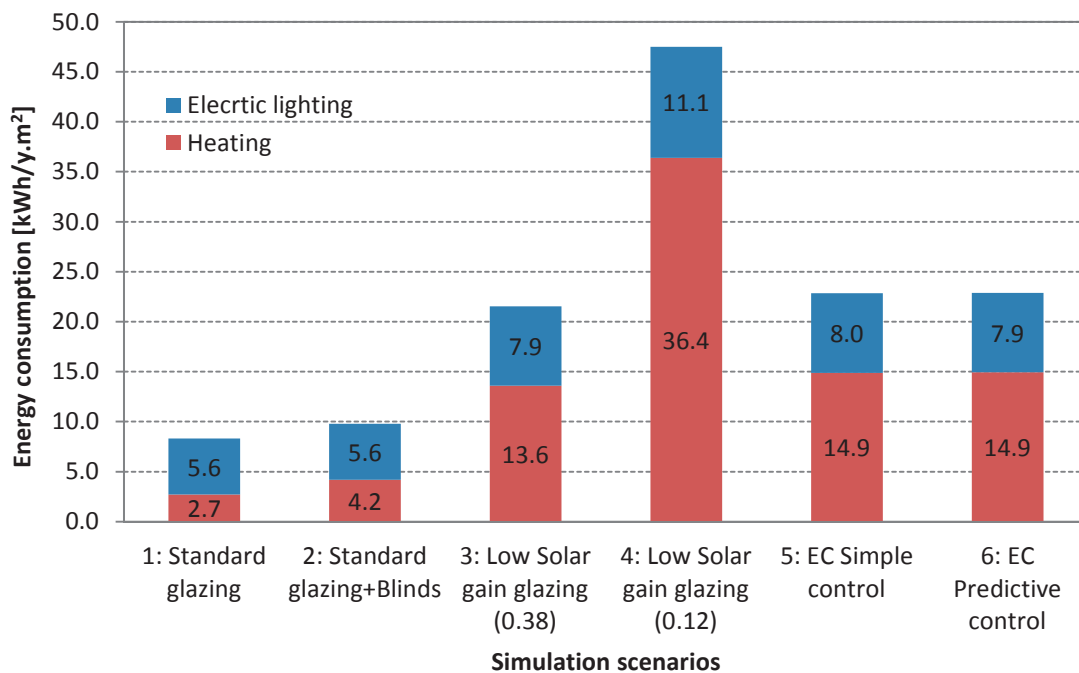


Figure 4-7. Annual energy demand for space heating and electric lighting for different simulation scenarios.

4.3.2. Thermal comfort

Indoor air temperature

As a first indication of thermal comfort, we compare the indoor temperature across the different simulation scenarios. We observe unacceptable temperatures for the cases with the standard glazing (1 and 2). In particular, scenario 1 demonstrates very high indoor air temperatures between 30-40°C for all months except those during winter (Figure 4-8). Scenario 2 is slightly improved but still unacceptable overheating occurs during some days in late winter and, to a lesser extent, during some days in late autumn with internal temperatures over 30°C (Figure 4-9). However, it should be noted that high temperatures are expected since neither cooling nor any form of ventilation is considered in the building model. Naturally, overheating can be partially mitigated by simply opening the window during mid-season or summer.

Scenario 4 (low solar gain glazing with SHGC=0.12) exhibits an indoor temperature that for almost the entire winter season stays stable at around the set-point temperature of 20°C (Figure 4-11), while in the warmest days of the non-heating period the indoor temperature is never over 25°C. However, during some intermediate season days in spring and fall when heating is not required, internal air temperature falls at 18°C or lower. Again, this is due to permanent glazing characteristic of cutting-off most of potential solar gains from entering

the room in days when they would have been beneficial for the conditioning of the space. However, it should be noted that the heating controller and thus the season definition are identical for all compared scenarios. In this one (4), where solar heat gains are largely prevented from entering the room and being stored in the heavy construction elements, it would be more realistic to modify the season definition to reflect the scenario's particular conditions (i.e. consider the season as "winter" if the average external temperature over the last 2-3 days is below 12°C (instead of the considered 10°C) or even follow a more advanced definition, like the one presented in Chapter 5).

Cases 3, 5 and 6 appear to have comparable energy consumption but when compared against the internal temperature significant differences are observed. In scenario 3 (low solar gain glazing with SHGC=0.38) internal temperature at around 30°C is observed for about 75 days during the year. In the scenarios with the EC windows (5, 6; Figure 4-12 & Figure 4-13), indoor temperature during non-heating season is at around 25°C, with the exception of some warm days during spring.

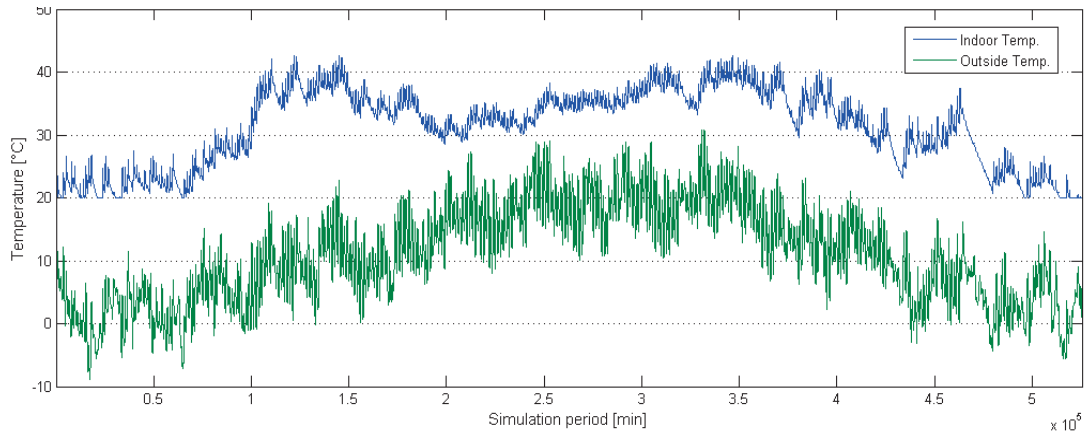


Figure 4-8. Temperatures variation for Scenario 1 (Standard glazing; no blinds). Overheating is observed from March to November.

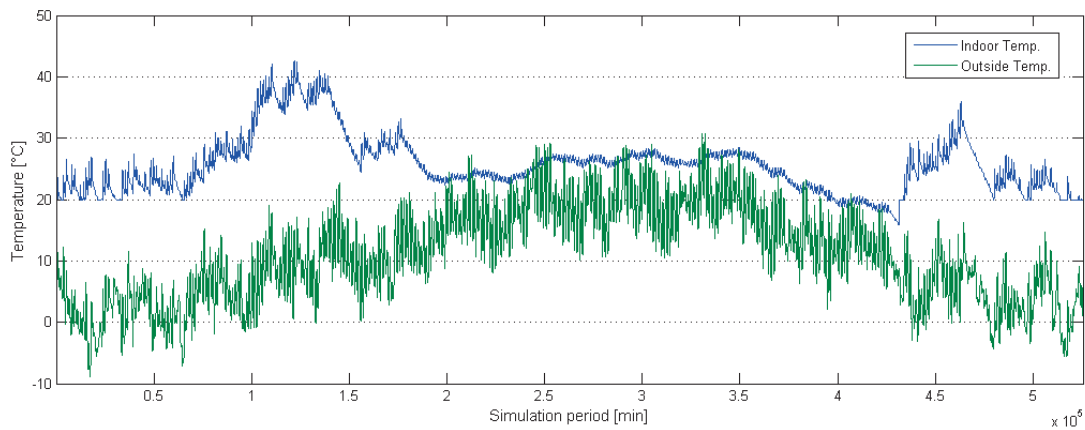


Figure 4-9. Temperatures variation for Scenario 2 (Standard glazing + blinds). Internal temperature exceeding 30°C is observed during intermediate season.

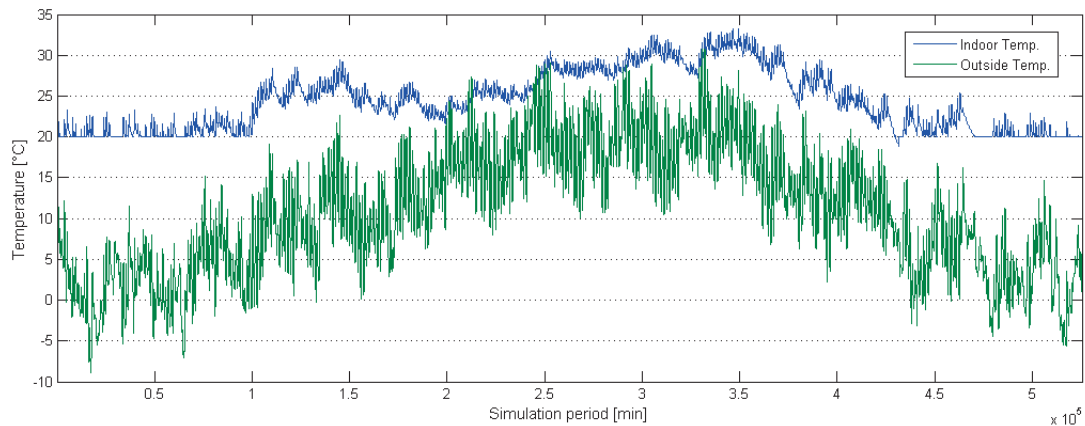


Figure 4-10. Temperatures variation for Scenario 3 (Low Solar gain glazing; SHGC=0.38). Internal temperatures around 30°C are observed for about 75 days during the year.

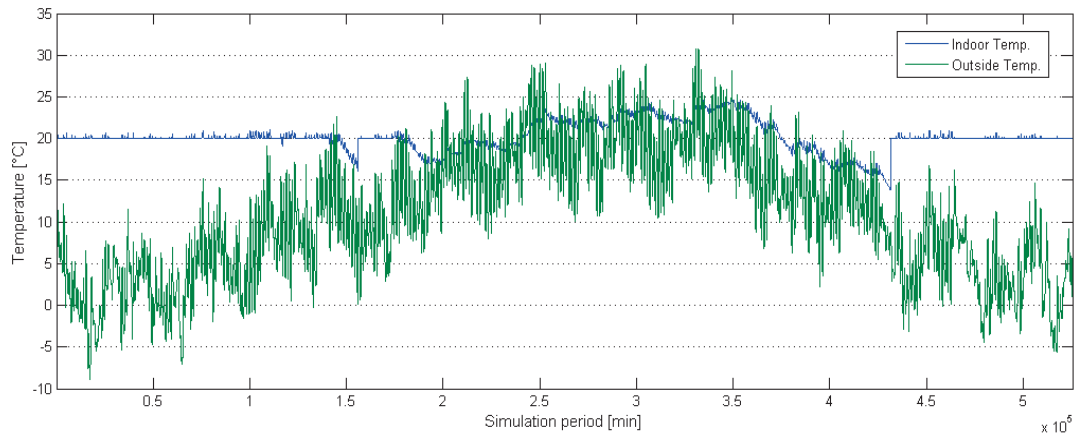


Figure 4-11. Temperatures variation for Scenario 4 (Low Solar gain glazing; SHGC=0.12).

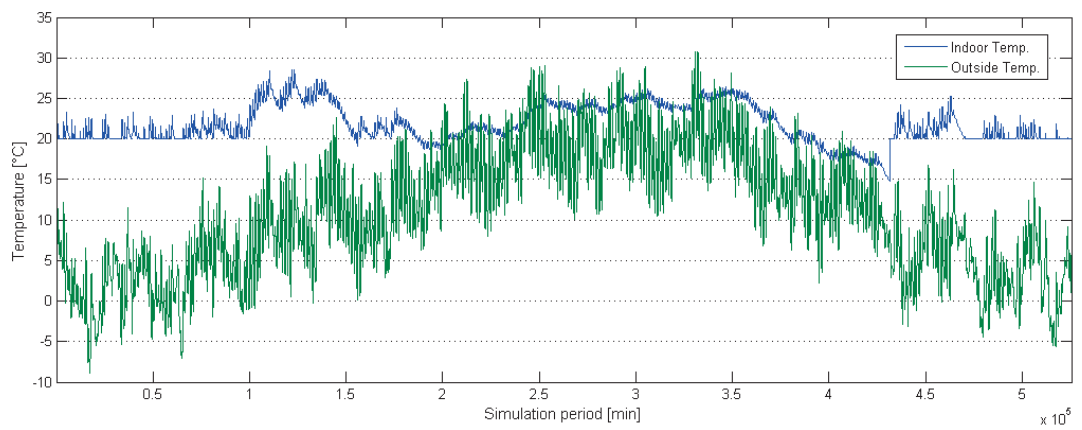


Figure 4-12. Temperatures variation for Scenario 5 (EC simple control).

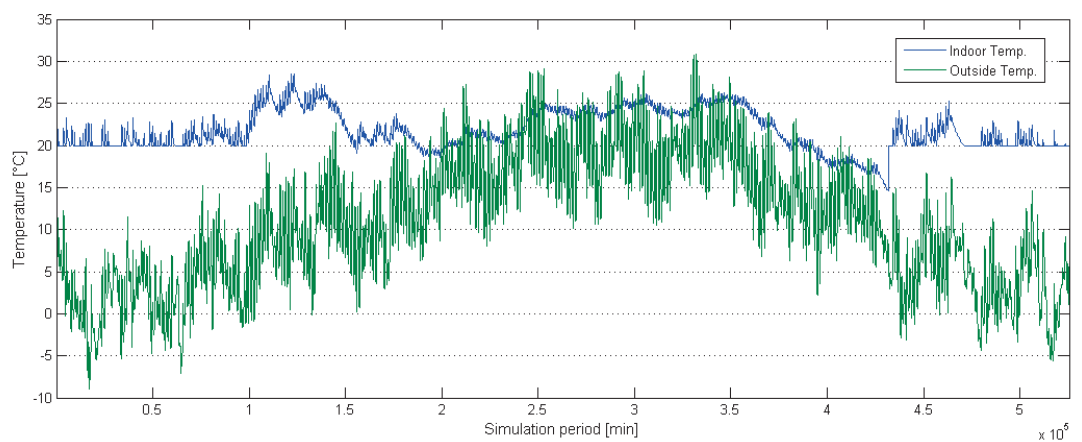


Figure 4-13. Temperatures variation for Scenario 6 (EC Predictive control)

Figure 4-14 displays a qualitative approach comparing the internal temperatures distribution for each of the six proposed simulation scenarios. Scenarios 1 and 4 appear immediately as the extreme cases. Scenario 4 is the one having less dispersion with most of the values close to the median (20°C), keeping the temperature steady throughout the year, in the expense of high energy consumption as we showed above.

Scenario 1 is having a median at around 33°C and values inside the 25th and 75th percentiles in the area of 26.2 - 36.4°C. Scenario 2 has a reduced interquartile range (22.7-27.5 °C), but its median is rather high (overheat risk) and the whiskers extend far from this range, both over and under. The significance of these distributions becomes crucial next, when we calculate the Predicted Percentages of Dissatisfied (PPD).

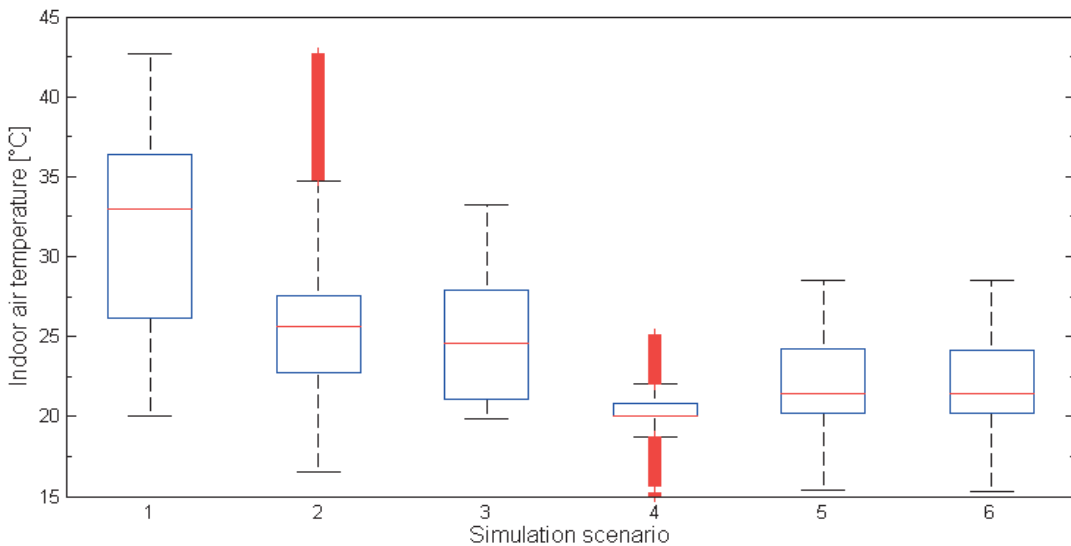


Figure 4-14. Distribution of indoor air temperature values for the six different simulation scenarios for a period of one year. The blue bottom and top of the box represent the 25th and 75th percentile respectively; the red mark inside the box is the 50th percentile (the median); whiskers represent the minimum and maximum of data points not considered outliers^f (red points outside whiskers).

^f Points are drawn as outliers if they are larger than $q3 + w(q3 - q1)$ or smaller than $q1 - w(q3 - q1)$, where $q1$ and $q3$ are the 25th and 75th percentiles, respectively. The value $w=1.5$ used here corresponds approximately to $\pm 2.7\sigma$ and 99.3 coverage if the data are normally distributed. The plotted whisker extends to the adjacent value, which is the most extreme data value that is not an outlier [36].

Predicted Percentages of Dissatisfied (PPD)

Thermal comfort was analyzed with the use of Fanger's model [12]. Using as input for every time step of the simulation the season, the radiant temperature in the room and the room's air temperature, the Predicted Percentages of Dissatisfied (PPD) and the Predicted Mean Vote (PMV) were generated for every working hour in the year. The comfort parameters of air humidity, air velocity, clothing insulation and metabolic heat production were set to fixed values and they are shown on Table 4-4.

Parameter	Heating period	Non-heating period
Clothing [clo]	1.0	0.50
Activity [met]	1.2	1.2
Air speed [m/s]	0.10	0.10
Relative humidity [%]	50.0	50.0
Operative temperature [°C]	19.2 - 23.8	23 - 26.3

Table 4-4: Comfort parameters and calculated operative temperature used in Fanger's model for a PPD<10%.

The operative temperatures for the heating and the non-heating seasons were calculated as the limits within which the PPD remains below from the generally accepted standard for office rooms of 10% ($-0.5 < PMV < 0.5$ or 90% of thermally satisfied occupants). These comfort limits are proposed by the ISO 7730 standard [13]. Clothing insulation was set to 0.5 clo for the non-heating period and to 1 clo during the heating period (for the definition of "season" see paragraph 4.2.6). The metabolic heat production was set to 1.2 met (light desk work) in all simulations.

The estimation of the thermal comfort for the whole period (1 year) was conducted to evaluate the ability of the simulated case studies to keep the internal air temperature within the comfort limits specified by the said standards (Table 4-4). The percentage of the working time when the air temperature is outside the range defined by the comfort limits was determined for all the simulation scenarios and seasons and it can be seen on Table 4-5 and Figure 4-15. Again, it should be noted that results should be put in perspective of the absence of cooling and of any form of ventilation. Hence, extreme temperatures and thermal discomfort are expected during mid-season and – most notably – during summer (i.e. non-heating periods).

Simulation scenario	Heating period [%]			Non-heating period [%]			Entire year [%]
	PMV < -0.5 (=feeling cold)	PMV > +0.5 (=feeling warm)	Total	PMV < -0.5 (=feeling cold)	PMV > +0.5 (=feeling warm)	Total	
1: Standard glazing	0	61.4	61.4	0	99.5	99.5	81
2: Standard glazing + Blinds	0	58.4	58.4	20.4	43.5	63.9	61.3
3: Low Solar gain glazing (0.38)	0	20.9	20.9	6.9	60	66.9	44.7
4: Low Solar gain glazing (0.12)	0	0	0	80.5	0	80.5	41.6
5: EC Simple control	0	15.6	15.6	49.9	0.8	50.7	33.7
6: EC Predictive control	0	15.6	15.6	50.2	0.4	50.6	33.6

Table 4-5: Percentage of working time during the simulation period where temperature is outside comfort limits (PMV<-0.5 or PMV>+0.5; PPD>10%), for each of the six considered simulation cases.

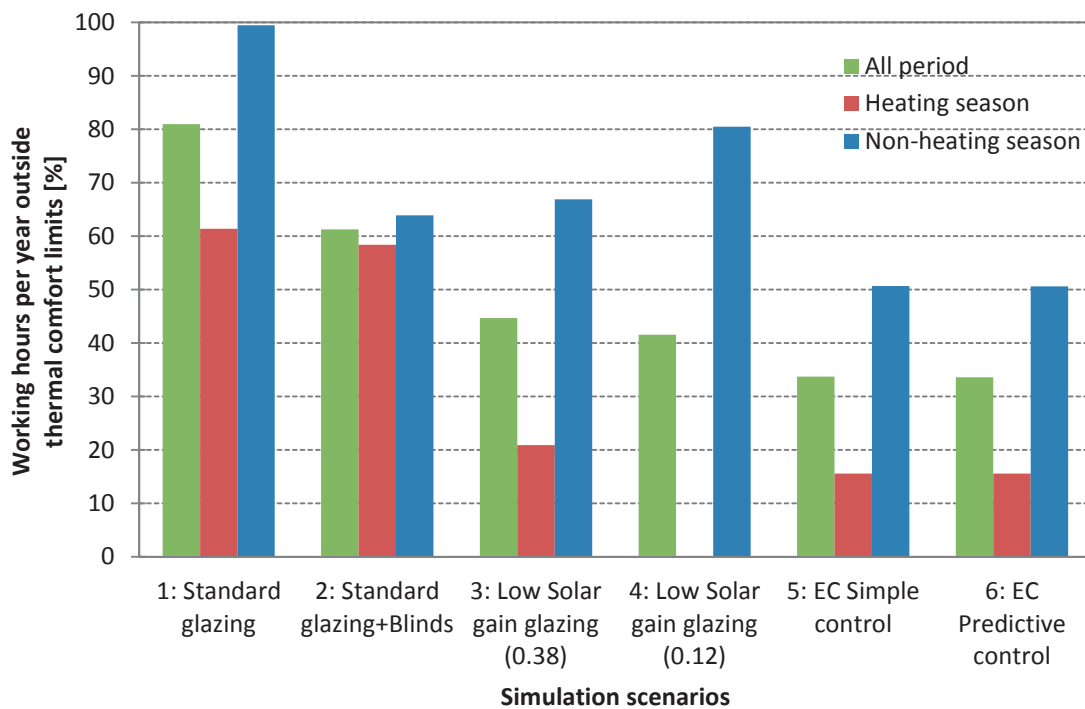


Figure 4-15. Percentage of working time during the simulation period where temperature is outside comfort limits (i.e. PPD is over 10%), for each of the six considered simulation cases.

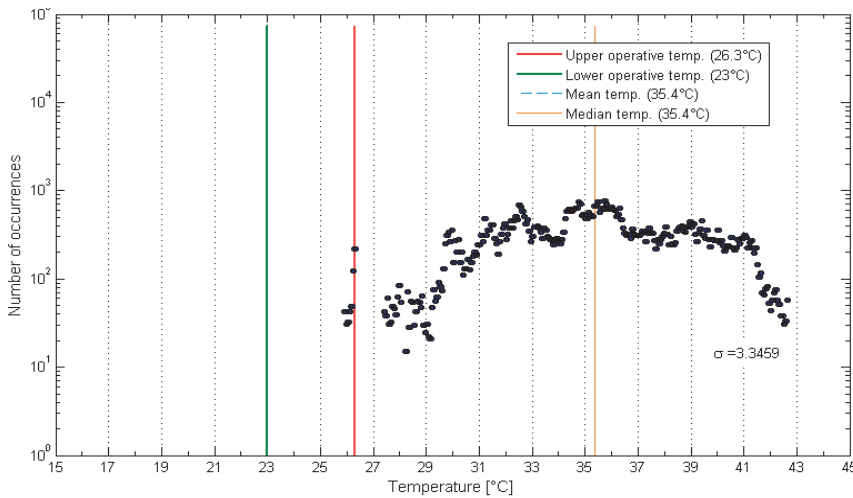
The comparison between all different scenarios shows clearly that automatically controlled EC windows (scenario 5 and 6) provide the best possible thermal comfort conditions with only a 15.6% of working time during the winter season found outside the thermal comfort limits. Scenario 3 also provides acceptable thermal comfort with 21% of working time during the winter season lying outside the thermal comfort limits. Standard glazing scenarios provide unacceptably high discomfort conditions. During winter, scenario 4 interestingly enough provides the “perfect” thermal comfort conditions with zero working time being outside comfort conditions. That is of course due to the excessive use of heating energy since almost all solar gains are rejected.

We kept separately the reports for the non-heating season on purpose. Since there is no active cooling system (and we chose not to implement night-cooling as well), temperatures during the “summer” days are more likely to fall outside thermal comfort criteria. But also in this case, EC windows scenarios are performing better than the others.

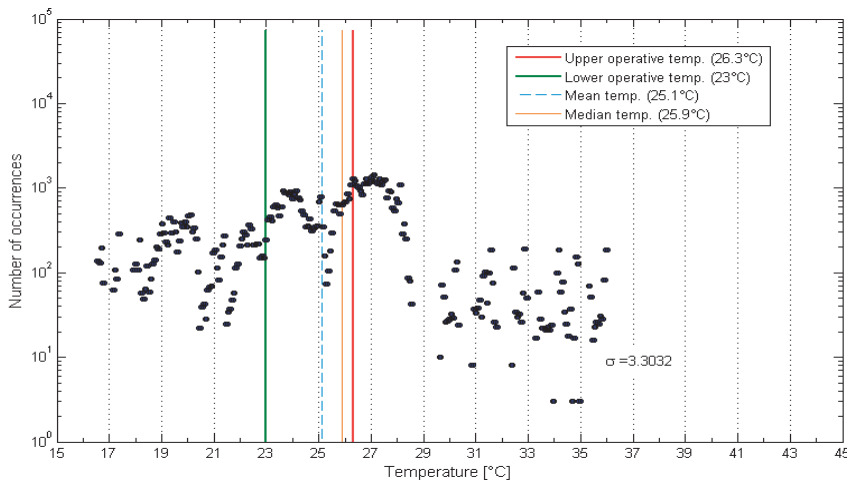
It is also interesting to note the distinction made on Table 4-5 concerning the PPD percentages between these that are due to overheating and those that occur due to risk of feeling cold. In this regard, during the heating period, the predicted percentages of dissatisfaction in all scenarios are all due to anticipated complaints of overheating ($PMV > +0.5$) and none for the contrary. This is expected, since the controller keeps the air temperature at 20°C minimum during the entire heating season (see Figure 4-17, Figure 4-16 & Figure 4-19). On the other hand, best performing cases (scenario 5 and 6) seem to suffer from excessive rejection of solar heat gains during the non-heating period and users are likely to complain because they are feeling cold. However, these complains would likely be mitigated with the adaptation of user clothing during this period (i.e. from 0.5 to 0.65 clo; see Table 4-4).

Figure 4-16, Figure 4-17, Figure 4-18 and Figure 4-19 below complete the picture in thermal comfort providing some additional qualitative information about the indoor temperature during the simulation periods. In particular, the distribution of indoor temperature (values, median, mean and standard deviation) during working hours for both the non-heating and the heating period is displayed together with the limits of the operative temperatures (green and red lines) for all simulation scenarios.

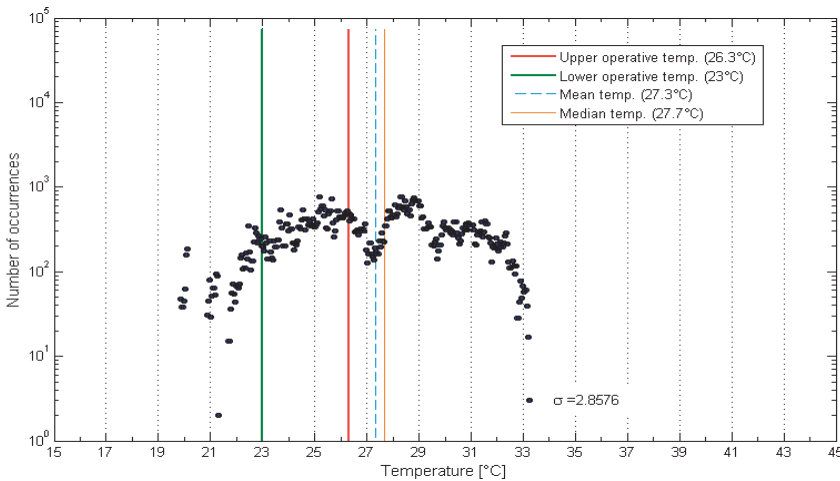
Air temperature distributions during working hours



(Scenario 1a)



(Scenario 2a)



(Scenario 3a)

Figure 4-16. Indoor temperature values distribution during working hours in non-heating period (a) for simulation scenarios 1-3. Displayed are the values (black points), median (orange line), mean (light blue dashed line) and standard deviation (σ) together with the limits of the operative temperatures (green and red lines).

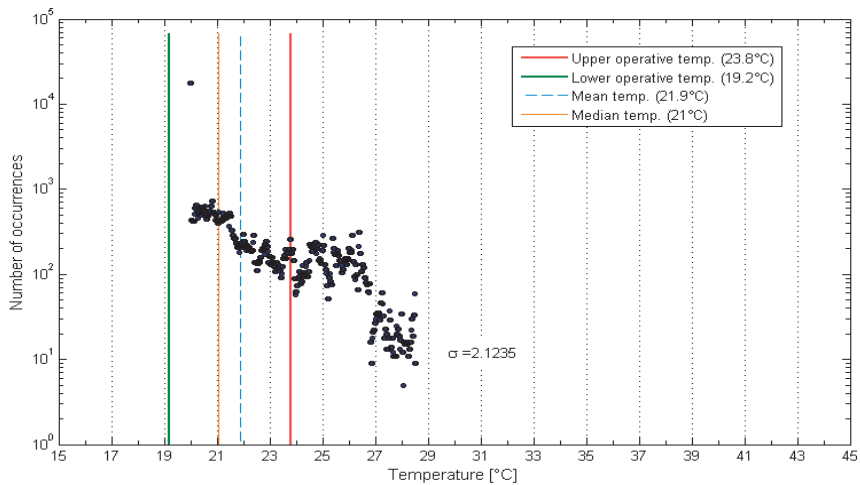
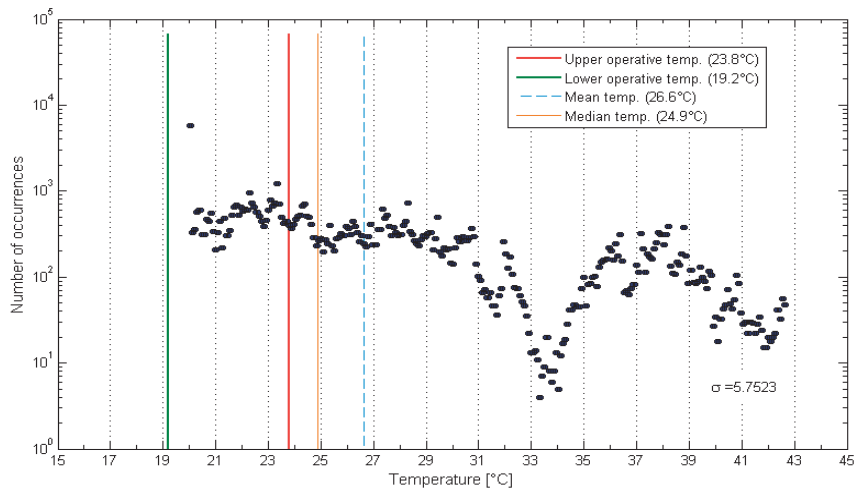
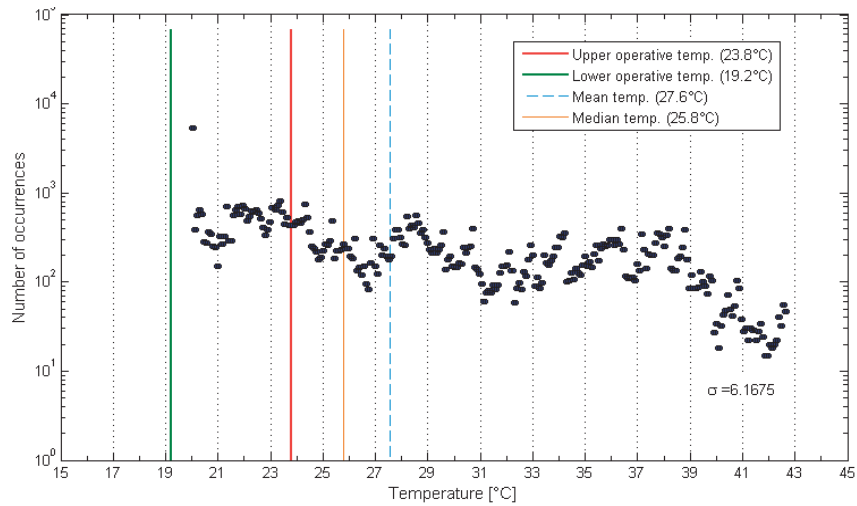
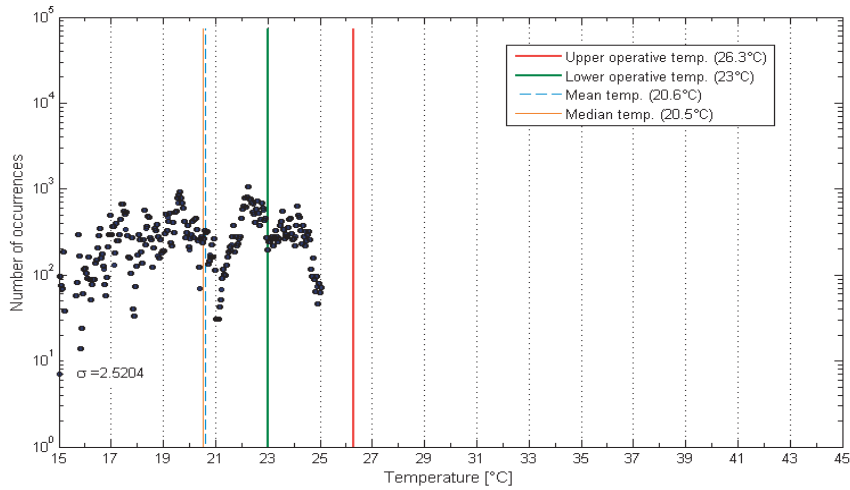
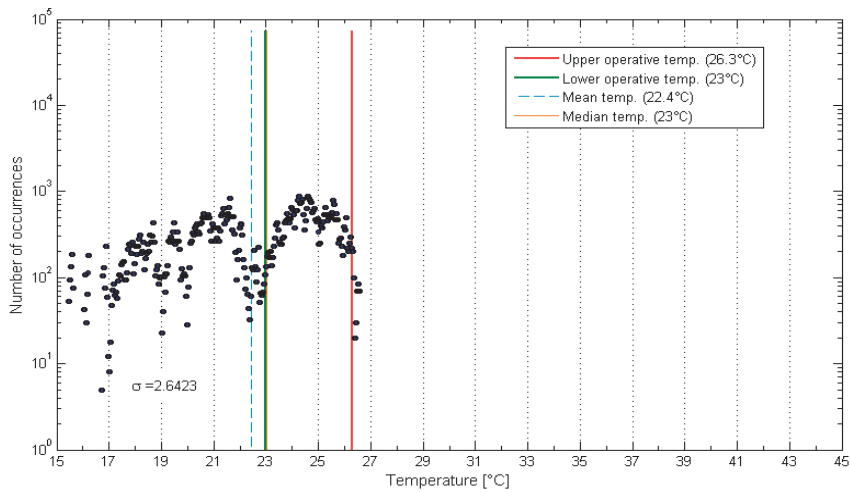


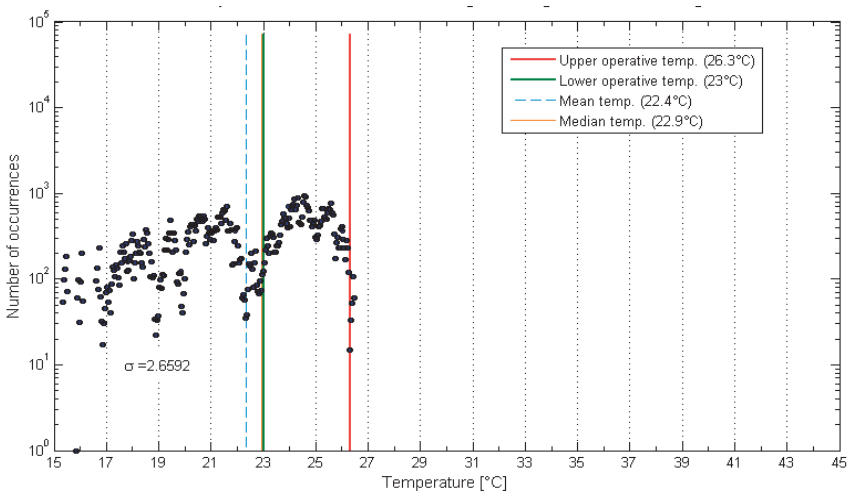
Figure 4-17. Indoor temperature values distribution during working hours in heating period (b) for simulation scenarios 1-3. Displayed are the values (black points), median (orange line), mean (light blue dashed line) and standard deviation (σ) together with the limits of the operative temperatures (green and red lines).



(Scenario 4a)



(Scenario 5a)



(Scenario 6a)

Figure 4-18. Indoor temperature values distribution during working hours in non-heating period (a) for simulation scenarios 4-6. Displayed are the values (black points), median (orange line), mean (light blue dashed line) and standard deviation (σ) together with the limits of the operative temperatures (green and red lines).

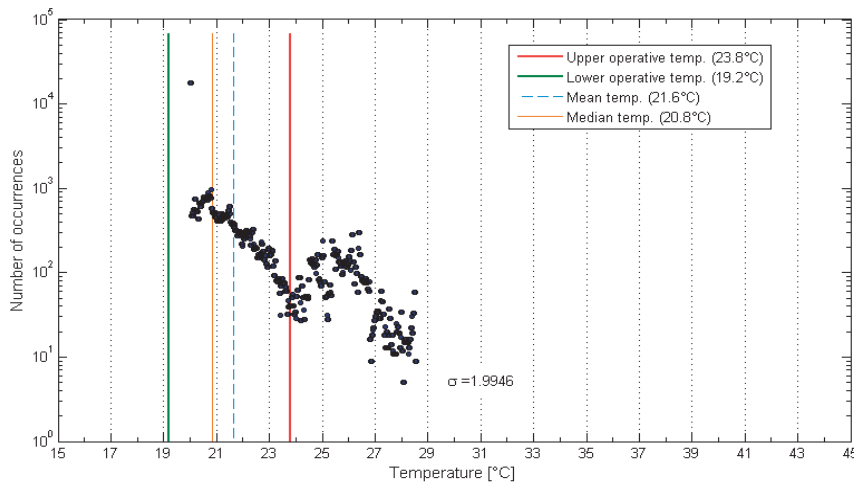
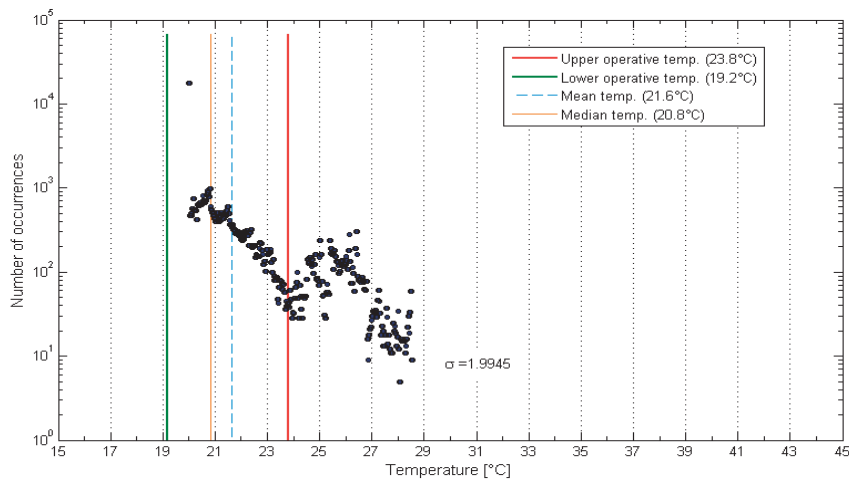
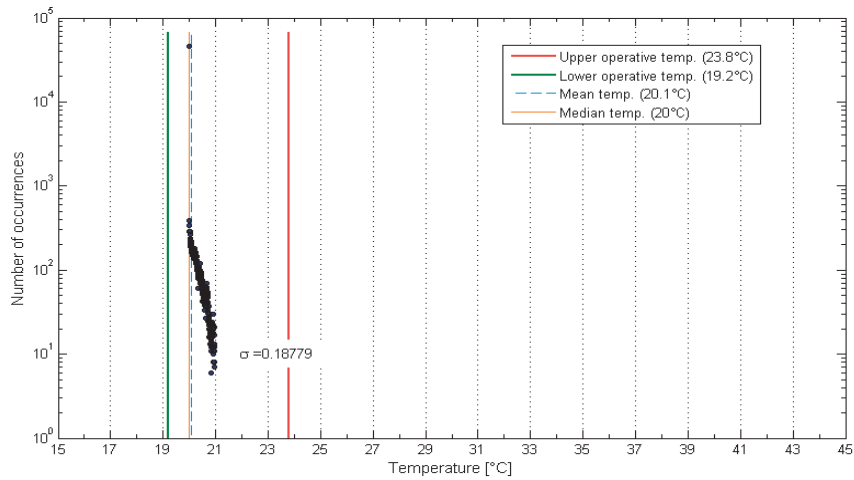


Figure 4-19. Indoor temperature values distribution during working hours in heating period (b) for simulation scenarios 4-6. Displayed are the values (black points), median (orange line), mean (light blue dashed line) and standard deviation (σ) together with the limits of the operative temperatures (green and red lines).

4.3.3. Visual comfort

Estimation of visual comfort in th(b) facis section is based on the work of Lindelöf [18] realised in LESO regarding the Bayesian optimization of visual comfort. Lindelöf calculates the user Visual Discomfort Probability (VisDP) as a function of the horizontal workplane illuminance (Figure 4-20), based on a large number (7273) of user actions on the blinds or on electric lighting⁹. Based on his work, we list the approximate illuminance limits for the VisDP as per Table 4-6:

Visual discomfort probability [-]	Workplane illuminance [lx]
< 0.30	400-500
< 0.35	300-720
< 0.40	250-1620
< 0.45	225-2000
< 0.50	210-2545
≥ 0.50	(outside the above limits)

Table 4-6: Ranges of workplane illuminance and their probability to cause visual discomfort to space occupants (approximate values derived from Figure 4-20).

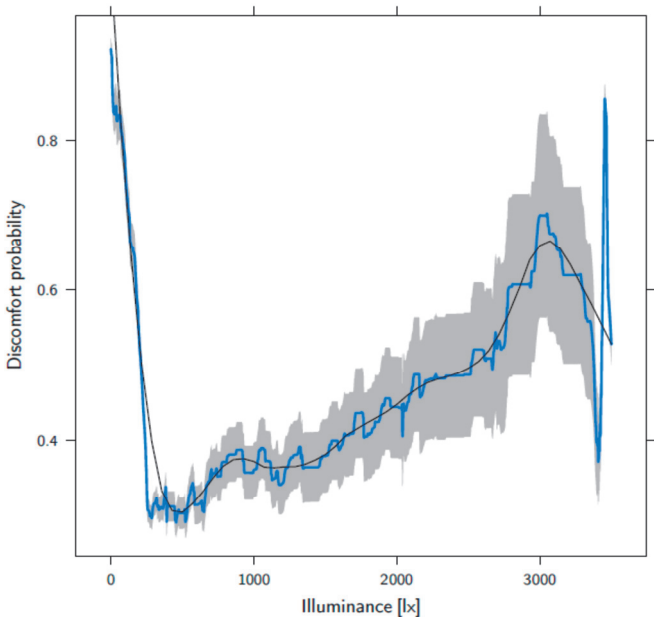


Figure 4-20. User discomfort probability as a function of horizontal workplane illuminance (values greater than ~3 klux should be ignored due to the saturation of the illuminance sensors of the study above this limit) [18] (image: ©Lindelöf).

⁹ For more details on visual comfort, please refer to Chapter 6.

Using as input for every time step of the simulation the desktop (workplane) illuminance, the VisDP was generated for every working hour in the year. The estimation of the visual comfort for the whole period (1 year) was conducted to evaluate the ability of the simulated case studies to keep the workplane illuminance within ranges (Table 4-6) which are less likely to cause discomfort to the occupants. The percentage of the working time where the visual discomfort probability is kept below 30, 35, 40, 45 and 50% was determined for all the simulation scenarios and it is presented on Table 4-7 and Figure 4-21.

Simulation scenario	Working hours/year [%] with visual discomfort probability below:				
	<=0.3	<0.35	<0.4	<0.45	<0.5
1: Standard glazing	4.7	10	26.2	29.9	35.2
2: Standard glazing + Blinds	4.7	10.1	29.2	36.9	49.2
3: Low Solar gain glazing (0.38)	13.9	25.5	58.3	65.9	74.4
4: Low Solar gain glazing (0.12)	24.9	46.4	87	94.8	99.8
5: EC Simple control	14.2	26.3	70.8	83.3	93.7
6: EC Predictive control	14	26.1	70.7	83.7	93.7

Table 4-7: Percentage of working time during the simulation period where visual discomfort probability is kept below fixed values, for each of the six considered simulation cases.

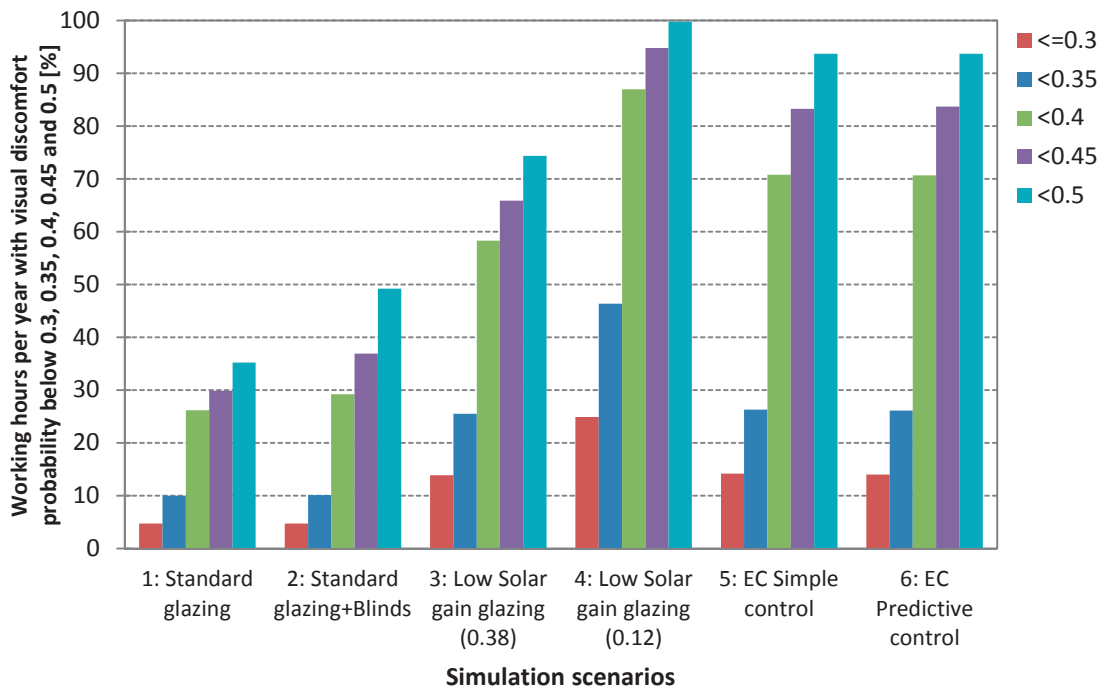


Figure 4-21. Percentage of working time during the simulation period where visual discomfort probability is kept below 30, 35, 40, 45 and 50%, for each of the six considered simulation cases.

It should be noted that predicted visual discomfort only accounts for the illuminance intensity on the workplane and does not take into consideration at all the visual discomfort due to glare phenomena.

Extreme-case scenario 4 demonstrated the best possible visual performance between the studied cases (87% of the working hours the VisDP is kept below 0.4), followed closely by the EC windows scenarios (5 and 6) and scenario 3, although that is true only for the illuminance ranges corresponding to discomfort probability below 0.35. For the thresholds of VisDP above 0.35, scenario 3 performance deteriorates as there is some dispersion of illuminance towards higher values (Figure 4-22, Figure 4-23 & Figure 4-24).

Figure 4-22 compares the distribution of desktop illuminance values of the studied scenarios. As with the temperature values, we observe the great dispersion and the high values of the standard glazing scenarios. On the other hand, scenario 4 appears “the perfect case” but we should consider that illuminances are kept to ideal only because a great deal of electric lighting is administered throughout the year. As in thermal comfort estimation, Figure 4-23 & Figure 4-24 provide additional qualitative and quantitative information about the workplane illuminance during the simulation periods. In particular, the distribution of illuminance during working hours for the entire period is displayed together with the range limits of the VisDP (Table 4-6) for each simulation scenario. Also noted on the figures are the percentages of working hours of the entire period measured inside the limits of each range.

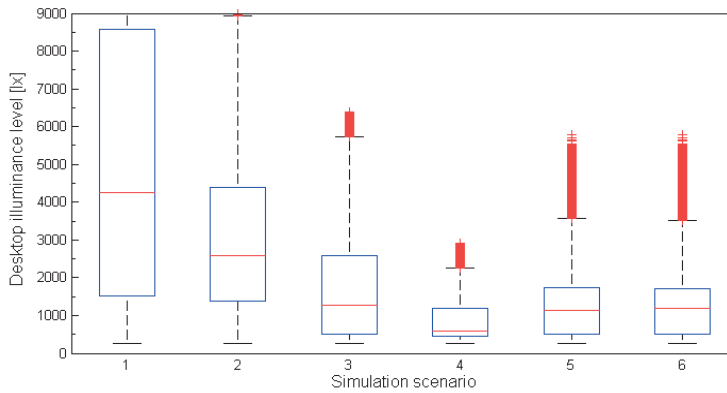
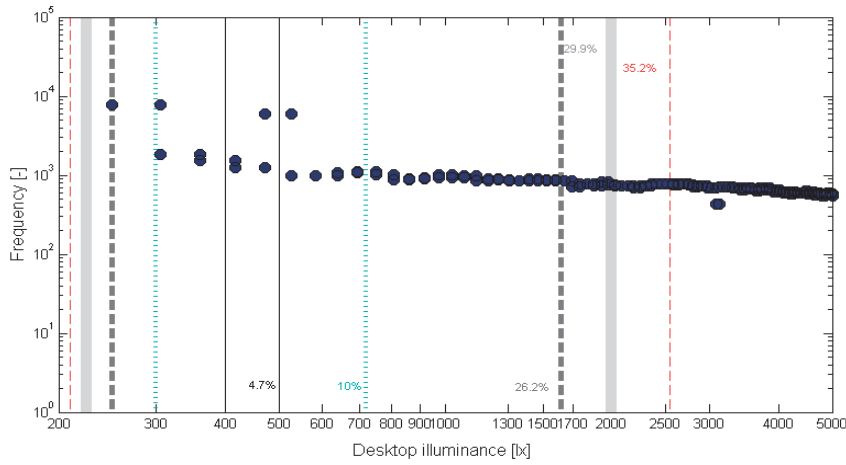


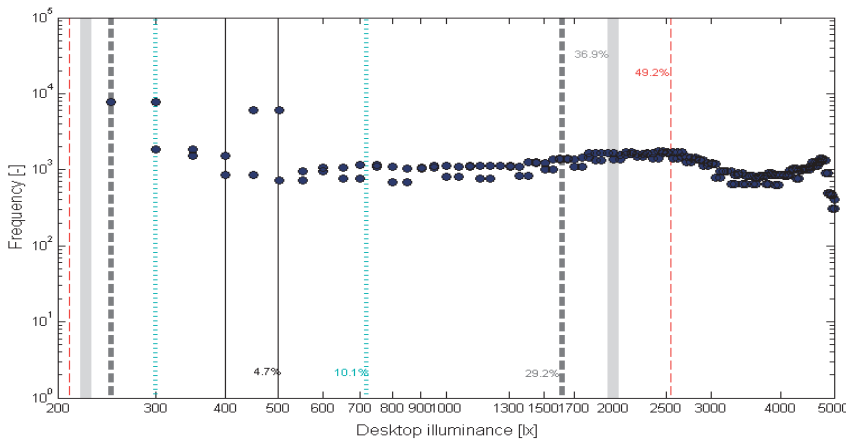
Figure 4-22. Distribution of desktop illuminance values for the six different simulation scenarios for a period of one year. The blue bottom and top of the box represent the 25th and 75th percentile respectively; the red mark inside the box is the 50th percentile (the median); whiskers represent the minimum and maximum of data points not considered outliers^h (red points outside whiskers). Top whisker of Scenario '1' is >9000 lx and it is not displayed here.

^h Points are drawn as outliers if they are larger than $q3 + w(q3 - q1)$ or smaller than $q1 - w(q3 - q1)$, where $q1$ and $q3$ are the 25th and 75th percentiles, respectively. The value $w=1.5$ used here corresponds to approximately $\pm 1.5\sigma$ and 99.3 coverage if the data are normally distributed. The plotted whisker extends to the adjacent value, which is the most extreme data value that is not an outlier [36].

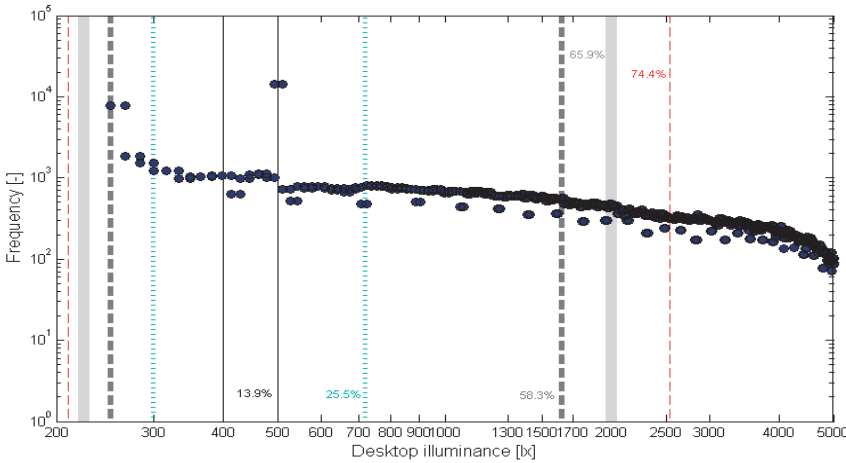
Desktop illuminance distributions during working hours



(Scenario 1)



(Scenario 2)



(Scenario 3)

Figure 4-23. Simulation scenarios 1-3: Desktop illuminance values distribution during working hours for the entire simulation period. The illuminance limits for every range of the VisDP are marked with 2 identical vertical lines for every range (see Table 4-6 for the range limits). Displayed next to the limit lines with the same colour as them are the percentages of working hours of the entire period with illuminance inside the limits of each range.

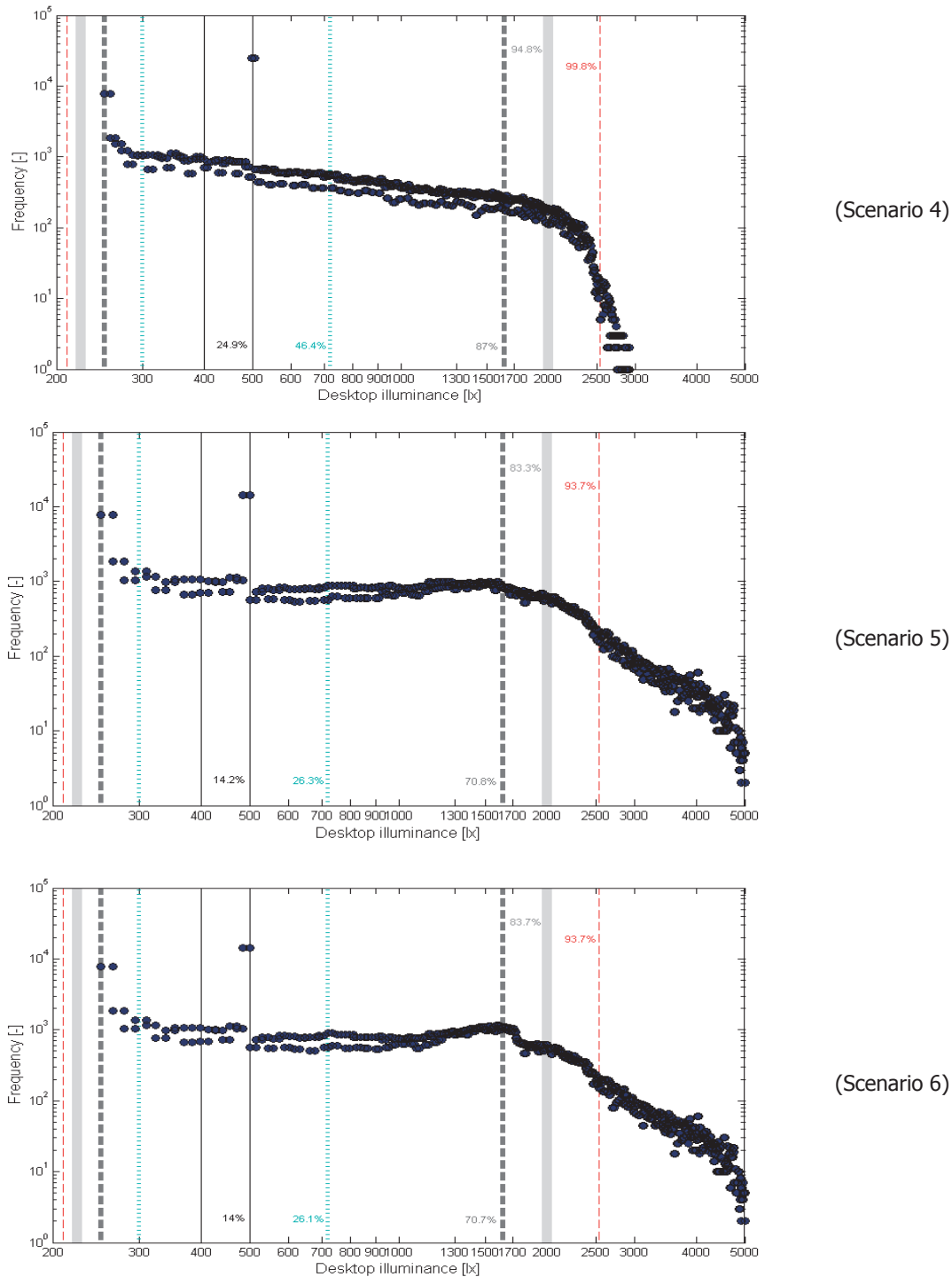


Figure 4-24. Simulation scenarios 4-6: Desktop illuminance values distribution during working hours for the entire simulation period. The illuminance limits for every range of the VisDP are marked with 2 identical vertical lines for every range (see Table 4-6 for the range limits). Displayed next to the limit lines with the same colour as them are the percentages of working hours of the entire period with illuminance inside the limits of each range.

From the results presented thus far, scenarios 5 and 6 appear to achieve same levels of visual comfort in this analysis. Nevertheless, a close look to workplane illuminance values when comparing the two scenarios against the same weather conditions and time period (Figure 4-25), reveals that predictive control strategy (scenario 6) maintains workplane illuminance more stable compared to simple control (scenario 5).

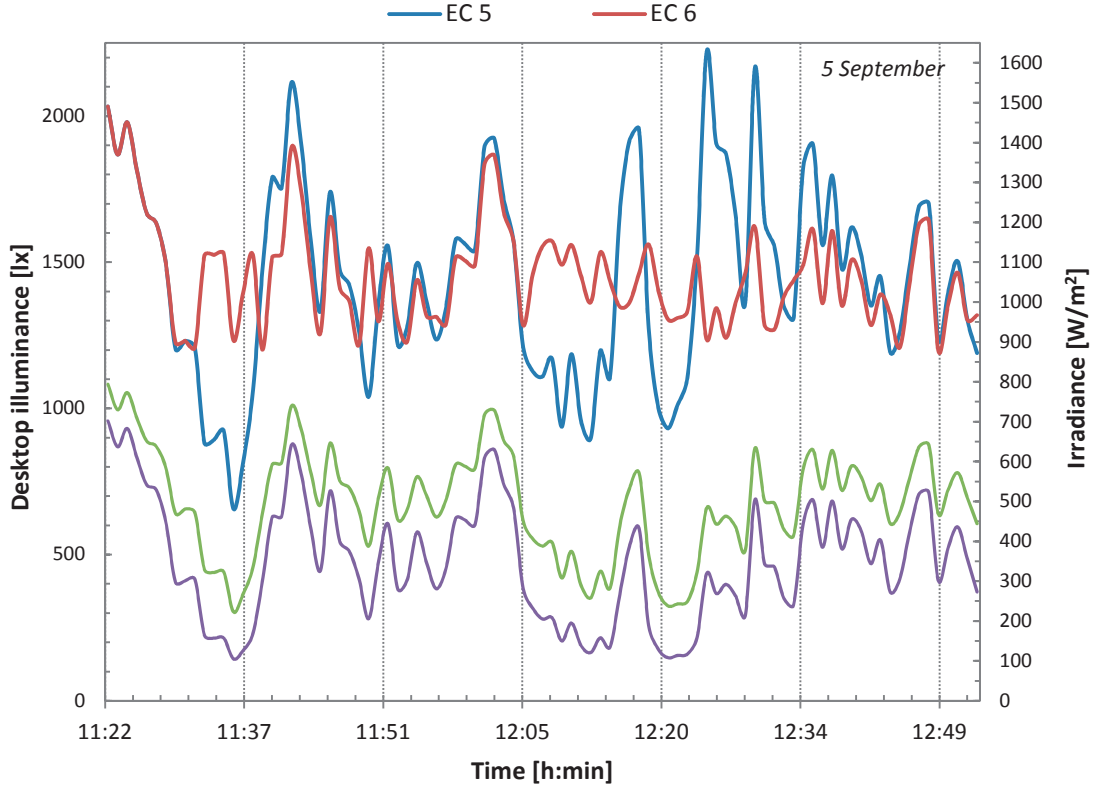


Figure 4-25. Desktop illuminance (EC 5; EC 6), Global Horizontal Irradiance (IgHor) and Vertical South Global Irradiance (IgvSouth) fluctuation around noon time on a day with intermediate sky conditions (September 5th; non heating period) for 2 different EC windows control strategies (Scenario 5 and 6).

Workplane illuminance in non-predictive control tends to fluctuate in almost perfect agreement with external irradiance levels. This is especially true under constantly varying sky conditions where the switching-time inertia of the system is in the same order as the sky variations. Matching illuminance levels for the two scenarios occur when Vertical South Global Irradiance (IgvSouth) exceeds the upper cut-off limit of solar gains (300 W/m^2) and EC glazings keep in both cases a steady transmission value of $T_v=15\%$.

4.4. Conclusion

In this section we present the evaluation of the performance of the proposed sky prediction EC control algorithm via (limited) field measurements and a parametric study.

Simulations showed that the elaborated algorithm for the automatic control of EC windows can provide better thermal and visual comfort conditions when compared to standard glazing coupled with blinds and still exhibit acceptable levels of energy consumption for space heating and electric lighting. Permanently tinted windows (solar protection windows) with a SHGC=0.38 (the same as the clear state of EC windows) can offer competitive conditions as EC windows, exhibiting slightly worse thermal and visual behaviour, especially during days when solar gains are high (sunny days) which is expected since they cannot modify their transmission and block unwanted solar radiation.

As it became evident during the comprehensive parametric study, the developed sky prediction algorithm does not outperform a simpler closed-loop algorithm based on external irradiation with no EC switching-time compensation when considering energy consumption aspects. In respect to visual comfort, the two control systems perform similarly when analysed for the Visual Discomfort Probability (VisDP). However, under varying intermediate sky conditions predictive control strategy minimizes workplane illuminance fluctuation when compared to simple control and thus, it provides a more stable luminous working environment.

The short field survey showed that user acceptance of a daylight control system including EC windows is severely impaired by the unnatural colour rendering of the room and of the view when looking outside. Also, a bigger dynamic range of possible transmissions would be positively seen by most users. As it was expected, glare issues were mentioned by some users and blinds were employed in these occasions. However, most users are willing to oversee any inconveniences or disadvantages when comparing EC windows with a standard daylight control system such as blinds, mainly favouring the unobstructed view that EC windows offer at all times.

As discussed before (Section 4.1.5), future field work including long-term measurements of the implemented EC control as well as detailed user surveys will allow for the comprehensive evaluation of the system by real users, the validation of simulation results and possible improvements of the control algorithm.

Closing, it is our belief that the research presented herein so far has confirmed the hypothesis that advanced building systems such as EC windows when integrated into a holistic building control scheme (heating, cooling, electric lighting) can create a comfortable visual and thermal environment and can be considered as a future replacement to standard window glazings with mobile solar shadings or to permanently tinted solar protection glazings.

5. SEASON MODELLING USING STATE-BASED STOCHASTIC DATA-DRIVEN MODELS

This section presents a novel approach to model the “season” variable used in building control systems by using state-based stochastic data-driven models such as the Hidden Markov Models (HMMs). In Section 5.1 we provide a comprehensive definition of the variable and identify the main factors affecting it. Next, Section 5.2 discusses the ways these factors are taken into account in the domain of building control, both in common practice and in relevant research. As the presented state-of-the art reveals, there is a scarcity of models that properly address all parameters that influence the season variable. This lack of models motivated the elaboration of a novel HMM-based season approach in Section 5.3, building on the analysis of real-life time series data obtained in the course of an 8-year period in The LESO solar experimental building. The key advantages of the proposed model are: it does not require a thorough comprehension of the underlying physical process; it is building-independent and it can be adapted to new or modified building configurations; it incorporates information of the building characteristics, the weather conditions and the user behaviour (hence, it learns from and adapts to the user preferences). The novel approach’s ability to maintain the user’s thermal comfort while preserving energy for space heating is explored in Section 5.4 and the first results (obtained through simulations) are encouraging. Finally, Section 5.5 discusses several points in relation with the proposed model and recommends possible future work.

Preliminary results on the subject of this chapter have been published by Ridi, Zarkadis et al. [87] and they are cited in-text as appropriate.

5.1. Introduction

In the domain of Heating, Ventilation and Air Conditioning (HVAC) equipment or solar protection systems control, the “season” variable plays an important role. In the very context of this thesis, in Section 3.4.2, the season is based on average external temperatures over a period of 48 hours and it is used as an input for the control of EC windows and blinds. On the simulations presented in Section 4.2, season is used again into EC windows and blinds control and it is also incorporated into the heating controller; in that later case, it is defined as a two-value variable: The value “heating season” is assigned if the average external temperature over the last 7 days is below 10°C and the value “non-heating

season” is applied for the remaining hours/days of the year. But, where do these two different definitions stem from? And which of the two – if any – is the correct one?

5.1.1. General definition of the "season" variable

In building control, season depends heavily on the weather conditions but it is not associated with the calendar seasons in a strict way. When only a heating system is present, as it is the case with the LESO solar experimental building, two seasons are usually considered: heating season and non-heating season. In buildings where full HVAC systems are installed, cooling season has also to be considered and three seasons may be distinguished: heating season, cooling season, and no heating/no cooling season. However, as we explain next, these three seasons can (and should) be considered in all buildings, independently of whether a complete HVAC is deployed. By generalising, the three different values of the “season” variable can be defined as follows:

Heating season

The heating season is defined when heating is needed to avoid that the inside temperature is getting lower than the optimal user comfort temperature. During this period, the available heat gains (i.e. passive solar, appliances, persons) are always welcome and they allow for a reduction of the heating power provided by the HVAC equipment.

Cooling season

On the other hand, the cooling season is the season when cooling is required to maintain the internal room temperature inside the occupant’s comfort limits. This can be achieved either by mechanical means (HVAC) or by other techniques such as passive night cooling or protection against solar gains (i.e. EC windows, blinds). During this period, the heat gains are never welcome (since they increase the cooling load) and they must be rejected. If the structure of the building permits so (e.g. heavy construction with significant thermal mass), “cold” should be stored in the heavy parts of the building (i.e. heavy walls or slabs) during the relatively cooler periods.

Intermediate season

While in the other two seasons there is a clear demand for either heating or cooling, the intermediate season (mid-season) is defined as the period where well-designed buildings are neither heated nor cooled actively by an HVAC system. Passive measures (i.e. accepting or rejecting solar gains, opening or closing the windows, night cooling) should be enough to regulate the inside climate and maintain the occupants’ thermal comfort. Heavier constructions hold again an advantage because the effect of short periods of relatively hot weather or relatively cool weather can be attenuated by the heat storage in the thermal mass of the building. In the extreme (hypothetical) case where a building has no thermal mass whatsoever, the mid-season is either completely absent or severely shrunk and

heating and cooling may be used successively (often in the same day) to preserve thermal comfort.

5.1.2. Factors affecting the "season" in buildings

As it becomes readily evident from the definitions given above, weather conditions (i.e. outside temperature T_{ext} or solar irradiation) is not the only factor which influences the "season" variable in building control. Season is also depended on the design characteristics of the building (heat transmission coefficient of the envelope, effective thermal mass, passive solar gains penetration and storage capability) and its use. For instance, in the case of an office building with an important number of appliances such as computers and extensive use of electric lighting, the available internal heat gains can shorten significantly the heating season but they can also extend the duration of the intermediate or cooling seasons.

Regarding the building construction characteristics, they also influence the duration of the seasons and the switching from one season to the other can be longer or shorter. As mentioned before, in the worst case scenario, poorly-designed buildings would require during the same day heating (during the morning) and cooling (during the afternoon) following closely the outside temperature variations. This (rather extreme) situation can be observed when there is an absence of enough thermal storage in the building which, in normal conditions, provides the necessary thermal inertia against external temperature fluctuations. To describe one building's thermal storage capacity, thermal mass (or thermal capacitance C) alone is not a sufficient indicator; even in cases where a construction has a relatively small thermal mass, if the building envelope has a very low heat transmission coefficient then it would allow for a satisfactory temperature smoothing. A good indicator for the quality of the building for absorbing transient heat gains is the time constant of the building τ , which is related to the response of a building to outside temperature changes [88] and it is defined as follows:

$$\tau = \frac{C}{H_L}, \quad (5-1)$$

where C ($Wh/^\circ K$) is the effective heat capacity of the building and H_L ($W/^\circ K$) denotes its overall heat loss coefficient (See Section 5.3.3). A heavy construction has a longer time constant and therefore the passage from one season to the next requires more time than in a lightweight one.

Concerning the succession of "seasons", it should be noted here that the passage from one season to the next it does not follow the "common sense", calendar-like season sequence shown in Figure 5-1(a), where seasons are succeeding one another in a periodic circle. Instead, for instance, a mid-season period in the spring can be followed by the return of a short period of heating season before switching directly to the cooling season after an abrupt rise in external temperatures. Figure 5-1(b) illustrates this sort of possible transitions.

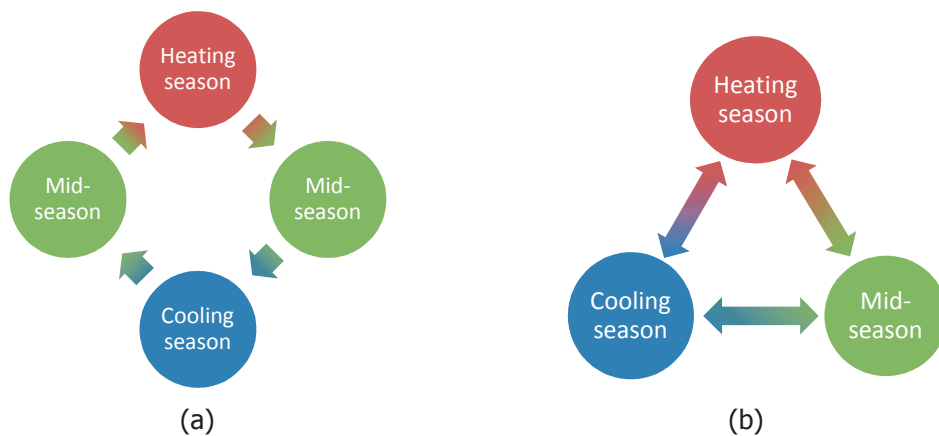


Figure 5-1. Season succession over the course of one year in (a) the classical, calendar definition of the season and (b) in season definition in building control.

Another factor that has an important impact on the aforementioned season definition orbits around the operation of the buildings by their users. Identical buildings in the same location but each having a different use integrate different kind of equipment (appliances, etc.), which in return, as discussed earlier, can prolong or reduce the duration of seasons. But even inside the same building, seasons can differ, for example, between two identical office rooms because of their users: as it is well established in related bibliography (i.e. [14; 12]), the perception of thermal comfort is strongly subjective and therefore the notion of providing a “comfortable indoor temperature” can greatly differ from person to person. Last, building occupants tend to behave differently under a given environment and this different behaviour can affect the season variable: a more eco-conscious person will be likely inclined to control the available building systems in a way that, for instance, solar heat gains are totally rejected during the cooling season and totally accepted in the heating season period.

5.2. Current practice and research status

In the previous section we set the definition and the possible values of the “season” variable in the context of building control and we identified the key factors that have a direct impact on it (weather conditions, building construction characteristics and use). In this section we present which of these factors and in what way are taken into account in the domain of building control in common practice as well as in the relevant research.

5.2.1. Calendar definition of season

As show in several studies [58; 61], the calendar definition of the season variable is still in widespread use as far as the control of heating systems is concerned. In this definition, the

heating season is fixed between two, rather arbitrarily, chosen days in the year based on the empiric knowledge of outside climate where “normally” the building is heated and the building users do not complain about feeling too cold in the building. For a building located in a temperate climate zone (i.e. Switzerland), one could define the value of the variable as being “heating season” between the 1st October and the 31st of May. In different climate zones (i.e. Mediterranean or North European), different values must be of course considered. During the heating season, the heating is turned on the entire period and rudimentary control strategies can be present depending for instance on a threshold of the outdoor or indoor temperature [61; 89], and including possibly a night setback or night cut-off. On office buildings a fixed-schedule operation based upon anticipated occupancy and use of the building is usually applied [90]. Similar considerations are taken into account for the cooling season.

In their simplicity, these control strategies that base their operation on fixed-term schedules have important drawbacks. Risk of overheating and wasting heating energy is eminent when the control strategy is not good; likewise, instances of inadequate heating can arise when cool periods occur out of the arbitrarily set heating period. Additionally, heating systems that operate in standby mode even when they are not needed, they waste energy as all systems or appliances when in standby. And when comparing these control schemes against the ones based on the season definition we attempted earlier in this chapter, we notice that the building’s characteristics are completely ignored (at least explicitly^a) while the weather conditions and the building’s use are taken into account only partially (external temperature and fixed-occupancy schedules).

Although advanced control systems are being proposed for several decades (as we will see next), their adoption in practice has been slow and hindered by mainly the requirements in hardware and software that the majority of these control systems require and secondly by the lack of properly trained commission engineers able to setup these rather complex systems [91].

5.2.2. Average outdoor temperature approach

In this approach, season definition is based on the average temperature over a defined number of n past days. The number of days should be chosen to reflect the time constant τ of the building, which ranges typically from 2 to 10 days. A temperature threshold is considered, taking into account the heating setpoint temperature, the normal free heat

^a Setting fixed-time schedules for the operation of building systems may actually incorporate an approximate empiric consideration of the building’s response curve to alternating weather conditions (i.e. the case of an attentive superintendent). However, the building’s characteristics are not used explicitly as variables in the said controllers.

gains, and the insulation characteristics of the building. This is an improvement compared to the calendar-based definition, because the building characteristics are also taken explicitly into consideration. Automatic control systems including that feature are not common, but they have been investigated by researchers, for instance for the control of heating and blinds [33; 29; 92]. This type of control was also used in three instances in the framework of the present thesis (Sections 3.4.2, 4.2 & 5.3.8).

5.2.3. Average outdoor temperature and solar radiation approach

This is an improvement over the previous definition; solar gains are additionally taken into account. At the same time, this definition requires some sort of prediction of the solar gains which is the main difficulty when implementing control schemes based on this approach. A recent study by Oldewurtel et al. [93] which uses hourly weather predictions over the next three days coupled with a Stochastic Model Predictive Control (SMPC), confirmed the high performance potential of such control strategies. Likewise, such strategies are on the forefront of research and application, forming the current state-of-the art on the building control domain, as presented next.

5.2.4. State of the art

Fuzzy Logic

One important tool for elaborating smart control algorithms is Fuzzy Logic, which allows to express domain knowledge as rules and represents facts as fuzzy sets expressing linguistic knowledge (for instance the terms “very cold”, “cold”, “medium”, “warm” or “hot” can be employed to specify temperature) [94]. Dounis et al. [95] presented a living space thermal comfort control based on Fuzzy Logic. The thermal comfort is expressed in terms of the PMV (Predicted Mean Vote) comfort index [12], which is together with the outdoor temperature the only input to the system. The system has three actuators: heater, cooler and natural ventilation (window opening). The fuzzy system was tested on a model for two different climate conditions, in summer and in winter. The results show that the system is able to keep the PMV level within the predefined range. However, no statement is made about the energy efficiency or expected energy saving of the system. A similar system was proposed by Calvino et al. [96], which tries to keep the PMV at a certain level by controlling the speed of the heating fan. Tests took place in a real room during wintertime; the system performed well, but again no information was provided given about possible energy savings.

For solar shading, Fuzzy Logic is for instance used in the system proposed by Trobec Lah et al. [97] for controlling a roller blind in respect to the lighting environment in the building. The input information of the system is: internal illuminance, global and diffuse solar radiation, and current position of the roller blind. The thermal comfort and the building characteristics are not considered by the system. Kolokotsa et al. [98] presented a fuzzy logic controller for indoor thermal, visual comfort and air quality based on a EIB building bus

and Matlab. The fuzzy logic controller is fed with the following information: PMV, outdoor temperature, heating or cooling requirement, window opening, indoor illuminance, status of electric lighting and solar shading and it generates as an output the electric lighting and solar shading position. The system was tested during a short time period in an experimental chamber of 2 m³ equipped with various sensors and results showed good performance in term of keeping the target values. No indications on energy savings were available. More recently, Kurian et al. [99] developed a combined system for controlling shading devices and electric lighting. Their system consisted of three fuzzy logic controls (glare, visual comfort, and energy effectiveness when user was absent), and an adaptive neuro-fuzzy inference system for prediction and lighting control. The control system has been compared with a simple on/off scheme and reported energy savings were between 5% and 60%. Last, in the framework of the present thesis (Section 3.4.2), fuzzy logic has been used to control EC windows, blinds and electric lights by using the available instantaneous weather information (Irradiances and illuminances, external temperature) and building state (room occupancy, user wishes/actions on building systems, workplane illuminance, and internal air temperature).

Genetic algorithms and genetic rule selection

As stated previously, fuzzy logic is based on linguistic rules established by experts. However in certain situations, experts might fail to accurately define at once the rules with optimal performance. The optimization of these rules is known as tuning and it consists of adjusting the connexions between the rules after their establishment. Genetic algorithms are used to optimize progressively the rule bases in a three step approach: evaluation, selection and alteration/mutation. Over the generations, better and better solutions appear, increasing the quality of the rule base versions. In the domain of HVAC control, Alcala et al. [100] proposed the use of weighted linguistic fuzzy rules in combination with a rule selection process where the main criteria was the energy efficiency, while maintaining the required level of thermal comfort, the indoor air quality, and the system stability. The control system was compared with a simple on/off strategy and the results showed energy savings of 14% with the rule base optimization as compared to a 9% energy saving without the optimization. In the field of shading device control, Guillemin and Morel [33; 92] applied genetic algorithm for the optimisation process of a blinds and electric light controller which adapts to the user wishes and it is optimized for energy savings when the user is not present. The controller allowed for 26% of energy savings when compared to a manual system, whereas when compared to an non-adaptive algorithm, it consumed slightly more energy but it achieved a 5% rejection rate from the users as opposed to 25% of the non-adaptive controller.

Artificial neural networks

Artificial neural networks (ANN) are mathematical models replicating the biological neural networks. An ANN is an interconnected group of artificial neurons, and it processes information using a connectionist approach for computation. Basically, an ANN is an adaptive

system that changes its structure and parameters based on external or internal information that flows through the network during the learning phase. The corresponding models being non-linear, ANN can be used to capture complex relationships between inputs and outputs, or to find patterns in data. Yang et al. [101] developed an ANN for predicting the optimal start time of the heating system in a non-residential building. For training the ANN, a building simulation program was used to collect training data for various conditions. The following input variables were used: indoor temperature, varying rate of indoor temperature, outdoor temperature, varying rate of outdoor temperature. From these factors, the start time of the heating system was predicted by the ANN. Morel et al. [59] used an ANN for the thermal model of a building to optimize the sequence of control commands for the heating in a time horizon of 12 hours. The model was progressively adapted to the real building characteristics, using the data measured by sensors.

Predictive optimization algorithms

These algorithms allow the optimization of a future control sequence over a given time horizon, using a model of the building and building services to be controlled and an algorithm to optimize a "cost function". Dounis et al. [95] use a thermal model of the building and a dynamic programming optimization process. In this case, the cost function is a weighted sum of the energy consumption and thermal discomfort, both factors being considered as inconveniences. To use such an optimization algorithm, the future evolution of the boundary conditions (weather conditions) within the time horizon has to be provided. In this controller, this prediction was using an ANN. In research carried out by Nygard Ferguson [61], the prediction of boundary conditions was done by considering the evolution of the weather within the time horizon modelled by a Markov chain.

Stochastic machine learning algorithms

Markov chains or Markov Models are stochastic approaches that have been used in research to identify parameters connected to the buildings use such as presence and activity patterns [14] or appliance recognition [102]. Gaussian Mixture Models (GMM) and Hidden Markov Models (HMM) are state-based stochastic approaches that can be used for machine learning and modelling of complex systems. Dong et al. [90; 103] proposed a building controller, which integrates local weather forecasting (temperature, solar radiation and wind speed) with occupant behaviour pattern detection (number of occupants and occupancy duration) into a real-time Model Predictive Control (MPC) design. In this context, GMM are used for the categorization of the changes of the selected features. These categorizations are then used as the observations input vector for an HMM which estimates the number of occupants. Machine learning algorithms coupled MPC design were further explored by Domahidi et al. [91] where building controllers were constructed from building data through a process that minimizes the number of input data (i.e. sensors) needed and their performance is found to be building-independent when tested in different building types.

From the preceding literature review we can conclude that in the domain of intelligent building control there is a plethora of advanced solutions and techniques available in the last decades. However, according to the definition of “season” variable given in the beginning of this chapter, there are three main factors that an ideal controller must be based on:

- Building characteristics relate to design and the construction of the envelope
- Present and anticipated weather conditions (i.e. outside temperature and solar irradiation)
- User preferences, user behaviour and building use.

By looking closely at the relevant research, there are few instances where all these factors are properly addressed. This scarcity of “all-inclusive” models is the main driver that propels our research towards a new comprehensive season model.

5.3. Methodology

The approach we follow herein builds on data mining and machine learning processes where the developed model is learnt from the analysis of time series data. The advantages of this approach are several: data-driven techniques and self-learning algorithms do not require a comprehension of the underlying physical process; the model can be adapted to new or modified building configurations (making it building-independent) as soon as new observation data are available; model incorporates information for the building characteristics, the modus operandi of its users and some statistical information concerning the dominant weather conditions [87].

5.3.1. Model framework (Hidden Markov Models) and definitions

In specific, we use HMMs which are state-based stochastic approaches. Historically they have been applied in many domains such as speech recognition, handwriting recognition, biometric authentication and financial time series analysis [104; 105], but in the later years they have been increasingly used in building control, principally in the field of occupant pattern detection [90; 106] and appliance identification [107]. HMMs offer a robust probabilistic framework to model time series, where the system being modelled is assumed to be a Markov process with hidden states (unlike the standard Markov models, where states are directly visible). In HMMs, the output tokens are visible and dependent on the (hidden) state. For instance, when modelling the season variable we “cannot see” the state in which the variable is found (heating, cooling or mid-season) but the parameters of the model are visible (e.g. external temperature or user actions with the blinds). To the best of the author’s knowledge, this is the first attempt to model season using HMMs.

Following on the example given, we consider an HMM where the “season” variable can take the value of one the following 3 hidden states:

- Heating season (HS)
- Cooling season (CS)
- Intermediate season or Mid-season (MidS)

The exact definition of the 3 hidden states is given in the introduction of this chapter (Section 5.1.1); the variable is considered “ergodic”^b and the possible transitions from one state to the next are shown in the Figure 5-1b.

5.3.2. Observations (features) vector and data mining

To be able to model and identify “season”, a feature vector $X = \{x_1, x_2, \dots, x_n\}$ with n different components is chosen. The components x_1, x_2, \dots, x_n are the system variables which combined can give an indication of the current (hidden) state. As explained previously, there are 3 main factors that affect season and the following selection of features reflect all three of them. Selection of course is always limited by data availability. In this study, we involve the signals from HVAC, window opening, window blinds, external and internal temperature and solar irradiation [87]. Data used comes from the LESO database which includes over eight years of multiple sensor and actuator data recordings. More details concerning the database can be found in Section 2.2.2 as well as in an article by Zarkadis et al. [28].

Vector components

The feature vector has $n=8$ components and consists of the signals of 7 actuators and sensors^c and of one calculated parameter (τ). The signal of an 8th actuator, the heating power switch, is used as the “ground truth” for the value “HS” of the season and it verifies the outcome of the model.

$$X = \{T_{ext}, T_{int}, Window, Blind, I_{gh}, \tau\} \quad (5-2), \quad \text{where:}$$

- T_{ext} is the instantaneous outside temperature and it is one of the two parameters that provide information on the weather conditions.
- T_{int} is the internal temperature.
- $Window$ gives the information about user interactions with the windows. This information can be interpreted in (at least) two ways: the opening of windows is

^b In this context, it is meant that any state can be reached from any other state at any given step (Figure 5-1b).

^c The components “blinds” and “window actions” are constituted from the output of 2 actuators (and 2 sensors respectively) each: there are 2 blinds in the room, one for the anidolic window and one for the lower part as well as two openable windows. T_{ext}, T_{int}, I_{gh} correspond each to the output of a separate sensor. Hence, 7 actuators/sensors in total provided data to the observation vector.

either linked to the need of air exchange between inside and outside for sanitary reasons or to overheating (or both). Measurement of inside pollution may allow to distinguish between the former and the need to exchange inside air and cooler outside air, which is a clear indication of overheating risk and therefore of being currently in the cooling season.

- *Blind* denotes the user actions with the available blinds. Their use may also be triggered by two situations: daylighting glare (during any season) or protection against overheating (during CS only).
- I_{gh} represents the instantaneous global horizontal solar irradiance and it is the second parameter that gives information on the weather conditions.
- τ denotes the time constant of the building, as it is defined in Section 5.1.2 and is the parameter that gives valuable information on building characteristics. It does not derive from recorded data but it is calculated as shown next.

5.3.3. Building's time constant

As mentioned earlier, a good indicator for the quality of the building for absorbing transient heat gains is the time constant τ of the building, which is related to the response of a building to outside temperature changes [88] and it is defined as follows:

$$\tau = \frac{C}{H_L} \quad (5-3),$$

where C ($Wh/^\circ K$) is the effective heat capacity^d of the building and H_L ($W/^\circ K$) denotes its overall heat loss coefficient. It's inclusion into the elaborated model is important for the portability of the model in other buildings or in unseen configurations. The overall heat loss coefficient is calculated using the expression:

$$H_L = \sum_{j=1}^k U_j A_j + \rho C_p V, \quad (5-4)$$

Where U_j is the overall heat-transfer coefficient ($W/^\circ K m^2$), A_j is the outdoor surface (m^2) of each of the k external building elements of the envelope (i.e. exterior walls, roof and fenestration); ρ (kg/m^3) and C_p ($J/kg ^\circ K$) are the density and the specific heat of the air, respectively, and V denotes the volume-flow rate of the infiltration and ventilation air (m^3/s). The total heat capacity of the building can be expressed:

^d The effective heat capacity C relates to the ability of the building to smooth down the diurnal (short-term) temperature variations and it is only a fraction of the building's total heat capacity C' , which expresses the long-term thermal storage capacity of the building due to its entire mass. The relation connecting the two can be written as: $C = a_0 C'$, where $a_0 \in (0,1]$ is a correction coefficient.

$$C' = \sum_{i=1}^l V_i \rho_i C_i, \quad (5-5)$$

where V_i (m^3), ρ_i (kg/m^3) and C_i ($\text{J}/\text{kg } ^\circ\text{K}$) are the volume, the density and the specific heat of each of the l different structure elements of the building inside of the insulation layer (i.e. slabs, walls, furniture, etc.) [108].

This is the generally formulated expression of the building time constant. However, Antonopoulos and Tzivanidis [108] claim that “an experimental investigation, as well as comparisons with more elaborate time-constant models, showed that [the above equations] lead to overestimations of τ exceeding 100%”. Reddy et al. [109] use the presented calculation method but they point out that it is based on heating losses and not on cooling load; therefore small differences may occur when one attempts to use it also for cooling load estimation. Antretter et al. [110] use the above equations with the addition of 2 coefficients, but this transformation was adapted to “continuously heated buildings (heated more than 12 hours per day)”.

Following the relevant bibliography and based on the above equations, we calculated the LESO time constant, for which we have the empiric knowledge of being a heavy building with an increased time constant that is approximately 7 days. We found that the use of a coefficient $a_0 = 0.5$ corresponds well to the ground truth and it confirms the claims of Antonopoulos and Tzivanidis [108] for a 100% overestimation resulting from the calculations above. Subsequently, the final expression for the calculation of the time constant becomes:

$$\tau = 0.5 \frac{C'}{H_L} \quad (5-6)$$

It should be noted however that this expression is valid for the LESO building and is probably accurate to a certain extent for rather heavy building constructions. It should be used with caution to other buildings.

5.3.4. Data pre-processing

Before their inclusion into the HMM toolbox, data had to be prepared and structured accordingly. Four main data types were structured: training sets (cTr), testing sets (cTs) and their corresponding label vectors: labTr for the training data sets and labTc for the testing data sets. Both training and testing sets are clustered into three categories that correspond to the three different hidden states we attempt to identify: HS, CS and MidS. The label vectors are used as indexes which indicate the category of each set. Although it may seem counter-intuitive, labelling the test sets is required by the HMM toolbox in order to output the identification accuracy of the resulted model in the confusion matrices (see Section 5.3.6).

The training and testing sets are structure arrays^e that group related data using data containers called fields. They contain D observations. Every observation O in both training and test set has to be an element "c" of the structure and access to the data of the structure is possible through the use of dot notation of the form $c1(i).c$. The observations are allowed to have different lengths (T) but they must have the same dimensionality (P). Hence, every observation is a matrix of $P \times T$ dimensions. In this case, the observations have always $P = 8$ dimensions (exactly as the components of the observations vector; see Section 5.3.2). Their length varied from about 800 to 1800, depending on data granularity (see next).

Before the preparation of data into data structures of testing and training sets, the observation vector data had been extracted from the original MySQL database (Section 2.2.2) and filtered out. The filtering consists of:

- Excluding periods of time where data recording has been problematic (i.e. interruptions in recording due to data logging malfunction).
- Homogenization of the data. When multiple values of a recorded variable exist per hour (i.e. in the case of I_{gh}), an averaged value was considered over a fixed time-step. Multiple training/testing cycles were attempted with data averaged down to fixed time-steps of 1h, 30 and 15 min (which are sufficient when thermal comfort is regarded).

5.3.5. Labelling rules of data sets

As described in section 5.3.4, labelling^f of the training and testing sets had to be performed. The following rules were applied to assign one of the 3 possible hidden states to the observations:

- HS: When heating has been switched on over the last 24h.
- CS: When $\bar{T}_{ext} > 25^{\circ}C$ over the last 24h or if the windows have been kept open for more than 15 min over the last 1h^g.
- MidS: All the remaining time series.

^e Matlab "struct arrays"

^f = spitting data into three categories (classes) that correspond to the three different hidden states we attempt to identify: HS, CS and MidS.

^g When the outside temperature is too high, windows are likely to be kept closed; on the other hand, when they are opened up for a brief time only (15 min), we consider that the user wants to exchange the air of the room with fresh air from outside, not to deal with overheating risks.

5.3.6. Model training and testing

After pre-processing, data structures were ready to be trained. An HMM toolbox in Matlab with a comprehensive library has been built in the framework of the Green-Mod research project by A. Ridi^h. Therefore, it should be noted that the work presented in this subsection describes work not performed by the author of this PhD thesis; however, and on the grounds of completeness, a general description of the process and of the main algorithms used is provided herein.

The training of the HMMs consists in the creation of a transition matrix and the emission matrix, which is expressed by the Sigma, the Mean and the Weight matrices (see definitions next). For every class, a model is created characterized by those matrices.

In specific, training is composed of three main phases:

- Initialization of the transition matrix
- Initialization of Mean, Sigma, PComp (weight) matrices
- Convergence of the model

For the first phase, we initialize the transition matrix having N states (including the first-entry and last-exit, which are non-emitting). A simple example with an ergodic variable ($N=4$) is given in Table 5-1. In this example, we have 2 "real" states plus the start and end state (4 in total). When starting, there is a 0.5 probability of transiting to each of the 2 states. When we are in state 1 or 2, 3 transitions with the same probability (0.33) exist: we can switch to 1, 2 or exit (end). Once ended, we cannot return back.

	Start	1	2	End
Start	0	0.5	0.5	0
1	0	0.33	0.33	0.33
2	0	0.33	0.33	0.33

Table 5-1: Transition probability matrix of an ergodic variable ($N=4$).

For the second phase of the initialization of Mean, Sigma, PComp (weight) matrices, we proceed as follows:

1. An initialization function takes as input all the training observations of a specific model, the number of states N and the vector of Gaussians K . As a first step, a

^h PhD candidate specialized in data-driven machine-learning algorithms in the University of Applied Sciences of Western Switzerland (HES-SO), Fribourg, Switzerland.

vector containing all the set of points of all the observations associated to a specific state is created.

2. Then, we create a number of vectors equal to the number of states. For every vector we have a series of points in a P -dimensional spaceⁱ. For those points, we perform k-means clustering, using as a number of clusters the number of Gaussians K . That way, we use this clustering as a starting configuration for the next step.
3. We then use the Expectation-Maximisation (EM) iterative algorithm for computing the distribution of the Gaussian Mixture Models. A GMM is a parametric probability density function computed as a weighted sum of Gaussian component densities [107]:

$$p(x_n|M_i) = \sum_{i=1}^I \omega_i N(x_n, \mu_i \Sigma_i) \quad (5-7),$$

where x_n is the feature vector, I is the number of mixtures, ω_i is the weight, N the Gaussian densities, μ_i is the mean ($P \times 1$ vector), Σ_i is the ($P \times P$) covariance matrix and M_i is the model for the Gaussian mixture i . It should be noted that the following constraint is satisfied:

$$\sum_{i=1}^M \omega_i = 1$$

Next, we assume that the selected features of the observation vector are not correlated. That way we simplify the GMM computation by using diagonal covariance matrices. An additional assumption regarding the independence of the measurements used, allow us to compute the global likelihood score S_i for the sequence of our feature vectors:

$$X = \{x_1, x_2, \dots, x_n\},$$

given a model M_i , as follows:

$$S_i = p(X|M_i) = \prod_{n=1}^N p(x_n|M_i) \quad (5-8)$$

To compute this expression and to fit a mixture model to a given set of training data, we call the EM algorithm [111]. For each state of the season variable, all data

ⁱ P is equal to the number of the components of the observations vector.

sets labelled with that state are used to compute the model M_i . Since the EM works in an iterative way, we use the starting configuration of the k-means clustering discussed above in (2) as the starting point (as initial values of the Gaussian distributions $N(x_n, \mu_i, \Sigma_i)$). Assuming equal priors, the likelihood performs the classification according to the Bayes rule (see also 6.2.3).

4. Following the implementation of the EM algorithm, we obtain K Gaussians. Inside a specific model, we have a certain number of states; we make the hypothesis that the number of Gaussians K is constant within the states: we have the same number K of Gaussians for every state in the same model. In this way we build the following matrices:

- $MI(p, i, k)$ is the matrix of means. It is a 3-dimensional matrix where p is the dimension (P the total), i is the state (out of total M) and k denotes the Gaussian (K in total).
- $SIGMA(p, i, k)$ is the matrix of standard deviations. It is also a 3-dimensional matrix (annotations as before).
- $PComp(i, k)$ is the weight in the mixture of Gaussians. It is a 2-dimensional matrix (with annotations as above). It is not depended on the dimension; hence p is absent.

Regarding the EM algorithm, it calculates a diagonal matrix. For this reason the MI and the $SIGMA$ matrices are of the same dimension.

In the next phase, the convergence of the model is computed by calculating the probabilities and the alignment through the Viterbi algorithm, through the following steps:

- Verifying the presence of enough observation vectors to initialize all states.
- Calculation of the probabilities and the alignment using the Viterbi algorithm.
- Re-estimation of HMM (re-estimation of transition matrix).

The Viterbi algorithm is a dynamic programming algorithm used to find the best state sequence (among hidden states) that results in a sequence of observed events (our training data). We test all the models against the test data sets and we search the most probable among the models. Along with the observation, we take as input the three matrices that derived earlier from the training as well as the transition matrix which had been initialized during the first phase. Then, we test a specific observation $\{O_x\}$ using the Viterbi algorithm, which computes the alignment and the associated probability (best score). This time we take into account only the probability in order to find the most probable model. We create a vector of probability, one for every model, and we chose the most probable. Rabiner [112] describes this process as follows:

If $Q = \{q_1, q_2, \dots, q_T\}$ is the best single state sequence for a given observation sequence $O = \{O_1, O_2, \dots, O_T\}$, we define for the model λ as $\delta_t(i)$ the best score (highest probability) along a single path at time t (accounts for the first t observations) that ends in state S_i :

$$\delta_\tau(i) = \max_{q_1, q_2, \dots, q_{t-1}} P [q_1 q_2 \dots q_t = i, O_1 O_2 \dots O_t | \lambda] \quad (5-9)$$

By induction:

$$\delta_{\tau+1}(j) = [\max_i \delta_\tau(i) a_{ij}] \cdot b_j(O_{t+1}) \quad (5-10),$$

where a_{ij} denotes the state transition probability between states i and j and b_j represents the emission probabilities of state j . To get the actual state sequence, we keep track of the argument which maximised (5-10), for every t and j .

The Viterbi algorithm is executed for every observation and finally the confusion matrix is given as output. The confusion matrix presents the classification performance for every hidden state of the HMM on the test data sets. Given that the test data are not imperatively balanced among the classes, the confusion matrix is constituted by the number of observations and not by their percentage. However, to improve presentation and to easy comparisons between models, the numbers in the matrix (observations correctly identified) are divided by the population of every class so that the accuracy per class expressed in percentages is presented, like in the Table 5-2 below.

Confusion matrices

In the end of each training/testing campaign, we obtained the confusion matrices which summarize the identification accuracy of the developed HMM-based season model. As also reported by Ridi et al. [107], best results are obtained with a number K of Gaussians greater than 15. However, no significant differences were found between observation vectors with different granularities (15, 30 min and 1-h averaged data) concerning the same training/testing periods. Multiple tests revealed that a training period of 6 to 9 months of recorded data is necessary to produce a satisfactory model. The best results obtained are presented in Table 5-2 and show that HS was identified with an accuracy of 91% followed by CS and MidS.

	HS	CS	MidS
HS	91	0	9
CS	0	85	15
MidS	19	12	69

Table 5-2: Confusion matrix showing accuracy per class (in percentages). Results were obtained with 9-month training data with 1-h granularity for the GMMs with 17 mixtures.

“Higher accuracy is observed when identifying heating or cooling seasons, while it drops significantly for the intermediate season. This is expected behaviour as intermediate season is not a crisp state and it is far more hard to define and thus to correctly identify. Also, the absence of active cooling in LESO building adds a further difficulty in the validation of our model, as it would have provided us with an (accurate) indication of the cooling season” [87].

5.3.7. Model simplification: Feature selection

The model that was obtained through the process above it is a satisfactory first attempt to model season using HMMs. However, two questions arose after our first results:

- *Is HMM-based season modelling just a purely academic exercise, or can it be used in the building control domain?*
- *If yes, can we simplify the observation vector and make our model applicable in buildings where a limited set of sensors/data is available?*

To answer the first question, it has been decided that simulations would be the logical first step to evaluate the model’s performance. The use of the developed model “as is” for the simulations (i.e. keeping the observations vector intact), it requires the utilisation of synthetic values for user’s actions on windows and blinds, either based on simple occupancy heuristic rules or on stochastic approaches, such as the discrete-time Markov process proposed by Haldi [14 pp. 39-102]. The necessary modules for windows and shading devices would then have to be built and incorporated in to the Matlab simulation code (see next Section) or a suitable simulation tool, such as IDA/ICE, would have to be used and customized accordingly. However, when also considering the second question above, it was decided to reduce the terms of the observation vector so it can be used in building configurations where only a minimum set of sensors is installed. The new reduced observation vector is comprised of 3 terms:

$$X' = \{T_{ext}, I_{gh}, \tau\}. \quad (5-11)$$

The indoor temperature too was eliminated from the observations for practical reasons related to the simulations^j; however we feel that it should probably make sense to be included in a future final version of the model.

^jOn data recorded in real buildings, T_{int} is usually readily available and, as such, it can feature in the observation vector fed to the HMM algorithm. However, in (dynamic) thermal simulations it is calculated at every time step given a number of different parameters (i.e. T_{ext} , etc.). The inclusion of T_{int} in the simplified model, it would have required the “live” connection between the thermal simulation code and the HMM season code at every iteration instead of just once per simulation run (see 5.3.8), which would be impractical.

The initial selection of the seven features that constituted the original observations vector was based on an “expert’s knowledge” decision. The subsequent elimination of features from the observations has been performed on the grounds of facilitating the simulation process and catering to sensor-poor buildings. To avoid subjective or even erroneous decisions, a formalised approach for feature selection (and reduction) could have been used. For instance, Domahidi et al. [84] utilize the *GML AdaBoost Matlab Toolbox* to assign weighting factors to all available features; future selection is performed by selecting the sensors or actuators that contribute to the highest weighting factors. In the framework of the Green-Mod project mentioned earlier, the developer of the HMM algorithm will likely include a module for a feature selection in the future.

Confusion matrix of the simplified model

Following the feature elimination and the creation of the new observation vector, multiple training/testing campaigns were performed. Best results are obtained with a number K of Gaussians greater than 21. This time, only 1-h averaged data were used for training/testing. The best results obtained follow the pattern of the first model where HS is much more accurately detected (83%) than CS and MidS (Table 5-3). General accuracy however is reduced when compared to the first model (Table 5-2), with CS being particularly affected (15% less accurate than before) while both HS and MidS are 9% less accurate when compared to the first model.

	HS	CS	MidS
HS	83	1	16
CS	1	72	27
MidS	22	15	63

Table 5-3: Confusion matrix showing accuracy per class (in percentages) for the simplified modes (3-feature observation vector). Results were obtained with 12-month training data with 1-h granularity for the GMMs with 21 mixtures.

5.3.8. Simulations

To assess the efficiency of the newly developed model (the simplified one) when it is integrated into building control, we ran simulations of different control schemes and construction types against the varying meteorological conditions of one year. The simulations (presented next in Sections 5.4.1 and 5.4.2) employed the same nodal thermal model described in Section 4.2.2 and focused on the energy consumption for space heating and on the estimation of thermal comfort.

The Matlab code was further expanded to include a new module for calculating the building’s time constant discussed earlier which is fed as an input in the “season’s” observation vector (and thus taken into account in the heating controller). A connection module was implemented which interfaces with the HMM Matlab code described above. In an iterative process, the observation vectors of each time step are fed into the HMM season model and

the season value is returned for each step and stored in a “season” matrix, which is used later during the simulations. The chosen time step for the simulation was one hour, which is sufficient when only heating and thermal comfort aspects are considered and it is also remarkably less computationally expensive than when shorter time steps are chosen.

Simulated scenarios

The parametric study compared the following four cases of a South-facing office room:

1. A typical LESO office with standard heating/blinds control;
2. A typical LESO office with control based on the HMM season definition;
3. An office room in a light-weight building with standard heating/blinds control;
4. An office room in a light-weight building with control based on the HMM season definition.

Description and characteristics of the simulated office rooms

The office room used in the first two simulation cases is a simplified nodal model of a typical South-facing LESO office room, exactly as described in full detail in Sections 2.1.1 and 4.2.4.

Construction elements	LESO office room	Office room in a light-weight, non-insulated building
Floor area	15.7 m ²	
Room height	2.8 m	
South façade wall (layer 1)	2 cm plaster panel	
South façade wall (layer 2)	12 cm thermal insulation [0.04 W/m·K]	5 cm concrete
South façade wall (layer 3)	3 cm wood	
Window area (including frames)	5.10 m ² (frames area: 17%)	
Glazing	SHGC=0.4; U-value=1.1 W/m ² K (same U-value the for the frames)	
Blinds	Textile tissue with 20% solar gains transmission when completely drawn	
Partition walls (internal)	10 cm (concrete bricks)	5 cm (concrete bricks)
Floor screed	6 cm (concrete)	4 cm (concrete)
Ceiling slab	25 cm (concrete)	5 cm (concrete)

Table 5-4: Main characteristics of the two different office rooms in the considered simulations. (Wall layer 1 is the inside layer and layer 3 is the outside one).

The only difference is that no EC glazings are present; instead, standard IGUs are considered with a SHGC transmission of 40% (equivalent to low solar gain windows). U-value, frame-to-window ratio and all other characteristics remained unchanged.

Regarding simulation scenarios 3 and 4, an office room identical to the typical LESO room above was considered, the only exceptions being the absence of insulation^k and that the building structure considered is a much lighter one with low thermal mass (i.e. much thinner walls, slabs, etc.). The main characteristics of the two different rooms are summarized in the Table 5-4.

Meteorological data

The meteorological data used for the simulation are synthetic values for one year generated by the Meteorm software [84] for the village of Ecublens near EPFL and LESO building. Time interval was set to one (1) hour which is also the simulations' time-step as explained above. The generated data which were used in the simulations included hour of the day, day and month of the year, external temperature, global horizontal and global vertical south solar radiation. The values of T_{ext} and I_{gh} additionally went through the structure transformation needed by the HMM module (See section 5.3.4).

Standard heating control system

In simulation scenarios 1 and 3, we use a simple, closed-loop control system based on the internal air temperature and the season definition as given in the Section 5.2.2. The set point for the heated zone temperature is 20°C (no night setback schedule is implemented). At every time step the controller checks whether the temperature is below the set point and if the season is set to "heating season"; if both conditions are met, then it injects the necessary amount of energy in the room so that the temperature can reach the set point value (no hysteresis is implemented). A time step is considered as heating season if the average external temperature over the last 7 days is below 10°C.

To reflect the current situation of LESO building neither active nor passive cooling system is employed. Also, as mentioned earlier, ventilation is only through infiltration and windows remain closed at all times (see 4.2.4).

Heating controller based on the HMM season definition

In simulation scenarios 2 and 4, the heating controller bases its operation on the novel season model developed in this study (simplified model). Again, the set point for the internal temperature is set at 20°C with no implementation of night setback or occupancy schedule.

^k Although it can be argued that the absence of insulation is an extreme scenario, it has been chosen to test the capabilities of the developed model under difficult conditions.

The operation of the controller stays the same as above when a simulation step is labelled as "heating season". However in this case, the season can take three values (Heating, Cooling or Mid-season) and is dependent on the values of the input vector $X' = [T_{ext}, I_{gh}, \tau]$, at each time step as described in Sections 5.3.2 & 5.3.7. When the season is labelled as cooling or mid-season, the controller stays idle as no cooling system is considered (same as above). However, these seasons are used by the blind controller as it can be seen next.

Blinds controller

For simulation scenarios 1 and 3 (standard heating/blinds control), a simple closed-loop control is used based on the global vertical south solar radiation (I_{gvs}), internal air temperature (T_{int}) and the season (as defined in the section *Standard heating control system* above). During the "heating season", if the T_{int} is lower than 25°C then solar gains are welcome and the blinds are completely open. If the temperature is over that limit, solar gains are rejected and blinds are completely closed. In the "non-heating season", if the T_{int} is over 23°C, solar gains are rejected to the maximum. In the case that the temperature is lower than 23°C¹, blinds are kept fully open for an I_{gvs} below 100 W/m²; fully closed if it exceeds 300 W/m² and assigned linearly interpolated open/closed ratio values for solar radiation values between 100 and 300 W/m²^m.

For simulation scenarios 2 and 4 (HMM season definition), when the label "cooling season" is applied by the new season model, the controller blocks as much as possible the solar heat gains by keeping the blinds fully deployed keeping up with the season definitions given in the beginning of this chapter (Section 5.1.1). Likewise, in the winter (heating season) they are kept fully open. When the time step is labelled as "mid-season", then the simple control strategy based on the I_{gvs} and T_{int} described above for the non-heating season is applied.

Occupancy schedule

For the estimation of thermal comfort we consider the presence of a single occupant only during the working hours with a 9-hour daily schedule of 08.00 to 18.00 with a lunch break (absence) from 12.00 to 13.00, 5 days per week.

¹ Approximate lower temperature limit where an average person feels comfortable inside an office room during the summer period given a set of parameters; please refer to Section 4.3.2 and to Fanger's model [12] for more details.

^m The open/closed ratio is '1' for 100 W/m² and '0' at 300 W/m².

5.4. Results

5.4.1. Energy consumption

The results of the parametric study regarding the energy consumption for space heating for the four different considered cases are shown on Figure 5-2. As expected, under the same conditions a building with heavy structure and good insulation (i.e. LESO) requires much less energy (-30%) for space heating during one year than a building with low thermal mass.

When comparing the control schemes that were applied, we note that a 7% reduction in energy consumption can be achieved when a LESO office room is controlled with the newly developed HMM season model. On the other hand, for a light-weight building, the energy consumption practically stays the same. This is expected behaviour: structures with increased thermal inertia require a more delicate energy planning because of their intrinsic slow response in external temperature variations. It seems that the incorporation of the building's time constant in the decision for the season identification (and hence the heating and blinds control) contributes in this direction. On light-weight structures, the demand of a good (predictive) control is less crucial and simple control schemes based on the outside temperature are likely to yield satisfactory results. Notwithstanding the foregoing, when it comes to poor building constructions (i.e. low thermal mass, inadequate insulation, etc.), primarily focus should be given to improving the structures themselves before considering the application of intelligent control algorithms.

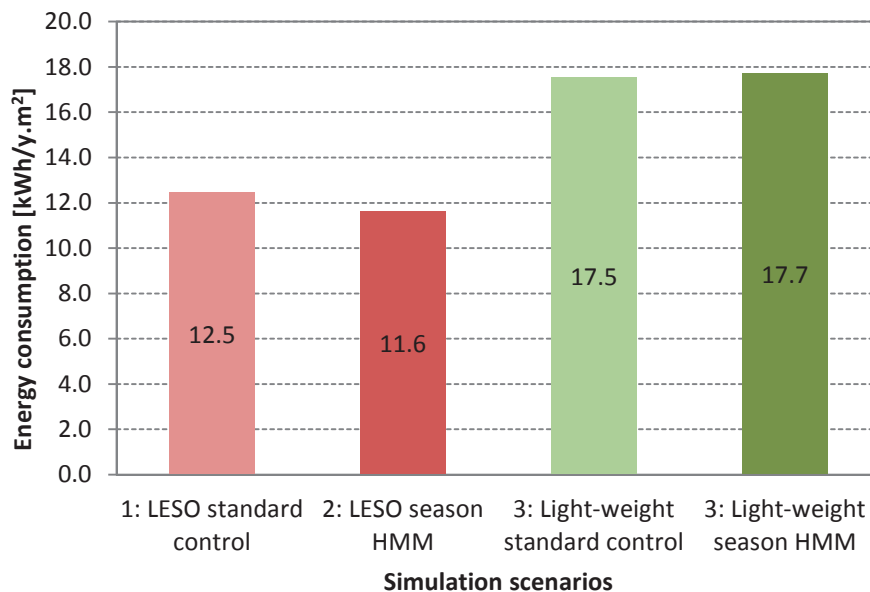


Figure 5-2. Annual energy demand for space heating for different simulation scenarios.

However, the comparison of energy consumption it should be viewed against the quality of the indoor environment that each of the compared test cases offers to potential occupants. With this in mind, these 4 scenarios are compared in respect to the predicted thermal comfort in the next Section.

5.4.2. Thermal comfort

Indoor air temperature

Akin to what was presented previously in Section 4.3.2, as a first indication of thermal comfort, we compare the indoor temperature across the different simulation scenarios. In Figure 5-3, Figure 5-4, Figure 5-5 and Figure 5-6, we can immediately notice the strain to keep the indoor temperature from being either too high or too low during some intermediate season days in March and September. However, when comparing the HMM control scenarios (2 and 4) with the standard control ones (1 and 3), it is evident that the HMM-based control copes much better with the mid-season difficulty. And, in the case of autumn, it notably raises and keeps the T_{int} around 20-22°C and it does so without spending extra energy for heating; apparently the good season identification manages to deploy much more efficiently the blinds and thus, take advantage of the free solar heat gains. On the other hand, the “standard” controller apparently is cutting-off most of potential solar gains from entering the room in days when they would have been beneficial for the conditioning of the space.

When comparing the cases 1 and 2 (heavy construction) with the 3 and 4 (light weight construction), we can observe that the internal temperature tends to fluctuate in the later cases much more than it does in the first ones. This is of course due to the important thermal mass of the heavier building which is capable of smoothing out to a good degree the variations of weather disturbances. But, even in the case of a poorly designed building, the HMM-based control seems capable of partially reducing the amplitude of the fluctuations of the internal temperature (Figure 5-5 & Figure 5-6).

However, it should be noted that the high temperatures observed in March and September are expected since neither cooling nor any form of ventilation is considered in the building model. In an actual case, users would mitigate the overheating risk can by simply opening the window during mid-season or summer.

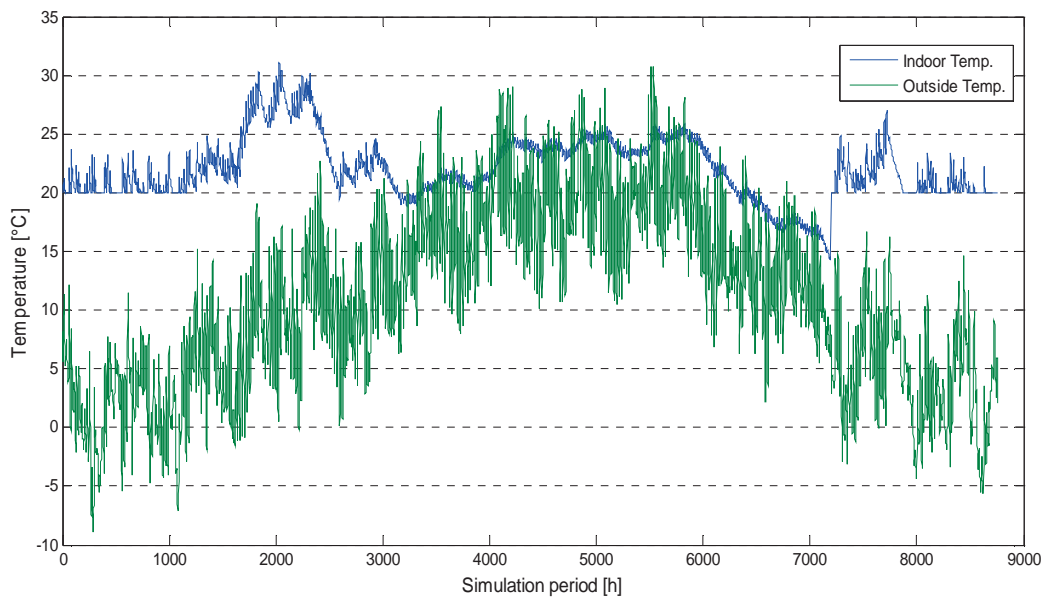


Figure 5-3. Temperatures variation for Scenario 1 (LESO office-room with standard control).

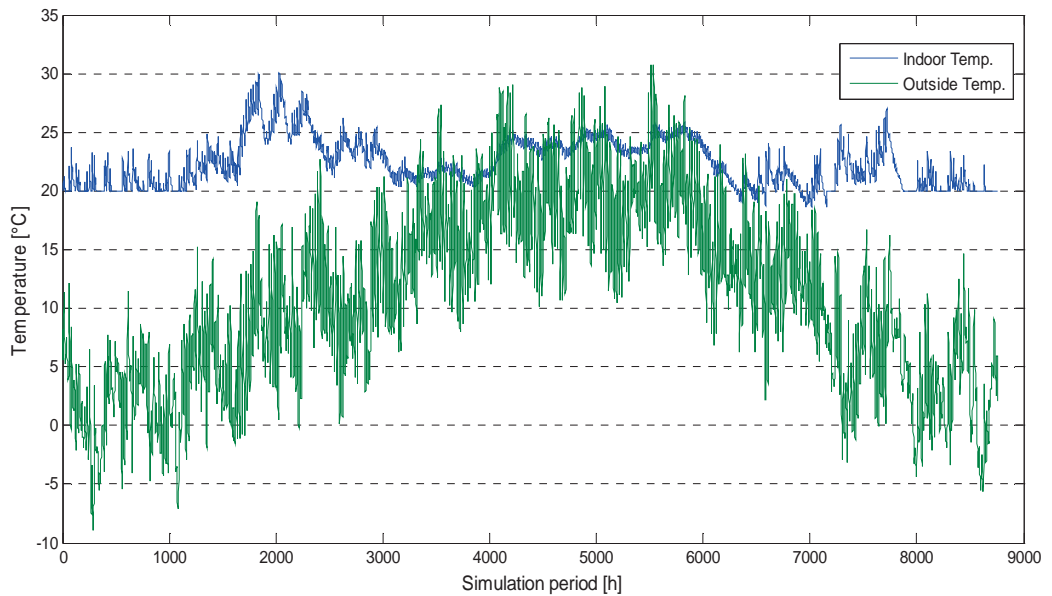


Figure 5-4. Temperatures variation for Scenario 2 (LESO office-room with HMM control).

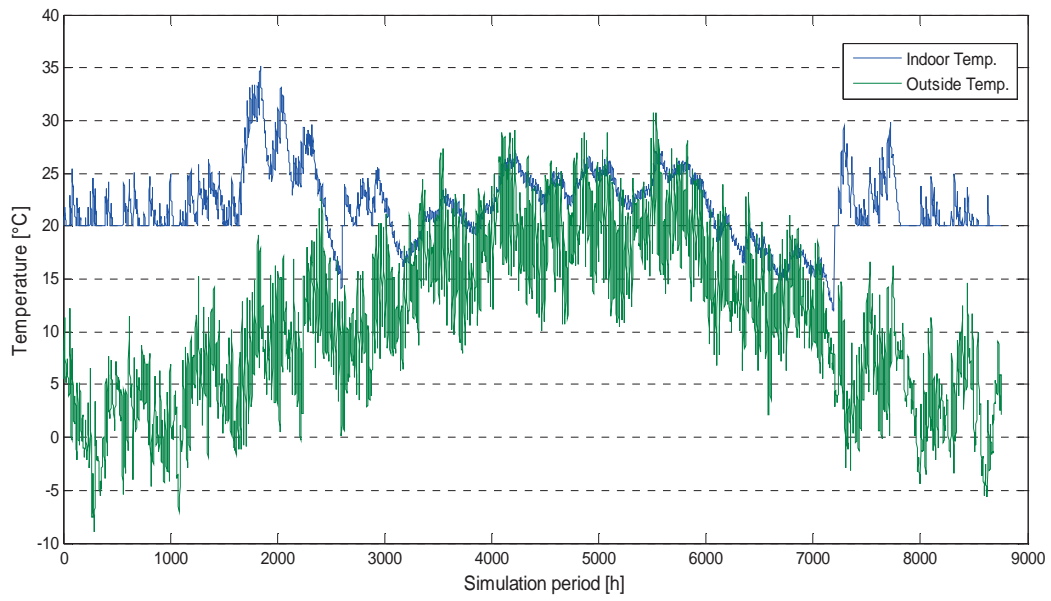


Figure 5-5. Temperatures variation for Scenario 3 (Light-weight structure with standard control).

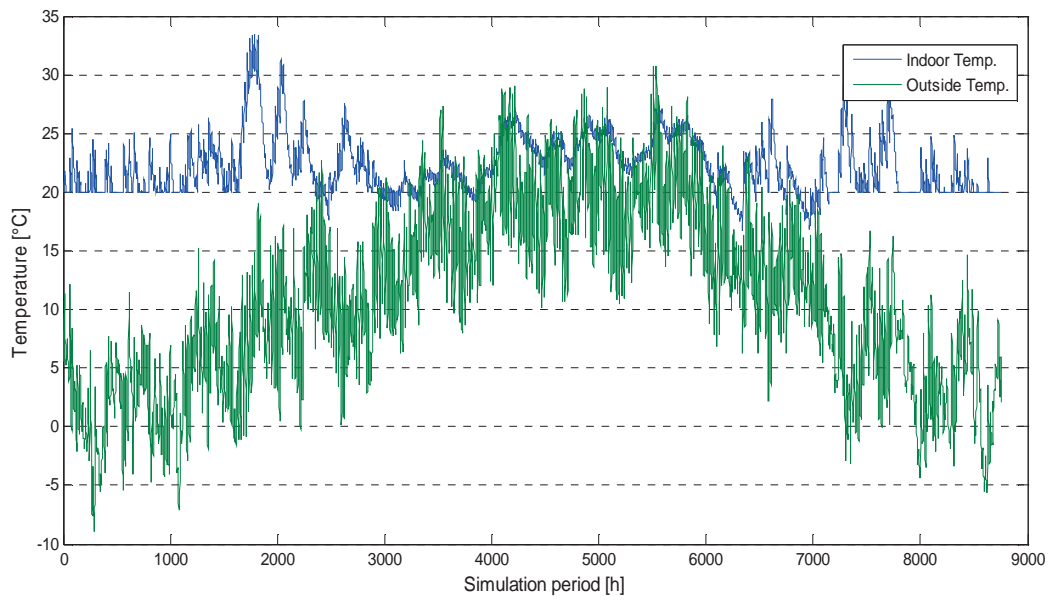
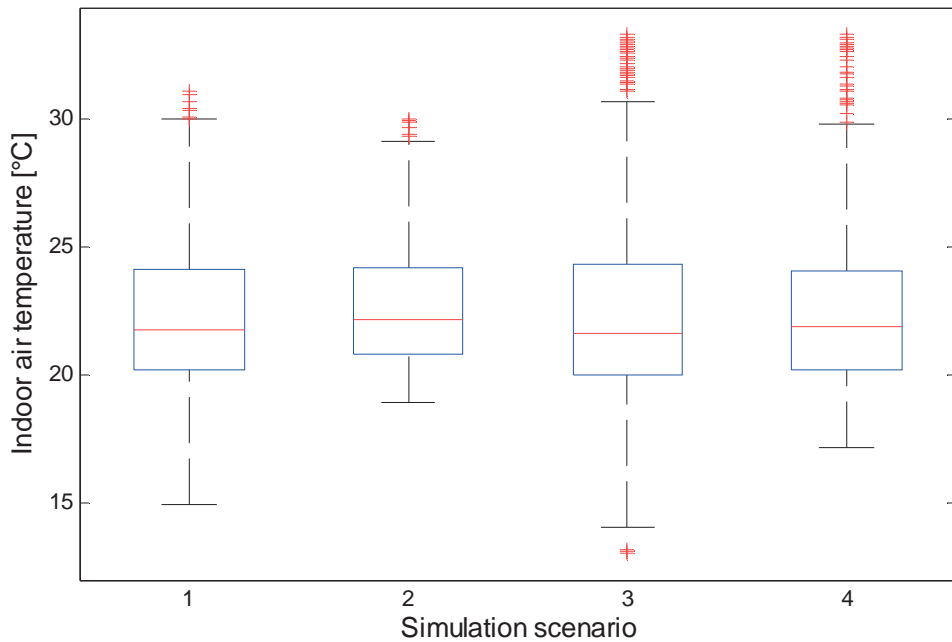


Figure 5-6. Temperatures variation for Scenario 4 (Light-weight structure with HMM control).

Figure 5-7 displays a qualitative approach comparing the internal temperatures distribution for each of the four proposed simulation scenarios over the entire simulation period. All scenarios appear to have approximately the same 25th and 75th percentiles and exhibit satisfactory dispersion with an interquartile range of about only 4°C. Nonetheless, we observe that HHM-based control (scenarios 2 and 4) have less outliers and their whisker extremes are much closer to the median. However, this relatively good and uniform performance of all the simulated cases is not recurring when next we calculate the Predicted Percentages of Dissatisfied (PPD).



Predicted Percentages of Dissatisfied (PPD)

In the same way as before in this thesis, the thermal comfort was analyzed with the use of Fanger's model [12]. Using as input for every time step of the simulation the season, the radiant temperature in the room and the room's air temperature, the Predicted Percentages of Dissatisfied (PPD) and the Predicted Mean Vote (PMV) were generated for every working hour in the year. The comfort parameters of air humidity, air velocity, clothing insulation and metabolic heat production are shown on Table 5-5; they were set to the same values as in the parametric study presented in Section 4.3.2, where the reader is referred to, should they need more details.

Parameter	Heating period	Non-heating period
Clothing [clo]	1.0	0.50
Activity [met]	1.2	1.2
Air speed [m/s]	0.10	0.10
Relative humidity [%]	50.0	50.0
Operative temperature [°C]	19.2 - 23.8	23 - 26.3

Table 5-5: Comfort parameters and calculated operative temperature used in Fanger's model for a PPD<10%.

The estimation of the thermal comfort for the entire period (1 year) was conducted to estimate the ability of the simulated case studies to keep the internal air temperature within the specified comfort limits (Table 5-5). The percentage of the working time when the air temperature is outside the range defined by the said limits was determined for all the simulation scenarios and it is presented separately for the heating and non-heating periods and it can be seen on Table 5-6 and Figure 5-8.

The comparison between all different scenarios shows clearly that HMM-based control greatly improves thermal comfort for both heavy structures like LESO and poorly-designed buildings. In the heating period, it does not seem to affect heavy structures, while it does improve thermal comfort in light-weight ones by 27%. During the non-heating, period results are overwhelmingly positive for the HMM-based control where it ameliorates thermal comfort by approximately 50% in the case of LESO and by 37% in the case of the light-weight building.

When comparing the PPD percentages between these that are due to overheating and those that occur due to risk of feeling cold, during the heating period, the predicted percentages of dissatisfaction in all scenarios are all due to anticipated complaints of overheating ($PMV > +0.5$) and none for the contrary. This is expected, since the controller keeps the air

temperature at 20°C minimum during the entire heating season (see parts (b) on Figure 5-9 & Figure 5-10).

Simulation scenario	Heating period [%]			Non-heating period [%]			Entire year [%]
	PMV < -0.5 (=feeling cold)	PMV > +0.5 (=feeling warm)	Total	PMV < -0.5 (=feeling cold)	PMV > +0.5 (=feeling warm)	Total	
1: LESO standard control	0	20	20	52.2	1.5	53.7	37.5
2: LESO HMM control	0	21.4	21.4	27.6	0	27.6	24.4
3: Lightweight standard control	0	28.1	28.1	59.4	2.7	62	45.6
4: Lightweight HMM control	0	20.4	20.4	36.1	2.8	38.9	29.6

Table 5-6: Percentage of working time during the simulation period where temperature is outside comfort limits (PMV<-0.5 or PMV>+0.5; PPD>10%), for each of the four considered simulation cases.

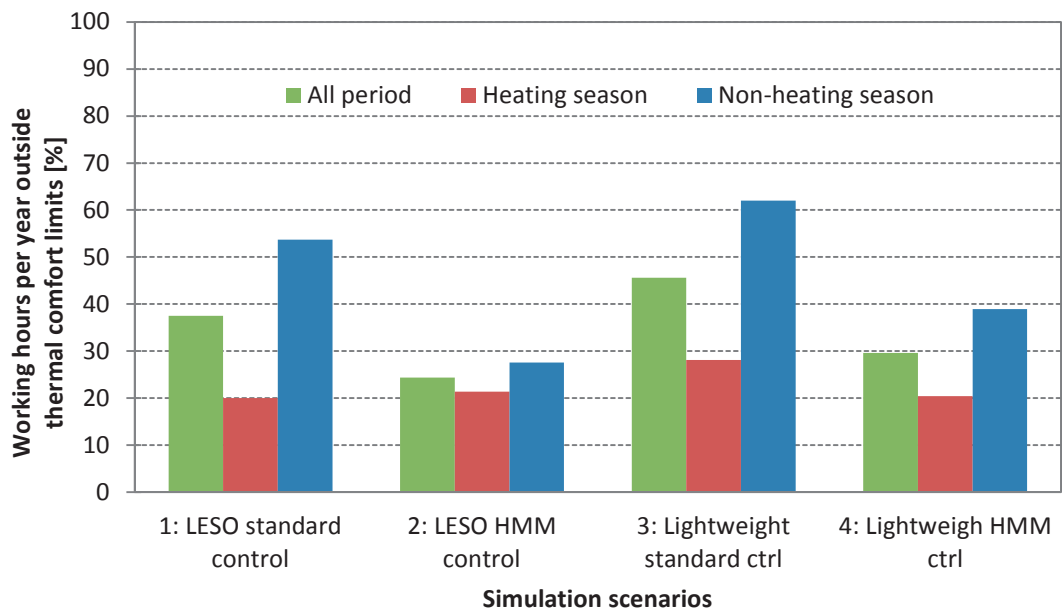


Figure 5-8. Percentage of working time during the simulation period where temperature is outside comfort limits (i.e. PPD is over 10%), for each of the four considered simulation cases.

It should be stressed that results presented in this analysis ought to be put in perspective of the absence of cooling and of any form of ventilation. Hence, higher-than-normal temperatures and thermal discomfort are expected during mid-season and – most notably – during summer (i.e. non-heating periods). But if that is true, then why during this period we expect occupants to be dissatisfied because they are feeling cold, as seen on Table 5-6?

One possible explanation could be that the controllers somehow suffer from excessive rejection of solar heat gains during the non-heating period. On a different rationale, we should reflect on the fact that even if we consider three different “seasons” for the HMM-based control, we present the results by distinguishing between a heating and a non-heating period to keep up with the presence of only heating in the tested scenarios. This binary distinction it’s quite likely to introduce some bias in favour of the results concerning the heating season: in fact, the mid-season comfort operative temperatures are lower than the ones of the non-heating period. However, mid-season occurrences in our study are judged by the highest, non-heating, limits. This may partially justify the high PDD values due to feeling cold in the non-heating period ($PMV < -0.5$). As also argued previously in Section 4.3.2, these instances of high PPD during the non-heating season would be largely mitigated with the adaptation of user clothing (i.e. from 0.5 to 0.65 clo; see Table 5-5).

Air temperature distributions during working hours

Figure 5-9 and Figure 5-10 conclude the results presentation regarding the estimation of thermal comfort providing some additional qualitative information about the indoor temperature during the simulation periods.

In particular, the distribution of indoor temperature (values, median, mean and standard deviation) during working hours for both the non-heating and the heating period is displayed together with the limits of the operative temperatures (green and red lines) for all simulation scenarios.

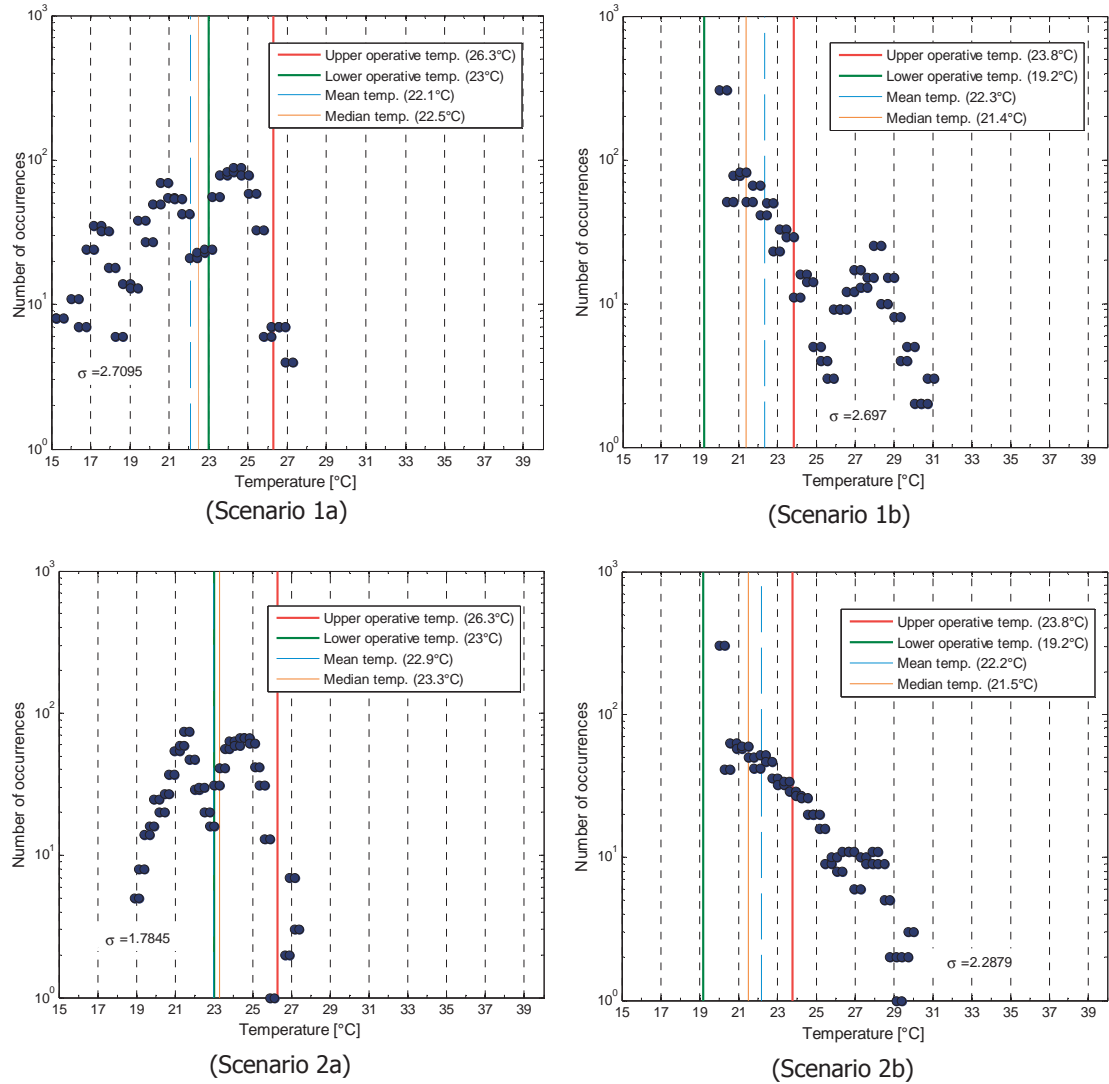


Figure 5-9. Indoor temperature values distribution during working hours in (a) non-heating and (b) heating period for simulation scenarios 1-2. Displayed are the values (black points), median (orange line), mean (light blue dashed line) and standard deviation (σ) together with the limits of the operative temperatures (green and red lines).

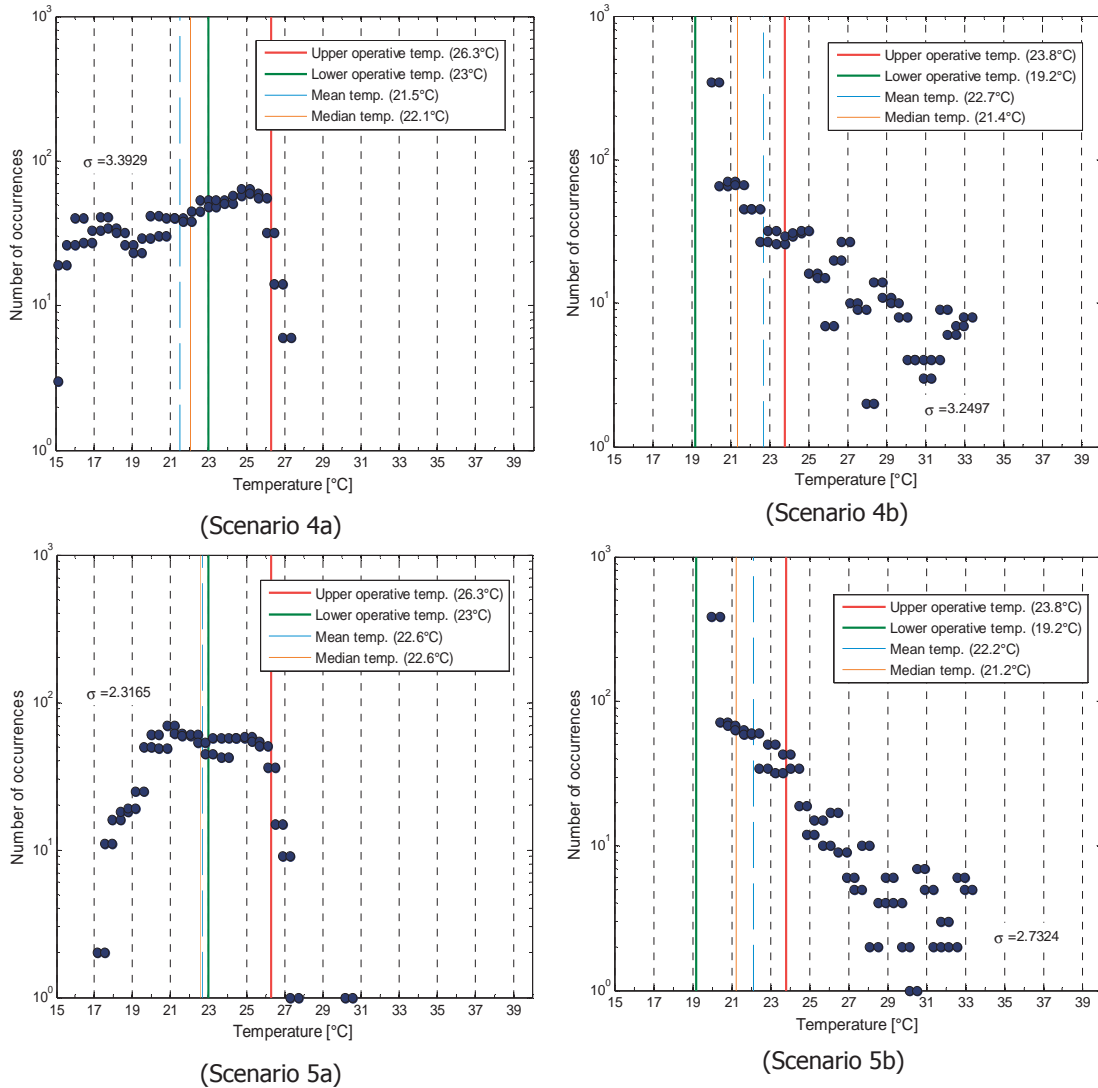


Figure 5-10. Indoor temperature values distribution during working hours in (a) non-heating and (b) heating period for simulation scenarios 2-4. Displayed are the values (black points), median (orange line), mean (light blue dashed line) and standard deviation (σ) together with the limits of the operative temperatures (green and red lines).

5.5. Discussion and outlook

When commissioning HVAC systems or solar protection devices, the most important questions that an engineer, building manager or user have to answer is *when* and *under which conditions* should these systems start and stop their operation in order that occupants' comfort is maintained with the minimum possible energy use and economic cost. In this chapter we attempted to answer these questions (with respect to the thermal comfort) through the definition and modelling of a "season" variable using stochastic state-based approaches and HMMs. To the best of our knowledge, this is the first attempt in this

direction and, as such, several points for further discussion are raised that may lead to the model's refinement:

- The elaboration of the proposed methodology was based on the hypothesis that 3 seasons exist when controlling building equipment for thermal comfort (Section 5.1.1). While the definition of cooling and heating seasons is more or less crisp, the introduction and definition of the intermediate season is possible that could be debated from the scientific community or professionals. For instance, one could object to the ergodic character of the model (Section 5.3.1), according to which direct transitions between the heating and the cooling season are possible without switching first to the mid-season. Another point of consideration related to these definitions is whether they could also manage the visual comfort aspects of building control.
- The inclusion of a building time constant τ seems an appropriate approach in order to account for each building's thermo-physical characteristics in the control of HVAC systems and generalize the developed model so it can be useful in multiple buildings or unknown configurations. Even so, τ in its present form is based partially on intuition and "expert's knowledge" (correction coefficient of $a_0=0.5$; see Section 5.3.3). Although we strongly believe our methodology is correct in practice, further research, probably requiring extensive experimental validations, could be carried out as to accurately define the model's coefficients and fine tune its final expression.
- The required data mining and machine learning for the development of the season as an HMM was based on data recorded over a long period in LESO. While it is hard to find other databases to match the quality and (mainly) the length of the LESO database, it is safe to assume that the developed model would have performed better (especially in the cooling season) had it been developed with data originating from a building with a full HVAC system deployed (and not only with heating, as it is the case of LESO).
- As reported in Sections 5.3.6 and 5.3.7, for obtaining satisfactory season identification results from the season HMM, the model requires training data that span several months (9 to 12). While this does not pose a problem when studying the model in a parametric study such as the performed simulations in 5.4, it may be problematic when attempted to use the elaborated model on a real-life building control application (especially on new buildings where data is not yet available). In this case, such a lengthy training period is hardly accepted nowadays where other smart control algorithms need much less time for adaptation and optimization. However, as demonstrated also in the simulations in Section 5.4, it seems as a very

promising approach to building control and it could be used in such framework if further explored and fine-tuned.

- In the first attempt to build an HMM-based model we aspired to include in it parameters from all main factors that affect “season” (see 5.1.2 and 5.3.2). For practical reasons, we performed the simulation analysis with a simplified model which did not include the ‘use’ element (apart a simple occupancy feature which nonetheless did not influence the controller’s decisions; it was only used for thermal comfort estimation purposes). As a suggestion for future work, we believe that it would be worthwhile to simulate user actions like window openings and actions on shading devices or incorporating advanced occupancy and activity models, as discussed previously (5.3.7). Also discussed on the same Section, in the future the fine tuning of the model could be performed with a formalised approach of feature selection and elimination. However, even in that case, producing a generalized model with high portability (i.e. excluding features that cannot be easily made available in the majority of buildings) should remain a priority.

Following a (possibly) improved version of the model which may be introduced after the points above are considered, we believe that the next topics are worth investigating in future research work:

- After the decision to include the time constant of the buildings in the elaborated model, it would be interesting to study the performance of the model (i.e. the energy conservation potential) by comparing different building structures against different climate zones. The study should include a large number of buildings for better comparison.
- Another interesting study would be to compare the energy, thermal and visual comfort performance of a controller that employs the season HMM against other intelligent algorithms (Fuzzy, ANN, Genetic, MPC, etc.).
- In its present form, the HMM-based season algorithm outputs a crisp value of the season. It would be very interesting in our opinion to modify the algorithm, so it outputs season as a fuzzy variable.

5.6. Conclusion

In this chapter we propose a novel approach to building control through the elaboration of a season model using stochastic, data-driven, state-based approaches such as Hidden Markov Models. In the proposed model, the season variable is unique to every building (or even to every room if the building systems permit individual, room-based control) and it depends on meteorological conditions around the building, user behaviour and building construction. In this regard, three seasons are defined and identified in each building by the novel HMM

approach: heating, cooling and mid-season. Two HMM-based season models are considered. The first is a comprehensive one that includes the inputs of outside and indoor temperature, solar irradiation, HVAC and user actions on windows and shading devices. To reflect each building's unique construction and thermal inertia, the time constant is calculated and it is likewise inserted in the model. The season identification accuracy was 91, 85 and 69% for the heating, cooling and intermediate season, respectively. The second model was a simplified one with only three inputs (outside temperature, solar irradiation and the time constant). It exhibited 10% lower prediction accuracy and it required a slightly longer training set compared to the comprehensive model; however, it can be used in buildings which possess only a limited sensor network and less-than-average infrastructure.

The performance of the simplified model was evaluated through simulations that compared two different controllers (one incorporating the new HMM model and one that used as indication for the season variable the average outside temperature over the last 7 days) in two different building construction types (a building with important thermal mass storage and increased time constant and a poorly designed one with a low time constant). The results were very promising for the HMM-based controller, which manages to save energy for heating and at the same time improves thermal comfort for the occupants by keeping indoor temperatures inside comfort limits, even in the case of a poorly designed building.

6. **VISUAL COMFORT MODELLING BASED ON STOCHASTIC DATA-DRIVEN MODELS**

This section presents a novel approach to model visual comfort based on state-based stochastic data-driven models such as the Hidden Markov Models (HMMs). Proposed models are based on horizontal plane illuminance measurements already available in LESO database and on new monitoring of the vertical illuminance at the observer's eye (pupillary illuminance) using wearable sensors. In specific, Section 6.1 introduces the notion of visual comfort and Section 6.2 attempts a state-of-the-art overview of the current tools that quantify or estimate it, identifying possibilities for improvement. Section 6.3 describes the development of the proposed models and discusses why finally only workplane measurements are employed in the HMM development. Finally, Section 6.4 presents the results of this new modelling approach which include comparison with other state-of-art classifiers (Bayesian and k-Nearest Neighbours) as well as an innovative analysis that demonstrates the model's inherent capability to be seamlessly integrated and used in building control systems built on fuzzy logic. Other strong points of the proposed HMM are the perspectives of the model to improve greatly over the various existing discomfort glare indices and metrics.

6.1. **Introduction**

Light has important visual and non-visual effects on human beings [113] and the provision of proper lighting inside buildings is of paramount importance in shaping a healthy, productive and pleasant indoor environment [3; 5]. In this chapter, we focus on the visual effects of light and, in specific, on the estimation of the user's visual discomfort probability inside their working environment.

6.1.1. Definition of visual discomfort

Although no universally accepted definition for visual comfort exists, we can attempt to define it as the situation where visual discomfort phenomena do not occur. As for visual discomfort, it is caused principally by three reasons:

- Insufficient illuminance
- Discomfort glare
- Excessive illuminance

The first reason is quite straight-forward and it relates to situations where the available light is not enough to adequately lit the internal space. Building codes, norms and lighting handbooks generally provide the minimum values or the range of values for the different types of possible tasks. For instance, the International Commission on Illumination (CIE^a) recommends workplane illuminances of 200 to 500 lx for task with simple visual requirements, 300 to 750 lx for tasks requiring medium visual requirements and 500 to 1000 lx for visually-demanding tasks [114]. By *discomfort glare*, one defines the annoying sensation due to excessive luminous contrasts in the field of view, usually caused by bright surfaces perceived in a much darker environment (such as a patch of sunlight on the desk in an otherwise dim office). Except non-uniform distribution of illuminances on the workplane, disability glare can also be caused by saturation of the visual system when a large amount of light is oriented directly towards the user's retina (such as direct sunlight beams hitting the eyes for instance) [81]^b. The third reason of discomfort refers to the cases when our visual environment is generally over-lit.

As we will see next, most models that try to assess objectively the visual discomfort, aim at estimating glare, which is undoubtedly the most subtle issue of the three.

6.2. Previous research work

6.2.1. Visual discomfort indices

Today, a number of methods and indices are available for the estimation of discomfort glare due to daylight, although none is unanimously recognized as a standard at the international level [81]. However, as we will see next, most of them agree that visual comfort depends on the illuminance on the user's pupillary plane and on the luminances of light sources and their position in the field of view of the user.

One of the first efforts to quantify visual discomfort was made in the 1950 when Petherbridge and Hopkinson [115] developed the British Glare Index (BGI). In their model, glare was rated according to a four-point scale as *just noticeable*, *just acceptable*, *just*

^a From the French: *Commission Internationale de l'Eclairage*.

^b Glare is further divided into two types, discomfort glare and disability glare. Discomfort glare causes discomfort without necessarily impairing the vision of objects [124] (and usually results in an instinctive desire to look away from a bright light source or difficulty in seeing a task. Disability glare impairs the vision of objects without necessarily causing discomfort [123].

uncomfortable and *just intolerable*. They developed empirically an equation, which however was limited to small glaring sources of and was not adapted to larger ones, such as day-lit windows. The Cornell equation or Daylight Glare Index (DGI) is a modification of the BGI and was adapted to predict glare from a large luminance source (i.e. a window) [116]. The equation is as follows:

$$DGI = 10 \log_{10} 0.48 \sum_{i=1}^n \frac{L_{s,i}^{1.6} \Omega_{s,i}^{0.8}}{L_{b,i} + 0.07 \omega_{s,i}^{0.5} L_{s,i}}, \quad (6-1)$$

where $L_{b,i}$ denotes the background luminance (cd/m^2), $L_{s,i}$ is the glare source luminance (cd/m^2), $\Omega_{s,i}$ is the solid angle subtended by the glare source (sr), $\omega_{s,i}$ is the solid angle of the luminous parts of each source as viewed from the observer's eye and $n(-)$ is the number of luminous sources i causing glare. This index uses a numeric scale from 16 to 28 to represent glare sensations that span as above from *just noticeable* (16) to *just intolerable* (28), with the DGI of 22 being on the *Borderline between comfort and discomfort*.

Another index developed to overcome the limitation of the BGI regarding multiple glare sources and to compensate between different national systems was the CIE Glare Index (CGI) by the CIE, which was based on a formula proposed by Einhorn:

$$CGI = 8 \log_{10} 2 \frac{[1 + (E_d/500)]}{E_d + E_{in}} \sum_{i=1}^n \frac{L_{s,i}^2 \omega_{s,i}}{p_i^2}, \quad (6-2)$$

where E_d is the direct vertical illuminance at the eye level due to all sources (lx), E_{in} is the indirect illuminance (lx) at the eye level (excluding the glare sources) and $p_i(-)$ is Guth's position index, which attributes different weights to the luminous sources relative to their azimuth and elevation in the observer's field of view [18 pp. 21-22]. Other annotations are as above.

Later, in 1992, the CIE [117] proposed the Unified Glare Rating (UGR) to evaluate glare sensations for an artificial lighting system (restricted to sources within a solid angle of $3 \cdot 10^{-4}$ to 0.1 sr). The UGR combines elements of both the CGI and the BGI and it is expressed with the following equation:

$$UGR = 8 \log_{10} \frac{0.25}{L_b} \sum_{i=1}^n \frac{L_{s,i}^2 \omega_{s,i}}{p_i^2}, \quad (6-3)$$

Wienold and Christoffersen note that the equation-based glare indices presented above "try to estimate possible glare sensation of a so-called 'standard observer'. Although this is not completely wrong, a word of warning is needed, since large variations of rating discomfort glare are normally found when comparing individual subjects" [116]. Subsequently, when

they compared the calculations of the DGI and the CGI in a real-life test environment against the responses of 349 real users, they reported that “these indices showed a weak correlation with how subjects reported discomfort glare in an experimental set-up with three different façade layouts, two different view directions and three different solar shading systems”. To deal with the limitations of existing models to properly reflect the truth, they subsequently proposed a new metric called Daylight Glare Probability (DGP):

$$DGP = 5.87 \cdot 10^{-5} E_v + 9.18 \cdot 10^{-2} \log_{10} \left(1 + \sum_i \frac{L_{s,i}^2 \omega_{s,i}}{E_v^{1.87} p_i^2} \right) + 0.16, \quad (6-4)$$

where E_v is the vertical eye illuminance (lx); $L_{s,i}$ the luminance of the source i (cd/m²); $\omega_{s,i}$ the solid angle of the source i and $p_i(-)$ its position index. This metric has been validated for a range of DGP between 0.2 and 0.8 and has been derived from real tests in rooms with day-lit windows. Further, it promotes the vertical eye illuminance as a crucial glare evaluation parameter without ignoring at the same time the central sum of the glare sources term used in the CIE glare indices (UGR and CGI).

6.2.2. Limitations of visual discomfort indices

As Lindelöf [18] promptly pointed out, there are three principal inconveniences and/or limitations related to the aforementioned formulae.

First, they require a detailed knowledge of luminance distributions in the field of view of the user. Usually, this knowledge entails the use of multiple illuminance sensors, scientific-grade CCD cameras and special lenses, the application of techniques for luminance mapping such as High Dynamic Range (HDR) photography as well as information on the photometric characteristics of the rooms (i.e. reflectances of internal surfaces) [81; 83; 116]. In practice, that level of needed detail would hinder their integration in automatic lighting controllers in other than experimental buildings, where the availability of the relevant information is limited.

Secondly, the indices presented herein attempt to quantify numerically the visual discomfort experienced by an average user as a function of lighting stimuli. However, as noted already in the introduction of this thesis (Section 1.1.1), visual comfort is perception-based and as such, differences at preferred illuminance levels are to be expected between individuals [17; 18]. Consequently, such methods do not take into account the individual preferences and behaviour of different users.

Last, these formulas only estimate discomfort glare (which is of course the most delicate cause to cater to), without addressing discomfort caused by insufficient or excessive lighting conditions.

6.2.3. User-adaptive, data-driven approaches

To overcome these limitations, Lindelöf [18] proposed a very interesting approach to model visual discomfort. In specific, he used a Bayesian method to calculate the user Visual Discomfort Probability (VisDP) as a function of a single variable (the horizontal workplane illuminance), by means of the following equation:

$$\Pr(C = F|E = e) = \frac{\Pr(E = e|C = F)\Pr(C = F)}{\Pr(E = e|C = F)\Pr(C = F) + \Pr(E = e|C = T)\Pr(C = T)}, \quad (6-5)$$

where C the event *user comfortable*; E the horizontal workplane illuminance (lx); $T=True$ and $F=False$ the possible values of C ; e a possible illuminance value of E (lx) and the terms $\Pr(C = F)$ and $\Pr(C = T)$, are the Bayesians' priors, which in this study was set to 0.5^c. Based on the assumption that:

"The set of situations immediately preceding and immediately following a user action provides us with a data pool of transitions from uncomfortable to (presumably) comfortable situations for that user"^d,

he applied this equation on a large number (7273) of user actions on the blinds or on electric lighting recorded in the course of 26 months at the LESO solar experimental building (see Section 2.2). The outcome of the proposed model is the curve used previously in this thesis in Section 4.3.3 (and shown in Figure 4-20), where the VisDP reaches a global minimum (~0.3) at around 500 lx. Outside the 500 lx region, the probability of discomfort increases sharply for lower illuminance values while it increases more gradually for values between 500 and 2500 lx, after which VisDP increases sharply.

On-site testing of a lighting controller based on the Bayesian modelling of visual comfort revealed good adaptation of the model to the user, where the user's interactions with the blinds or the electric lighting have been reduced to half. Simulations also demonstrated very good performance of a controller integrating this model: the average yearly discomfort probability was reduced from 0.44 in manual mode to 0.33 in controller mode; the energy for artificial lighting has been reduced by 61.3% on average and the energy for heating/cooling in south-oriented rooms has been reduced by 9% at a central European office room and by 35% at a South European one.

^c The choice of a prior equal to 0.5 corresponds to a complete lack of information as to the occupant's prior probability of being uncomfortable. As demonstrated by Lindelöf [18], "a different choice of priors does not affect the shape of the probability curve but tends to 'squash' it to higher or lower values".

^d This assumption is only valid for single-occupant office rooms.

The main advantage of Lindelöf's Bayesian approach over the discomfort metrics presented earlier is obviously the ability to adapt to each user's behavioural patterns in a relatively short period of time^e by using only a single variable (horizontal workplane illuminance), which in practice is not difficult to have access to. Further, and along with Wienold and Christoffersen's DGP, the outcome of the model is an intuitive, readily interpretable probability and not a score on a numeric scale.

However, despite the clear strengths of his model, Lindelöf [18] agrees that using additional variables and especially the eye-level pupilar illuminance is recommended and would likely improve the visual comfort modelling. In the same direction, Wienold and Christoffersen [116] observed after experimental measurements that "the correlation between the linear function of vertical eye illuminance and the probability of disturbed persons was stronger than all other tested functions". Osterhaus [118] also suggests that direct vertical illuminance on the eye level should be taken under consideration when evaluating visual discomfort since it has been shown that calculations of glare based on CGI, UGR (and DGI to a lesser extent) showed reasonable correlation with the measured direct vertical illuminance values.

From the above, we can conclude that visual comfort modelling using data driven approaches, which learn from and adapt to the user are promising. Nevertheless, since these approaches are not yet fully explored, there is still space for new ideas and improvement; this is what we attempt to pursue next in the models we propose.

6.3. Methodology

In this section, we discuss the development of a visual comfort model that correlates illuminances measured at the eye-level pupilar plane and on the task workplane with the use of electric lighting and external blinds and hence, the probability of visual discomfort^f. Following the promising implementation of data mining and machine learning processes for the modelling of the season variable in Chapter 5, we attempt to apply these techniques for the modelling of visual comfort. In specific, our goal is to move from the Bayesian approach described above to a Hidden Markov Model (HMM) one, using data mining on historic as well as on newly collected data in the LESO building. As it was the case with the season modelling, to the best of the author's knowledge, this is the first attempt to model visual

^e Assuming an average of four user events per day, five days per week, Lindelöf [18] estimated that 7–8 weeks are sufficient for the optimal adaptation of his model to the user.

^f Actually, two different models are discussed in this Section: one with both parameters (Sections 6.3.1 – 6.3.4) and one with workplane illuminance alone (Sections 6.3.5 – 6.4.4). As it is thoroughly explained next, only the later was pursued further into the development of the HMM.

comfort using HMMs. As a note, in this Section we try to avoid unnecessary repetition; for more details concerning HMM, the reader is kindly referred to Chapter 5.

6.3.1. Initial model definition: A two-variable model

By definition, in a HMM the system being modelled is assumed to be a Markov process with hidden states and visible output tokens, which are dependent on the (hidden) state. In this case, we propose to build a HMM where the visible output tokens are the illuminances measured (at the horizontal workplane and at the eye-level pupilar plane) while the “visual comfort” variable can take the value of one of the following three hidden states:

- Comfort
- Discomfort because of glare and/or low illuminances
- Discomfort because of glare and/or high illuminances

In Section 6.1.1 we attempted a definition of these states and as it becomes apparent, we have chosen to group glare with both low and excessive lighting conditions, as glare can occur in both situations. But, while it may be intuitive that glare phenomena can arise under high illuminance conditions, the contrary is probably not so evident. Let us consider the following situation:

A user is working behind a desk which faces a west-looking window and the late evening sun is close to the horizon. The available daylight can be rather weak on his/her workplane (= “low illuminances” as may be detected by a ceiling-mounted sensor), despite the fact that blinds or other shading devices are not deployed. However, at the same time the user can sense glare, as the direct component of the sun’s irradiation is penetrating into the room and is falling against the user’s eyes. We argue that by using a second sensor measuring the illuminance at the eye-level pupilar plane we could more finely distinguish between different discomfort-generating situations.

Nevertheless, as it will be illustrated in the next Sections, slight modifications to this definition will become necessary for the development of the HMM.

6.3.2. Data sources

Regarding the output tokens (the visible observations dependent on the state), we followed the recommendations of previous studies as presented in the Section 6.2 and thus we chose to include two variables in our observations vector: the illuminance measured on the vertical eye-level plane (E_v) and the workplane illuminance (E_{desk}).

Workplane illuminance data comes from the LESO management system (EIB/KNX) and database (see Sections 2.2 & 6.3.7 for details); data concerning the pupilar illuminance derived from the newly installed EnOcean sensor network (Section 2.4) and their acquisition is described below.

6.3.3. Monitoring procedure

Pupilar plane illuminance measurements were carried out in six South-facing, single-occupant offices in the LESO solar experimental building between 2 June and 18 July 2014 (six weeks) under mostly clear and intermediate sky conditions. Four of the offices were situated on the first floor of the building and two on the second. The detailed description of the LESO building is provided in Section 2.1. The six subjects that participated in the study were LESO staff members with an average age of about 43 years (ranging in age from 35 to about 53). They were three scientists and three administrative staff; three female and three male persons.

Measurements were carried out with the minimum possible interference on the regular workflow of the subjects. Each subject was given a lightweight, relatively small, autonomous wearable illuminance sensor (see Section 2.4.1), which they were told to hang around the neck (as seen in Figure 6-1) for as long as possible during their working day while they were carrying out their normal day-to-day work activities.



Figure 6-1. Picture that shows one of the six users that participated in the field measurements of pupilar plane illuminance, bearing the autonomous EnOcean illuminance/motion sensor as a pendant.

Before the beginning of the monitoring campaign, they were briefly informed on practical matters concerning the measurements and the correct handling of the sensors and were given a short text with useful information that served as a “user guide” (provided in Appendix A.6).

In parallel with the pupilar plane illuminance measurements, the building management system (EIB/KNX; Section 2.1) of the LESO building was also recording data regarding desktop illuminance, user presence, user interactions with the blinds and the electric lighting, etc.

6.3.4. Evaluation and usability of the eye-level plane illuminance measurements taken during the monitoring procedure

Following the commissioning of the EnOcean sensors network, we proceeded to calibration measurements to verify that the values provided by the sensors correspond to the ground truth. For that, multiple measurements were carried out including the six new illuminance sensors and a hand-held lux meter⁹ (Figure 6-2).



Figure 6-2. Chauvin Arnoux C.A 811 Light-Meter (Image: ©Chauvin Arnoux Group).

⁹ This is not a precision instrument; from tests we performed against a high precision, reference lux meter, it was found that in the region of 200-800 lx, it constantly overestimates illuminance by a factor of ≈ 1.16 . However, inaccuracies of this magnitude were not crucial, as it will be evident next.

The sensors were repeatedly tested inside the LESO building, principally on horizontal surfaces against different illuminance levels (not under direct sunlight) and varying outside weather conditions. During the measurements, the sensors were all placed at the same spot; the sensor of the hand-held lux meter was placed among them to minimise the bias due to the positioning of the instrument.

Figure 6-3 displays the results of the test measurements, where we can see that the sensors gave almost double or more of the actual illuminance value. Additionally, large dispersion is observed in the values of each sensor (coefficient of determination stays below 0.76 for the linear regressions of each of the sensors), which demonstrate almost random behaviour under the same lighting conditions (e.g. the sensor 3, for a real value at ~ 300 lx, one time provided a value at ~ 300 lx and another time gave a reading of ~ 1350 lx).

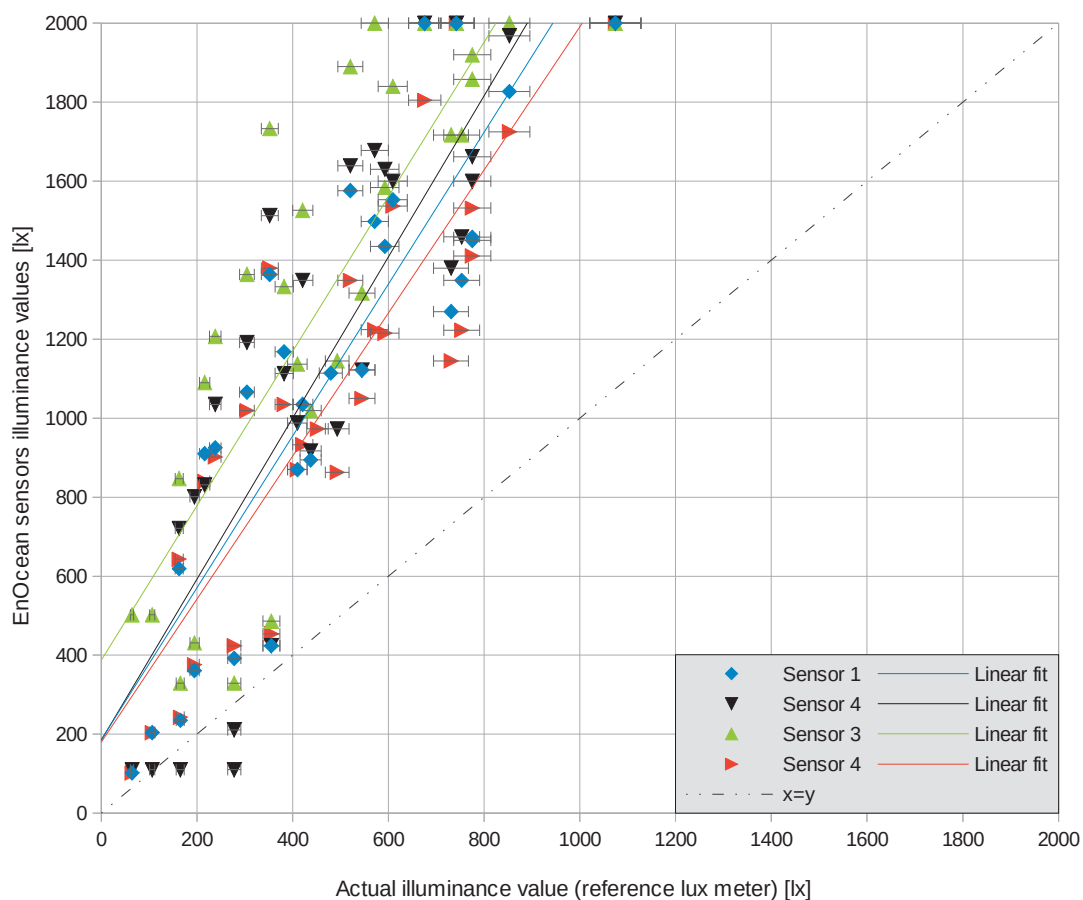


Figure 6-3. Comparison of simultaneous illuminance measurements taken with the Chauvin Arnoux C.A 811 Light-Meter (corrected with a coefficient of 0.86 to reflect actual values and assuming an additional 5% measurement error [error bars]) and four of the EnOcean sensors.

Also, for the same illuminance level (e.g. ~ 400 or ~ 750 lx), there are large discrepancies between the illuminance values provided by the EnOcean sensors. Further, as described in Section 2.4.1, according to their specification sheet the effective range of the sensors is between 0 and 2000 lx. This is not verified by our measurements, where sensors saturated (gave a reading of 2000 lx) for illuminance values between ~ 600 and ~ 1100 lx and greater.

After the first measurements, we suspected that an erroneous multiplier must have been inserted in the software on the gateway that handles the reception and the recording of the values. Nonetheless, after we consulted the persons responsible for the sensors deployment and commissioning, it seemed that no such error had occurred. Without ruling out the possibility of faulty hardware (for all the sensors), we assumed (and much later, verified from the technical specifications provided by the manufacturer) that these type of sensors are not destined for precision illuminance measurements but they are rather intended for simple automatic control applications (i.e. turning the lights on and off after an approximate threshold value has been reached).

After this unexpected turn, we felt strongly against using these measurements of pupilar illuminance for an HMM development concerning visual comfort; hence, we considered alternative paths, such as:

- Use only the workplane illuminance (E_{desk}) on the same data that Lindelöf [18] employed to develop an HMM approach with three hidden states as described in Section 6.3.1 but not for glare (in the LESO building, no E_v values are available globally for that period).
- Use (test) the developed model by using only the E_{desk} on the data collected during our experiments.
- Repeat the measurements campaign using new, scientific-grade wearable sensors and use both the E_v and the E_{desk} of the new data collected to develop a new model (as above but including estimation of glare probability) and then compare it with the previous one.

As this is an ongoing study that continues well beyond the time frame of this thesis^h, it has been decided to proceed in the design of a new portable illuminance sensor using commercially available EnOcean sensor kits coupled with a reliable sensor which will be scientifically sound. Once such a prototype sensor is ready, we also envisage performing longer data acquisition campaigns which we believe they will result in a much better training data pool for machine learning algorithms. However, this decision is part of a future endeavour which is outside the scope of the current work.

^h The research presented in this chapter has been carried out in the framework of the Green-Mod project which will continue until March 2016.

Concerning the short term perspectives inside the scope of this thesis, we decided to pursue the HMM development independently from the EnOcean sensors' present shortcomings and future improvements. Thus, this research continued following the first alternative path described above: Elaboration of a Hidden Markov Model approach for the estimation of visual comfort by using the same pool of data used in the past for the development of the VisDPⁱ and by utilising only one variable: the horizontal workplane illuminance.

6.3.5. New model definition: Observation vector with one variable

As opposed to our initial aspirations (of using two features) as well as to the season HMM approach explained in the Section 5 (where 3 to 6 features have been used), this time an observations vector with only one feature is selected for the modelling and the identification of the visual comfort:

$$X = \{E_{desk}\} \quad (6-6),$$

where E_{desk} is the horizontal workplane illuminance (lx) preceding and following the interaction of the user with any system that alters the luminous environment (in the case of LESO that is the blinds and the electric lights). The feature selection is limited by the lack of other relevant variables recorded at LESO solar experimental building and by the untrustworthiness of newly collected data, as explained in Section 6.3.4 above.

The choice of only one variable imposes a slight modification to the initial model definition since the lack of illuminance information on the pupillary plane of the user seriously hinders any attempt to identify glare independently from the workplane illuminance levels (i.e. morning light can cause glare when directed on the user's eyes but at the same time might not be sufficient to properly illuminate the user's work plane). As a result, in the proposed HMM the "visual comfort" variable can take the value of one the following three hidden states:

- Comfort
- Discomfort-L (Discomfort because of Low illuminances)
- Discomfort-H (Discomfort because of High illuminances)

Last, concerning the possible transitions from one state to the other, we consider an ergodic model, where we consider that any state can be reached from any other state at any given step (i.e. Figure 5-1b).

ⁱ See Section 6.2.3 for more details on VisDP.

6.3.6. Labelling the data sets

In the presented implementation of HMMs it is important to indicate during the training phase of the algorithm which observations (of horizontal workplane illuminance) represent the "Comfort" state and which the two discomfort states (labelling process^j). Building on the assumption mentioned in Section 6.2.3, where it is considered that the conditions before the user action(s) are indicative of an uncomfortable situation whereas those immediately after indicate a mostly comfortable environment, the following rules were applied to assign one of the 3 possible states to the observations:

- Comfort: E_{desk} recorded immediately after a user action.
- Discomfort-L: E_{desk} recorded before a user action which resulted in an increase of the workplane illuminance.
- Discomfort-H: E_{desk} recorded before a user action which resulted in a decrease of the workplane illuminance.

It should be noted that even though originally the illuminance measurements we handle are continuous data ranging from 0 to about 3,500 lux measured in the course of time, the described labelling process results in data sets that are populated with discrete, non-continuous illuminance values. For instance, a data set labelled "Comfort" with the following illuminance values (lx):

$$Data_1(Comf) = \{403, 784, 399, 1201, \dots\},$$

is not a continuous temporal sequence where the values have been recorded the one after the other. Rather, each of these is an illuminance value "recorded immediately after a user action" which means that in fact, between two consecutive values in this dataset there are an unknown number of values filtered out and the real elapsed time between two consecutive values in this example can be anything from a few minutes to hours or even days.

6.3.7. User actions, data processing and verification

To be able to compare and validate our model against one that had already been developed, we chose to use the same data employed by Lindelöf [18] for his VisDP model development. As such, data recorded between the January 2003 and mid-January 2005^k were pulled from

^j The assignment of a state to a data set.

^k The data range of "mid-November 2002 to mid-January 2005" referred to by Lindelöf [18] did not contain complete information for all of 4 sensor/actuator data considered: blinds, electric lights, presence and desktop illuminance.

the LESO database (details in Section 2.2). In specific, the following sensor and actuator data were used to filter out and create our final E_{desk} data sets:

- Presence
- Blinds: only actions performed by the user
- Electric lighting data: only actions performed by the user

To ensure our data match those employed by the aforementioned study, we filtered out successive user actions that occurred in a time window of one minute and considered them as part of the same action (where i.e. the user is fine-tuning the electric lighting level or the blinds position). Similarly, we excluded actions that took place two or less minutes before the user's departure from the room (it is assumed that these do not relate to improving the visual comfort but to the user's departure). The same study also showed that LESO office room '104' has had the most user actions during the time period considered and thus it is a good starting point for the development of a model which is heavily dependent on user actions. Unless otherwise stated, all development mentioned hereafter concerns this single-occupant room.

Of a total of 736695 telegrams recorded in the LESO database during the considered period and concerned the blinds and the electric lights, only 11749 of them were user actions (representing 14 rooms) that met the selection criteria above. Finally, 1347 user actions¹ that concerned the chosen office room were considered (11.5% of the actions in all the 14 LESO rooms during the same period). As explained in the previous Section, these 1347 user actions were employed to filter out, create and label the E_{desk} data sets used in the model development.

To verify the integrity and usability of the selected data, we implemented a simplified Bayesian approach to estimate the visual discomfort probability and then we compared our findings with Lindelöf's [18] Bayesian discomfort model. First, we separated the illuminance values recorded before and after the user actions and presented them in histograms by selecting a bin of 100 lux (Figure 6-4). Then, we applied the equation (6-5), where we considered:

- $\Pr(E = e|C = F)$: The workplane illuminance distribution BEFORE the user actions,
- $\Pr(E = e|C = T)$: The workplane illuminance distribution AFTER the user action (histograms of Figure 6-4).

¹ As compared to 983 user actions selected by the previous study.

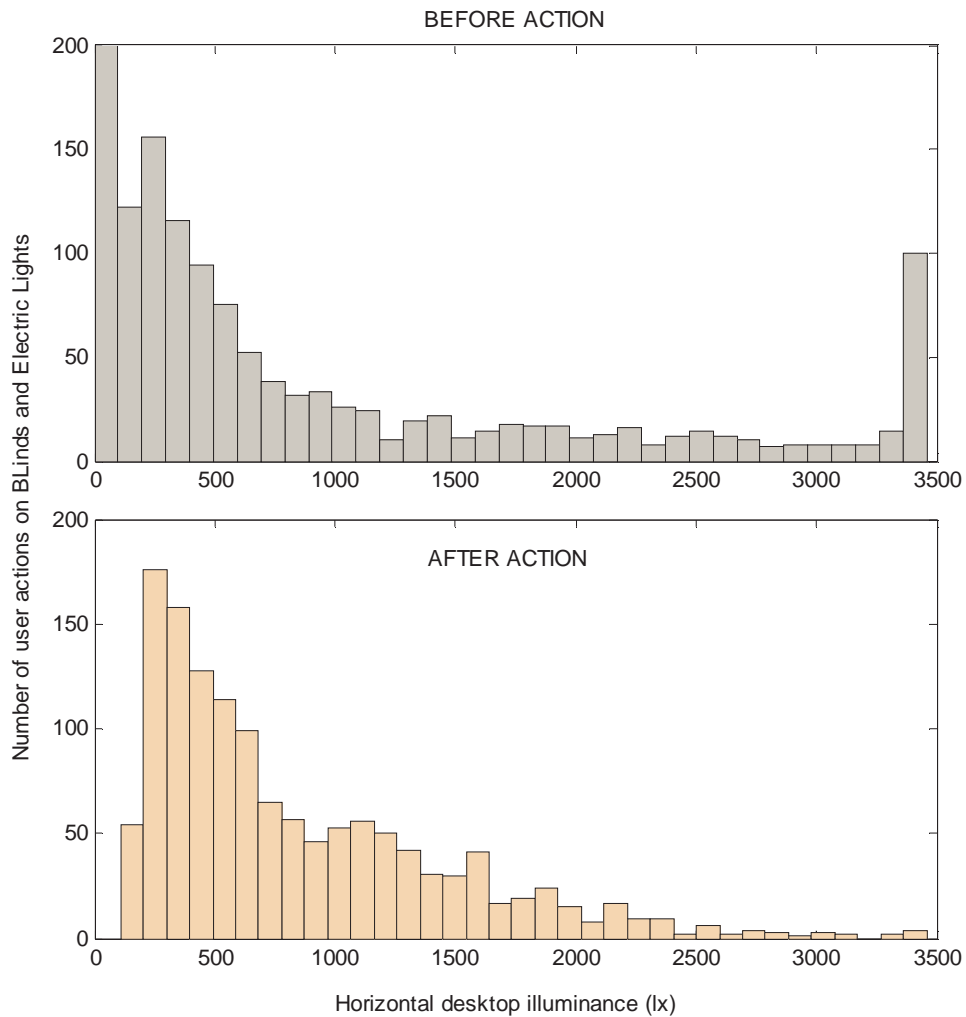


Figure 6-4. Illuminance distribution, before and after user action, in office room 104 (Histogram bin width: 100 lux). Combinations of user actions spaced apart not more than one minute in time are considered as part of the same user action. Actions performed less than two minutes before the user has left the office were excluded. A total of 1347 actions are considered for the period January 2003 – January 2005.

By selecting an equal value of 0.5 for the priors (the terms $\Pr(C = F)$ and $\Pr(C = T)$ of the equation (6-5)), we derived a simplified Bayesian approach of the discomfort probability as a function of the horizontal workplane illuminance as depicted in Figure 6-5. When comparing this result with the VisDP by Lindelöf [18 p. 100] (refer also to Figure 4-20), we observe the same general trend: a zone approximately between 300 and 1700 lx where the discomfort probability is equal or below 0.4. Outside this zone, the probability of discomfort increases sharply for lower illuminance values while it increases more gradually for values greater than 1700 lx.

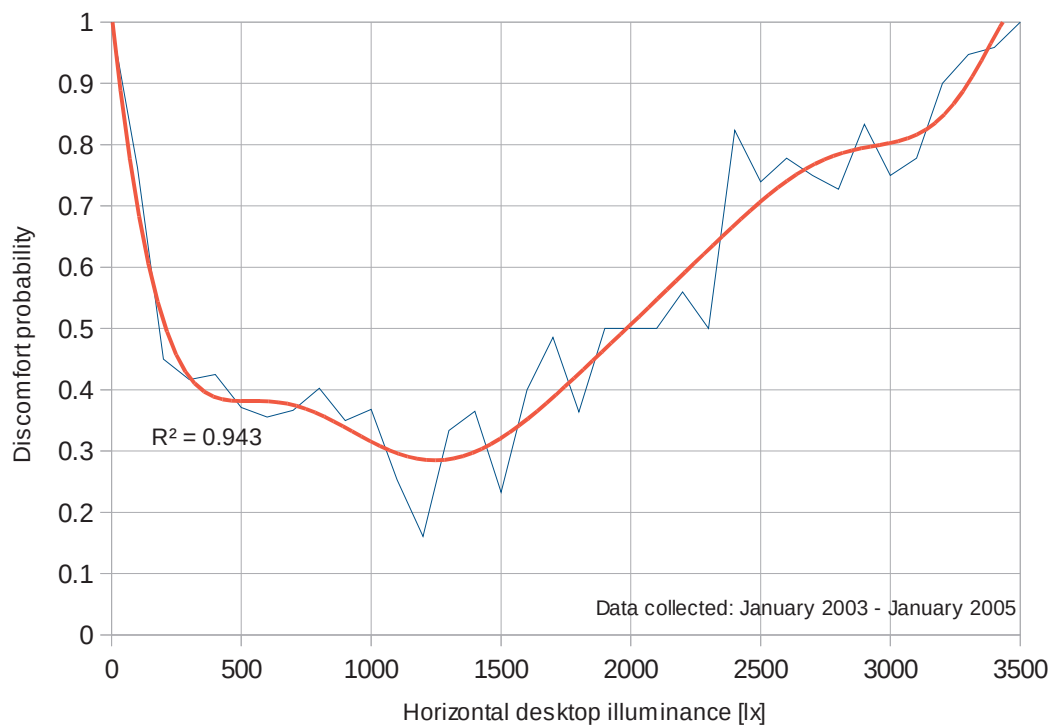


Figure 6-5. Simplified Bayesian estimation of discomfort probability as a function of the horizontal workplane illuminance with polynomial regression (red line). Data were collected in LESO office room 104 between January 2003 and January 2005.

This comparison exercise verified the integrity of the selected data which were subsequently used to develop the HMM Visual Comfort approach. Similarly to the process detailed in Section 5.3.4, observation data (E_{desk}) had to be structured in training and testing sets which are Matlab structure arrays. Considering the data quantity, we built 6 training and testing data sets for each of the 3 states (Comfort, Discomfort-L & Discomfort-H; see Section 6.3.6)^m and each data set contained a sequence of illuminances that varied in length (T) from 97 to 271 values. As detailed earlier (Section 6.3.5) the observation vector contained only one feature, hence the dimension of the observations in this case is $P=1$.

Following the data processing and preparation, multiple training and testing cycles of the model took place using the Matlab toolbox and procedure as detailed in Section 5.3.6. The results of the process and the model itself are presented in the next Section.

^m $6 \times 3 = 18$ data sets in total

6.4. Results

This section presents the results acquired during the development of a Visual Comfort model using HMM approaches and based on horizontal plane illuminance measurements only (the second model defined in Section 6.3.5).

6.4.1. Identification accuracy using the structured data sets: Confusion Matrices

In the end of each training/testing campaign, we obtained a confusion matrix which summarizes the identification accuracy of the developed HMM-based Visual Comfort model. As we had 6 data sets in our disposition for each of the hidden states, we first kept 5 for training and the remaining for the testing (every time a different set of 5x3 was randomly picked for the training of the model). Then we started reducing one by one the number of training sets. For each training/testing cycle, a different number of Gaussian mixtures (k) were tried.

k: 1-10	Discomfort-L	Comfort	Discomfort-H
Discomfort-L	100	0	0
Comfort	0	100	0
Discomfort-H	0	0	100

Table 6-1: Confusion matrix showing accuracy per state (in percentages). Results were obtained using 2 to 5 training tests (equivalent to about 8 to 20 months of observations) for the GMMs with 1-10 mixtures (k).

k: 13	Discomfort-L	Comfort	Discomfort-H
Discomfort-L	75	25	0
Comfort	0	100	0
Discomfort-H	0	0	100

Table 6-2: Confusion matrix showing accuracy per state (in percentages). Results were obtained with only one training test (equivalent to about 4 months of observations) for the GMMs with 13 mixtures (k).

The results are presented in Table 6-1 and demonstrate that a 100% identification accuracy of the visual comfort states can be achieved when tested against real data collected from the same office room. Multiple tests revealed that a training period of 4 to 8 months of recorded data is necessary to keep the model's accuracy at this percentage, even when using a low number of k . As also shown in Table 6-2, when using only one training set (which roughly corresponds to using 4-month data) an overall 92% identification accuracy can be achieved (75% for the 'Discomfort-L' state). It should be noted that when using

higher values of k with less training tests then the algorithms fail to converge after a finite number of iterations (multiple iteration values were tested).

6.4.2. Visual comfort identification using random illuminance values: The HMM as a classifier

The above tests were performed against real illuminance data recorded in the specific LESO room and showed very promising results. Thinking of how we can implement an HMM visual comfort model in a real-life application, we asked the following questions: Once enough data is available to train and build a visual comfort model, how would this model then classify newly recorded illuminance values? Or, what visual comfort state would be assigned to different workplane illuminance values?

To answer, we considered a base visual comfort HMM trained with all 6x3 available data sets (24 months) and tested against synthetic illuminance values that ranged from 0 to 3500 luxⁿ and for different GMM mixtures (k) raising from 1 to 40. The results of the 1400 testing cycles are summarized in Figure 6-6. We observe that already for a k greater than 5, the "Comfort" state identification pattern is stabilised in the region between 500 and 1300 lux while illuminances below and above this zone are identified as Discomfort-L and Discomfort-H, respectively. HMMs with higher number of k (greater than 15) start to produce more fine results and reveal subtleties that include a visual comfort zone on and slightly past the 1500 lux mark (however, these are not prevailing hence they do not appear on the average state identification of all the models). Indeed, these patterns can also be observed in the results of discomfort probability for the office room 104 produced by Lindelöf [18 p. 100].

ⁿ In every test, the model was tested against 10 illuminance values randomly generated within a specific illuminance zone. The spectrum of 0-3500 lux was evenly distributed into 35 zones of 100 lux each.

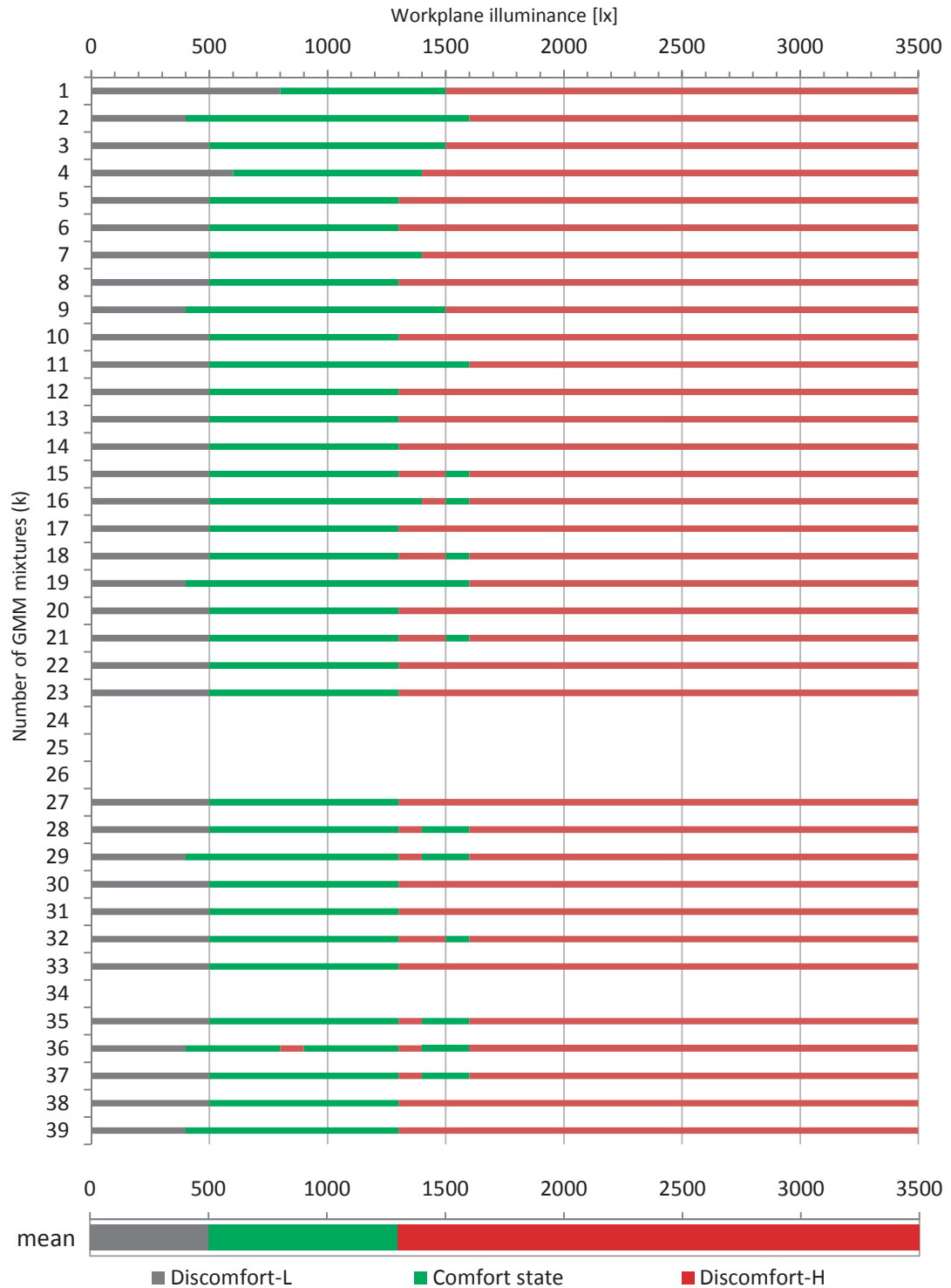


Figure 6-6. Visual comfort state identification against different workplane illuminance values for 35 different HMMs, each having (k) GMM mixtures ranging from 1 to 40 (models for k equal to 24-26, 34 and 40 are omitted because of non-convergence). The mean values of state identification for all the models are presented on the bottom.

6.4.3. Comparison of the HMM with other classifiers: Simple Bayesian and k-Nearest Neighbors

A first comparison of the developed HMM with other classifiers can be readily made with the simplified Bayesian approach presented in Section 6.3.7. Intuitively, we can decide on a threshold value for the discomfort probability, below which we assume the occupant's state as "mostly comfortable" or "probably comfortable". For the applied value of 0.5 for the Bayesian priors, we can argue that a decision rule (threshold) of 0.4 for the VisDP would represent a sensible choice. Thus, by applying this arbitrary however intuitive and reasonable rule and considering those E_{desk} illuminance levels where the discomfort probability is equal or lower than 0.4, we observe that a "Comfort" state is established between the 450 and 1600 lux region, with an additional "comfort island" at around 1800 lux. By comparing this to the HMM developed, we notice the similarities with the principal 500 – 1300 lux comfort zone, as well as with the narrower one at 1500 – 1600 lux of several high-k HMM ($k > 15$).

For a more formalised evaluation, we compare the developed HMM-based visual comfort models with k-Nearest Neighbor (k-NN) classifiers. K-NN classifiers are based on the calculation of the distance in the feature space between the test object (that we want to classify) and the training examples. The object is classified by performing a majority vote among the class labels of the k nearest neighbors that are closest to the test object. When $k=1$, the test object is simply assigned the class of its nearest neighbor. The distance computation depends on the nature of the feature space and includes distance metrics as Euclidean, City-block, Chebychev, Minkowski, Mahalanobis, etc. [107]. In our case, after testing several distance metrics, the Euclidean distance has been chosen. For the construction and the implementation of the k-NN classifiers, the Statistics Toolbox in Matlab has been used. As half of our data (training sets) concerned are labelled by definition as "Comfort" (the E_{desk} immediately following a user action), a prior of 0.5 was attributed to this class. The classes "Discomfort-L" and "Discomfort-H" concern the other half of the data, 32 and 18%, respectively. Following their classes' frequencies, they have been attributed a prior of 0.32 and 0.18, respectively.

Following multiple tests and iterations while changing several parameters (i.e. distance metrics, priors), we finally trained and tested the best 40 different k-NN classifiers, each having a k from 1 to 40. Figure 6-7 provides a qualitative evaluation of the built classifiers as a function of the number of Nearest Neighbors (k) used in each model. The Resubstitution loss is the fraction of misclassifications that can occur when testing with known data (training data), while the Cross-validation loss is the lack of precision when classifying new data not used on training (assuming that the new data feature a distribution similar to that of the training data). The first thing we observe is that the classification accuracy quickly decreases (for $k > 1$) and never gets better from about 70%, even when testing against known data. In comparison, the developed HMM-based model had an

accuracy of 100% even when using a part of the available data and 92% when only a sixth of the data were used to train the model.

When testing against new data (synthetic illuminance values generated exactly as described previously in Section 6.4.2), the classification results for each of the 40 k-NN classifiers are presented in Figure 6-8. When comparing with the classification results from the HMM, it becomes immediately apparent (when focusing on models with $k > 20$) that the “Comfort” class now occupies a much broader spectrum than before (especially towards the high end). We can argue that this is rather an improvement over the HMM models since we know that in this (identified) region between 300 to 2000 lux most people can perform their tasks comfortably, especially if the illuminances are due to natural daylight [14; 17]. Additionally, this is verified by the Bayesian analysis presented in Section 6.2.3 where we observed that below the 300 – 400 lx region “the probability of discomfort increases sharply for lower illuminance values while it increases more gradually for values between 500 and 2500 lx”. However, one should be cautious when building a k-NN classifier: as seen in the presented results, the classification for $k < 20$ is much less stable and is on the borderline of being erratic for $k < 10$.

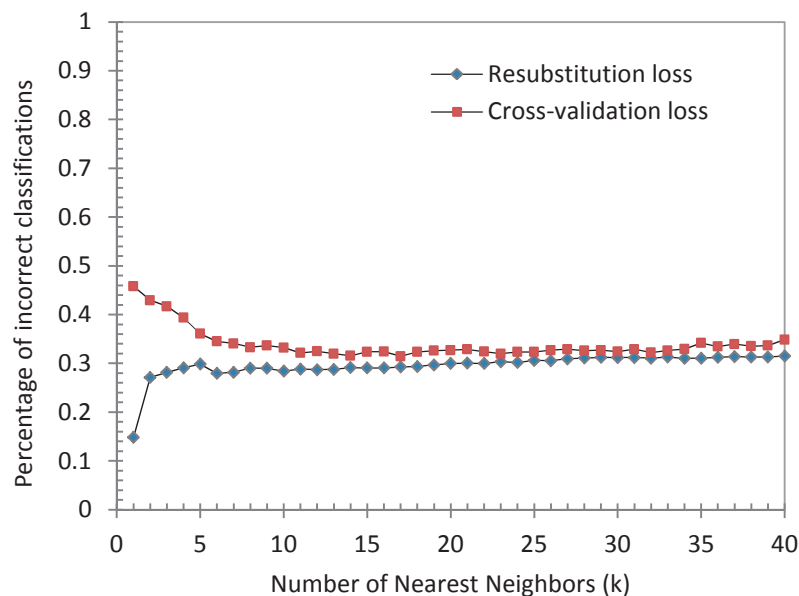


Figure 6-7. Quality of k-NN classifiers as a function of the number of Nearest Neighbors (k) used in each model. The Resubstitution loss is the fraction of misclassifications concerning the training data, while the Cross-validation loss is the lack of precision when classifying data not used on training (assuming that the new data has about the same distribution as the training data).

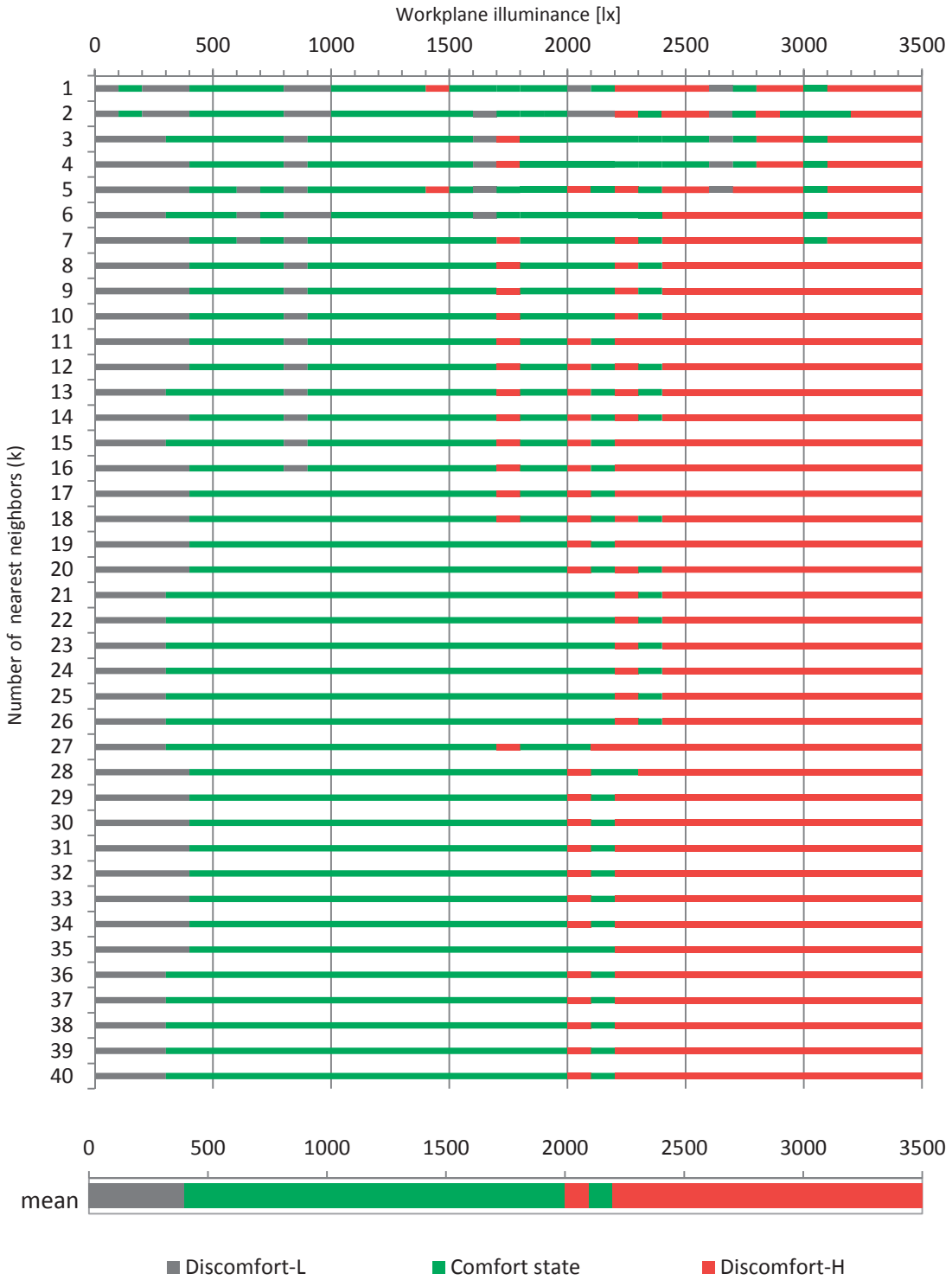


Figure 6-8. Visual comfort state identification against different workplane illuminance values for 40 different k-NN based classifiers, each having (k) Nearest Neighbors ranging from 1 to 40. The mean values of state identification for all the models are presented on the bottom.

6.4.4. State identification certainty of the HMM: Likelihood of selected states

As we can see from the results presented in Section 6.4.2, our HMM-based model intrinsically does not output an index or a probability for the visual comfort. Instead, it processes a given set of illuminance observations and outputs the best state that matches them. Although this output of the model is a crisp state regarding the occupant's visual comfort, it would be interesting to go beyond the crisp answer and see what does "best state" means in terms of quantifiable metrics or, in other words, to explore the certainty with which the model decides on one state over the other two.

To do so, we use the output of the Viterbi algorithm (See 5.3.6), which tests every observation separately against each of the 3 possible states and finds the most likely state that this observation sequence belongs into. This is realised via a log-likelihood and it is computed on a one-to-one basis (each observation to one single state) so it cannot be directly employed for a likelihood comparison between the different states. Instead, we proceed in normalisation of the acquired log-likelihoods of the 3 states: We first subtract the biggest value (the one of the most probable state) from the values of all the states. If X_1 is the log likelihood representing the most probable state, we now have 3 values that look like:

$$\text{Log likelihoods} = \{X_1, X_2, X_3\} \quad , \quad \text{where } X_1 = 0 \text{ \& } X_2, X_3 < 0 \quad (6-7)$$

Their normalised relative likelihoods for each state i are then calculated as follows:

$$\text{Normalised likelihood}_i = e^{X_i} / \sum_{i=1}^3 e^{X_i} \quad (6-8)$$

Figure 6-9 presents the results of the normalised relative likelihoods for each identified state in each of the 35 different HMM as a function of the horizontal workplane illuminance while Figure 6-10 gathers in one graph all the normalised relative likelihoods (scattered points) and their means (lines). The first point to notice is that the decision-making of the model does not always resemble a binary process. Despite the fact that the normalised values are often of the form $\{1,0,0\}$ in the 0-3500 lx range (showing great decision confidence), the uncertainty becomes evident for the illuminance values close to the states transition.

Great caution should be exercised in the interpretation of these results. That is because the visual comfort likelihoods presented in this context should not be confused with the probability of the occupant feeling comfortable or uncomfortable at a given desktop illuminance level; the discomfort probability is better reflected in other models, like the DGP or VisDP presented in Section 6.2. Instead, we should be constantly reminded that the proposed HMM approach identifies and outputs crisp states and the likelihoods presented here merely reflect the confidence (relative likelihood) with which the model took the decision to identify one of the three different states.

That being clarified, one could however safely deduce from these results and the ease or not of the model to decide between different states, that the comfort of the occupant of the room 104 is likely to be maximised between 600 – 1250 lx, where the normalised relative likelihood is close to one (and thus the model's confidence is maximized) and it is likely to drop as the illuminances approach the limits of the "Comfort" state on Figure 6-6.

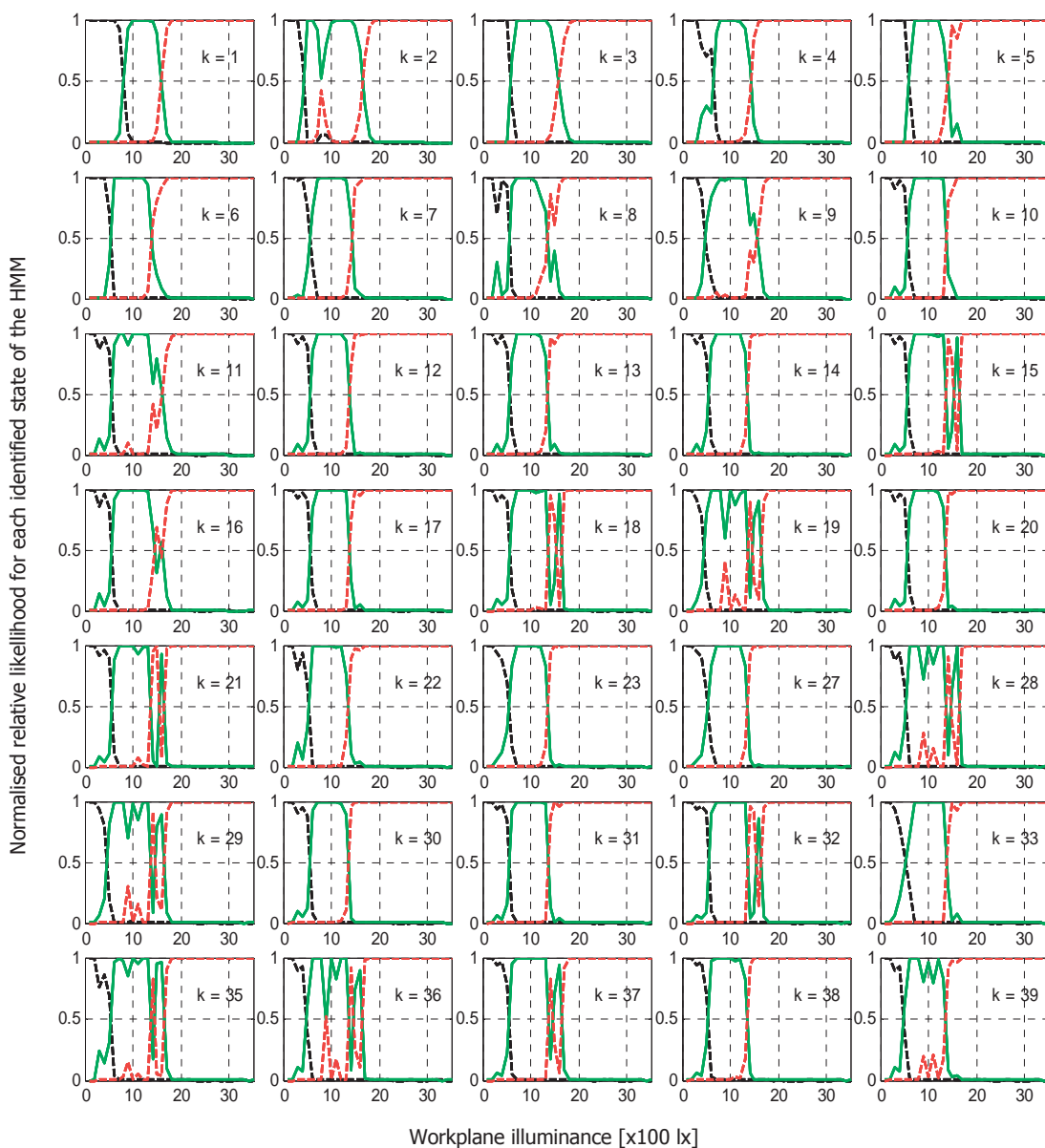


Figure 6-9. Normalised relative likelihood for each identified state in the 35 different HMM as a function of the horizontal workplane illuminance. Black colour represents Discomfort-L, green Comfort & red Discomfort-H.

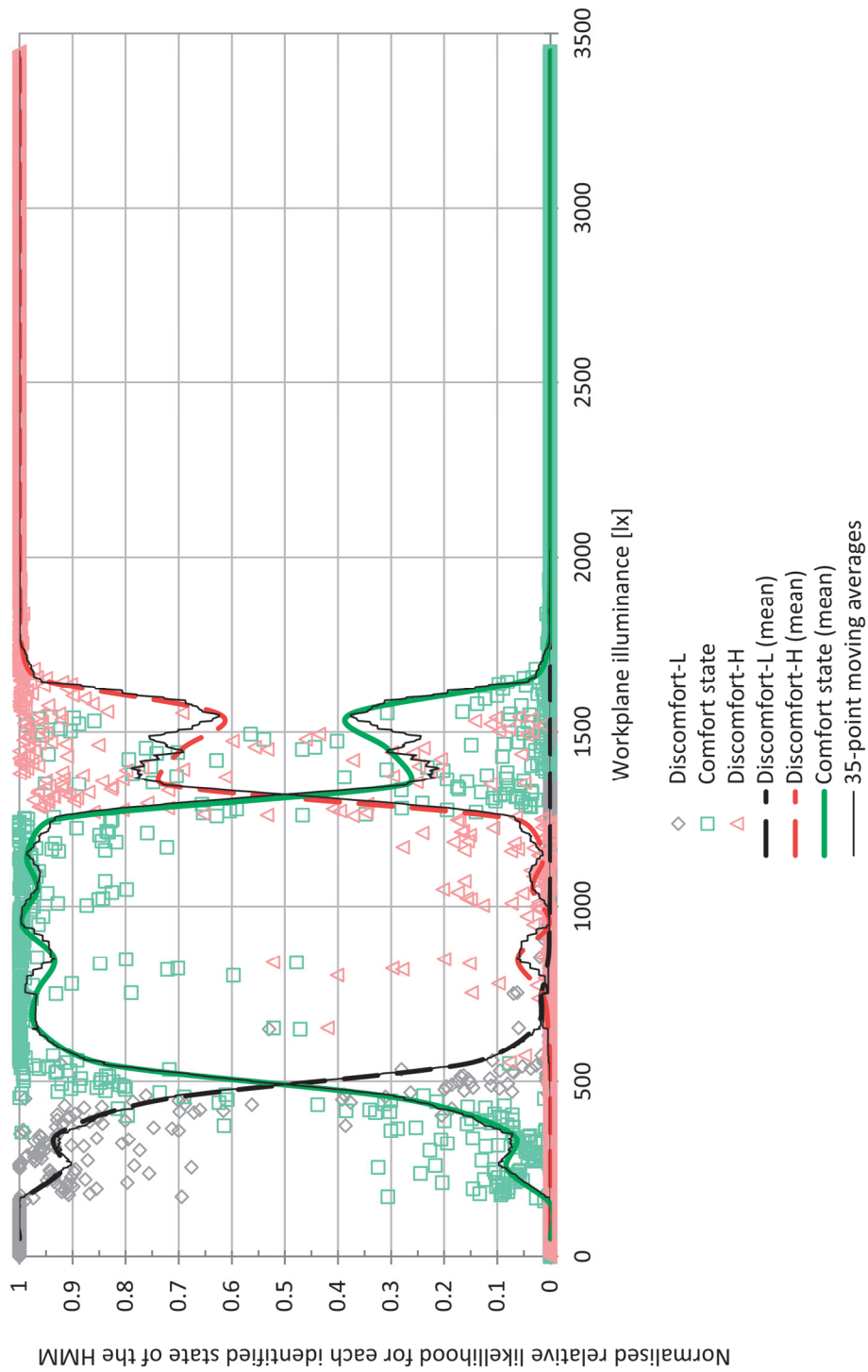


Figure 6-10. Normalised relative likelihoods of the identified states in all the 35 different HMM (scattered points) and their means (lines) as a function of the horizontal workplane illuminance.

This assumption is verified, when cross-checked once more with the results for the office room 104 produced by Lindelöf [18 p. 100], where the global minimum values of discomfort probability (less than 0.35) are achieved for exactly that range of desktop illuminances.

6.5. Conclusion

This chapter presents the development of a novel model for the estimation of visual comfort. As we have demonstrated, there exist today several metrics that evaluate discomfort glare; however they are met with important limitations. In the approach we suggest, we build on previously performed work to produce a model that is adapted to each user's perception of comfort and that for the first time includes Hidden Markov Models with an innovative measurement method to measure pupilar illuminances on the eye-level plane of the user.

The five main points that constitute the proposed approach an improvement in relation to the established indices in the field, are:

- It does not require detailed knowledge of the user visual environment (the input variables are easily obtained with the minimum possible interference with the user).
- It makes use of the vertical illuminance at the pupillary level, which all studies indicate as the variable that correlates the most with the visual comfort^o.
- It takes into account the individual preferences and behaviour of different users.
- It attempts to address discomfort caused also by insufficient or excessive lighting conditions (as opposed to only estimating glare).
- When compared with other state-of-the art classifiers shows remarkably improved classification accuracy rates.

What is more, the results of the developed model have been compared with a previous study performed using the same data and the conclusion is that the newly developed model successfully reproduces the findings of the older one while using the completely different and innovative HMM approach.

Last, on the perspective of employing the proposed model in a building controller, we identify two clear advantages:

- Firstly, the model makes a clear decision whether the occupant experiences or not visual discomfort and this decision could be directly passed on to a controller that would undertake the proper actions.
- Secondly, the fine analysis performed in Section 6.4.4 concerning the normalised relative likelihoods of the identified states revealed that these metrics could be an

^o Not incorporated in the presently developed model but scheduled for inclusion in the future.

ideal input to building automation systems based on fuzzy logic. Indeed, the forms of the normalised curves resemble (and could serve as) the membership functions of a fuzzy inference input i.e. for the control of electric lighting (see for example Appendix A.2). In this way, the crisp state decided by the HMM could be turned into a fuzzy one, which in some cases might be preferable.

7. CONCLUSION AND OUTLOOK

7.1. Main achievements

In this section we review and discuss the key contributions of this doctoral thesis, where we developed novel stochastic models and algorithms for predictive building control, which maintain the occupants' comfort, while at the same time mitigate the energy demand taking into account the ever-changing outdoor conditions, the thermo-physical features of the building and the user preferences. More specific, in the framework of this research we achieved the following novelties:

- A novel sky-scanner prediction algorithm for the automatic control of electrochromic windows which addresses for the first time the slow reaction which characterizes this type of advanced glazing. The developed algorithm does not regard the EC windows as an isolated building sub-system, as it is often the case. Instead, it integrates them in a holistic approach, where, together with the blinds and artificial lighting, are part of an advanced daylighting system. We demonstrated that this system can create a comfortable visual and thermal environment (without excessive energy consumption) and can be considered as a future replacement to standard window glazings with mobile solar shadings or to permanently tinted solar protection glazings.
- A novel approach for building control based on the modelling of the "season" variable using Hidden Markov Models. Apart from the originality due to the use of HMMs, this model is innovative in that: (a) it addresses all parameters that influence the season variable (the building characteristics, the weather conditions and the user behaviour); (b) its elaboration does not require a thorough comprehension of the underlying physical processes; (c) it is building-independent and can be adapted to new or modified building configurations; (d) it demonstrated the ability to maintain the user's thermal comfort while mitigating energy for space heating.
- A novel approach for the estimation of visual comfort using HMMs, which, when compared with the current best practices, shows five clear improvements: (a) as it makes use of only two easily obtainable input variables (illuminance measured at the eye-level pupilar plane and on the task workplane), it does not entail complex calculations which require detailed knowledge of the visual environment of the user;

(b) it makes use of the vertical illuminance at the pupillary level, which all studies indicate as the variable that correlates the most with the visual comfort; (c) proposes a new method (EnOcean wireless autonomous sensors) for obtaining the vertical illuminance at the pupillary level, without much interference with the user's normal day-to-day tasks; (d) it takes into account user preferences and behaviour; (e) it attempts to enlarge the notion of visual discomfort to also cover insufficient or excessive lighting conditions (as opposed to only estimating glare).

From the summary of the above contributions brought about by this research, we can conclude (and thus confirm our constitutive hypothesis) that indeed "a sound automatic control which integrates successfully the different subsystems, respects user wishes and adapts to the building's own characteristics as well as to outdoor variations can reduce the energy consumption and provide for a better visual and thermal environment for the users".

7.2. Future outlook

Nevertheless, the confirmation of a thesis' hypothesis is almost never too exhaustive; as such, the perspectives for performing additional work that builds on the research presented herein or improving the novel concepts proposed seem almost endless. In this context, the following suggestions (alongside the ones discussed in detail at the end of each chapter) could constitute either points of improvement or of a new depart:

- The novel sky-scanner prediction algorithm for the control of electrochromic windows has been evaluated via a statistical analysis and later through a comprehensive parametric study. In the future, it would be interesting to evaluate its on-site performance in a real-life, long term field study which will also include detailed evaluation by users.
- On the technical side, it would also be interesting to slightly adapt the proposed sky-scanner algorithm by adding a fish-eye camera, which will almost certainly allow for a wider prediction window.
- Regarding the elaboration of the visual comfort model using Hidden Markov Models, it is very important to improve the quality (and time duration) of the vertical plane measurements by using a reliable sensor. However, this should not be on the expense of portability or the autonomous character of the sensor (two factors that were greatly appreciated by the subjects in this study).
- Also concerning the state-based developed models, we believe the next logical step would be their integration into smart control algorithms for building services as well as performing extensive field testing and measurements. This has been partly done for the season model (at least on the simulation level), and it is proposed but is not yet explored for the visual comfort one. Both developed HMM should benefit

however from the future development of the innovative analysis discussed in Section 6, which demonstrated the models' intrinsic capability to be seamlessly integrated and used in building control systems built around the fuzzy logic concept.

Last, it should be mentioned that the completion of the visual comfort modelling using HMMs and illuminance measurements at the eye-level pupilar plane has been kept on purpose outside this list of proposed future work, as it is currently the subject of an ongoing research in the framework of the Green-Mod research project which will carry on until March 2016.

APPENDIX

A.1. Communication protocol of "EControl-Glas" glazings

(Information presented in this section is an English translation of a German EControl-Glas document written by Tobias Wesenberg; errors may exist)

A.1.1. General description

The EControl unit for an EControl glazing can be used either as standalone control for a single glazing (control unit with a manual control ESS/BT), or as integrated in an advanced automatic control system (control unit ESS without manual control capability, as a UP style unit), controlled by a EC-Group control unit (GSG). The GSG includes additionally an RS 485 serial interface, which can be connected either to a PC or to a EIB/KNX, LonWorks, or Ethernet network through an interface.

A.1.2. EC-Bus

A protocol with variable data length is used for the communication between GSG and ESS. The tables below describe the protocol, the addresses, and the coding of commands and errors. For data and addresses including more than 1 byte, the most significant byte (High-Byte) is transmitted first.

Protocol format on the EC-Bus

Address	Command	Length	Data	Checksum
1 byte	1 byte	1 byte	max 20 bytes	1 byte

Serial transmission protocol: 19200 bauds, no parity, 1 stop-bit

Addresses

Address	Function
0	Feedback to GSG
1-30	ESS
200	Broadcast
251-254	Not implemented
255	Device not addressed (delivery status)

Commands

Remark: the commands 1 and 2 can be sent as broadcast, since these commands are checked periodically by the GSG. For that, the periodic sending (command 13) must be activated.

Number	Length	Description	Broadcast	Single	Answer
1	0 bytes	Glazing initialization	X	X	
2	1 byte	Start glazing transmission setting in % (18 ... 64)	X	X	
3	0 byte	Request short info		X	60
4	0 byte	Request measured values for current glazing temperature and current glazing transmission		X	61
7	1 byte	Request error list (0 ... 4)		X	60/63
8	0 byte	Request HW and SW status		X	60/64
9	0 byte	Request number of cycles		X	60/65
13	1 byte	Cyclic request of all ESS on EC-bus by the GSG: 0 = not active (reading of the individual ESS or ESS/BT by the GSG) 1 = active (default)			
30	7 bytes	Set clock: byte 1 = seconds (0 ... 59) byte 2 = minutes (0 ... 59) byte 3 = hours (0 ... 23) byte 4 = day of the month (1 ... 31) byte 5 = day of the week (0 ... 6, 0 = Sunday) byte 6 = month (1 ... 12) byte 7 = year (0 ... 99)		X	60
31	0 byte	Read system time		X	60/69

Feedback

All feedback data take place at address 0 (GSG).

Number	Length	Description	Broadcast	Single	Answer
60	1 byte	General feedback negative --> error code positive: 0 = ready, 1 = currently changing, 2 = init cycle Feedback "cyclic request" negative --> error code positive: 30 = not active, 31 = active			

		Feedback "set clock" negative --> error code positive: 40 = clock set			
61	20 bytes	Feedback from command "request measured values": glazing temperature (hi-byte 14, low-byte 15) glazing transmission (byte 18)			
63	10 bytes	Feedback from command "request error list" last 5 errors with time stamp: error number (0-4), error code (1), cycle number (3, see below), timestamp (5 bytes, see below)			
64	4 bytes	Feedback from command "request HW and SW status": bytes 1 and 2 --> hardware status xxxx bytes 3 and 4 --> software status yy.yy			
65	3 bytes	Feedback from current cycle number (3 bytes: lo, hi, LO)			
69	7 bytes	Feedback from command "request current system time", coded BCD: byte 1 = seconds (0 ... 59) byte 2 = minutes (0 ... 59) byte 3 = hours (0 ... 23) byte 4 = day of the month (1 ... 31) byte 5 = day of the week (0 ... 6, 0 = Sunday) byte 6 = month (1 ... 12) byte 7 = year (0 ... 99)			

Remark: the temperature is a signed (-/+) 16-bit number.

Error codes

Error number	Description
-15	checksum error EC-bus
-16	checksum error building bus
-30	temperature sensor broken or not connected
-31	temperature sensor broken or short-circuited
-38	glazing temperature too high (transmission coefficient adjustment stopped until $T < T_{max} - \text{hysteresis}$)

-39	glazing temperature too low (transmission coefficient adjustment stopped until $T > T_{min}$)
-----	--

Explanation "feedback to": errors that stop the adjustment of transmission coefficient are stored in the error memory of the EEPROMs. The errors can be retrieved by the command "request short info" through the bus, until a reset takes place. Errors whose cause is a bus access (checksum errors, status errors) are directly fed-back. When errors with other codes take place, please contact EControl-Glas.

Error memory organization

(BCD coding)

byte 1	error code
byte 2	cycle number low byte
byte 3	cycle number mid-byte
byte 4	cycle number high byte
byte 5	year
byte 6	month
byte 7	day of the month
byte 8	hour
byte 9	minute

Error request by GSG

The GSG polls cyclically every ESS on the EC-bus. By command number 3 ("request short info"), the current status (ready, currently adjusting transmission coefficient, initialized, or error code when an error happens) is provided.

A.1.3. Interface for an automatic control system

The RS485 interface of the GSG can be connected to a building bus through an additional interface, or to a PC. The telegrams on the EC-bus are directly transmitted to the RS485 interface, without any change of protocol.

A.1.4. Control of glazing transmission coefficient

The transmission coefficient of the glazing can be adjusted between 18 % (dark) and 64 % (clear).

A.1.5. Example: request short info from controller #2

1. De-activate cyclic sending:

Address	Command	Length	Data	Checksum
0	13	1	0	14

2. Wait answer from GSG:

Address	Command	Length	Data	Checksum
0	60	1	30	91

3. Request short info from controller #2:

Address	Command	Length	Data	Checksum
2	3	0	-	5

4. Answer controller #2:

Address	Command	Length	Data	Checksum
0	60	1	1	62

5. Re-activate cyclic sending:

Address	Command	Length	Data	Checksum
0	13	1	1	15

6. Answer from GSG:

Address	Command	Length	Data	Checksum
0	60	1	31	92

A.2. Fuzzy logic controller of Electrochromic Windows

A.2.1. User Present, "EC Tv" Fuzzy Rule Base

Inputs (fuzzy values):

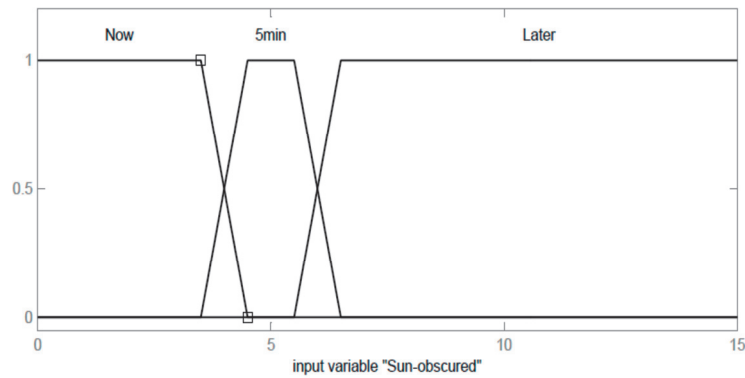


Figure A-1. Fuzzy variable "Sun-obscured" (sky obscured probability) [min].

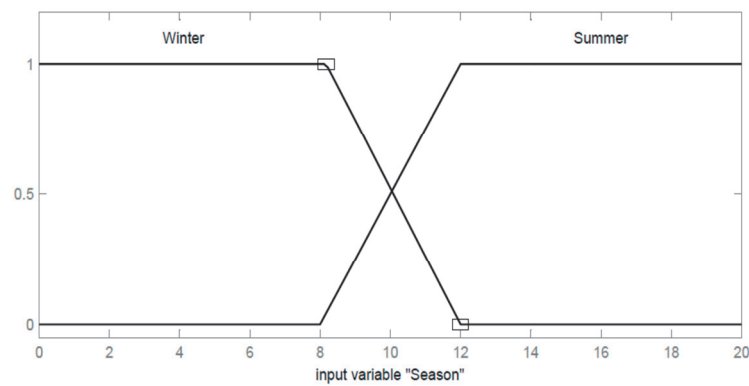


Figure A-2. Fuzzy variable "Season" (outdoor average temperature on the last 48 hours) [°C].

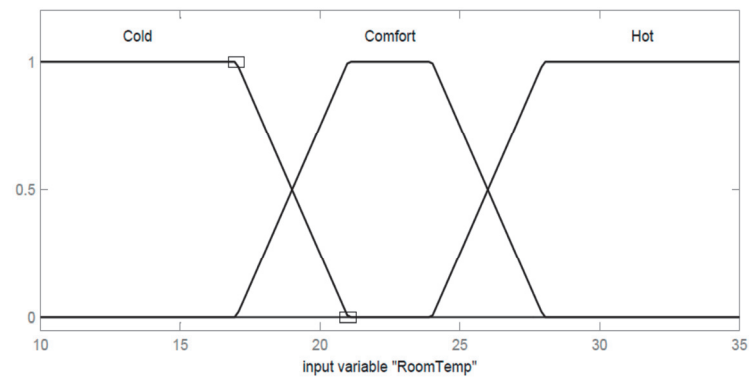


Figure A-3. Fuzzy variable "Roomtemp" (instantaneous air temperature) [°C].

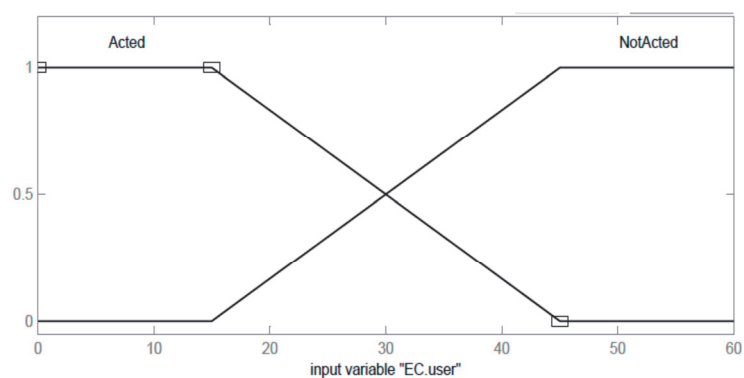


Figure A-4. Fuzzy variable "EC.user" (user interaction with EC windows) [min].

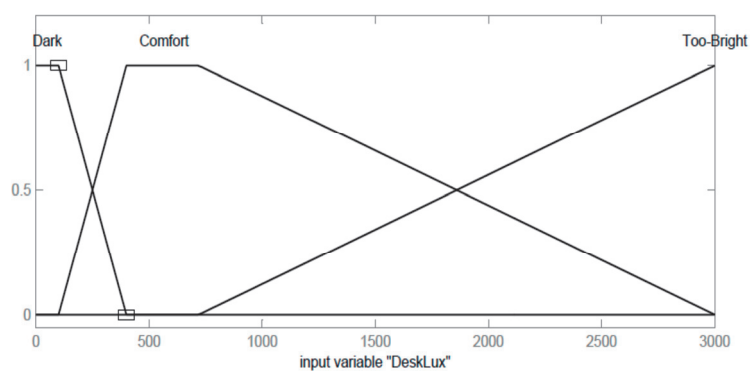


Figure A-5. Fuzzy variable "DeskLux" (minute-averaged workplane illuminance) [lx].

Output (crisp value):

Low = 15%
 MediumLow = 24%
 Medium = 32.5%
 MediumHigh = 41%
 High = 50%
 C = Leave unchanged

Table A-1. Output crisp value "EC-Tv" (EC windows visible light transmission)

Complete rule base (23 rules):

Fuzzy rules

- (1) If EC.user is "Acted" then EC-Tv is "C"
- (2) If Sun-obscured is "Later" and DeskLux is "Comfort" and EC.user is "NotActed" then EC-Tv is "C"
- (3) If Sun-obscured is "Later" and DeskLux is "Too-Bright" and Season is "Summer" and RoomTemp is "Hot" and EC.user is "NotActed" then EC-Tv is "Low"
- (4) If Sun-obscured is "Later" and DeskLux is "Too-Bright" and Season is "Summer" and RoomTemp is "Cold" and EC.user is "NotActed" then EC-Tv is "MediumLow"
- (5) If Sun-obscured is "Later" and DeskLux is "Dark" and Season is "Summer" and RoomTemp is "NOT Hot" and EC.user is "NotActed" then EC-Tv is "MediumHigh"
- (6) If Sun-obscured is "Later" and DeskLux is "Too-Bright" and Season is "Winter" and RoomTemp is "Cold" and EC.user is "NotActed" then EC-Tv is "Medium"
- (7) If Sun-obscured is "Later" and DeskLux is "Too-Bright" and Season is "Winter" and RoomTemp is "Comfort" and EC.user is "NotActed" then EC-Tv is "MediumLow"
- (8) If Sun-obscured is "Later" and DeskLux is "Too-Bright" and Season is "Winter" and RoomTemp is "Hot" and EC.user is "NotActed" then EC-Tv is "MediumLow"
- (9) If Sun-obscured is "Later" and DeskLux is "Dark" and Season is "Winter" and RoomTemp is "Cold" and EC.user is "NotActed" then EC-Tv is "High"
- (10) If Sun-obscured is "Later" and DeskLux is "Dark" and Season is "Winter" and RoomTemp is "Comfort" and EC.user is "NotActed" then EC-Tv is "High"
- (11) If Sun-obscured is "Later" and DeskLux is "Dark" and RoomTemp is "Hot" and EC.user is "NotActed" then EC-Tv is "MediumHigh"
- (12) If Sun-obscured is "5min" and Season is "Winter" then EC-Tv is "High"
- (13) If Sun-obscured is "5min" and Season is "Summer" then EC-Tv is "MediumHigh"
- (14) If Sun-obscured is "Now" and DeskLux is "Dark" and RoomTemp is "Cold" and EC.user is "NotActed" then EC-Tv is "High"
- (15) If Sun-obscured is "Now" and DeskLux is "Dark" and RoomTemp is "Comfort" and EC.user is "NotActed" then EC-Tv is "High"
- (16) If Sun-obscured is "Now" and DeskLux is "Dark" and RoomTemp is "Hot" and EC.user is "NotActed" then EC-Tv is "MediumHigh"
- (17) If Sun-obscured is "Now" and DeskLux is "Comfort" and EC.user is "NotActed" then EC-Tv is "C"
- (18) If Sun-obscured is "Now" and DeskLux is "Too-Bright" and Season is "Winter" and RoomTemp is "Cold" and EC.user is "NotActed" then EC-Tv is "High"
- (19) If Sun-obscured is "Now" and DeskLux is "Too-Bright" and Season is "Winter" and RoomTemp is "Comfort" and EC.user is "NotActed" then EC-Tv is "High"
- (20) If Sun-obscured is "Now" and DeskLux is "Too-Bright" and Season is "Winter" and RoomTemp is "Hot" and EC.user is "NotActed" then EC-Tv is "MediumHigh"
- (21) If Sun-obscured is "Now" and DeskLux is "Too-Bright" and Season is "Summer" and RoomTemp is "Cold" and EC.user is "NotActed" then EC-Tv is "MediumHigh"
- (22) If Sun-obscured is "Now" and DeskLux is "Too-Bright" and Season is "Summer" and RoomTemp is "Comfort" and EC.user is "NotActed" then EC-Tv is "Medium"
- (23) If Sun-obscured is "Now" and DeskLux is "Too-Bright" and Season is "Summer" and RoomTemp is "Hot" and EC.user is "NotActed" then EC-Tv is "Medium"

Table A-2. Complete rule base of control scheme *User Present*, "EC Tv" in verbose format.

A.2.2. User Absent, "EC Tv" Fuzzy Rule Base

Inputs (fuzzy values):

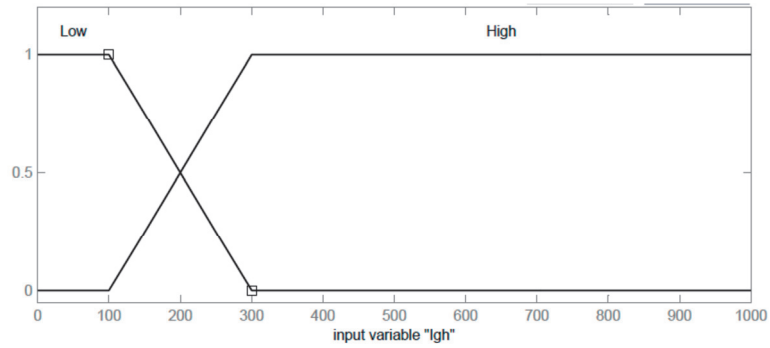


Figure A-6. Fuzzy variable "Igh" (global horizontal solar irradiation) [W/m²].

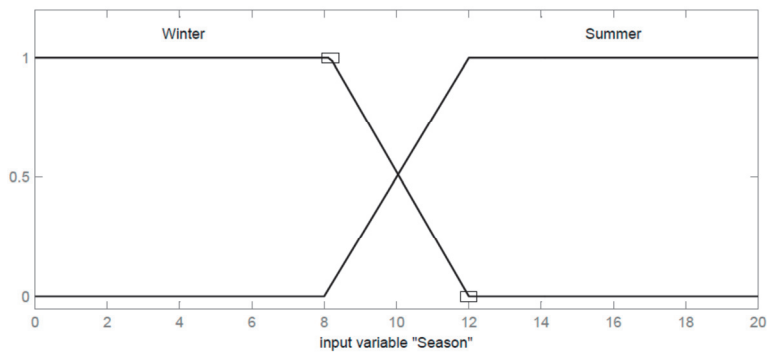


Figure A-7. Fuzzy variable "Season" (outdoor average temperature on the last 48 hours) [°C].

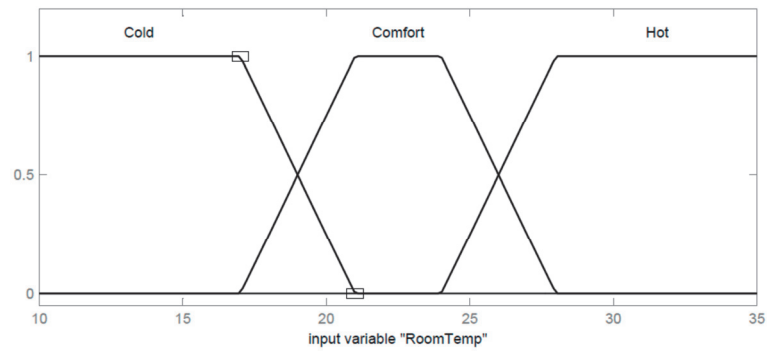


Figure A-8. Fuzzy variable "RoomTemp" (instantaneous air temperature) [°C].

Output (crisp value):

Low = 15%
MediumLow = 24%
Medium = 32.5%
MediumHigh = 41%
High = 50%

Table A-3. Output crisp value "EC-Tv" (EC windows visible light transmission)

Complete rule base (10 rules):

Fuzzy rules

-
- (1) If Season is "Summer" and RoomTemp is "Hot" then EC-Tv is "Low"
 - (2) If Igh is "High" and Season is "Summer" and RoomTemp is "Comfort" then EC-Tv is "MediumLow"
 - (3) If Igh is "High" and Season is "Summer" and RoomTemp is "Cold" then EC-Tv is "Medium"
 - (4) If Igh is "Low" and Season is "Summer" and RoomTemp is "Comfort" then EC-Tv is "Medium"
 - (5) If Igh is "Low" and Season is "Summer" and RoomTemp is "Cold" then EC-Tv is "MediumHigh"
 - (6) If Igh is "High" and Season is "Winter" and RoomTemp is "Hot" then EC-Tv is "Medium"
 - (7) If Igh is "High" and Season is "Winter" and RoomTemp is "Comfort" then EC-Tv is "MediumHigh"
 - (8) If Igh is "Low" and Season is "Winter" and RoomTemp is "Hot" then EC-Tv is "MediumHigh"
 - (9) If Igh is "Low" and Season is "Winter" and RoomTemp is "Comfort" then EC-Tv is "High"
 - (10) If Season is "Winter" and RoomTemp is "Cold" then EC-Tv is "High"
-

Table A-4. Complete rule base of control scheme *User Absent*, "EC Tv" in verbose format.

A.2.3. *User Present*, "Blinds" Fuzzy Rule Base

Inputs (fuzzy & crisp values):

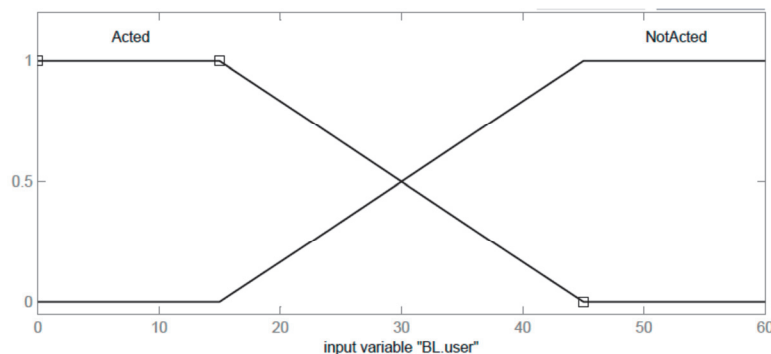


Figure A-9. Fuzzy variable "BL.user" (user interaction with the blinds) [min].

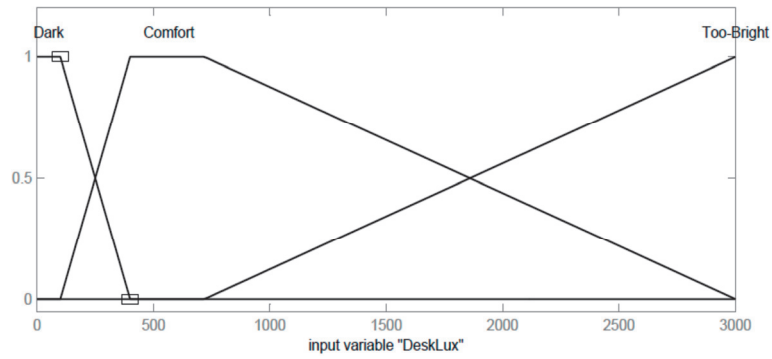


Figure A-10. Fuzzy variable "DeskLux" (minute-averaged workplane illuminance) [lx].

Low = 15%
 MediumLow = 24%
 Medium = 32.5%
 MediumHigh = 41%
 High = 50%

Table A-5. Input crisp value "EC-Tv" (EC windows visible light transmission)

Output (crisp value):

0
 0.4
 0.6
 0.8
 1
 C (Leave unchanged)

Table A-6. Output crisp value " a_{blind} " (Blinds position: 1: completely open; 0: completely closed).

Complete rule base (8 rules):

Fuzzy rules

- (1) If BL.user is "Acted" then alpha-blind is "C"
- (2) If DeskLux is "Dark" and BL.user is "NotActed" then alpha-blind is "1"
- (3) If DeskLux is "Comfort" and BL.user is "NotActed" then alpha-blind is "C"
- (4) If DeskLux is "Too-Bright" and BL.user is "NotActed" and EC-Tv is "Low" then alpha-blind is "0.4"
- (5) If DeskLux is "Too-Bright" and BL.user is "NotActed" and EC-Tv is "MediumLow" then alpha-blind is "0.6"
- (6) If DeskLux is "Too-Bright" and BL.user is "NotActed" and EC-Tv is "Medium" then alpha-blind is "0.8"
- (7) If DeskLux is "Too-Bright" and BL.user is "NotActed" and EC-Tv is "MediumHigh" then alpha-blind is "1"
- (8) If DeskLux is "Too-Bright" and BL.user is "NotActed" and EC-Tv is "High" then alpha-blind is "1"

Table A-7. Complete rule base of control scheme *User Present*, "Blinds" in verbose format.

A.2.4. *User Absent*, "Blinds" Fuzzy Rule Base

Inputs (fuzzy & crisp values):

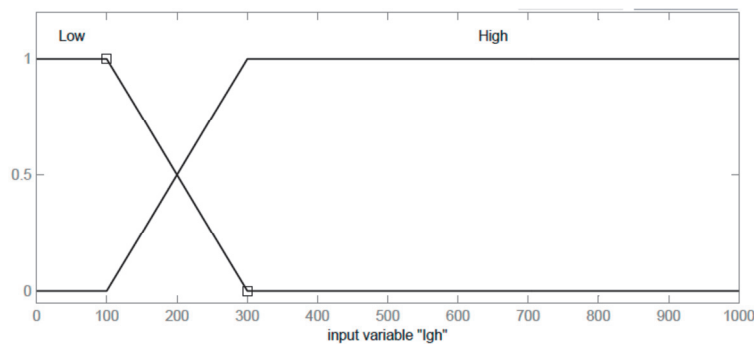


Figure A-11. Fuzzy variable "Igh" (global horizontal solar irradiation) [W/m²].

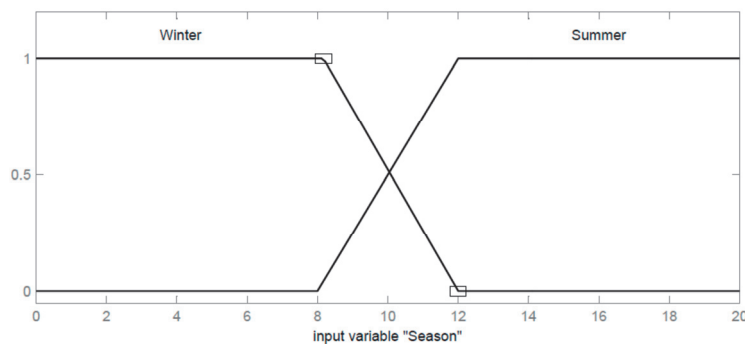


Figure A-12. Fuzzy variable "Season" (outdoor average temperature on the last 48 hours) [°C].

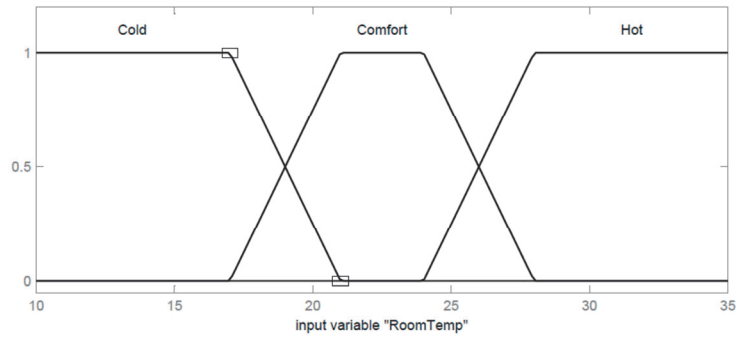


Figure A-13. Fuzzy variable "RoomTemp" (instantaneous air temperature) [°C].

Low = 15%
 MediumLow = 24%
 Medium = 32.5%
 MediumHigh = 41%
 High = 50%

Table A-8. Input crisp value "EC-Tv" (EC windows visible light transmission)

Output (crisp value):

0
 0.4
 0.6
 0.8
 1

Table A-9. Output crisp value " α_{blind} " (Blinds position: 1: completely open; 0: completely closed).

Complete rule base (9 rules):

Fuzzy rules

- (1) If EC-Tv is "Low" and Igh is "High" and Season is "Summer" and RoomTemp is "Hot" then alpha-blind is "0"
 - (2) If EC-Tv is "MediumLow" then alpha-blind is "0.4"
 - (3) If EC-Tv is "Medium" and Igh is "High" and Season is "Summer" and RoomTemp is "Cold" then alpha-blind is "0.4"
 - (4) If EC-Tv is "Medium" and Igh is "Low" and Season is "Summer" and RoomTemp is "Comfort" then alpha-blind is "0.6"
 - (5) If EC-Tv is "Medium" and Igh is "High" and Season is "Winter" and RoomTemp is "Hot" then alpha-blind is "0.8"
 - (6) If EC-Tv is "MediumHigh" and Igh is "Low" and Season is "Summer" and RoomTemp is "Cold" then alpha-blind is "0.6"
 - (7) If EC-Tv is "MediumHigh" and Igh is "High" and Season is "Winter" and RoomTemp is "Comfort" then alpha-blind is "1"
 - (8) If EC-Tv is "MediumHigh" and Igh is "Low" and Season is "Winter" and RoomTemp is "Hot" then alpha-blind is "1"
 - (9) If EC-Tv is "High" then alpha-blind is "1"
-

Table A-10. Complete rule base of control scheme *User Absent*, "Blinds" in verbose format.

A.2.5. *User Present, "Lights" Fuzzy Rule Base*

Inputs (fuzzy & crisp values):

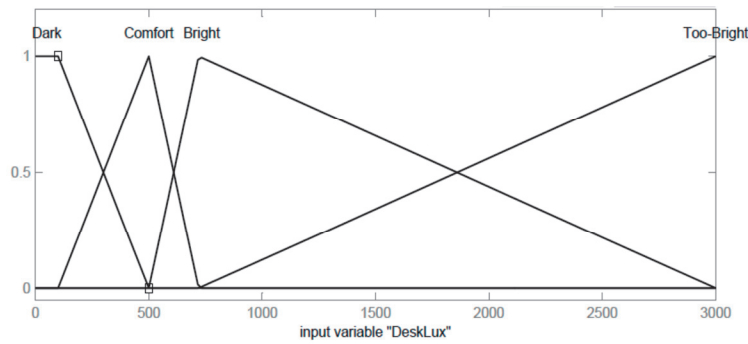


Figure A-14. Fuzzy variable "DeskLux" (minute-averaged workplane illuminance) [lx].

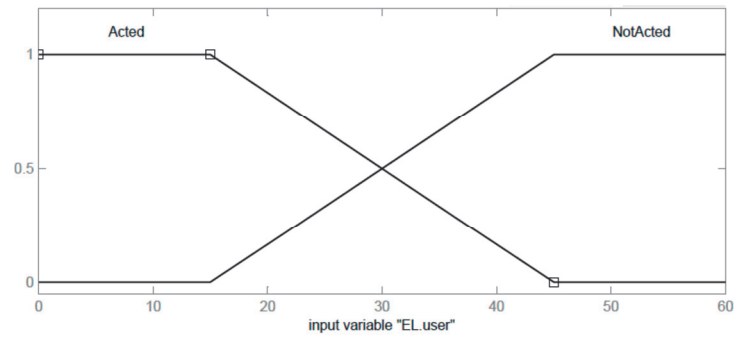


Figure A-15. Fuzzy variable "EL.user" (user interaction with the electric lights) [min].

Low = 15%
MediumLow = 24%
Medium = 32.5%
MediumHigh = 41%
High = 50%

Table A-11. Input crisp value "EC-Tv" (EC windows visible light transmission)

0
0.4
0.6
0.8
1

Table A-12. Input crisp value "ablind" (Blinds position: 1: completely open; 0: completely closed).

Output (crisp value)^a:

0
1
C (LeaveUnchanged)

Table A-13. Output crisp value "P.lights" (fraction of applied electric lighting power in dimmable luminaires; 1: fully on; 0: completely off).

Complete rule base (8 rules):**Fuzzy rules**

-
- (1) If DeskLux is "Comfort" and EL.user is "Acted" then P.lights is "C"
 (2) If DeskLux is "Comfort" and EL.user is "NotActed" then P.lights is "C"
 (3) If DeskLux is "Too-Bright" and EL.user is "NotActed" then P.lights is "0"
 (4) If DeskLux is "Dark" and EL.user is "NotActed" and EC-Tv is "NOT High" and alpha-blind is "NOT 1" then P.lights is "0"
 (5) If DeskLux is "Dark" and EL.user is "NotActed" and EC-Tv is "NOT MediumHigh" and alpha-blind is "NOT 1" then P.lights is "0"
 (6) If DeskLux is "Dark" and EL.user is "NotActed" and EC-Tv is "High" and alpha-blind is "1" then P.lights is "1"
 (7) If DeskLux is "Dark" and EL.user is "NotActed" and EC-Tv is "MediumHigh" and alpha-blind is "1" then P.lights is "1"
 (8) If DeskLux is "ComfortBright" and EL.user is "NotActed" then P.lights is "0"
-

Table A-14. Complete rule base of control scheme *User Present*, "Lights" in verbose format.

^a Although set to a crisp value, the output of the rules (as well as the one used for the control of electric lights) is a fraction in the region of [0,1].

A.4. Switching time curves of electrochromic windows

Measurements have been performed as explained in Section 4.1.1 with EC reported temperature at about 26°C.

A.4.1. From clear to tinted state

Time [min]	Tv EC [%]	Tv IGU [%]	SHGC [%]
0	64	50.0	38.0
1	58.8	46.3	35.8
2	53.2	42.1	32.9
3	48.2	38.4	30.3
4	43.7	35.0	27.9
5	39.7	32.0	25.7
6	36.1	29.3	23.7
7	33	27.0	22.0
8	30.3	24.9	20.5
9	28	23.2	19.1
10	26	21.6	17.9
11	24.3	20.3	16.9
12	23	19.3	16.1
13	21.9	18.5	15.3
14	21	17.7	14.7
15	20.3	17.2	14.2
16	19.8	16.8	13.8
17	19.5	16.5	13.5
18	19.2	16.3	13.2
19	19.1	16.2	13.1
20	19	16.1	13.0
21	18.9	16.0	12.9
22	18.8	16.0	12.8
23	18.7	15.9	12.8
24	18.5	15.8	12.7
25	18.3	15.7	12.7
26	18	15.0	12.0

A.4.2. From fully tinted to clear

Time [min]	Tv EC [%]	Tv IGU [%]	SHGC [%]
0	18.0	15.0	12.0
1	19.4	16.4	13.4
2	20.4	17.5	14.5
3	21.5	18.4	15.4
4	22.7	19.4	16.3

5	24.0	20.6	17.2
6	25.8	21.9	18.3
7	27.8	23.6	19.5
8	30.3	25.6	21.1
9	33.2	27.9	22.9
10	36.5	30.6	24.9
11	40.2	33.5	27.2
12	44.1	36.6	29.5
13	48.1	39.7	31.9
14	52.1	42.8	34.2
15	56.0	45.6	36.1
16	59.5	48.0	37.6
17	62.4	49.7	37.9
18	64.0	50.0	38.0

A.5. Short survey questionnaire

Electrochromic Windows short survey (LESO, Office LE003)

Time required: ~10min

Part A: Background information

Date:

Start time:

End Time:

A1. What is your gender?

- ☐ Male
- ☐ Female

A2. How old are you?

- ☐ Under 30
- ☐ 30-39
- ☐ 40-49
- ☐ 50-59
- ☐ 60 and over

A3. Are you colour blind?

- ☐ No
- ☐ Yes: Red/Green; Blue/Yellow (please underline one pair)
- ☐ I am not sure

A4. On a scale from 1 to 5, how familiar you would say you are with the Electrochromic (EC) Windows applications in buildings? [1=Not at all, 5=Very familiar]

Part B: Survey

B1. During this session, what percentage of your time was spent on each of the following tasks:

- a. Reading (from paper) : %
- b. Computer: %
- c. Writing by hand: %
- d. Other: %, please specify:

B2. During this session, what percent of your time were you facing the following directions:

- a. Side wall : %
- b. Windows: %
- c. Back wall/Door: %
- a. Other: %, please specify:

B3. Please assign a rating of 1,2,3,4 or 5 with all the following lighting/thermal conditions during the time you spent in the test office.

- a. Room Temperature [1=Too cold, 3=Just right, 5=Too hot]:
- b. Light level [1=Too dark, 3=Just right, 5=Too bright]:
- c. Light distribution [1=Very bad, 5=Excellent]:
- d. Room colours [1=Very unnatural, 5=Natural]:
- e. Colours when looking outside [1=Very unnatural, 5=Natural]:
- f. Glare sensation [1=None, 3=Acceptable, 5=Intolerable]:

B4. Please rate with **1,2,3,4 or 5** your satisfaction regarding **all** of the following aspects of the Electrochromic (EC) Windows during the time you spent in the test office. [1=Very Dissatisfied, 5=Very Satisfied]

- a. Ease of use of EC windows manual control panels:
- b. Time to switch to desired transmission level (lighten/darken):
- c. Other (Please specify):_____

B5. During your stay in this office, did you use **the blinds**?

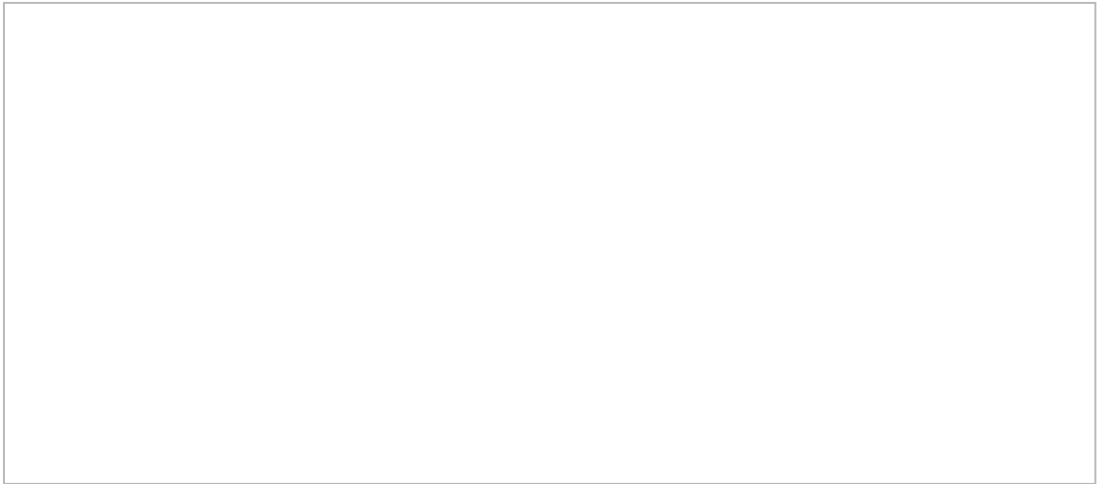
- ☐ No
- ☐ Yes, for the following reason(s): [Choose as many as appropriate]
- ☐ To deal with overheating issues
 - ☐ To deal with glare issues
 - ☐ To reduce illuminance levels
 - ☐ EC windows were difficult to adjust to desired levels of light transmission
 - ☐ EC windows took a lot of time to change their light transmission levels
 - ☐ Privacy
 - ☐ Other (Please specify): _____

B6. During your stay in this office, did you use **the electric lighting**?

- ☐ No
- ☐ Yes, for the following reason(s): [Choose as many as appropriate]
- ☐ To increase lighting level
 - ☐ Other (Please specify): _____

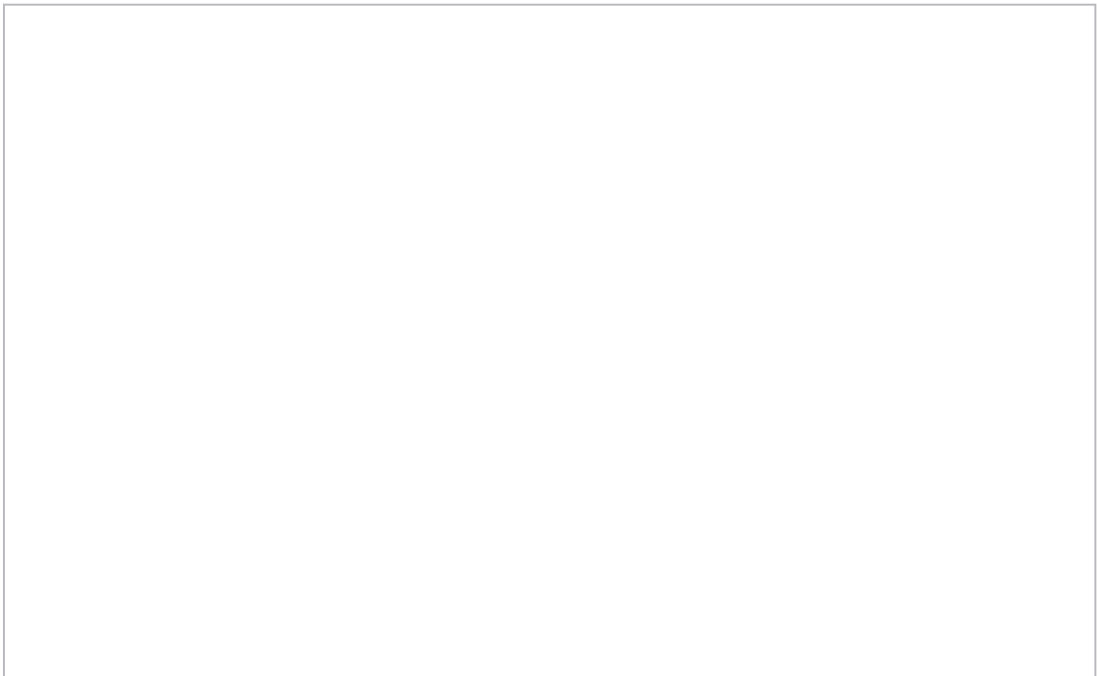
B7. Regarding the natural light conditions, **what did you appreciate** during the time you spent working in this office? (e.g. you can compare with your usual workplace in LESO)

B8. Regarding the natural light conditions, **what did you not like** during the time you spent working in this office? (e.g. you can compare with your usual workplace in LESO)



B9. Please freely add below any additional remarks, comments or suggestions you may have regarding the time you spent working in this office.

Also, in the view of a thorough survey we are planning for the future on the subject of users' satisfaction with an advanced automatic control system of Electrochromic Windows, you're also kindly asked to comment on the survey itself and help us improve the questionnaire and research protocol.



A.6. Useful information concerning the portable illuminance sensor 'EnOcean'

(This text was handed out to the subjects that participated in the measurements campaign described in Section 6.3.3).

To ensure the study's success you are kindly requested to follow these simple guidelines concerning the portable illuminance sensor. If you have any questions whatsoever, please do not hesitate to contact us (turn over for details). Thank you for accepting to participate!

- **Please hang the sensor around your neck as soon as you start your working day in the office.** If for any reason you omit it, just note down the time & date and inform us so we can exclude the time that you were in your office without wearing it from our analysis. (You can still put the sensor on at a later time during the day; it will just mean less useful data for the study).
- Feel free to adjust the length of the belt (loose or tighten the knot as appropriate) to keep it as comfortable as possible for you. Just make sure **the sensor is not (partly) hidden beneath your desk while you work, nor it is hindered by any garments** (scarf, tie, jacket etc.).
- Each sensor bears a name on the bottom side; this is for your convenience and to avoid accidental swaps of the sensors. Please also note that this study is about single-occupant offices; **do not give the sensor to another person who might be working in your office.**
- If another person is present or working in your office while you're there, there is not a problem; just carry on normally with your work! However, **if another person is using your office while you're not there for the whole day or a big part of it, then please tell us so we can exclude measured data from our study.**
- Please don't change your habits, preferences or visual comfort levels because of study: **Feel absolutely free to adjust the electric lights or the blinds in your office** to match your preferences and comfort levels. However, please give priority to electrically powered devices (roller tissue blinds and dimmable lights) over manually controlled devices (i.e. vertical venetian blinds of the anidolic windows).
- When not wearing the sensor (i.e. when out of office or at the end of the day), please **leave it to a luminous spot with as much daylight as possible, face up** (not upside down or under papers or other objects). This way the PV panel around the sensor will keep your sensor's battery charged!
- **Keep the sensor on you as often as possible when inside your office.** That being said, you don't have to take it off each time you step outside your office: no data will be recorded or processed when you are out of office, even if you keep it on you. (Of course, you might want to take it off for your own comfort when out of office!). Similarly, **feel free to work wherever/however you like inside your office: at your desk, at the round table, on your white board, arrange your files etc.**

...and the most important:

Carry on with your normal activities as if you were not wearing the sensor!

NOMENCLATURE

ADS	Anidolic Daylighting System(s)
ANN	Artificial Neural Networks
Ave	Average
BGI	British Glare Index
CCD	Charge-coupled device (i.e. sensor in digital cameras)
CGI	CIE Glare Index
CIE	Commission Internationale de l'Eclairage (International Commission on Illumination)
DC	Direct Current
DGI	Daylight Glare Index
DGP	Daylight Glare Probability
Discomfort-H	Discomfort because of High illuminances
Discomfort-L	Discomfort because of Low illuminances
EC	Electrochromic
Egh	Global Horizontal Illuminance [lx]
EIB	European Installation Bus
EM	Expectation-Maximisation (algorithm)
EPFL	École Polytechnique Fédérale De Lausanne
Evgs	Global vertical South illuminance [lx]
FOV	Field-of-view

GMM	Gaussian Mixture Models
HMM	Hidden Markov Model
HTTP	Hypertext Transfer Protocol
HVAC	Heating, Ventilation and Air Conditioning
I_{gh}	Global horizontal solar irradiation [W/m ²]
IGU	Insulating Glass Unit
I_{gvs}	Global vertical south solar radiation [W/m ²]
LAN	Local Area Network
LC	Liquid Crystal
LED	Light Emitting Diode
LESO(-PB)	Laboratoire d'Énergie SOLaire et de Physique du Bâtiment (Solar Energy and Building Physics Laboratory)
MPC	Model Predictive Control
PMV	Predicted Mean Vote
PPD	Predicted Percentage of Dissatisfied
SHGC	Solar Heat Gain Coefficient
SP	Electrophoretic or Suspended-Particle
Stdv	Standard deviation
T_{ext}	Outside (external) temperature [°C]
T_{int}	Internal air temperature [°C]
T_v	Visible Transmittance
UGR	Unified Glare Rating
VisDP	Visual Discomfort Probability
WoT	Web-of-Things

LIST OF FIGURES

Figure 1-1. General scheme representing the scope of the doctoral thesis.....	4
Figure 2-1. LESO building: (a) ground floor; (b) first floor; (c) second floor; (d) southern façade [28].	9
Figure 2-2. Vertical section detail of an office room located in the South façade of LESO building which showcases the conventional window on the lower part and the ADS on the upper one [32].	9
Figure 2-3. Pictures and plan drawing of the LESO solar experimental building and office room LE 003 where the EC glazings have been installed.	12
Figure 2-4. EC glazings in the bleached (clear) and fully tinted (dark) states.	13
Figure 2-5. Schematic view and cross section of installed EC glazings (images: ©EControl-Glas GmbH).	13
Figure 2-6. One of the two control units of the EC glazings with the manual control panel in the front (right image) and its position inside the office room LE 003.....	14
Figure 2-7. EnOcean gateway connected to Ethernet and to DC power supply (left image) and autonomous EnOcean illuminance/motion sensor with the solar cells around the sensor (image on the right).	16
Figure 2-8. Connection topology of EnOcean sensors with the gateway and the local area network (LAN) via Ethernet.	16
Figure 3-1. (a) Outside and (b) inside view of the skylight in the office room where the camera was placed; the red circles indicate the point where the camera was placed during the measurements; (c) the USB camera "BulletHD PRO 1080p" used for the study, at an angle ' α ' from the zenith. (Image taken while the camera was off-duty, placed on a desk).	24
Figure 3-2. Sky prediction image-processing – part I: (a) and (b) show two consecutive original images taken on 2012.06.07 at 10h29m40s and at 10h29m45s (UTC+2), respectively.	25
Figure 3-3. Sky prediction image-processing – part II: (c) shows the combined image of the two original images with motion vectors grid overlaid; (d) presents the	

decision image including sun disc position (area inside orange circle), the vectors corresponding to (parts of) clouds heading towards the sun disc (in red) and the part of clouds that can potentially obscure the sun with the time prediction for each of them (blue numbers in min).	26
Figure 3-4. Prediction accuracy of the sky scanner algorithm as a function of the variability of the sky conditions (as represented by the hourly standard deviation of the Global Horizontal Irradiance) for the four days analysed.	30
Figure 4-1. Switching decay curve (blue marks) of the EC element (laminated unit) for the installed EC glazing showing Tv levels (%) vs. switching time (min) during transition from bleached to coloured states for a given temperature ($\sim 26^{\circ}\text{C}$). The black line is the polynomial fit with displayed equation and coefficient of determination.	39
Figure 4-2. Switching decay curve (blue marks) of the EC element (laminated unit) for the installed EC glazing showing Tv levels (%) vs. switching time (min) during transition from coloured to bleached states for a given temperature ($\sim 26^{\circ}\text{C}$). The black line is the polynomial fit with displayed equation and coefficient of determination.	39
Figure 4-3. Daylight factors for the two extreme Tv levels of the EC windows (50 and 15%) as a function of the distance from the windows (measurement errors: 15% for the DF and $\pm 0.1\text{m}$ for the distances). The apparent non-homotheticity of the curves can be attributed to measurement errors and to the presence of the ADS in the upper window.	41
Figure 4-4. Desktop illuminance and Global Horizontal Irradiance (IgHor) measurements before and around noon time on 31 August 2012 (day with intermediate sky conditions).	43
Figure 4-5. A schematic of the thermal model used in the simulations as an equivalent electric circuit.	46
Figure 4-6. Electric lights usage as a function of the natural light-induced desktop illuminance.	50
Figure 4-7. Annual energy demand for space heating and electric lighting for different simulation scenarios.	52
Figure 4-8. Temperatures variation for Scenario 1 (Standard glazing; no blinds). Overheating is observed from March to November.	54
Figure 4-9. Temperatures variation for Scenario 2 (Standard glazing + blinds). Internal temperature exceeding 30°C is observed during intermediate season.	54
Figure 4-10. Temperatures variation for Scenario 3 (Low Solar gain glazing; SHGC=0.38). Internal temperatures around 30°C are observed for about 75 days during the year.	54

Figure 4-11. Temperatures variation for Scenario 4 (Low Solar gain glazing; SHGC=0.12).	55
Figure 4-12. Temperatures variation for Scenario 5 (EC simple control).	55
Figure 4-13. Temperatures variation for Scenario 6 (EC Predictive control).....	55
Figure 4-14. Distribution of indoor air temperature values for the six different simulation scenarios for a period of one year. The blue bottom and top of the box represent the 25th and 75th percentile respectively; the red mark inside the box is the 50th percentile (the median); whiskers represent the minimum and maximum of data points not considered outliers (red points outside whiskers).	56
Figure 4-15. Percentage of working time during the simulation period where temperature is outside comfort limits (i.e. PPD is over 10%), for each of the six considered simulation cases.	58
Figure 4-16. Indoor temperature values distribution during working hours in non-heating period (a) for simulation scenarios 1-3. Displayed are the values (black points), median (orange line), mean (light blue dashed line) and standard deviation (σ) together with the limits of the operative temperatures (green and red lines).	60
Figure 4-17. Indoor temperature values distribution during working hours in heating period (b) for simulation scenarios 1-3. Displayed are the values (black points), median (orange line), mean (light blue dashed line) and standard deviation (σ) together with the limits of the operative temperatures (green and red lines).....	61
Figure 4-18. Indoor temperature values distribution during working hours in non-heating period (a) for simulation scenarios 4-6. Displayed are the values (black points), median (orange line), mean (light blue dashed line) and standard deviation (σ) together with the limits of the operative temperatures (green and red lines).	62
Figure 4-19. Indoor temperature values distribution during working hours in heating period (b) for simulation scenarios 4-6. Displayed are the values (black points), median (orange line), mean (light blue dashed line) and standard deviation (σ) together with the limits of the operative temperatures (green and red lines).....	63
Figure 4-20. User discomfort probability as a function of horizontal workplace illuminance (values greater than ~ 3 klux should be ignored due to the saturation of the illuminance sensors of the study above this limit) [18] (image: ©Lindelöf).....	64
Figure 4-21. Percentage of working time during the simulation period where visual discomfort probability is kept below 30, 35, 40, 45 and 50%, for each of the six considered simulation cases.	65
Figure 4-22. Distribution of desktop illuminance values for the six different simulation scenarios for a period of one year. The blue bottom and top of the box represent the 25th and 75th percentile respectively; the red mark inside the box is the 50th	

percentile (the median); whiskers represent the minimum and maximum of data points not considered outliers (red points outside whiskers). Top whisker of Scenario '1' is >9000 lx and it is not displayed here.	66
Figure 4-23. Simulation scenarios 1-3: Desktop illuminance values distribution during working hours for the entire simulation period. The illuminance limits for every range of the VisDP are marked with 2 identical vertical lines for every range (see Table 4-6 for the range limits). Displayed next to the limit lines with the same colour as them are the percentages of working hours of the entire period with illuminance inside the limits of each range.	67
Figure 4-24. Simulation scenarios 4-6: Desktop illuminance values distribution during working hours for the entire simulation period. The illuminance limits for every range of the VisDP are marked with 2 identical vertical lines for every range (see Table 4-6 for the range limits). Displayed next to the limit lines with the same colour as them are the percentages of working hours of the entire period with illuminance inside the limits of each range.	68
Figure 4-25. Desktop illuminance (EC 5; EC 6), Global Horizontal Irradiance (IgHor) and Vertical South Global Irradiance (IgvSouth) fluctuation around noon time on a day with intermediate sky conditions (September 5 th ; non heating period) for 2 different EC windows control strategies (Scenario 5 and 6).	69
Figure 5-1. Season succession over the course of one year in (a) the classical, calendar definition of the season and (b) in season definition in building control.	74
Figure 5-2. Annual energy demand for space heating for different simulation scenarios.....	93
Figure 5-3. Temperatures variation for Scenario 1 (LESO office-room with standard control).....	95
Figure 5-4. Temperatures variation for Scenario 2 (LESO office-room with HMM control).....	95
Figure 5-5. Temperatures variation for Scenario 3 (Light-weight structure with standard control).	96
Figure 5-6. Temperatures variation for Scenario 4 (Light-weight structure with HMM control).	96
Figure 5-7. Distribution of indoor air temperature values for the four different simulation scenarios for a period of one year. The blue bottom and top of the box represent the 25th and 75th percentile respectively; the red mark inside the box is the 50th percentile (the median); whiskers represent the minimum and maximum of data points not considered outliers (the red points outside whiskers).....	97
Figure 5-8. Percentage of working time during the simulation period where temperature is outside comfort limits (i.e. PPD is over 10%), for each of the four considered simulation cases.	99

- Figure 5-9. Indoor temperature values distribution during working hours in (a) non-heating and (b) heating period for simulation scenarios 1-2. Displayed are the values (black points), median (orange line), mean (light blue dashed line) and standard deviation (σ) together with the limits of the operative temperatures (green and red lines). 101
- Figure 5-10. Indoor temperature values distribution during working hours in (a) non-heating and (b) heating period for simulation scenarios 2-4. Displayed are the values (black points), median (orange line), mean (light blue dashed line) and standard deviation (σ) together with the limits of the operative temperatures (green and red lines). 102
- Figure 6-1. Picture that shows one of the six users that participated in the field measurements of pupilar plane illuminance, bearing the autonomous EnOcean illuminance/motion sensor as a pendant. 114
- Figure 6-2. Chauvin Arnoux C.A 811 Light-Meter (Image: ©Chauvin Arnoux Group). 115
- Figure 6-3. Comparison of simultaneous illuminance measurements taken with the Chauvin Arnoux C.A 811 Light-Meter (corrected with a coefficient of 0.86 to reflect actual values and assuming an additional 5% measurement error [error bars]) and four of the EnOcean sensors. 116
- Figure 6-4. Illuminance distribution, before and after user action, in office room 104 (Histogram bin width: 100 lux). Combinations of user actions spaced apart not more than one minute in time are considered as part of the same user action. Actions performed less than two minutes before the user has left the office were excluded. A total of 1347 actions are considered for the period January 2003 – January 2005. 121
- Figure 6-5. Simplified Bayesian estimation of discomfort probability as a function of the horizontal workplane illuminance with polynomial regression (red line). Data were collected in LESO office room 104 between January 2003 and January 2005. 122
- Figure 6-6. Visual comfort state identification against different workplane illuminance values for 35 different HMMs, each having (k) GMM mixtures ranging from 1 to 40 (models for k equal to 24-26, 34 and 40 are omitted because of non-convergence). The mean values of state identification for all the models are presented on the bottom. 125
- Figure 6-7. Quality of k-NN classifiers as a function of the number of Nearest Neighbors (k) used in each model. The Resubstitution loss is the fraction of misclassifications concerning the training data, while the Cross-validation loss is the lack of precision when classifying data not used on training (assuming that the new data has about the same distribution as the training data). 127
- Figure 6-8. Visual comfort state identification against different workplane illuminance values for 40 different k-NN based classifiers, each having (k) Nearest Neighbors

ranging from 1 to 40. The mean values of state identification for all the models are presented on the bottom.	128
Figure 6-9. Normalised relative likelihood for each identified state in the 35 different HMM as a function of the horizontal workplane illuminance. Black colour represents Discomfort-L, green Comfort & red Discomfort-H.	130
Figure 6-10. Normalised relative likelihoods of the identified states in all the 35 different HMM (scattered points) and their means (lines) as a function of the horizontal workplane illuminance.	131
Figure A-1. Fuzzy variable "Sun-obscured" (sky obscured probability) [min].	144
Figure A-2. Fuzzy variable "Season" (outdoor average temperature on the last 48 hours) [°C].	144
Figure A-3. Fuzzy variable "Roomtemp" (instantaneous air temperature) [°C].	144
Figure A-4. Fuzzy variable "EC.user" (user interaction with EC windows) [min].	145
Figure A-5. Fuzzy variable "DeskLux" (minute-averaged workplane illuminance) [lx].	145
Figure A-6. Fuzzy variable "Igh" (global horizontal solar irradiation) [W/m ²].	147
Figure A-7. Fuzzy variable "Season" (outdoor average temperature on the last 48 hours) [°C].	147
Figure A-8. Fuzzy variable "RoomTemp" (instantaneous air temperature) [°C].	147
Figure A-9. Fuzzy variable "BL.user" (user interaction with the blinds) [min].	148
Figure A-10. Fuzzy variable "DeskLux" (minute-averaged workplane illuminance) [lx].	149
Figure A-11. Fuzzy variable "Igh" (global horizontal solar irradiation) [W/m ²].	150
Figure A-12. Fuzzy variable "Season" (outdoor average temperature on the last 48 hours) [°C].	150
Figure A-13. Fuzzy variable "RoomTemp" (instantaneous air temperature) [°C].	151
Figure A-14. Fuzzy variable "DeskLux" (minute-averaged workplane illuminance) [lx].	152
Figure A-15. Fuzzy variable "EL.user" (user interaction with the electric lights) [min].	152

LIST OF TABLES

Table 2-1: Principal characteristics of the installed EC glazings.	13
Table 3-1: Accuracy of the sky prediction algorithm to predict sun-obscureness in 5-min forecast horizons for each day and tested hour.....	29
Table 4-1: Switching speed of EC Glazings (time required by the EC glazings to execute a certain percentage of the total switching depth).....	40
Table 4-2: Daylight factors for the 2 extreme Tv levels of the EC windows and for each point.	40
Table 4-3: Annual energy demand for space heating and electric lighting for different simulation scenarios.	51
Table 4-4: Comfort parameters and calculated operative temperature used in Fanger's model for a PPD<10%.....	57
Table 4-5: Percentage of working time during the simulation period where temperature is outside comfort limits (PMV<-0.5 or PMV>+0.5; PPD>10%), for each of the six considered simulation cases.	58
Table 4-6: Ranges of workplane illuminance and their probability to cause visual discomfort to space occupants (approximate values derived from Figure 4-20).	64
Table 4-7: Percentage of working time during the simulation period where visual discomfort probability is kept below fixed values, for each of the six considered simulation cases.	65
Table 5-1: Transition probability matrix of an ergodic variable (N=4).....	84
Table 5-2: Confusion matrix showing accuracy per class (in percentages). Results were obtained with 9-month training data with 1-h granularity for the GMMs with 17 mixtures.	87
Table 5-3: Confusion matrix showing accuracy per class (in percentages) for the simplified modes (3-feature observation vector). Results were obtained with 12-month training data with 1-h granularity for the GMMs with 21 mixtures.	89
Table 5-4: Main characteristics of the two different office rooms in the considered simulations. (Wall layer 1 is the inside layer and layer 3 is the outside one).	90

Table 5-5: Comfort parameters and calculated operative temperature used in Fanger's model for a PPD<10%.	98
Table 5-6: Percentage of working time during the simulation period where temperature is outside comfort limits (PMV<-0.5 or PMV>+0.5; PPD>10%), for each of the four considered simulation cases.	99
Table 6-1: Confusion matrix showing accuracy per state (in percentages). Results were obtained using 2 to 5 training tests (equivalent to about 8 to 20 months of observations) for the GMMs with 1-10 mixtures (k).	123
Table 6-2: Confusion matrix showing accuracy per state (in percentages). Results were obtained with only one training test (equivalent to about 4 months of observations) for the GMMs with 13 mixtures (k).	123
Table A-1. Output crisp value "EC-Tv" (EC windows visible light transmission)	145
Table A-2. Complete rule base of control scheme <i>User Present</i> , "EC Tv" in verbose format.	146
Table A-3. Output crisp value "EC-Tv" (EC windows visible light transmission)	148
Table A-4. Complete rule base of control scheme <i>User Absent</i> , "EC Tv" in verbose format.	148
Table A-5. Input crisp value "EC-Tv" (EC windows visible light transmission)	149
Table A-6. Output crisp value "a _{blind} " (Blinds position: 1: completely open; 0: completely closed).	149
Table A-7. Complete rule base of control scheme <i>User Present</i> , "Blinds" in verbose format.	150
Table A-8. Input crisp value "EC-Tv" (EC windows visible light transmission)	151
Table A-9. Output crisp value "a _{blind} " (Blinds position: 1: completely open; 0: completely closed).	151
Table A-10. Complete rule base of control scheme <i>User Absent</i> , "Blinds" in verbose format.	151
Table A-11. Input crisp value "EC-Tv" (EC windows visible light transmission).	152
Table A-12. Input crisp value "ablind" (Blinds position: 1: completely open; 0: completely closed).	152
Table A-13. Output crisp value "P.lights" (fraction of applied electric lighting power in dimmable luminaires; 1: fully on; 0: completely off).	153
Table A-14. Complete rule base of control scheme <i>User Present</i> , "Lights" in verbose format.	153

BIBLIOGRAPHY

- [1]. **Turiel, Isaac.** *Indoor Air Quality and Human Health*. s.l. : Stanford University Press, 1985. ISBN: 9780804712552.
- [2]. Indoor Environments. *Environmental Law Institute*. [Online] [Cited: 11 23, 2010.] http://www.eli.org/Program_Areas/indoor_environments.cfm.
- [3]. **Fisk, W.J. and Rosenfeld, A.H.** Estimates of Improved Productivity and Health from Better Indoor Environments. *Indoor Air*. 1997, Vol. 7, 3, pp. 158-172.
- [4]. **Olesen, B.W. and Parsons, K.C.** Introduction to thermal comfort standards and to the proposed new version of EN ISO 7730. *Energy and Buildings*. 2002, Vol. 34, 6, pp. 537-548.
- [5]. **Knez, Igor.** Effects of indoor lighting on mood and cognition. *Journal of Environmental Psychology*. 1995, Vol. 15, 1, pp. 39-51.
- [6]. **Li, D.H.W and Lam, J.C.** Evaluation of lighting performance in office buildings with daylighting controls. *Energy and Buildings*. 2001, Vol. 33, 8, pp. 793-803.
- [7]. **Goldberg, M.L.** Lighting in Commercial Buildings. *Report of U.S. Department of Energy, Energy Consumption Series*. 1992.
- [8]. **Perez-Lombard, L., Ortiz, J. and Pout, C.** A review on buildings energy consumption information. *Energy and Buildings*. 2008, Vol. 40, 3, pp. 394-398.
- [9]. **Bodart, M. and De Herde, A.** Global energy savings in offices buildings by the use of daylighting. *Energy and Buildings*. 2002, Vol. 34, 5, pp. 421-429.
- [10]. Directive 2010/31/EU of the European Parliament and of the Council of 19 May 2010 on the energy performance of buildings. *Official Journal of the European Union*. 18.6.2010, L 153/13.
- [11]. ASHRAE Standard 55-2004: Thermal Environmental Conditions for Human Occupancy. 2004.
- [12]. **Fanger, P.O.** *Thermal comfort analysis and applications in environmental engineering*. New York : McGraw-Hill, 1970.
- [13]. **7730:2005, EN ISO.** *International standard: Ergonomics of the Thermal Environment-Analytical Determination of Thermal Comfort by Using Calculations of the PMV and PPD Indices and Local Thermal Comfort Criteria*. Geneva : International Standard Organization for Standardization, 2005.

- [14]. **Haldi, F.** *Towards a Unified Model of Occupants' Behaviour and Comfort for Building Energy Simulation*. PhD thesis no. 4587, EPFL. 2010.
- [15]. **Nicol, F. and Humphreys, M.** Derivation of the adaptive equations for thermal comfort in free-running buildings in European standard EN15251. *Building and Environment*. January 2010, Vol. 45, 1, pp. 11-17.
- [16]. **Linhart, F.** *Energetic, visual and non-visual aspects of office lighting*. PhD thesis no. 4634, EPFL. 2010.
- [17]. **Nabil, A., & Mardaljevic, J.** Useful daylight illuminance: a new paradigm for assessing daylight in buildings. *Lighting Research and Technology*. March 2005, Vol. 37, 1, pp. 41-57.
- [18]. **Lindelöf, D.** *Bayesian optimization of visual comfort*. PhD thesis no. 3918, EPFL. 2007.
- [19]. **Galasiu, A. D. and Veitch, J. A.** Occupant preferences and satisfaction with the luminous environment and control systems in daylit offices: a literature review. *Energy and Buildings*. July 2006, Vol. 38, 7, pp. 728-742.
- [20]. **Scartezzini, J.-L. and Courret, G.** Anidolic daylighting systems. *Solar Energy*. 2002, Vol. 73, 2, pp. 123-135.
- [21]. **Macrelli, G.** Electrochromic windows. *Renewable Energy*. 1998, Vol. 15, 1-4, pp. 306-311.
- [22]. **Lee, E.S., et al.** Advancement of Electrochromic Windows. *Lawrence Berkeley National Laboratory*. 2006. LBNL-59821.
- [23]. **Baetens, R., Jelle, B.P. and Gustavsen, A.** Properties, requirements and possibilities of smart windows for dynamic daylight and solar energy control in buildings: A state-of-the-art review. *Solar Energy Materials and Solar Cells*. 2010, Vol. 94, 2, pp. 87-105.
- [24]. **Lee, E.S. and DiBartolomeo, D.L.** Application issues for large-area electrochromic windows in commercial buildings. *Solar Energy Materials and Solar Cells*. 2002, Vol. 71, 4, pp. 465-491.
- [25]. **Leaman, A. and Bordass, B.** Productivity in buildings: the 'killer'variables. *Building Research & Information*. 1999, Vol. 27, 1, pp. 4-19.
- [26]. **Oseland, N. A.** Predicted and reported thermal sensation in climate chambers, offices and homes. *Energy and Buildings*. December 1995, Vol. 23, 2, pp. 105-115.
- [27]. **Karjalainen, S. and Lappalainen, V.** Integrated control and user interfaces for a space. *Building and Environment*. 2011, Vol. 46, 4, pp. 938-944.
- [28]. **Zarkadis, N., Ridi, A. and Morel, N.** A multi-sensor office-building database for experimental validation and advanced control algorithm development. *Procedia Computer Science*. 2014, Vol. 32, The 5th International Conference on Ambient Systems, Networks and Technologies (ANT-2014), the 4th International Conference on Sustainable Energy Information Technology (SEIT-2014), pp. 1003-1009.
- [29]. **Zarkadis, N. and Morel, N.** Automatic control of an electrochromic window. *OFEN Final Report 103320/154379, Solar Energy and Building Physics Laboratory, EPFL, Lausanne*. October 2012.
- [30]. **Courret, G., et al.** Design and assessment of an anidolic light-duct. *Energy and Buildings*. 1998, Vol. 28, 1, pp. 79-99.

- [31]. **Altherr, René and Gay, J.-B.** A low environmental impact anidolic facade. *Building and Environment*. 2002, Vol. 37, 12, pp. 1409-1419.
- [32]. **Morel, N.** Description of the LESO Building. *Ecco-Build, Technical Report #9, Solar Energy and Building Physics Laboratory, EPFL, Lausanne*. 2004.
- [33]. **Guillemin, A.** *Using genetic algorithms to take into account user wishes in an advanced building control system*. PhD thesis no. 2778, EPFL. 2003.
- [34]. **Page, J., et al.** On-site performance of electrochromic glazings coupled to an anidolic daylighting system. *Solar Energy*. 2007, Vol. 81, 9, pp. 1166-1179.
- [35]. *EControl-Glas*. [Online] [Cited: 01 07, 2011.] <http://www.econtrol-glas.de>.
- [36]. MathWorks Inc. Official Website. [Online] <http://www.mathworks.com/>.
- [37]. **Eltako-Electronics, GmbH.** Wireless sensor; Motion/brightness sensor FBH63AP. *Technical specifications leaflet*. 11 2012.
- [38]. **Bovet, G. and Hennebert, J.** A Web-of-Things Gateway for KNX Networks. *In Proceedings of the IEEE European Conference on Smart Objects, Systems and Technologies (Smart SysTech)*. 2013.
- [39]. **Zarkadis, N. and Morel, N.** Advanced Control of Electrochromic Windows. *Proceedings of CISBAT 2013 Cleantech for Smart Cities and Buildings*. 2013, Vol. 1, EPFL-CONF-195697, pp. 543-548.
- [40]. **Granqvist, C.G.** Electrochromic tungsten oxide films: Review of progress 1993–1998. *Solar Energy Materials and Solar Cells*. 2000, Vol. 60, 3, pp. 201-262.
- [41]. **Sbar, N. L., et al.** Electrochromic dynamic windows for office buildings. *International Journal of Sustainable Built Environment*. June 2012, Vol. 1, 1, pp. 125-139.
- [42]. **Clear, R.D., Inkarojrit, V. and Lee, E.S.** Subject responses to electrochromic windows. *Energy and Buildings*. July 2006, Vol. 38, 7, pp. 758-779.
- [43]. **Scartezzini, J.-L., et al.** Intensive Use of Daylight in Buildings through Coupling of Electrochromic Glazings and Anidolic Daylighting Systems. *Final Report fo the VELUX Fondation, Solar Energy and Building Physics Laboratory, EPFL, Lausanne*. 2003.
- [44]. **Lee, E.S., et al.** A Design Guide for Early-Market Electrochromic Windows. *Lawrence Berkeley National Laboratory*. 2006. LBNL-59950.
- [45]. **Lee, E.S., DiBartolomeo, D.L. and Selkowitz, S.E.** Daylighting control performance of a thin-film ceramic electrochromic window: Field study results. *Energy and Buildings*. January 2006, Vol. 38, 1, pp. 30-44.
- [46]. **Fasano, G., et al.** A detailed characterization of commercial electrochromic devices for building applications. *Proceedings of EUROSUN 2002, June 2002, Bologna, Italy*.
- [47]. **Zinzi, M.** Office worker preferences of electrochromic windows: a pilot study. *Building and Environment*. 2006, Vol. 41, 9, pp. 1262-1273.
- [48]. **Czandernaa, A.W., et al.** Durability issues and service lifetime prediction of electrochromic windows for buildings applications. *Solar Energy Materials and Solar Cells*. 1999, Vol. 56, 3-4, pp. 419-436.
- [49]. **Sullivan, R., et al.** Effect of switching control strategies on the energy performance of electrochromic windows. *Proceedings SPIE*. 1994, Vol. 2255/443.
- [50]. **Assimakopoulos, M.N., et al.** Integrated energetic approach for a controllable electrochromic device. *Energy and Buildings*. 2004, Vol. 36, 5, pp. 415-422.

- [51]. **Jonsson, A. and Roos, A.** Evaluation of control strategies for different smart window combinations using computer simulations. *Solar Energy*. 2010, Vol. 84, 1, pp. 1-9.
- [52]. **Lee, E.S. and Tavit, A.** Energy and visual comfort performance of electrochromic windows with overhangs. *Building and Environment*. 2007, Vol. 42, 6, pp. 2439-2449.
- [53]. **Gugliermetti, F. and Bisegna, F.** Visual and energy management of electrochromic windows in Mediterranean climate. *Building and Environment*. 2003, Vol. 38, 3, pp. 479-492.
- [54]. **Assimakopoulos, M.N., et al.** Comparing the energy performance of an electrochromic window under various control strategies. *Building and Environment*. 2007, Vol. 42, 8, pp. 2829-2834.
- [55]. **Piccolo, A. and Simone, F.** Effect of switchable glazing on discomfort glare from windows. *Building and Environment*. 2009, Vol. 44, 6, pp. 1171-1180.
- [56]. **Klems, J.H.** Net energy performance measurements on electrochromic skylights. *Energy and Buildings*. 2001, Vol. 33, 2, pp. 93-102.
- [57]. **Tenner, A.D. and Zonneveldt, L.** Switchable Facades and Visual Comfort. *Right Light Conference, Nice, France*. May 29-31, 2002.
- [58]. **Bauer, M., et al.** DELTA, a blind controller using fuzzy logic. *OFEN Final Report 50.943, Solar Energy and Building Physics Laboratory, EPFL, Lausanne*. 1996.
- [59]. **Morel, N., et al.** Neurobat, a predictive and adaptive heating control system using artificial neural networks. *International journal of sustainable energy*. 2001, Vol. 21, 2, pp. 161-201.
- [60]. **Bosch, J.L., Zheng, Y. and Kleissl, J.** Deriving cloud velocity from an array of solar radiation measurements. *Solar Energy*. January 2013, Vol. 87, pp. 196-203.
- [61]. **Nygard F., A.M.** *Predictive thermal control of building systems*. PhD thesis no. 876, EPFL. 1990.
- [62]. **Gonzalez, R.C., Woods, E. and Eddins, S.L.** *Digital image processing using MATLAB*. 2nd Edition. s.l. : Gatesmark Publishing, 2009. ISBN 978-0-9820854-0-0.
- [63]. **Evans, A.N.** Cloud motion analysis using multichannel correlation-relaxation labeling. *Geoscience and Remote Sensing Letters, IEEE*. 2006, Vol. 3, 3, pp. 392-396.
- [64]. **Zafarifar, B. and With, P.H.N.** Blue sky detection for picture quality enhancement. *Advanced Concepts for Intelligent Vision Systems*. 2006, Vol. 4179, pp. 522-532.
- [65]. **Lalonde, J.-F., Narasimhan, S. and Efros, A.** What Do the Sun and the Sky Tell Us About the Camera? *International Journal of Computer Vision*. 2010, Vol. 88, 1, pp. 24-51.
- [66]. **Perez, R., Seals, R. and Michalsky, J.** All-weather model for sky luminance distribution - Preliminary configuration and validation. *Solar Energy*. 1993, Vol. 50, 3, pp. 235-245.
- [67]. **Horn, B. K. and Schunck, B. G.** Determining optical flow. *1981 Technical Symposium East*. International Society for Optics and Photonics, 1981, pp. 319-331.
- [68]. **Barron, J.L., Fleet, D.J. and Beauchemin, S.S.** Performance of optical flow techniques. *International Journal of Computer Vision*. 1994, Vol. 12, 1, pp. 43-77.
- [69]. **Chow, Chi Wai, et al.** Intra-hour forecasting with a total sky imager at the UC San Diego solar energy testbed. *Solar Energy*. November 2011, Vol. 85, 11, pp. 2881-2893.

- [70]. **Marquez, R. and Coimbra, C.F.M.** Intra-hour DNI forecasting based on cloud tracking image analysis. *Solar Energy*. May 2013, Vol. 91, pp. 327-336.
- [71]. **Li, Q., Lu, W. and Yang, J.** A Hybrid Thresholding Algorithm for Cloud Detection on Ground-Based Color Images. *Journal of Atmospheric and Oceanic Technology*. October 2011, Vol. 28, 10, pp. 1286–1296.
- [72]. **Mori, N. and Chang, K.-A.** Introduction to MPIV. *User reference manual*. <http://www.oceanwave.jp/software/mpiv>, 2003, p. 14p.
- [73]. **Reda, I., Andreas, A.** *Solar position algorithm for solar*. s.l. : National Renewable Energy Laboratory (NREL), 2003. Technical report NREL/TP-560-34302.
- [74]. **Lee, E.S., et al.** Monitored Energy Performance of Electrochromic Windows Controlled for Daylight and Visual Comfort. *Lawrence Berkeley National Laboratory*. 2005. LBNL-58912.
- [75]. **Fernandes, LL., Lee, E.S. and Ward, G.** Radiance-Mathematica optimization study of electrochromic window and daylighting control systems. *Advancement of Electrochromic Windows final report, Lawrence Berkeley National Laboratory. California Energy Commission, PIER Program*. 2006. CEC-500-2006-052-AT5.
- [76]. **Daum, D.** *On the Adaptation of Building Controls to the Envelope and the Occupants*. PhD thesis no. 4935, EPFL. 2011.
- [77]. **Lee, C. C.** Fuzzy logic in control systems: fuzzy logic controller. II. *Systems, Man and Cybernetics, IEEE Transactions*. March/April 1990, Vol. 20, 2, pp. 419-435.
- [78]. **Chung, F. L. and Duan, J. C.** On multistage fuzzy neural network modeling. *Fuzzy Systems, IEEE Transactions*. April 2000, Vol. 8, 2, pp. 125 - 142.
- [79]. **Crispim, E.M., Ferreira, P.M. and Ruano, A.E.** Prediction of the solar radiation evolution using computational intelligence techniques and cloudiness indices. *International Journal of Innovative Computing, Information and Control*. 2008, Vol. 4, 5, pp. 1121–1133.
- [80]. **Hygge, S. and Lofberg, H.A.** User Evaluation of Visual Comfort in Some Buildings of the Daylight Europe Project. *Right Light*. 1997, Vol. 2, 4.
- [81]. **Borisuit, A., Scartezzini, J.-L. and Thanachareonkit, A.** Visual discomfort and glare rating assessment of integrated daylighting and electric lighting systems using HDR imaging techniques. *Architectural Science Review*. 2010, Vol. 53, 4, pp. 359-373.
- [82]. **Borisuit, A., et al.** A new device for dynamic luminance mapping and glare risk assessment in buildings. *Proc. SPIE 8485, Nonimaging Optics: Efficient Design for Illumination and Solar Concentration IX*. October 11, 2012, Vol. 8485.
- [83]. **Inanici, MN.** Evaluation of high dynamic range photography as a luminance data acquisition system. *Lighting Research and Technology*. 2006, Vol. 38, 2, pp. 123-134.
- [84]. Meteonorm official website. [Online] <http://meteonorm.com/home/>.
- [85]. **Perez, R., et al.** Modeling daylight availability and irradiance components from direct and global irradiance. *Solar Energy*. 1990, Vol. 44, 5, pp. 271-289.
- [86]. **Andrew, J.M.** RADIANCE and Daylight Factors. *Natural Frequency*. 11 2007, 004.
- [87]. **Ridi, A., et al.** Towards Reliable Stochastic Data-Driven Models Applied to the Energy Saving in Buildings. *Proceedings of CISBAT 2013 Cleantech for Smart Cities and Buildings*. 2013, Vol. 1, EPFL-CONF-195696, pp. 501-505.

- [88]. **Chartered Institution of Building Services Engineers, (CIBSE).** Dynamic Behaviour of Buildings. 16387: *Environmental Engineering Science* 2, <http://ecotect.com/system/files/CIBSE+Factor.pdf>.
- [89]. **Bauer, M.** *Gestion bio-mimétique de l'énergie dans le bâtiment*. PhD thesis no. 1792, EPFL. 1998.
- [90]. **Dong, B., Lam, K.P. and Neuman, C.** Integrated building control based on occupant behavior pattern detection and local weather forecasting. *Twelfth International IBPSA Conference. Sydney: IBPSA Australia*. 2011, pp. 14-17.
- [91]. **Domahidi, A., et al.** Learning near-optimal decision rules for energy efficient building control. *Proceedings of the 51st IEEE Conference on Decision and Control*. December 2012, pp. 7571-7576.
- [92]. **Guillemin, A. and Morel, N.** An innovative lighting controller integrated in a self-adaptive building control system. *Energy and Buildings*. May 2001, Vol. 33, 5, pp. 477-487.
- [93]. **Oldewurtel, F., et al.** Use of model predictive control and weather forecasts for energy efficient building climate control. *Energy and Buildings*. February 2012, Vol. 45, pp. 15-27.
- [94]. **Zadeh, L.A.** Fuzzy algorithms. *Information and control*. February 1968, Vol. 12, 2, pp. 94-102.
- [95]. **Dounis, A. I. and Manolakis, D. E.** Design of a fuzzy system for living space thermal-comfort regulation. *Applied Energy*. June 2001, Vol. 69, 2, pp. 119-144.
- [96]. **Calvino, F., et al.** The control of indoor thermal comfort conditions: introducing a fuzzy adaptive controller. *Energy and Buildings*. 2004, Vol. 36, 2, pp. 97-102.
- [97]. **Trobec Lah, M., et al.** Daylight illuminance control with fuzzy logic. *Solar Energy*. 2006, Vol. 80, 3, pp. 307-231.
- [98]. **Kolokotsa, D., et al.** Design and installation of an advanced EIB fuzzy indoor comfort controller using Matlab. [ed.] 1092. *Energy and buildings*. 2006, Vol. 38, 9, p. 1084.
- [99]. **Kurian, C. P., et al.** Robust control and optimisation of energy consumption in daylight—artificial light integrated schemes. *Lighting Research and Technology*. 2008, Vol. 40, 1, pp. 7-24.
- [100]. **Alcalá, R., et al.** A genetic rule weighting and selection process for fuzzy control of heating, ventilating and air conditioning systems. *Engineering Applications of Artificial Intelligence*. 2005, Vol. 18, 3, pp. 279-296.
- [101]. **Yang, I. H., Yeo, M. S. and Kim, K. W.** Application of artificial neural network to predict the optimal start time for heating system in building. *Energy Conversion and Management*. 2003, Vol. 44, 17, pp. 2791-2809.
- [102]. **Wilke, U.** *Probabilistic Bottom-up Modelling of Occupancy and Activities to Predict Electricity Demand in Residential Buildings*. PhD thesis no. 5673, EPFL. 2013.
- [103]. **Dong, B. and Lam, K.P.** A real-time model predictive control for building heating and cooling systems based on the occupancy behavior pattern detection and local weather forecasting. *Building Simulation*. February 2014, Vol. 7, 1, pp. 89-106.
- [104]. **Rabiner, L. R. and Juang, B. H.** Fundamentals of speech recognition. *Englewood Cliffs: PTR Prentice Hall*. 1993.

- [105]. **Hennebert, J.** *Hidden Markov models and artificial neural networks for speech and speaker recognition*. PhD thesis no. 1860, EPFL. 1998.
- [106]. **Lu, J., et al.** The smart thermostat: using occupancy sensors to save energy in homes. *Proceedings of the 8th ACM Conference on Embedded Networked Sensor Systems*. 2010, pp. 211-224.
- [107]. **Ridi, A., Gisler, C. and Hennebert, J.** Automatic identification of electrical appliances using smart plugs. *Systems, Signal Processing and their Applications (WoSSPA), 2013 8th International Workshop on*. pp. 301-305.
- [108]. **Antonopoulos, K.A. and Tzivanidis, C.** Time constant of greek buildings. *Energy*. August 1995, Vol. 20, 8, pp. 785-802.
- [109]. **Reddy, T. A., Norford, L. K. and Kempton, W.** Shaving residential air-conditioner electricity peaks by intelligent use of the building thermal mass. *Energy*. July 1991, Vol. 16, 7, pp. 1001-1010.
- [110]. **Antretter, F., Klingenberg, K. and Pazold, M.** All-in-One Design Tool Solution for Passive Houses and Buildings - Monthly Energy Balance and Hygrothermal Simulation. *Thermal Performance of the Exterior Envelopes of Whole Buildings XII International Conference, ASHRAE*. 2003.
- [111]. **Dempster, A. P., Laird, N. M., Rubin, D. B.** Maximum likelihood from incomplete data via the EM algorithm. *Journal of the royal statistical society. Series B (methodological)*. 1977, Vol. 39, 1, pp. 1-38.
- [112]. **Rabiner, L.** A tutorial on hidden Markov models and selected applications in speech recognition. *Proceedings of the IEEE*. February 1989, Vol. 77, 2, pp. 257-286.
- [113]. **Webb, A. R.** Considerations for lighting in the built environment: Non-visual effects of light. *Energy and Buildings*. 2006, Vol. 38, 7, pp. 721-727.
- [114]. **CIE.** Guide on interior lighting, second edition. Technical report. *Commission Internationale de l'Eclairage*. 1986.
- [115]. **Petherbridge, P. and Hopkinson, R.G.** Discomfort Glare and the Lighting of Buildings. *Transaction of Illuminating Engineering Society*. 1950, Vol. 15, 39.
- [116]. **Wienold, J. and Christoffersen, J.** Evaluation methods and development of a new glare prediction model for daylight environments with the use of CCD cameras. *Energy and buildings*. July 2006, Vol. 38, 7, pp. 743-757.
- [117]. **CIE.** Discomfort Glare in the Interior Lighting, Commission Internationale de l'Eclairage (CIE), Technical committee TC-3.13, Division 4. *Interior Environment and Lighting Design*. 1992.
- [118]. **Osterhaus, W. K.** Discomfort glare assessment and prevention for daylight applications in office environments. *Solar Energy*. August 2005, Vol. 79, 2, pp. 140-158.
- [119]. **Michel, L.** *Méthode expérimentale d'évaluation des performances lumineuses de bâtiments*. EPFL. 1999. PhD thesis no. 2042.
- [120]. **Spasojevic, B. and Mahdavi, A.** Sky luminance mapping for computational daylight modeling. *Ninth International IBPSA Conference, Montreal, Canada*. August 15-18, 2005.

- [121]. **Thanachareonkit, A., Scartezzini, J.-L. and Andersen, M.** Comparing daylighting performance assessment of buildings in scale models and test modules. *Solar Energy*. 2005, Vol. 79, 2, pp. 168-182.
- [122]. **Chan, M., et al.** A review of smart homes: Present state and future challenges. *Computer Methods and Programs in Biomedicine*. July 2008, Vol. 91, 1, pp. 55-81.
- [123]. **CIE**. 17-330 disability glare. [Online] <http://eiv.cie.co.at/term/330>.
- [124]. —. 17-333 discomfort glare. [Online] <http://eiv.cie.co.at/term/333>.



Nikos ZARKADIS

Energy and Environmental Eng. M.Sc., PhD

Ecole Polytechnique Fédérale de Lausanne (EPFL)
Solar Energy and Building Physics Laboratory (LESO-PB)
LE 2 200, Station 18, CH-1015 Lausanne
Tel: +41 (0) 21 693 57 14
E-mail: nikoszarkadis@gmail.com

CURRICULUM VITAE

PERSONAL INFORMATION

Date of birth: 18 June 1979
City/Country of birth: Athens, GREECE

EDUCATION

2010 - 2015 **Ecole Polytechnique Fédérale de Lausanne**, Doctoral Program in Civil and Environmental Engineering, Solar Energy & Building Physics Laboratory (LESO-PB)

PhD Research, Thesis: Novel models for predictive control of advanced building systems and occupant comfort in buildings.

2004 - 2008 **University of Crete, Department of Chemistry**

M.Sc. in Environmental Protection Technologies

Dissertation: Towards A Methodology For An Integrated Assessment & Labelling For Sustainable Buildings In The EU.

1998 - 2003 **Technological Educational Institute of Crete (TEI of Crete), Department of Mechanical Engineering**

B.Sc. Degree in Energy and Environmental Technology

Dissertation: Energy and Environmental Assessment of Hospitals. The 'General University Hospital Of Heraklion' case study.

PAPERS, ARTICLES & CONFERENCES

N. Zarkadis, N. Morel, J-L. Scartezzini. Season Identification for Building Control Systems Based on Hidden Markov Models. (In preparation; provisional title).

N. Zarkadis, N. Morel, J-L. Scartezzini. A Novel Sun and Clouds Tracking and Prediction Sky-scanner Algorithm. (In preparation; provisional title).

N. Zarkadis, A. Ridi, N. Morel. A Multi-sensor Office-building Database for Experimental Validation and Advanced Control Algorithm Development, Procedia Computer Science, Volume 32, 2014, Pages 1003-1009, ISSN 1877-0509 (Presented at The 5th International Conference on Ambient Systems, Networks and Technologies, ICT-SB Workshop, June 2 - 5, 2014, Hasselt, Belgium)

A. Ridi, N. Zarkadis, G. Bovet, N. Morel and J. Hennebert. Towards Reliable Stochastic Data-Driven Models Applied to the Energy Saving in Buildings. CISBAT 2013, Lausanne, Switzerland, September 4-6, 2013.

N. Zarkadis and N. Morel. Advanced Control of Electrochromic Windows. CISBAT 2013, Lausanne, Switzerland, September 4-6, 2013.

N. Zarkadis, N. Sakkas, E. T. Samara. 1st SE Europe-Mediterranean Conference on Accessibility and Tourism: An Overview, ABACUS 2007 (Vol.2 No.2)

N. Zarkadis. Business Models in "Tourism For All" And The Role Of The Disability Movement, Accessibility and Tourism - 1st Regional Workshop, 29 & 30 June 2006

N. Zarkadis. Labeling For Sustainable Buildings – The LEnSE Project, Innovative policies and Technologies For The Built Environment, Technical Chamber of Greece Workshop (Eastern Crete Department), 22 June 2006

RESEARCH & PROFESSIONAL EXPERIENCE

2010 - **Ecole Polytechnique Fédérale de Lausanne / Solar Energy & Building Physics Laboratory**
Doctoral Assistant. Research in the fields of predictive building control, building physics, occupants visual and thermal comfort, energy saving. Teaching assistant in Building Physics I & II courses.

2004 - 2010 **Applied Industrial Technologies Ltd**
Independent contractor, researcher & technical consultant in the areas of: IT development, sustainable development and accessibility of the built environment, energy & environmental engineering, social economy and "tourism for all". Contracted to participate in several projects undertaken by the company.

2006 - 2008 **TEI of Crete/East Med Technology Transfer Unit (EMTTU)**
Independent contractor, researcher & technical consultant (same as above). Contracted to participate in TECH-TRANSFER, ICZM projects undertaken by the Institution.

2006 - 2007 **European Profiles SA**
Independent contractor & researcher. Contracted to participate in LEnSE project.

2002 - 2006 **Tsapalis Antonis Mech.Eng. Office**
Practical trainee and then employed on a full-time basis as Environmental Impact Assessor and Mech. Engineer & designer in building construction. Participated in small, medium and large scale private and public sector project assignments (i.e. University of Crete Campus Expansion, New Museum Of Natural History in Crete).

1999 - 2001 **Wind Energy Lab (TEI of Crete)**
Undergraduate researcher. Participated in several projects and R&D programmes undertaken by the Laboratory.

1997 - 1999 **Galanis Sports Data SA**
Employed on a part-time basis as a Sports Statistics Expert. Main duties included technical infrastructure setup and support; statistics generation, edit and

publication; display of sport statistics live (on real time) on national and international TV broadcasting networks.

SELECTED PROJECTS

2012 - 2015 **Green-Mod**, A joint EPFL/HES-SO Fribourg project; funded by the Hasler Foundation. Elaboration of models able to optimize energy consumption in buildings while preserving human comfort. Use of state-based stochastic modelling applied to temporal signals acquired from heterogeneous sources .

2010 - 2012 **ECControl, Automatic control of an electrochromic window**, OFEN, Switzerland. Development of an advanced predictive control algorithm for an electrochromic (EC) glazing for the optimal use of the direct solar gains and the (visual and thermal) comfort of the users.

2009 - 2010 **PERFECTION: Coordination Action For Performance Indicators For Health, Comfort And Safety Of The Indoor Environment**, EU; 7th Framework Programme (FP7)

Contracted to participate in Work Package 2: Development of IT framework for assessing the impact of Health, Comfort & Safety indicators on the indoor environment.

2005 - 2008 **The Social Economy in Greece. Framework, Pilot testing, and Support Structures**, EU & Greek Ministry of Employment And Social Affairs; EQUAL Initiative

Author of the 'Guide For The Creation And Operation Of Technology Aware Social Enterprises'. Designer and developer of the web based software for the Social Economy Observatory in Greece. Participated in elaboration of business plans of social economy pilot companies.

2006 - 2007 **LEnSE: Methodology Development towards a Label for Environmental, Social and Economic Buildings**, EU; 6th Framework Programme (FP6)

Contracted to participate in WP1, 2 & 3. Participated in research for the definition and development of sustainability indicators and methodology framework for assessing the sustainability of buildings. Responsible for the development of the prototype assessment tool and the pilot testing of the methodology (task leader). Participation and presentations in national and international meetings and events (Expert Workshops & Project Meetings).

1999 - 2000 **Wind Energy Lab Projects (TEI of Crete)**

Involved in wind systems research in the fields of: maps digitizing and management; wind energy potential assessments; wind energy calculations and synthesis of wind systems; wind energy management using Reverse Hydroelectric power plants.

Participated in the following projects:

- Feasibility study of Wind Park investment at St. Ioannis area in Lasithi, Crete.
- Technical and economic assessment of Wind Park at St. Ioannis area in Lasithi, Crete
- Combined management of Wind Energy and Water resources using Reverse Hydroelectric power plants in Malia Municipality, Crete.

- Combined management of Wind Energy and Water resources using Reverse Hydroelectric power plants in Mires Municipality, Crete.
- Studies, research and action plans for multilevel promotion of Renewable Energy Sources in Crete and Cyprus.

AWARDS AND HONOURS

- Award from REVOIL S.A. (Greek petroleum company) (June 2008) for best M.Sc thesis in Environmental studies
- Scholarship from “Greek State Scholarships Foundation” (February 2006) for excellency in M.Sc. Programme courses
- Scholarships (Excellence Awards) from “Greek State Scholarships Foundation” for 2 consecutive academic years (1998-1999 & 1999-2000) [B.Sc. courses excellency]

LANGUAGES

Greek (mother tongue), English (excellent), French (Very good), Italian & German (beginner).

GENERAL INTERESTS

- Producer and presenter of a 4-hour weekly radio show in university radio station (Studio FM1 105.4 MHz, <http://fm1.teiher.gr>) between 1999 and 2008. The show featured a wide range of music principally from 50s to 70s (Rock, pop, jazz, blues, folk, soul etc.). The show continued in Lausanne, at *Fréquence Banane*, Sundays 20h-22h (<http://vitaminzradio.wordpress.com/>).
- Music, literature, cinema, photography, travelling, good food.